Synthesis and Antimicrobial Activity of β-Hairpin Peptidomimetics Against *Pseudomonas aeruginosa*

and

Understanding the Mechanism of Action of the Insect Antimicrobial Peptide Thanatin

---

Dissertation

zur

Erlangung der naturwissenschaftlichen Doktorwürde

(Dr. sc. nat.)

vorgelegt der

Mathematisch-naturwissenschaftlichen Fakultät

der

Universität Zürich

von

Stefan Urs Vetterli

von

Stäfa, ZH

Promotionskommission

Prof. Dr. John A. Robinson (Vorsitz)

Prof. Dr. Oliver Zerbe

Prof. Dr. Nathan Luedtke

Zürich, 2017

This thesis is dedicated to the memory of my friend Peter Simon Frei
1985 – 2017

Contents

Summary

The increase in antimicrobial resistance against standard antibiotics and established therapies is a major concern for global health. The development of new antibiotics with new mechanisms of action is crucial in providing effective means of therapy for infected patients in the future. Antimicrobial peptides serve as a rich and as yet unexhausted source of potential new antibiotics. The three-dimensional character of peptides and peptidomimetics allows them to exploit a larger surface area on a biological target than traditional small organic molecules, potentially resulting in a strong and specific binding. This makes them ideal inhibitors of biological function. A novel class of β-hairpin peptidomimetics with high antimicrobial activity against the opportunistic pathogen *Pseudomonas aeruginosa* was recently discovered. The cyclic β-hairpin molecule L27-11 contains a 12 amino acid loop sequence (TWLKKRRWKKAK) connected to a ^{D}Pro-^{L}Pro template. It was proved, that L27-11 acts through a stereoselective interaction with the outer membrane protein LptD, a large β-barrel protein incorporated in the outer membrane of Gram-negative bacteria. LptD is part of the lipopolysaccharide (LPS) transport machinery, and is responsible for the final step in the transport of LPS from the inner membrane to the bacterial surface. Although important progress has been made in recent years in understanding the LPS transport and insertion process into the outer membrane, the binding site of L27-11 is still unknown.

The aim of the project described in the first part of this thesis was to expand the structure-activity relationship (SAR) profile of the closely related lead compound LB-01. N-methylation of backbone NH groups was chosen as a simple chemical modification to study the correlation between stable folded β-hairpins and antimicrobial activity. N-methylated analogues of LB-01 were synthesized and tested for their activity by determining their minimal inhibitory concentration (MIC). In-depth structural analysis was performed by solution NMR. Not only the previously suggested folding of the β-hairpin proved to be crucial for high antimicrobial activity, but several outward-facing NH groups sensitive to N-methylation could also be identified. These non-hydrogen bonding positions on both sides of the hairpin, likely make direct contact with a β-rich sequence in LptD through antiparallel strand-strand interaction. Further, the LB-01 scaffold was established as a non-toxic, cell penetrating peptide for delivery into mammalian cells.

In the second part of this thesis, the mechanism of action of the antimicrobial peptide thanatin was studied in detail in *E. coli*. Thanatin was first isolated from the hemipteran insect *Podisus maculiventris* in 1996. The peptide consists of 21 amino acids (GSKKPVPIIYCNRRTG KCQRM) with a disulfide bond between the two cysteines, forming a β-hairpin fold with a

flexible N-terminal sequence. Thanatin exhibits antimicrobial activity against a wide range of Gram-positive and Gram-negative bacteria and fungi. However, the all D-enantiomer of thanatin showed a complete loss of activity in *E. coli* and other Gram-negative bacteria, suggesting a stereospecific target in those organisms. A series of assays was performed to study the effect of thanatin on the membrane integrity in *E. coli*. Sytox® Green uptake, β-lactamase, and β-galactosidase release assays all ruled out a permeabilization of the cell membrane. Electron microscopy and confocal fluorescence microscopy was performed to learn more about changes in cell morphology as a direct effect of thanatin. Additionally, a fluorescence-labelled thanatin probe was used to study its localization inside the cell. The effect of thanatin on the macromolecular synthesis pathways of DNA, RNA, proteins, and the cell wall was studied by monitoring the incorporation of radioactive precursors. Only the incorporation of N-acetylglucosamine was upregulated, whereas the other pathways remained unaffected. A thanatin probe containing a biotin tag and a diazirine group suitable for photoaffinity labelling was used to identify potential interaction partners. Several crosslinked proteins could be identified by Western blotting of polyacrylamide gels in 1 and 2 dimensions and subsequent biotin detection. In a collaboration with the Wollscheid group at ETH Zurich, the crosslinking of LptD was confirmed by protein mass spectrometry, as well as the identification of LptA as a high-confidence interaction partner. These proteins play a crucial part in the LPS transport machinery, making it very likely that a perturbation of the LPS pathway is the cause of the antimicrobial activity of thanatin in Gram-negative bacteria. The periplasmic, LPS binding protein LptA was recombinantly expressed and binding affinity between the fluorescence-labelled thanatin analogue and LptA-His_6 was studied by fluorescence polarization. A K_d value of 12 ± 3 nM for this interaction was calculated and a competition experiment with native thanatin and D-thanatin confirmed the specific interaction with LptA-His_6. A key point mutation (Q62L) in LptA was identified, rendering *E. coli* bacteria that contain this mutation completely resistant against thanatin. These studies provide an important advance in revealing the mechanism of action of thanatin and propose the LPS pathway as a new major drug target in *E. coli* and other Gram-negative species.

Zusammenfassung

Die zunehmenden Resistenzen von Mikroorganismen gegenüber herkömmlichen Antibiotika und etablierten Therapien, stellen eine grosse Gefahr für die globale Gesundheit dar. Die Entwicklung von neuen Antibiotika mit neuen Wirkungsmechanismen ist entscheidend, um auch in Zukunft infizierte Patienten effektiv behandeln zu können. Eine bei weitem noch nicht erschöpfte Quelle an potentiellen Antibiotika stellt die Klasse der antimikrobiellen Peptide dar. Die dreidimensionale Struktur von Peptiden und Peptidmimetika würde es erlauben, mit einer grösseren Interaktionsfläche auf einer biologischen Zielstruktur zu interagieren, als es traditionelle kleine organische Verbindungen in der Lage sind. Solch eine starke und spezifische Bindung macht Peptide und Peptidmimetika zu idealen Inhibitoren biologischer Vorgänge. Eine neuartige Klasse von β-Haarnadel Peptidmimetika mit hoher antimikrobieller Aktivität gegenüber dem opportunistischen Krankheitserreger *Pseudomonas aeruginosa* wurde kürzlich entdeckt. Das zyklische β-Haarnadel Molekül L27-11 besteht aus einer Schlaufe von 12 Aminosäuren (TWLKKRRWKKAK), die dabei mit einem ^{D}Pro-^{L}Pro Templat verknüpft wird. Es konnte nachgewiesen werden, dass L27-11 stereoselektiv mit LptD, einem Protein der äusseren Membran in Gram-negativen Bakterien, interagiert. LptD ist Teil der Lipopolysaccharid (LPS) Transport Maschinerie, welche LPS von der inneren Membran zur Oberfläche eines Bakteriums transportiert. Obwohl in den letzten Jahren enorme Fortschritte im Verständnis des LPS Transports und des Einfügungsprozesses in die äussere Membran gemacht wurden, ist die Bindungsstelle von L27-11 an LptD weiterhin unbekannt. Das Ziel der Arbeit, welche im ersten Teil beschrieben wird, war es die Struktur-Wirkungsbeziehung (SAR) der mit L27-11 eng verwandten Leitstruktur LB-01 zu erweitern. Die N-Methylierung von NH Gruppen am Rückgrat des Peptids wurde als einfache chemische Modifizierung gewählt, um die Beziehung zwischen stabil gefalteten β-Haarnadel Strukturen und antimikrobieller Aktivität zu studieren. N-Methylierte Analoga von LB-01 wurden synthetisiert und mittels Bestimmung ihrer minimalen Hemm-Konzentration (MIC) auf ihre antimikrobielle Aktivität getestet. Die strukturelle, dreidimensionale Analyse wurde eingehend durch Kernspinresonanz (NMR) durchgeführt. Es zeigte sich dabei, dass nicht nur, wie bereits früher angenommen wurde, die stabil gefaltete β-Haarnadel Struktur für die antimikrobielle Aktivität entscheidend ist sondern auch mehrere nach aussen zeigende NH Gruppen, welche empfindlich auf N-Methylierung reagieren. Diese nicht-bindenden Wasserstoffbrücken Positionen auf beiden Seiten der β-Haarnadel interagieren vermutlich direkt durch antiparallele Strang-Strang Interaktion mit einer β-reichen Sequenz in LptD. Weiter wurde das LB-01 Gerüst als nicht-toxisches, zellpenetrierendes Peptid etabliert, für den potentiellen, gezielten Wirkstofftransport in Säugerzellen.

Im zweiten Teil dieser Arbeit wurde der Wirkungsmechanismus des antimikrobiellen Peptids Thanatin in *E. coli* grundlegend untersucht. Thanatin wurde 1996 erstmals aus dem Insekt *Podisus maculiventris* der Ordnung Hemiptera isoliert. Es handelt sich dabei um ein Peptid bestehend aus 21 Aminosäuren (GSKKPVPIIYCNRRTGKCQRM) mit einer Disulfidbrücke zwischen den beiden Cysteinen, welche eine β-Haarnadel mit einer flexiblen N-terminalen Sequenz formt. Thanatin zeigte antimikrobielle Aktivität gegenüber einer Reihe von Gram-positiven und Gram-negativen Bakterien, sowie auch gegenüber von Pilzen. Das D-Enantiomer von Thanatin jedoch zeigte nur in *E. coli* sowie anderen Gram-negativen Bakterien einen kompletten Wirkungsverlust, was auf eine stereospezifische Zielstruktur hindeutete. Es wurden mehrere Messungen durchgeführt um die Wirkung von Thanatin auf die Membranintegrität von *E. coli* zu untersuchen. Die Sytox® Grün Aufnahme, sowie β-Laktamase und β-Galaktosidase Freigabe-Untersuchungen schlossen alle eine generelle Permeabilisierung der Zellmembran aus. Untersuchungen mittels Elektronenmikroskopie und konfokaler Fluoreszenzmikroskopie wurden durchgeführt, um mehr über morphologische Veränderungen als direkte Auswirkung von Thanatin zu erfahren. Zusätzlich wurde ein fluoreszenzmarkiertes Analoga synthetisiert um dessen Ansammlung innerhalb der Zelle zu studieren. Der Effekt von Thanatin auf die makromolekularen Synthesewege von DNS, RNS, Proteinen und der Zellwand wurde mittels Einlagerung von radioaktiven Vorläufern untersucht. Nur die Einlagerung von N-Acetylglucosamin in die Zellwand war erhöht, wobei die anderen Synthesewege sich unverändert zeigten. Eine Thanatin Probe, welche eine Biotin Markierung und eine funktionelle Diazirin Gruppe enthält, wurde zur Nutzung der Photoaffinitäts-markierung synthetisiert, um damit potentielle Interaktionspartner zu identifizieren. Dabei wurden mittels Westernblot von 1- und 2-dimensionalen Polyacrylamid-Gelen und anschliessender Biotin Detektion, mehrere quervernetzte Proteine identifiziert. Durch eine Kollaboration mit der Wollscheid Gruppe an der ETH Zürich wurde die Quervernetzung von LptD mittels Protein-Massenspektrometrie bestätigt, sowie ebenfalls mit hoher Wahrscheinlichkeit die Identifizierung von LptA als direkter Interaktionspartner. Das periplasmatische, LPS-bindende Protein LptA wurde rekombinant exprimiert und eine Schlüsselmutation in LptA (Q62L) wurde identifiziert, welche *E. coli* Bakterien komplett resistent gegenüber Thanatin werden lässt. Affinitätsstudien zwischen dem fluoreszenz-markierten Thanatin-Analoga und LptA-His_6 wurden mittels Fluoreszenzpolarisationsmessung durchgeführt. Dabei wurde ein K_d Wert von 12 ± 3 nM für diese Interaktion berechnet. Ein Kompetitionsexperiment mit dem ursprünglichen Thanatin und D-Thanatin bestätigten die spezifische Interaktion mit LptA-His_6. Zusammenfassend liefern diese Studien einen wichtigen Fortschritt im Verständnis des Wirkungsmechanismus von Thanatin in *E. coli* und anderen Gram-negativen Bakterien und erklären den LPS Transportweg zu einer bedeutenden Zielstruktur für die Arzneimitteltherapie.

1 Introduction

1.1 Antimicrobial Peptides

Antimicrobial peptides (AMPs) are part of the innate immune system in many different organisms. They serve as a first line of defense in the fight against invading microorganisms and viruses and are therefore also often referred to as host-defense peptides. Most AMPs are genetically encoded with a signal sequence and have a length of less than 100 amino acids. They usually bear multiple cationic charges and hydrophobic residues in an overall amphipathic structure that allows electrostatic attachment to the negatively charged surface of the membrane of invading pathogens. Many AMPs are then capable of disrupting membranes by forming pore-like structures, finally leading to cell lysis. They are released directly at infection sites by effector cells due to their unselective mechanism of action and the normally micromolar concentration that is needed for activity.[1] Lysis of mammalian cells (e.g. red blood cells) can cause toxicity issues under higher concentration, as well as when AMPs are administered systemically.[2] However, some AMPs also have mechanisms of action that do not involve membranolysis. Certain peptides have been shown to translocate across the cell membrane without disruption and bind to nucleic acids (buforin II[3], tachyplesin[4]), inhibit cell-wall synthesis (mersacidin[5]), inhibit protein synthesis (pleurocidin[6], indolicidin[7]) or protein folding (pyrrhocoricin[8]). Hundreds of AMPs have been identified thus far and characterized on the basis of their amino acid composition, secondary structures, and origins. AMPs can adopt a variety of secondary structures, such as α-helices, extended coils, and β-sheets, which often include the formation of disulfide bonds (Figure 1).[9]

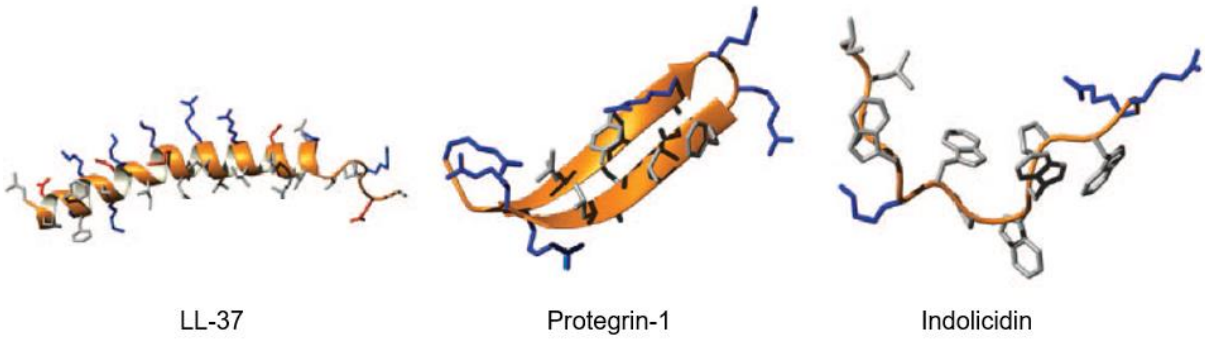

Figure 1 Different secondary structure elements found in AMPs: α-helix (LL-37), β-sheet (protegrin-1), extended coil (indolicidin). (Adapted from Nguyen *et al.*)[10]

In addition to their defensive role, AMPs also seem to play an important role in immunomodulatory activities, acting as cytokines at infection sites and signalling receptors.

They have been shown to modulate the host response of endotoxins such as LPS (lipopolysaccharides) and lipoteichoic acid from invading bacteria. Chemotactic recruiting of monocytes, lymphocytes, and neutrophils, promotion of histamine release from mast cells, inhibition of tissue proteases, and stimulation of wound healing are further processes in which AMPs are involved (Figure 2).[11]

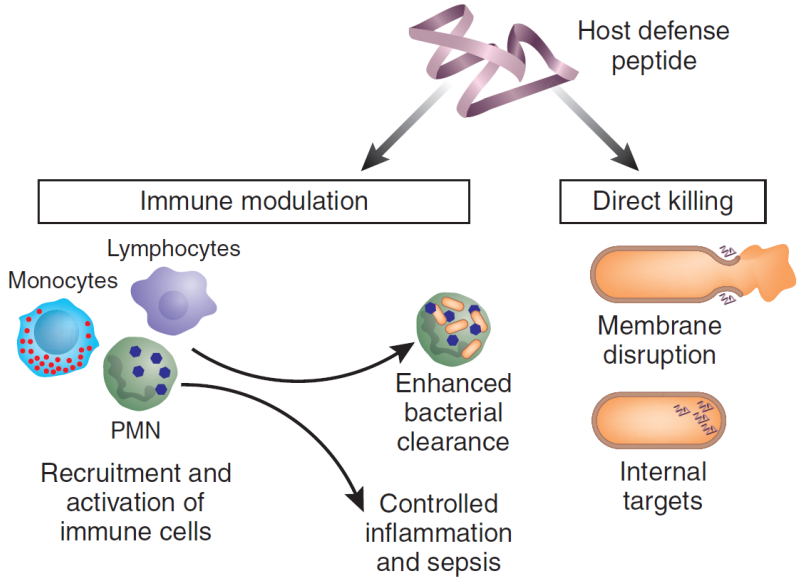

Figure 2 The two main biological roles of AMPs acting as host-defense peptides in mammals. (Reprinted from Hancock and Sahl)[12]

AMPs serve as a promising group of drug-leads in fighting a wide range of microorganisms and may not face the rapid emergence of resistance when compared with classical antibiotics, as bacteria are less likely to adapt to the physical disruption of cell membranes.[13] However, the use of peptides as drugs has traditionally been limited. This is due to their usually poor pharmacological properties, which include low metabolic stability towards proteases, low bioavailability, rapid clearance, and general toxicity issues.[14] Hence, intense efforts have been undertaken to improve the pharmacological properties of peptides. Medicinal chemists have developed an array of strategies to confront this problem, such as incorporating non-proteinogenic amino acids, cyclisation, peptide bond isosteres[15], peptoids[16], and retro-inverso peptides[17] to reduce protease cleavage, leading to a longer *in vivo* half-life. Additionally, conformationally constrained peptides can minimize binding to off-target receptors and increase binding affinity towards a desired receptor.[18]

1.2 Antibiotic Resistance in Bacteria

A global report on surveillance of antimicrobial resistance carried out by the Wold Health Organisation in 2014 states that resistance to bacteria has reached alarming levels in many parts of the world, and that few of the available treatment options remain effective for common infections. A post-antibiotic era, in which common infections and minor injuries can kill, might be a real possibility for the 21st century.[19] Resistance arises as a consequence of mutations in microorganisms through a selection pressure from antibiotic use that provides a competitive advantage for mutated strains. Sub-lethal antibiotic dosage enhances the stepwise selection of resistance. Resistance genes are borne on chromosomal and, increasingly, on transmissible genetic elements (e.g. plasmids). This spread is facilitated by inter-species gene transmission, poor sanitation and hygiene in communities and hospitals, and the increasing frequency of global disease transmission.[20] Recently, a plasmid-mediated polymyxin resistance mechanism (MCR-1), was reported for the first time in China. *E. coli* strain SHP45, isolated from food animals, showed a colistin (polymyxin E) resistance that was transferable to other Gram-negative species, with a high subsequent risk of spreading around the world.[21] Colistin is a last-resort antibiotic, only intended for difficult-to-treat infections, making this resistance emergence especially dangerous. Resistance mechanisms include the proteolytic degradation of AMPs, the expression of antibiotic efficacy reducing enzymes (e.g. β-lactamases that cleave and inactivate β-lactam-based antibiotics), the upregulation of efflux pumps, which actively transport antibiotics out of the cell, and changes in antibiotic targets through mutation and modification. Bacteria can also be intrinsically resistant to certain antibiotics. This is often the case for Gram-negative bacteria, which exhibit an additional outer membrane (cf. Introduction 1.4), hindering agents in crossing the outer membrane.[22] Six species of pathogen that currently cause the majority of infections in hospitals and effectively "escape" the effects of antibiotics are the so called "ESKAPE" pathogens, selected by the Infectious Diseases Society of America (IDSA). These include representatives from ***E****nterococcus faecium*, ***S****taphylo-coccus aureus*, ***K****lebsiella pneumoniae*, ***A****cinetobacter baumanii*, ***P****seudomonas aeruginosa*, and ***E****nterobacter* species.[23] There is clearly a need for new antibiotics with new mechanisms of action to combat antimicrobial resistance. Further requirements are a paradigm shift in the prescription of antibiotics, patient compliance, and prevention of spreading pathogenic microorganisms by screening, isolation, and containment of infected patients, as well as a reduction of the careless use of antibiotics in intensive animal farming.[24]

1.3 β-Hairpin Protein Epitope Mimetics

A primary reason for interest in peptides and proteins is that they bind with high specificity to their *in vivo* targets, resulting in exceptionally high potencies and relatively few off-target side effects. This high degree of selectivity of interaction is the product of millions of years of evolutionary selection for complementary shapes and sizes from among a huge array of structural and functional diversity. Thus, peptides have been fine-tuned to specifically interact with biological targets, evolving into potent endogenous hormones, growth factors, neurotransmitters, and signalling molecules, as well as immunologic and defense agents.[14] Protein epitope mimetics (PEMs) are specifically designed to mimic surface regions of proteins. Their three-dimensional character allows them to modulate protein-protein or protein-nucleic acid interactions where small organic molecules would fail. By exploiting a larger surface area on a protein target, they achieve a strong and specific binding, making them ideal inhibitors of biological function. A strategy in designing such modulators is to transplant a selected motif crucial for binding onto a stabilizing template. The template helps to orient the side-chain residues in the same direction as the native peptide, by rigidifying its three-dimensional structure. The most important secondary structure elements found in protein epitopes in nature are the β-hairpin and the α-helix. The β-hairpin (two antiparallel β-strands connected by a loop sequence) is an especially interesting scaffold, since it is used by many proteins for biomolecular recognition (e.g. antibodies or T-cell receptors), and it is readily amenable to mimetic design.[25] A β-turn occurs where the peptide strand reverses direction and consists of four amino acid residues designated i to i+3, in which the distance between $C\alpha_i$ and $C\alpha_{i+3}$ is ≤ 7 Å. Several different types of β-turns exist[26], depending on the dihedral angles Ψ and Φ of the i+1 and i+2 residues. Most normally abundant are type I and type II, and their mirror images I' and II' (Figure 3).[27]

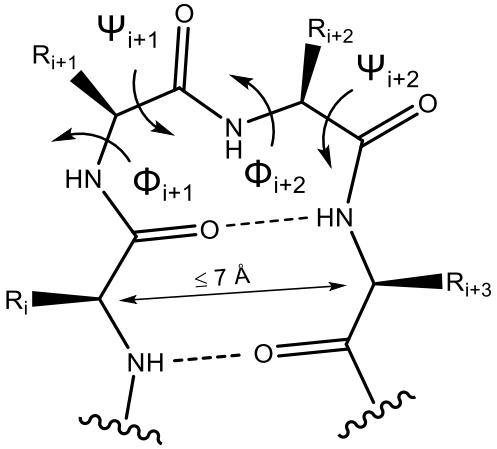

β-turns	Φ_{i+1}	Ψ_{i+1}	Φ_{i+2}	Ψ_{i+2}
I	-60	-30	-90	0
I'	60	30	90	0
II	-60	120	80	0
II'	60	-120	-80	0
III	-60	-30	-60	-30
III'	60	30	60	30

Figure 3 In a β-turn, the distance between $C\alpha_i$ and $C\alpha_{i+3}$ must be no longer than 7 Å. Dihedral torsion angles Ψ and Φ describe orientation along the backbone and define the β-turn type. (Adapted from Whitby *et al.*)[27]

In the case of the defensin, arenicin, tachyplesin, and protegrin families, the stability of the three-dimensional structure is enhanced by disulfide bridges, which hold the β-strands together (cf. Introduction 1.1).[12] A stem template, such as the dipeptide ^{D}Pro-^{L}Pro, holds the two strands in the correct H-bonding pattern, favouring a stable β-turn at the tip (Figure 4). Linear precursors of the loop can be synthesized by standard solid phase peptide synthesis, cyclized in solution, deprotected, and finally purified by HPLC – making the process amenable for combinatorial synthesis. These newly synthesized libraries of peptidomimetics may then be tested for biological activity.[28]

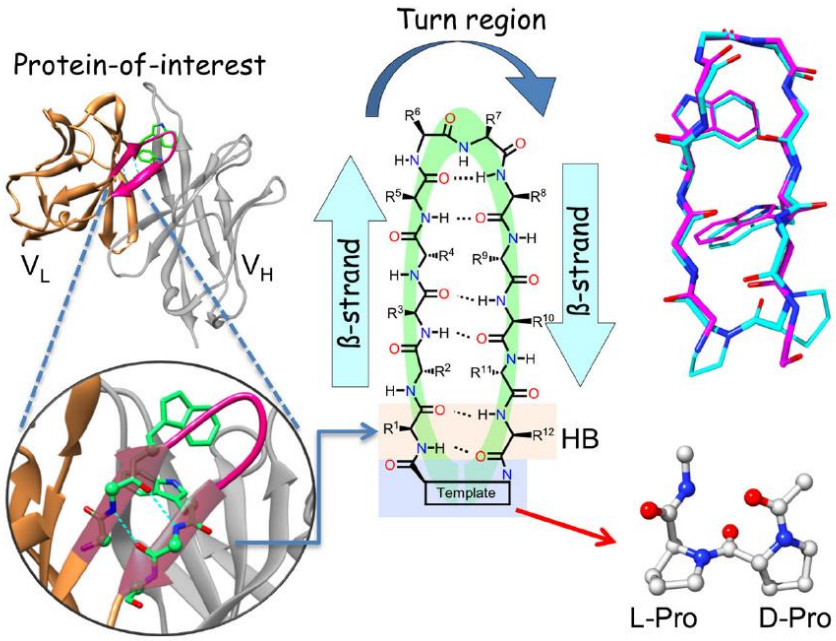

Figure 4 A β-hairpin loop identified in a crystal structure of an antibody complementarity-determining region (CDR) (left) can be transplanted onto a ^{D}Pro-^{L}Pro template (bottom right), resulting in a cyclic β-hairpin peptidomimetic (center). The template rigidifies and so nucleates the folded β-sheet. An NMR overlay of the CDR loop mimetic (blue) and the same loop in the crystal structure is shown on the top right. (Reprinted from Robinson *et al.*)[28]

With this approach, our group discovered new classes of β-hairpin peptidomimetics with different confirmed targets. L27-11 targets the LPS transport machinery in *P. aeruginosa* and will be described in detail in the following chapters. JB-95 exhibits high activity against *E. coli,* and its mechanism of action was revealed by Matthias Urfer.[29] PEM POL6326 (Balixafortide), which was developed by *Polyphor AG*, is derived from polyphemusin II, an 18-amino acid peptide isolated from the American horseshoe crab (*Limulus polyphemus*). POL6326 has been shown to inhibit CXCR4, a chemokine receptor of the G protein-coupled receptors (GPCRs) family. CXCR4 plays an important role in the mobilization of stem cells from the bone marrow into the circulating blood. POL6326 is currently in clinical trial phase Ib for stem cells transplantation and for a combination treatment in oncology.[30] A further PEM developed by *Polyphor AG* is POL6014, also currently in phase Ib, derived from the sunflower trypsin

inhibitor (SFTI)[31]. POL6014 is a selective inhibitor of the human serine protease neutrophil elastase (hNE) in immune cells, implicated in tissue degradation and inflammation in lung disease. The drug is intended for the treatment of cystic fibrosis and other severe lung diseases.[32]

1.4 Outer Membrane Proteins in Gram-negative Bacteria

Most bacteria can be categorized in two major groups (Gram-positive and Gram-negative), differentiated by their cell wall composition. Gram-positive bacteria exhibit a membrane with a thick peptidoglycan layer, whereas the Gram-negative bacteria are composed of an outer and inner membrane. LPS is incorporated in the outer leaflet of the outer membrane, covering the surface of the Gram-negative bacteria. The two membranes are separated by the periplasmic space (Figure 5).[33] The Gram-staining is a technique used to identify them under a microscope in a quick preliminary diagnostic procedure.[34]

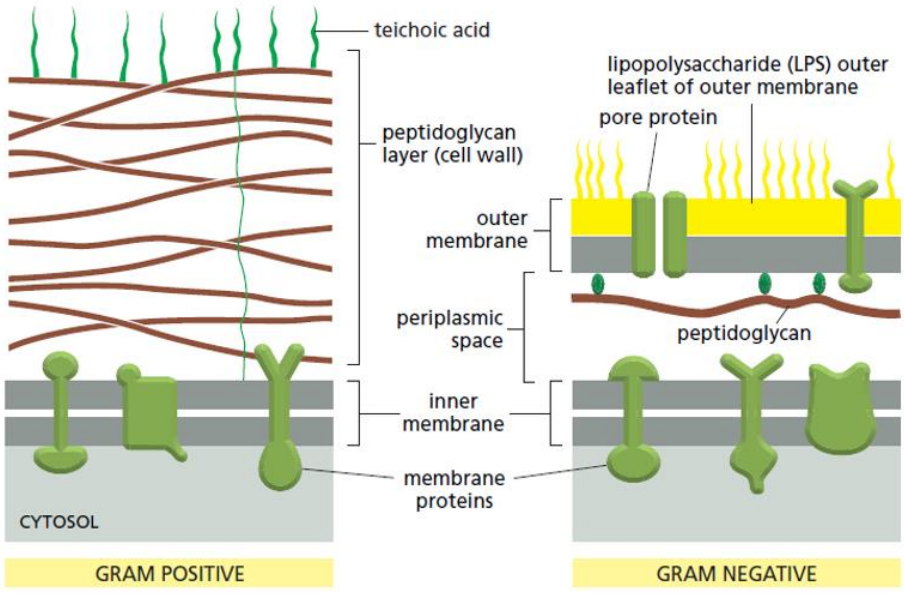

Figure 5 Comparison between a Gram-positive and a Gram-negative cell wall. In Gram-positive bacteria, there is a thick peptidoglycan layer, with proteins and teichoic acid incorporated. In Gram-negative bacteria, there is an additional asymmetric bilayer, separated by the periplasmic space. The outer leaflet is covered by LPS molecules. (Reprinted from Molecular Biology of the Cell (5th ed.))[33]

Membrane proteins are incorporated in both membranes, serving as signalling receptors, transporters, ion channels, and cellular anchors, regulating numerous processes in the cell. Integral membrane proteins of the inner membrane all have an α-helical fold, consisting of one or more α-helices, whereas in the outer membrane, proteins have a β-barrel fold consisting of several antiparallel β-strands. These so-called outer membrane proteins (OMPs) are folded and inserted by a multicomponent complex called the β-barrel assembly machinery (BAM

complex), consisting of the five subunits BamA-E. The crystal structure of the full BAM complex has recently been solved, providing a better understanding of the transport, folding, and insertion process of OMPs into the outer membrane in Gram-negative bacteria (Figure 6). OMPs are synthesized in the cytoplasm with a signal sequence that directs them to the Sec translocon, which in turn transports them over the inner membrane to the periplasmic space. Chaperones SurA and Skp then escort OMPs to the BAM complex, which folds and incorporates them into the outer membrane. 16-Stranded β-barrel BamA is the central component, with a periplasmic domain consisting of five polypeptide transport-associated (POTRA) domains. BamB-BamE are lipoproteins, and are assumed to have a stabilizing function.[35]

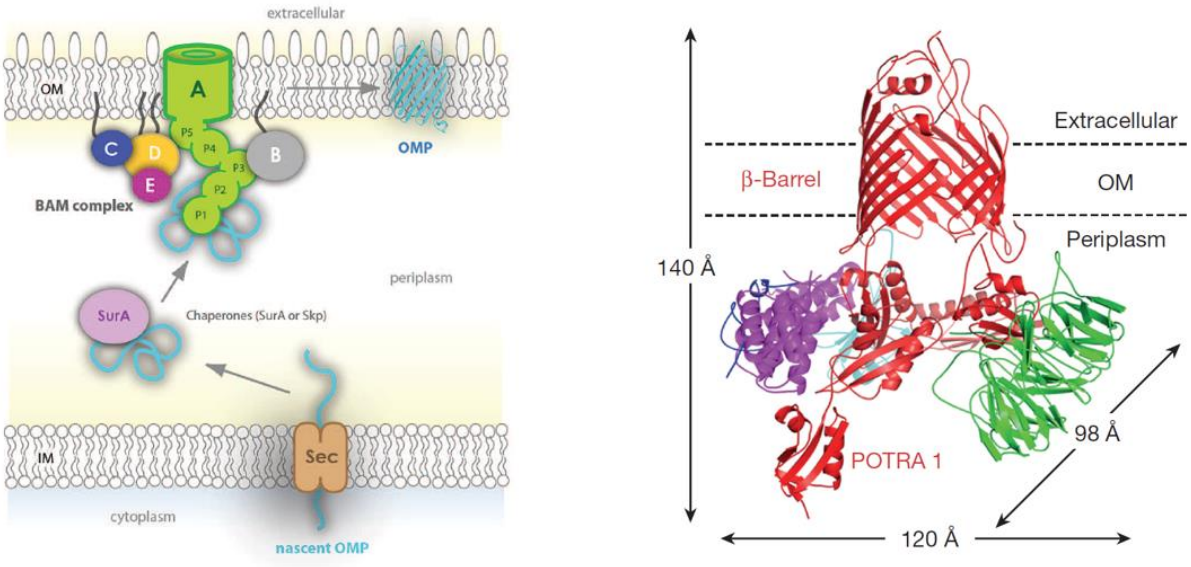

Figure 6 The folding and insertion process of β-barrel OMPs in Gram-negative bacteria (left). (Reprinted from Bakelar *et al.*)[35]. Structural representation of the full BAM complex in *E. coli*, consisting of BamA (red), BamB (green), BamC (blue), BamD (magenta), and BamE (cyan) (right) (Protein Data Bank (PDB) 5D0O). (Reprinted from Gu *et al.*)[36]

1.5 The LPS Transport Machinery

LPS in Gram-negative bacteria consist of three parts: lipid A, core-oligosaccharide, and the O-antigen (or O-oligosaccharide). The hydrophobic lipid A domain anchors the LPS molecules into the outer bacterial membrane. Lipid A is evolutionary conserved, and mainly responsible for the toxicity and immunogenic response of Gram-negative bacteria in a host. The core-oligosaccharide is attached to Lipid A, and contains several sugars as well as non-carbohydrate modifications, such as phosphates, amino acids, and phosphoethanolamines. The O-antigen is the most variable region, and contains a repetitive and often branched carbohydrate sequence crucial in protection and surface recognition.[37] LPS is assembled at

the inner leaflet of the inner membrane and then extracted and transported to the surface by the LPS transport machinery. Seven Lpt (lipopolysaccharide transport) proteins (LptA-G) have been identified in *E. coli*, forming a transport cascade across the entire cell wall (Figure 7). LPS is extracted from the inner membrane by an ATP hydrolysis driven ABC transporter composed of LptB, LptF, LptG, and probably LptC. LptA serves as a soluble, periplasmic chaperone that transports LPS to LptD/E for insertion into the outer membrane. LptD is a large β-barrel protein, complexed with the lipoprotein LptE, which acts as a "plug" inside the β-barrel. Although the fundamental process of LPS transport is still under investigation, all Lpt proteins are essential for the correct biogenesis of the bacterial cell wall and the survival of the bacteria.[38]

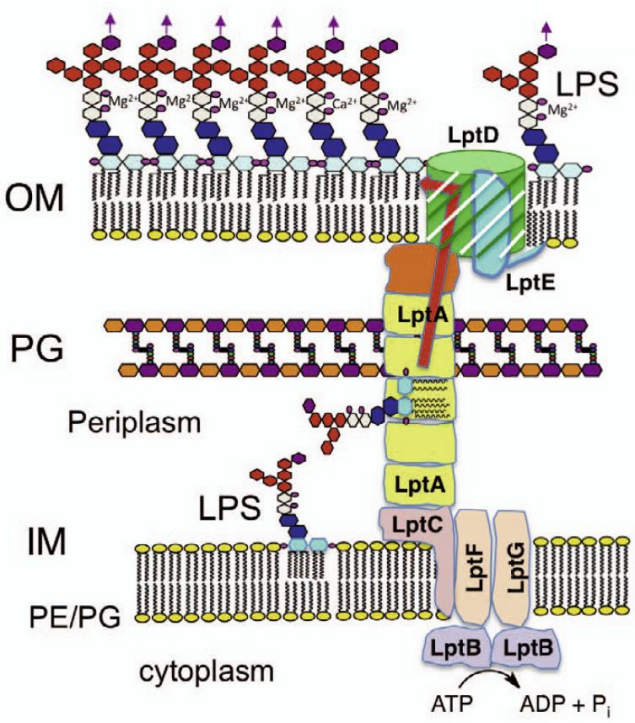

Figure 7 In Gram-negative bacteria, seven LPS transport proteins (LptA-G) transport LPS from the inner membrane over the periplasm to the bacterial surface. The insertion process into the outer leaflet of the outer membrane is guided by the large β-barrel protein LptD in complex with LptE. (Reprinted from Vetterli *et al.*)[39]

Important advances in understanding the structural basis of the LptD/E complex and LPS insertion have been made in recent years, with the reporting of the full length LptD/E crystal structures in *Shigella flexneri* (PDB 4Q35, Figure 8)[40] and *Klebsiella pneumoniae* (PDB 5IV9)[41], and lacking the N-terminal jelly roll domain in LptD: *Salmonella typhimurium* (PDB 4N4R)[42] and *P. aeruginosa* core complex (PDB 5IVA)[41]. The Lipid A moiety of LPS is funnelled through the hydrophobic β-jellyroll domain of LptA and LptC as well as the N-terminal domain of LptD (LptD_NT), and finally enters the LptD β-barrel with the carbohydrate headgroups making contact with the hydrophilic lumen of the LptD/E complex. The membrane-engulfed part of LptD is composed of twenty-six antiparallel β-strands (termed β1–β26),

making it the largest single-protein β-barrel observed to date. It is believed that strands β1 and β26 are able to dissociate from each other to create an exit gate for LPS molecules necessary for the insertion in the outer leaflet (Figure 9).[40]

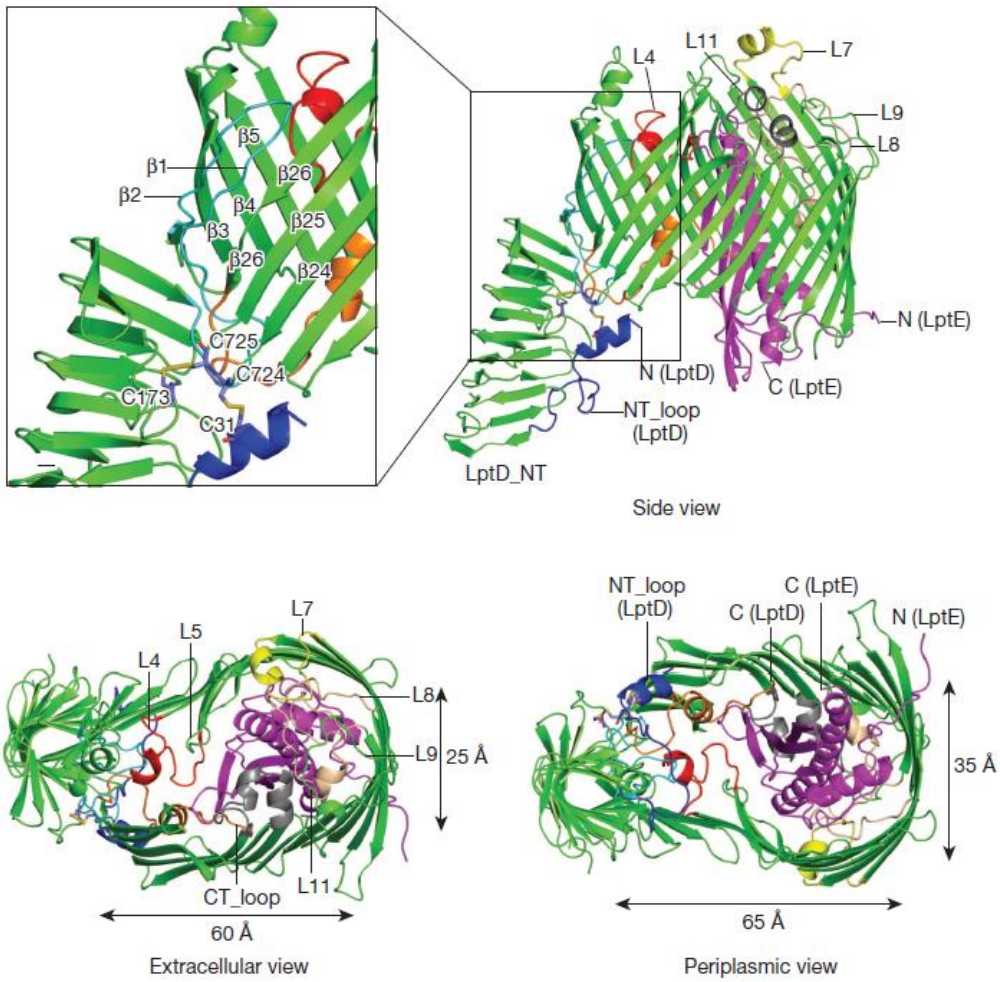

Figure 8 Structural representation of the LptD/E complex in *Shigella flexneri*, viewed in different orientation. Hairpin strands β1 and β2 are highlighted in cyan, LptE in purple. (Reprinted from Qiao *et al.*)[40]

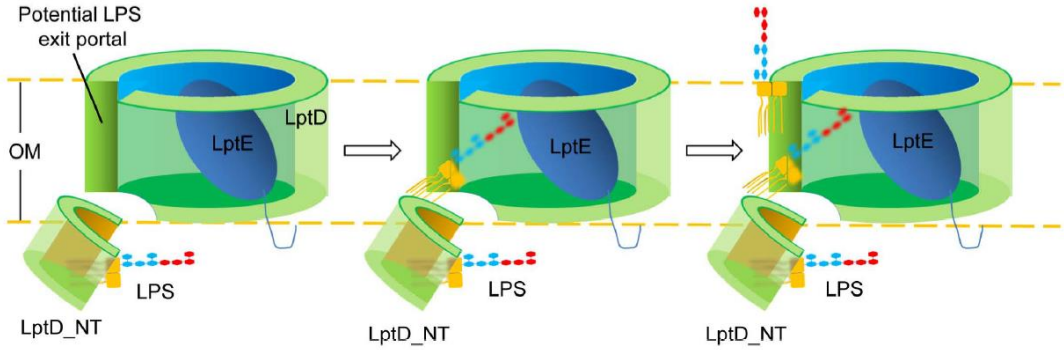

Figure 9 Proposed model for LPS insertion into the outer membrane: The hydrophobic moiety of LPS is believed to enter directly into the lipid bilayer, whereas the hydrophilic head groups make contact with the luminal LptE. LPS is then inserted through a lateral opening of the strands β1 and β26 in the β-barrel. (Reprinted from Qiao *et al.*)[40]

1.6 From Protegrin-1 to L27-11

Cationic AMP protegrin-1 was first isolated from porcine leukocytes, and consists of 18 amino acids highly enriched in arginine and cysteine, with a β-hairpin structure stabilized by two disulfide bridges. Its broad antimicrobial activity is exhibited in low micromolar concentrations.[43] Protegrin-1 served as a lead structure in the development of new peptidomimetics in our group, with higher activity and less hemolytic toxicity – a critical side effect that reduces its potential as a systemic antibiotic. Iterative cycles of library synthesis and screening led to the discovery of a new series of β-hairpin peptidomimetics. These peptidomimetics contain a sequence similarity to its ancestor; however, the loop is stabilized by the introduction of a ^{D}Pro-^{L}Pro template at the stem, which substitutes for the disulfide bridges to hold the two β-strands in place (Scheme 1).[44]

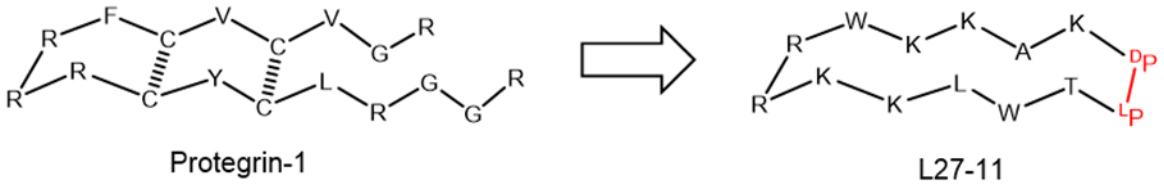

Scheme 1 Protegrin-1 served as a lead structure in the development of new peptidomimetics such as L27-11. A ^{D}Pro-^{L}Pro template (red) was introduced to stabilize the β-hairpin fold of the sequence and to substitute for the two disulfide bridges in protegrin-1.

L27-11 is a fully synthetic cyclic β-hairpin that was recently discovered in our group. With a minimal inhibitory concentration[45] (MIC) of 0.008 µg/ml against *Pseudomonas aeruginosa,* it is a highly potent antimicrobial peptide. Surprisingly, L27-11 only exhibits antimicrobial activity against *Pseudomonas spp*., indicating a specific mechanism of action. Indeed, it was found that L27-11 possesses no membranolytic activity, and a delayed bactericidal effect compared to protegrin-1. The enantiomeric form of L27-11 proved to be completely inactive against *P. aeruginosa,* suggesting a chiral target. A genetic screen for resistance determinants and a photoaffinity labelling experiment revealed outer membrane protein LptD as the target of L27-11 and inhibition of LPS transport as the assumed mechanism of action.[46,47] Related compounds have been synthesized for clinical application with improved ADME properties (absorption, distribution, metabolism, elimination). By substituting Lys and Arg residues for 2,4-diaminobutyric acid (Dab), protease cleavage sites were removed and plasma half-life was prolonged, with minimal effect on antimicrobial activity.[28] The structurally related clinical candidate drug POL7080 (Murepavadin), developed by *Polyphor AG*, successfully completed clinical trial phase I studies in 2013 and is currently under phase II evaluation for *P. aeruginosa* pneumonia infections.[48]

To study the contribution of a specific residue to the total activity of L27-11, an alanine scan was recently performed in our group by Schmidt *et al.*[49] In an alanine scan, each residue along the backbone of the β-hairpin loop is systematically substituted by an alanine. Most substitutions led to a 3-10 fold loss in activity. However, the substitutions of either Trp2 or Trp8 resulted in a complete loss of antimicrobial activity. NMR analysis showed no significant change in backbone conformation for mutant Trp2Ala compared to the native L27-11, whereas mutant Trp8Ala adopted a more flexible structure. Further substitutions of Trp2 and Trp8 to other aromatic residues (Phe and Tyr) were studied, and results showed that those substitutions lead to an about six fold drop in activity at position 2, and are even less tolerated at position 8. Summarizing, positions Trp2 and Trp8 are crucial for high antimicrobial activity in L27-11 (Figure 10).[49]

Peptide/mutant	MIC [µg/ml]
L27-11	**0.01**
Thr^{1}Ala	0.02
Trp^{2}Ala	>16
Leu^{3}Ala	0.1
Lys^{4}Ala	0.05
Lys^{5}Ala	0.1
Arg^{6}Ala	0.03
Arg^{7}Ala	0.06
Trp^{8}Ala	>16
Lys^{9}Ala	0.06
Lys^{10}Ala	0.06
Lys^{12}Ala	0.03
Trp^{2}Phe	0.06
Trp^{2}Tyr	0.06
Trp^{2}Leu	1.0
Trp^{8}Phe	0.1
Trp^{8}Tyr	0.3
Trp^{8}Leu	0.1

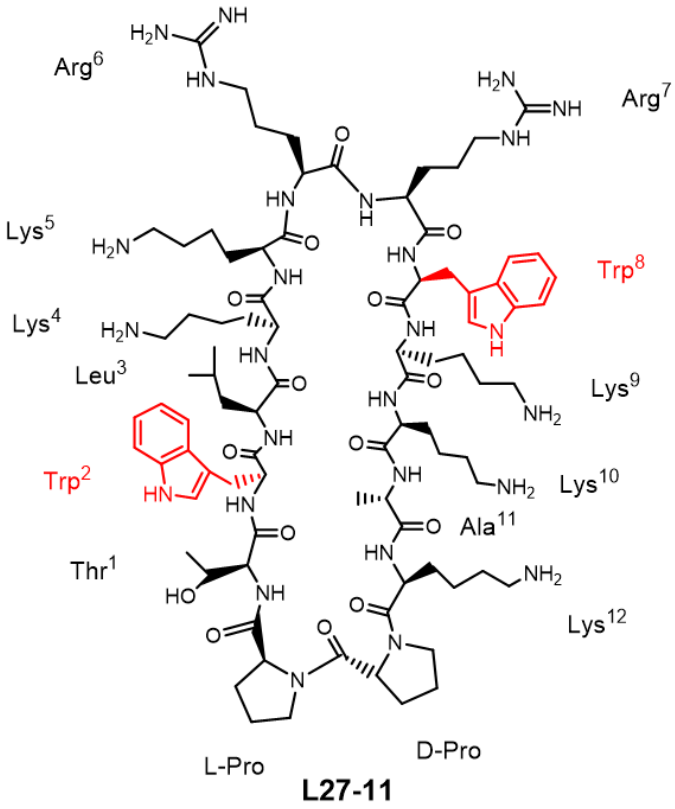

Figure 10 Peptidomimetic L27-11, with crucial positions Trp2 and Trp8 highlighted in red. The antimicrobial activity against *P. aeruginosa* ATCC27853 was determined in MH-I (Müller-Hinton broth) with addition of 0.02% BSA (bovine serum albumin). (Adapted from Schmidt *et al.*)[49]

1.7 LB-01 and NMR Studies

LB-01 (Figure 11) is a more suitable scaffold for studying NMR structures than L27-11. LB-01 differs from L27-11 in five positions (Table 1). Four lysines are substituted by ornithine and Dab to facilitate proton assignments. Otherwise, signal overlap would highly complicate assignments and structure calculations. Another difference is the Arg6 substitution by ^{D}Lys to give additional beta turn II' stability at the tip region. Despite these substitutions, LB-01 exhibits approximately the same high antimicrobial activity (MIC of 0.01 µg/ml) against *P. aeruginosa* as L27-11. The LB-01 scaffold was previously described by Schmidt *et al.*[49], emphasizing the importance of the β-hairpin fold in antimicrobial activity. LB-01 exists as a single rotamer (> 98%) in aqueous solution, with all peptide bonds *trans*. Analysis of coupling constants revealed $^{3}J_{HNH\alpha}$ values ≥ 8.5 Hz and mostly positive chemical shift deviation ($\Delta\delta = \delta_{observed} - \delta_{random}$)[50] for several residues, consistent with backbone conformations in β-sheet structures.[51] Characteristic long range cross-strand NOEs indicate a regular β-hairpin structure with a type II' β-turn in the tip region. It was also shown that the substitution of the ^{D}Pro-^{L}Pro template by ^{L}Pro-^{D}Pro results in a disordered, non β-hairpin-like structure, leading to a complete loss of antimicrobial activity.[49]

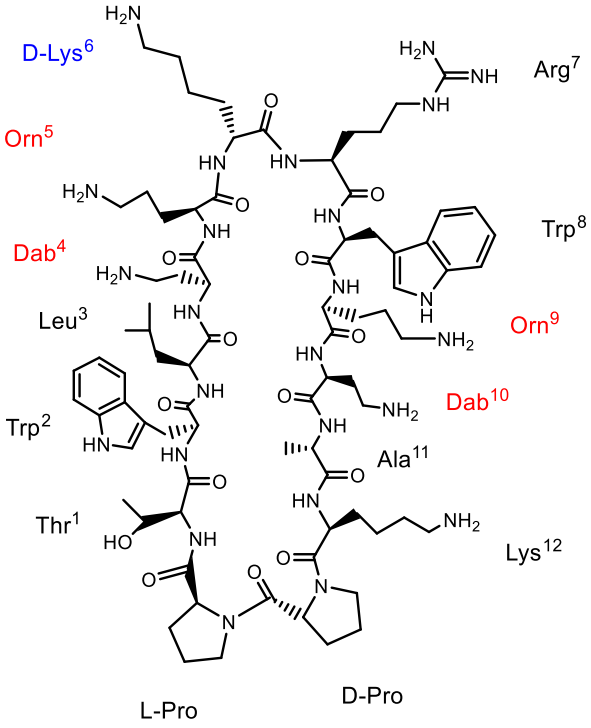

Figure 11 LB-01 scaffold with highlighted amino acids (red/blue) that differ from parent compound L27-11.

Table 1 Comparison of peptidomimetics L27-11 and its analogue LB-01.

	1	2	3	4	5	6	7	8	9	10	11	12	template	
L27-11	T	W	L	K	K	R	R	W	K	K	A	K	^{D}P	P
LB-01	T	W	L	Dab	Orn	^{D}K	R	W	Orn	Dab	A	K	^{D}P	P

1.8 N-Methylation

N-methylation is a modification that often occurs in Nature, and which regulates many biological functions. It is most prominent in epigenetics, where different degrees of DNA methylation regulate gene expression. DNA methylation occurs on the nucleosides adenine (N^6 position) and cytosine (C^5 position) through DNA methyltransferases. N-methylation on the side-chains of lysine and arginine in histone proteins leads to a change in chromatin structure and gene activity regulation. This so-called "histone code"[52] allows for a specific recognition by other proteins, leading to different gene expression patterns. However, N-methylation is not limited to histones and DNA modifications. There are many examples of naturally occurring N-methylated linear and cyclic peptides with interesting biological functions. They are mostly synthesized by non-ribosomal peptide synthetases (NRPSs), allowing the incorporation of different non-proteinogenic amino acids, leading to a high variety of molecules. A selection is described in the following (Figure 12): Enniatins, a group of cyclic depsipeptides[53] (the peptide bond is isosterically replaced by an ester group) was found in *Fusarium* fungi. They are able to target membranes by incorporating themselves into the cell membrane, acting as ionophores, subsequently causing membrane disruption. Enniatins have been shown to exhibit cytotoxic activity against human cancer cell lines.[54] Enniatin B has been found to inhibit the multidrug efflux pump Pdr5p in *Saccharomyces cerevisiae*, making it an interesting candidate for cancer therapy.[55] Hemiasterlins are a small group of cytotoxic N-methylated tripeptides derived from marine sponges. They are able to target microtubules, resulting in mitotic arrest of cells by preventing tubulin polymerization. Potent analogues of this drug have been synthesized and are currently evaluated as anti-cancer therapeutics. HTI-286, a synthetic analogue of hemiasterlin, is a potent inhibitor of proliferation (mean IC_{50} = 2.5 ± 2.1 nM in 18 human tumor cell lines), that also exhibits low interaction with multidrug resistance protein (P-glycoprotein).[56] Echinomycin, an antibiotic found in *Streptomyces echinatus*, targets DNA by intercalating between DNA bases, forming a complex that inhibits transcription by RNA polymerase.[57] Cyclosporin is a potent inhibitor of calcineurin, and a clinically widely used drug. Calcineurin is a Ca^{2+}- and calmodulin dependent protein phosphatase, and plays an important role in T-cell activation.[58] Its inhibition leads to an immunosuppressive effect, making cyclosporin especially important in preventing graft rejection in organ transplantation.[59,60]

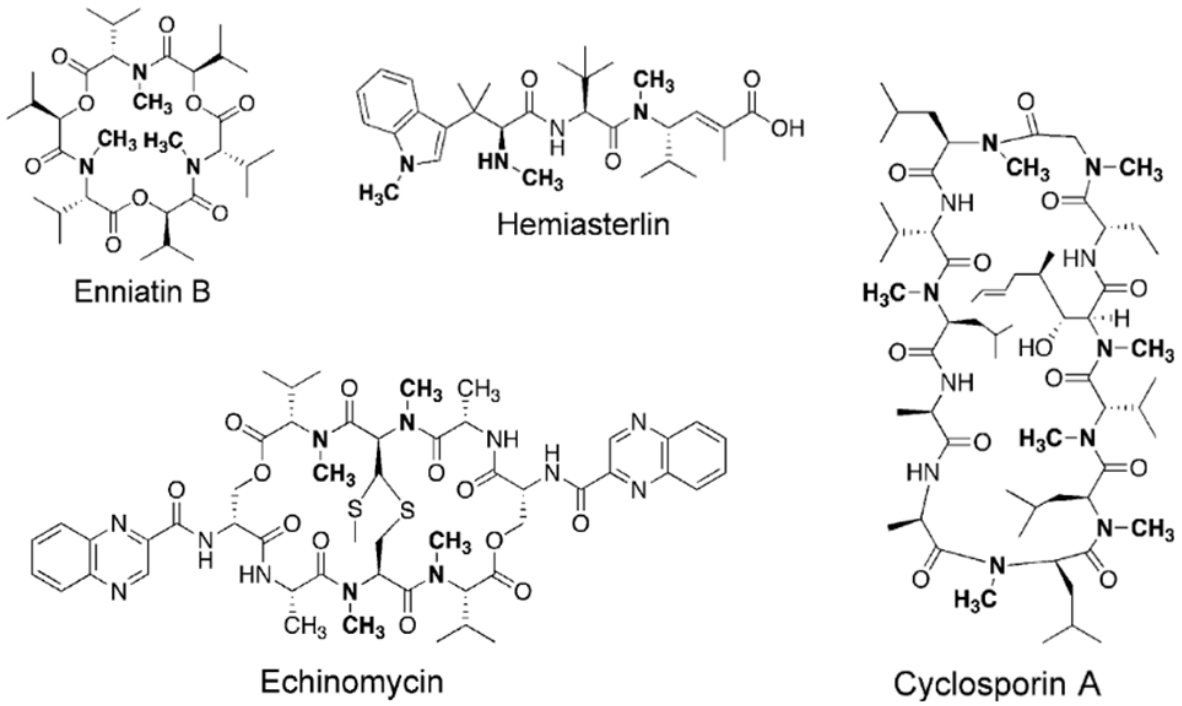

Figure 12 Selection of naturally occurring N-methylated peptides that act on different targets in the human body. (Adapted from Chatterjee *et al.*)[60]

Introducing an N-methyl group at the amide NH position of the peptide backbone has a direct effect on its flexibility. The additional steric hindrance influences the *cis-trans* equilibrium along the backbone, generally favouring a *cis* conformation of the adjacent residue. The rotational barrier of the *cis-trans* equilibrium is higher in energy, resulting in rotameric isomers (rotamers). Further, the removal of the amide hydrogen prevents the formation of hydrogen bonds. N-methylation therefore affects the ability to adopt secondary structure elements like helices and β-sheets in larger peptides. This obviously also strongly depends on the specific amino acid sequence and size and orientation of the residues.[61] N-methylation is a minimalistic approach to overcome obstacles in drug development, and has successfully been applied to improve bioavailability and metabolic stability of somatostatin analogues[62], G-protein ligands[63], and reduction of hemolytic activity in gramicidin S[64] towards human red blood cells. N-methylation was also applied to increase selectivity of ligands towards different integrin and melanocortin receptor subtypes.[65]

1.9 Cell-Penetrating Peptides

The cell membrane protects living cells from the outside environment, and, among many other tasks, regulates the permeation of compounds into the cell. Ions and small organic molecules are able to cross the lipid bilayer of cell membranes through specific transporter proteins, whereas larger and hydrophilic compounds usually cannot enter the cell interior unhindered.[33] In 1988, it was found that the 86 amino acid long TAT protein (trans-activator of transcription), derived from the human immunodeficiency virus (HIV-1), was efficiently taken up by cells from the surrounding media.[66] The transduction of large cargo molecules coupled to a short TAT peptide sequence was later demonstrated, substantially increasing the possibilities of drug delivery.[67] Hundreds of so-called cell-penetrating peptides (CPPs) have since been discovered, usually with a length of 5-35 amino acids, with a high abundance in basic residues such as arginine and lysine and/or an overall amphipathic structure. The guanidine headgroup of arginine was identified as a critical structural component responsible for the biological activity of polyarginines (containing six or more arginines), entering cells far more effectively than polymers of equal length composed of other residues.[68] However, the mechanism of cell entry by CPPs has not fully been understood. It is likely a combination of several mechanisms, ranging from energy-independent direct translocation to the active take-up by the endocytic pathway through phagocytosis and pinocytosis, including receptor mediated endocytosis (Figure 13).[69]

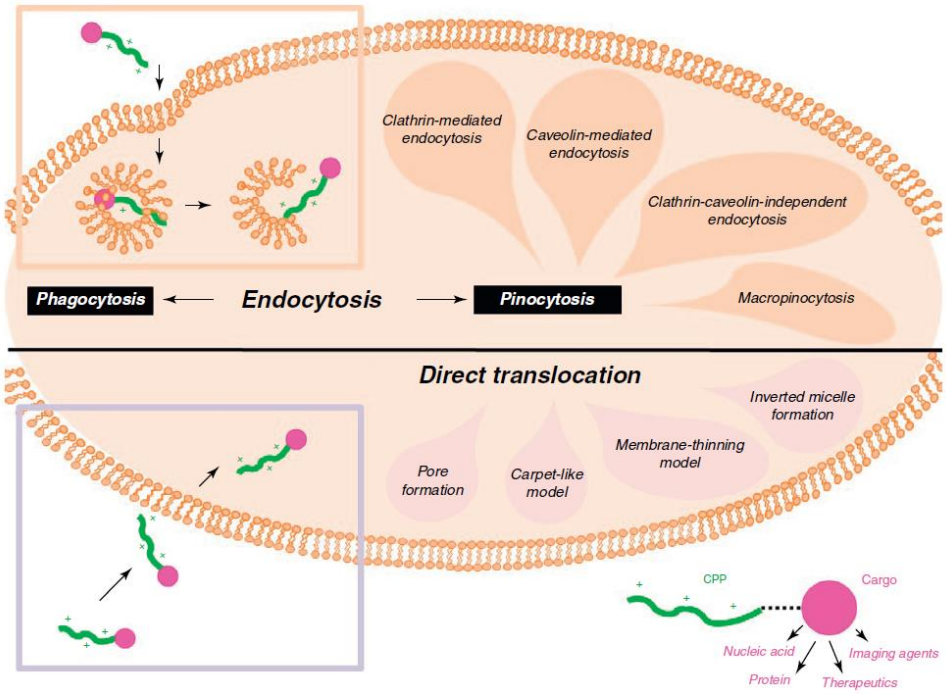

Figure 13 Mechanisms for CPP internalization: CPPs and CPP–cargo conjugates (e.g. nucleic acids, proteins, imaging agents, therapeutics), can penetrate cells using different endocytotic pathways: in particular pinocytosis, which includes macropinocytosis and clathrin-mediated, caveolae and clathrin- or caveolae-independent endocytosis or phagocytosis. Alternatively, CPPs can cross the membrane by energy-independent direct translocation. (Reprinted from Rizzuti *et al.*)[70]

1.10 Thanatin – an Insect Antimicrobial Peptide

Thanatin was first isolated from the hemipteran insect *Podisus maculiventris* (spined soldier bug) by Fehlbaum *et al.*[71] in 1996. The peptide consists of 21 amino acids (GSKKPVPIIYCNRRTGKCQRM) with a disulfide bond between Cys11 and Cys18 showing a sequence homology to the brevinin[72] family of antimicrobial defense peptides. Thanatin showed activity against a wide range of Gram-positive and Gram-negative bacteria and fungi (Table 2). A main factor distinguishing thanatin from other defense peptides of the innate immune system is its non-hemolytic activity towards red blood cells, indicating a mechanism of action that does not involve membrane permeabilization. Indeed, the cell membrane in *E. coli* was found to be intact upon thanatin addition by measuring potassium ion potential as well as respiratory activity (i.e. oxygen consumption) during the first hour. In order to investigate whether the activity derives from an interaction with a stereospecific cellular target, an all-D-enantiomer of thanatin was tested. Although activity on fungi and on certain representatives from Gram-positive bacteria did not change, a dramatic loss of activity on Gram-negative bacteria was observed with the enantiomer. This result points towards different mechanisms of action, dependent on the organism. Truncated isoforms of thanatin were tested for their MIC, revealing that a truncation of three to five N-terminal amino acids led to a fully active peptide in the case of K18M and a 50% reduction in activity for peptide V16M for both Gram-positive *A. viridans* / *M. luteus* and Gram-negative *E. coli* D31 / D22. A truncation of three amino acids from the C-terminus (G18C) led to a 25% active peptide in the Gram-positive test organisms and a complete loss of activity in *E. coli* (Table 3). High antifungal activity required the complete sequence. Four regions within the thanatin scaffold were therefore described essential for high antimicrobial activity: i) the C-terminal loop, ii) the C-terminal three amino acid extension, iii) a stretch of seven N-terminal, mostly hydrophobic residues and iv) three N-terminal residues necessary for high antifungal activity but dispensable for antibacterial activity.[71]

The first NMR solution structure of thanatin was published by Mandard *et al.*[73] in 1998, indicating a well-defined β-hairpin structure held together by the disulfide bond. The N-terminal region ranging from Gly1 to Pro7 consists of an extended, poorly defined region with high flexibility (Figure 14). The hydrogen bonding pattern of the molecule constitutes of regular hydrogen bonds characteristic for β-sheet structures between residues Asn12/Lys17, Tyr10/Gln19 and Ile8/Met21. At the tip region, there are two distorted CO(i) – NH(i+3) hydrogen bonds between Arg13 and Gly16 and between Asn12 and Thr15. The PDB file for thanatin is accessible under the code 8TFV.[73] An additional NMR study was performed by Imamura *et al.*[74] in 2008, in which Cys11 and Cys18 were substituted by serine or *tert*-butyl groups, disrupting the disulfide bond. The β-hairpin structure proved essential for antimicrobial activity

against Gram-negative *E. coli*, whereas activity on Gram-positive *M. luteus* was not affected by the change.[74]

A primary effect of *E. coli* cells treated with thanatin was an arrest of motility within seconds of its addition, followed by agglutination into larger clumps. This effect was attributed to a binding of the cationic thanatin to the negatively charged surface of bacteria, resulting in a reduction of the electrostatic repulsion between cells, leading to agglutination. This agglutination effect induced by thanatin was recently reproduced by Robert *et al.*[75], using artificial phospholipid vesicles. The influence of different cations and pH on antimicrobial activity was studied, indicating that thanatin is sensitive to the presence of higher concentration of cations, but insensitive to changes in pH in the range of pH 5-8.[76] Wu *et al.*[77] introduced S-thanatin, an analogue of thanatin, in which Thr15 was substituted by a serine, which exhibited improved antimicrobial properties and the ability to bind and neutralise LPS. Additional studies were conducted by Wu *et al.*[78] on the efficacy of S-thanatin in preventing septic shock in infected mice. Imamura *et al.*[79] cloned a synthetic thanatin gene into rice in 2010, generating a transgenic rice plant resistant to the blast fungus *Magnaporthe oryzae*. The potential of creating crops resistant to phytopathogenic fungi and bacteria was further reinforced by work in the model organism *Arabidopsis thaliana*.[80] However, despite all the advances since its discovery, a comprehensive mechanism of action of thanatin and a cellular target structure remains to be identified.

Table 2 Antimicrobial activity of thanatin and its enantiomer D-thanatin on certain Gram-positive, Gram-negative bacteria and fungi (values in µM MIC units). MIC values are expressed as intervals from the highest concentration tested at which bacteria were growing and the lowest concentration that caused 100% growth inhibition. ‡ : No activity was detected at the highest concentration tested (40 µM). (Reprinted from Fehlbaum *et al.*)[71]

Microorganism	Thanatin	D-thanatin
Gram-positive bacteria		
A. viridans	0.6–1.2	0.6–1.2
M. luteus	1.2–2.5	2.5–5
B. megaterium	2.5–5	0.6–1.2
B. subtilis	2.5–5	20–40
S. aureus	‡	‡
P. acidolactici	20–40	‡
Gram-negative bacteria		
E. coli D22	0.3–0.6	20–40
E. coli D31	0.3–0.6	20–40
E. coli 1106	0.6–1.2	‡
S. typhimurium	0.6–1.2	‡
K. pneumoniae	0.6–1.2	‡
E. cloacae	1.2–2.5	‡
E. carotovora	10–20	‡
P. aeruginosa	20–40	‡
Fungi		
N. crassa	0.6–1.2	0.6–1.2
B. cinerea	1.2–2.5	2.5–5
N. haematococca	1.2–2.5	1.2–2.5
T. viride	1.2–2.5	1.2–2.5
A. brassicola	2.5–5	2.5–5
F. culmorum	2.5–5	0.6–1.2
A. pisi	5–10	1.2–2.5
F. oxysporum	10–20	5–10

Table 3 Antimicrobial activities of truncated isoforms of thanatin, expressed as percentages of native thanatin. (Reprinted from Fehlbaum *et al.*)[71]

		Relative activities against test organisms, %		
Peptide	Amino acid sequence	*A. viridans* and *M. luteus*	*E. coli* D31 and *E. coli* D22	*N. crassa*
Thanatin	GSKKPVPIIYCNRRTGKCQRM	100	100	100
I11C	IIYCNRRTGKC	0.5	0	0
Y12M	YCNRRTGKCQRM	3	0	0
G18C	GSKKPVPIIYCNRRTGKC	25	0	5
I14M	IIYCNRRTGKCQRM	50	15	3
V16M	VPIIYCNRRTGKCQRM	50	50	5
K18M	KPVPIIYCNRRTGKCQRM	100	100	25

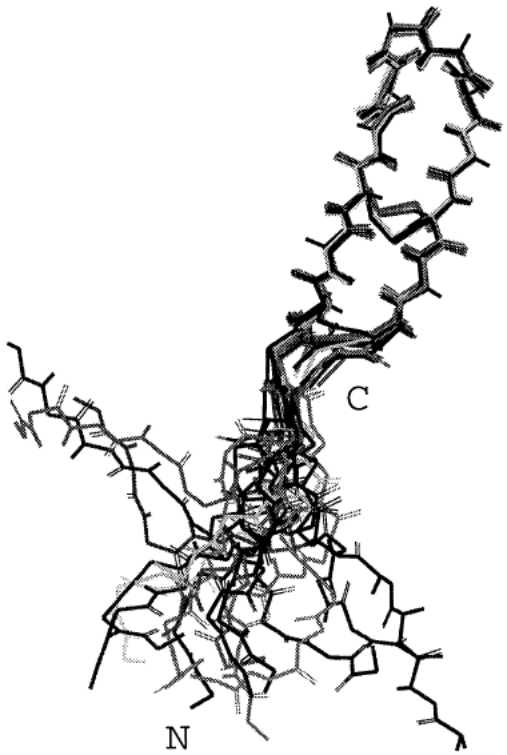

Figure 14 Superposition of 18 selected structures of thanatin fitted on the backbone atoms of residues 9-20. (Reprinted from Mandard *et al.*)[73]

2 Project Outline

2.1 LB-01

Intense efforts have been made in our group in the development of β-hairpin peptidomimetics with high activity against *P. aeruginosa*. As described above, outer membrane protein LptD has been identified as a target of lead structure L27-11. Recent NMR studies revealed a 3D solution structure of the β-hairpin conformation of L27-11 and LB-01, adding important structural information of how the peptide could interact and bind to LptD. The formation of a stable β-hairpin conformation seems to be important for high antimicrobial activity. An alanine scan of L27-11 identified the two opposing tryptophans as the most crucial residues for antimicrobial activity.[49] At the start of this project, no publication existed of a crystal structure of LptD alone or together with an inhibitor, which would give a better insight into the binding site of LptD. N-methylation of amide NH groups was chosen as an approach to add further information in building a detailed structure-activity relationship (SAR) profile of L27-11/LB-01. The aim of this project was to develop a reliable strategy for the synthesis of N-methylated analogues of LB-01. These new analogues would then need to be tested for their antimicrobial activity on *P. aeruginosa*. Solution structure NMR analysis would need to be applied to correlate 3D structure to antimicrobial activity. Further, the LB-01 scaffold makes a good candidate for a cell-penetrating peptide, and a study of its localisation and uptake into cells should give more insight into possible applications in drug delivery of this class of molecules.

2.2 Thanatin

Thanatin was chosen as a naturally occurring, insect derived peptide that targets a wide range of Gram-positive and Gram-negative bacteria and fungi. Since the antimicrobial activity is likely correlated with a stereoselective interaction with an unknown target in Gram-negative bacteria, the decision was made to study its mechanism of action in *E. coli*. The effect on the membrane integrity was investigated through a variety of assays; such as Sytox® Green uptake, β-lactamase, and β-galactosidase release in *E. coli*. Effects on the macromolecular pathways of DNA-, RNA-, Protein-, and cell wall biosynthesis were studied by radiolabelling methods. Further, a suitable photo-reactive analogue was designed to identify potential interaction partners through photoaffinity labelling. Electron microscopy studies were performed in order to reveal macroscopic changes in the cellular organelles and the overall shape of the bacteria. An analogue suitable for fluorescence confocal microscopy was designed in order to give additional information on the potential binding on the surface and cellular uptake of the molecule. Mass spectrometry and proteomic studies were applied to confirm the interaction partners found in the photoaffinity labelling experiments. With the identified proteins LptA and LptD, as well as the accumulated information from the other assays, a perturbation of the LPS transport pathway seemed very likely. Recombinant LptA was produced, and the binding interaction was studied by fluorescence polarization. A co-crystal structure of thanatin with the protein target LptA should give structural proof of the interaction and identification of key residues in LptA required for activity. This would open the field for SAR optimization and development of a high affinity drug with activity against a wide range of Gram-negative bacteria.

3 Results and Discussion

3.1 LB-01

3.1.1 LB-01 N-Methyl Scan

To investigate the influence of N-methylation of the amide backbone on structure and activity of β-hairpin peptidomimetics, the modifications were applied on the well-structured LB-01 as a reference compound. Twelve analogues of the LB-01 scaffold were synthesized according to the method of Srinivas *et al.*[46], with each amide position along the backbone N-methylated (Figure 15). N-methyl groups were either introduced by incorporating commercially available amino acid building blocks or by on-resin methylation following the *Kessler* protocol[81]. In the special case of the highly hindered amide position Thr1NMe, the dipeptide Fmoc-Pro-N-Me-Thr(OtBu)-OH was synthesized separately and then incorporated into the sequence by standard Fmoc chemistry[82].

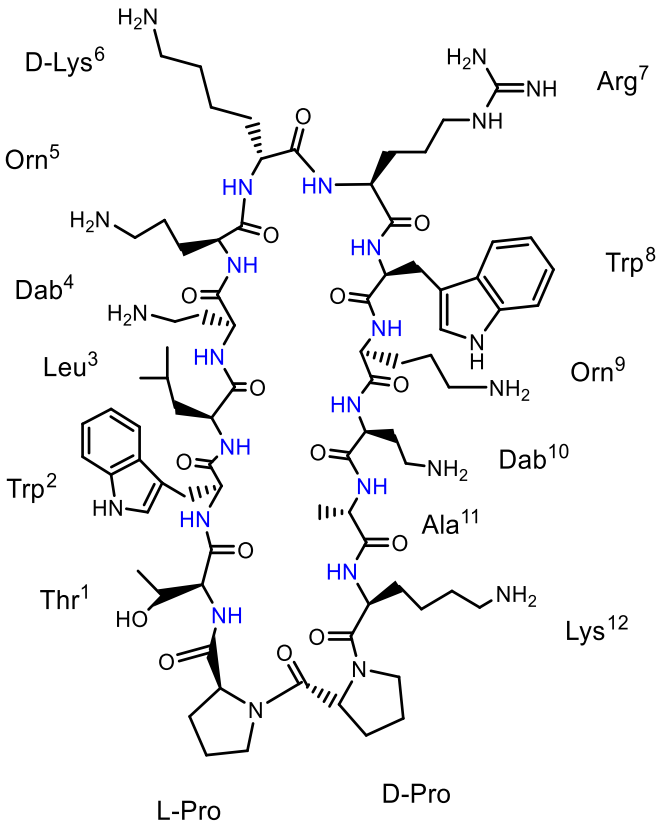

Figure 15 LB-01 scaffold with highlighted amide NH positions (blue) that have been individually methylated to give rise to 12 N-methyl analogues.

3.1.2 On-Resin Methylation

Regioselective methods for N-methylation of amino acids and peptides on solid support have been developed by Fukuyama *et al*.[83] and Miller and Scanlan[84]. The improved on-resin N-methylation method developed by Kessler *et al.*[81] is completely side-chain tolerant and regioselective for any amino acid: The free amine is temporarily protected by a nosyl group (2-nitrobenzenesulfonyl) and methylated under *Mitsunobu* conditions with methanol as the methyl donor. The nosyl group was then removed by treatment with mercaptoethanol and DBU (1,8-diazabicyclo[5.4.0]undec-7-ene) as a base, revealing the free N-methyl amine (Scheme 2). Generally high yields of > 90% were achieved in a reaction time of approximately 3 h for three steps in total.

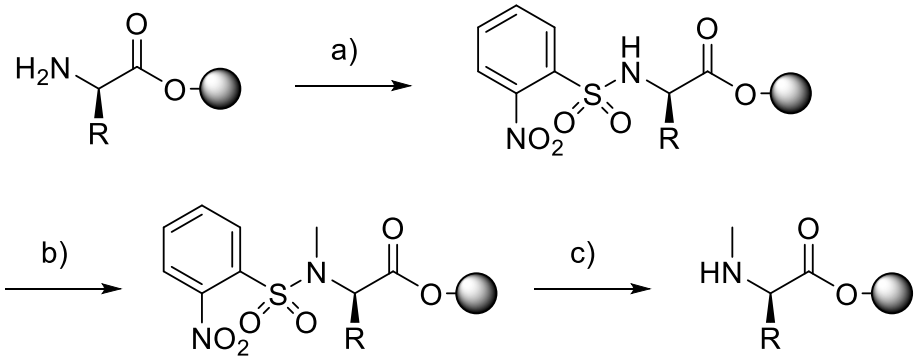

Scheme 2 a) o-NBSCl, sym-collidine, DMF, 40 min b) PPh_3, DIAD, MeOH, THF, 50 min. c) Mercaptoethanol, DBU, DMF 20 min.

This versatile strategy could be successfully used in the synthesis of all LB-01 N-methyl analogues except in the case of Thr1NMe, where steric hindrance in the sequence led to an unsuccessful coupling of the subsequent amino acid, as described in the next chapter.

3.1.3 Low Reactivity of N-Methyl Amines

One problem encountered when introducing N-methyl groups in a sequence was a decreased coupling efficiency on the following amino acid. Exemplified here by the highly hindered position at Thr1, three factors contribute to the low reactivity of the N-methyl amine: The N-methyl group itself, which substantially reduces the nucleophilicity of the amine, the beta branched side-chain of threonine, with a bulky *tert*-butyl protecting group, and the proline, with its five membered ring in close proximity to the carbonyl C (Scheme 3).

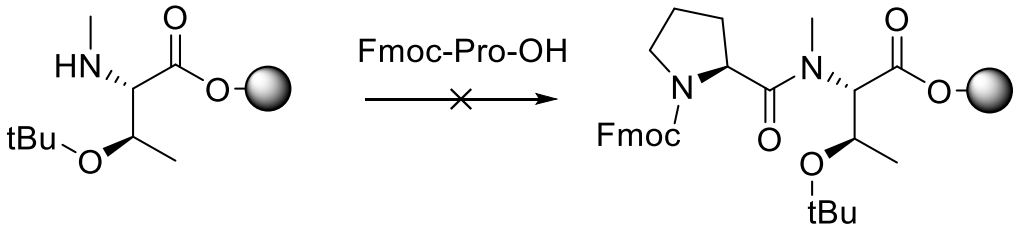

Scheme 3 Low reactivity of N-methyl amines, when a proline is coupled onto an N-methyl threonine on solid support.

Several unsuccessful attempts were made in this difficult coupling reaction. Coupling under standard conditions with HATU/HOAt[85] only led to a conversion of less than 5% determined by HPLC. Increasing equivalents of reagents, an extended reaction time, plus heating of the mixture to 50°C did not improve the extent of the conversion. The third generation coupling reagent COMU[86] showed a slightly better coupling efficiency under standard conditions, though still far from ideal. Microwave heating of the reaction mixture only led to a premature resin cleavage and was therefore not applicable for 2-chlorotrityl chloride supported resin (Table 4).

Table 4 Unsuccessful coupling of Fmoc-Pro-OH onto N-methyl Thr under different conditions.

Coupling reagents	Conditions	Product yield
HATU/HOAt/DIPEA	double coupling, 4 eq., 2h	< 5%
	overnight, 10 eq., 50°C	< 5%
COMU/DIPEA	3 eq.	< 10%
	microwave 50°C, 5 min	premature resin cleavage

The decision was thus made to synthesize an N-methylated dipeptide separately and incorporate it into the sequence through standard Fmoc chemistry.

3.1.4 Synthesis of Dipeptide Fmoc-Pro-N-Me-Thr(OtBu)-OH

Commercially available *Z*-Thr(*t*Bu)-OH was N-methylated and esterified to its methyl ester in a single step by treatment with iodomethane and silver oxide.[87] The carboxybenzyl group (Cbz) was then removed by catalytic hydrogenation and the crude free amine subjected to a peptide coupling reaction with Fmoc-Pro-OH and COMU as a coupling reagent. Saponification of the methyl ester proved to be difficult under strong basic conditions with NaOH and LiOH, as it led to the undesired deprotection of the Fmoc group. The ester was then finally cleaved by nonbasic lithium iodide in refluxing EtOAc with complete regioselectivity in good overall yield of 59% over three steps (Scheme 4).[88] The dipeptide served as a building block in the synthesis of the LB-01-Thr1NMe analogue.

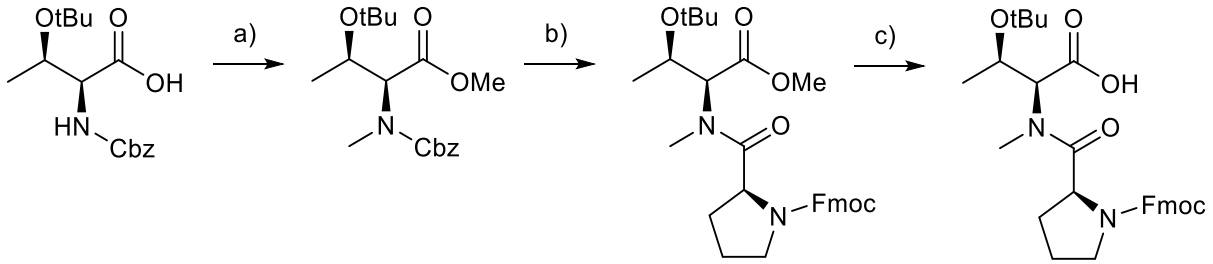

Scheme 4 a) MeI, Ag_2O, DMF, 16 h, 94%. b) Pd/C, H_2, THF, 30 min, then Fmoc-Pro-OH, COMU, DIPEA, DMF, 2 h, 72% over two steps. c) LiI, EtOAc reflux, 16 h, 87%.

3.1.5 Analysis of LB-01 N-Methyl Analogues

All LB-01 N-methyl analogues were subjected to high resolution mass spectroscopy and reversed-phase HPLC analysis. The occurrence of multiple charged ionic species in ESI mode (electron spray ionization) is typical for peptides with several basic residues (i.e. Lys, Orn, Dab, and Arg). The most abundant species were usually $[M+2H]^{2+}$, $[M+3H]^{3+}$ and $[M+4H]^{4+}$. All measured m/z values matched the calculated values with sufficient accuracy. HPLC retention times were in the range of 10-13 min, run with a linear gradient of 10 to 60% MeCN/H_2O with additional 0.1% TFA (Table 5). UV traces (226 nm, 254 nm, 278 nm) showed a purity of > 95% by integration of the 226 nm trace after preparative HPLC purification (Figure 16).

Table 5 Calculated mass and experimental m/z values of LB-01 N-methyl analogues measured by high resolution ESI. Retention times (t_R) were determined by HPLC chromatography. (Adapted from Vetterli *et al.*)[39]

Peptide	Exact mass (calc.)	m/z (HR-ESI)	Retention time t_R [min]
Thr1NMe	1706.02565	854.01996 $[M+2H]^{2+}$ 569.68292 $[M+3H]^{3+}$ 427.51393 $[M+4H]^{4+}$	11.4
Trp2NMe	1706.02565	854.02035 $[M+2H]^{2+}$ 569.68258 $[M+3H]^{3+}$ 427.51382 $[M+4H]^{4+}$	10.8
Leu3NMe	1706.02565	854.01884 $[M+2H]^{2+}$ 569.68228 $[M+3H]^{3+}$ 427.51364 $[M+4H]^{4+}$	12.6
Dab4NMe	1706.02565	854.01946 $[M+2H]^{2+}$ 569.68196 $[M+3H]^{3+}$ 427.51310 $[M+4H]^{4+}$	10.9
Orn5NMe	1706.02565	854.02013 $[M+2H]^{2+}$ 569.68328 $[M+3H]^{3+}$ 427.51416 $[M+4H]^{4+}$	12.0
^{D}Lys6NMe	1706.02565	854.01956 $[M+2H]^{2+}$ 569.68207 $[M+3H]^{3+}$ 427.51349 $[M+4H]^{4+}$	10.6
Arg7NMe	1706.02565	854.01911 $[M+2H]^{2+}$ 569.68236 $[M+3H]^{3+}$ 427.51394 $[M+4H]^{4+}$	11.7
Trp8NMe	1706.02565	854.01905 $[M+2H]^{2+}$ 569.68204 $[M+3H]^{3+}$ 427.51330 $[M+4H]^{4+}$	11.4
Orn9NMe	1706.02565	854.02048 $[M+2H]^{2+}$ 569.68328 $[M+3H]^{3+}$ 427.51441 $[M+4H]^{4+}$	12.1
Dab10NMe	1706.02565	854.01930 $[M+2H]^{2+}$ 569.68200 $[M+3H]^{3+}$ 427.51286 $[M+4H]^{4+}$	11.3
Ala11NMe	1706.02565	854.01880 $[M+2H]^{2+}$ 569.68178 $[M+3H]^{3+}$ 427.51305 $[M+4H]^{4+}$	11.0
Lys12NMe	1706.02565	854.01921 $[M+2H]^{2+}$ 569.68255 $[M+3H]^{3+}$ 427.51400 $[M+4H]^{4+}$	12.9

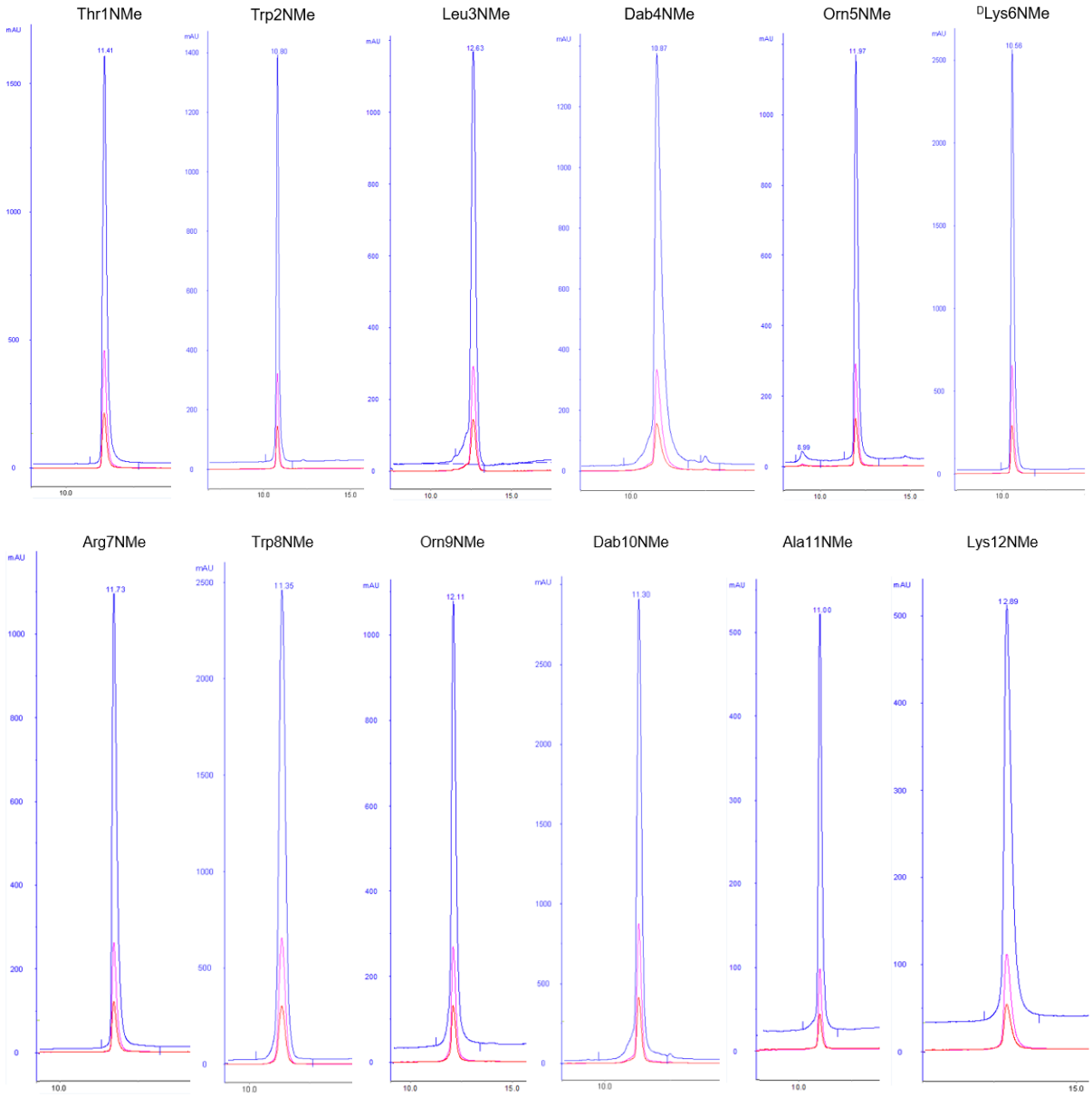

Figure 16 Analytical HPLC chromatograms of LB-01 N-methyl analogues, run with a linear gradient of 10 to 60% MeCN/H_2O with addition of 0.1% TFA on a C18 reverse-phase column. Wavelengths: 226 nm (blue), 254 nm (magenta), 278 nm (red). (Adapted from Vetterli *et al.* suppl. data)[39]

3.1.6 Antimicrobial Activity of LB-01 N-Methyl Analogues

MIC values were measured for all twelve mono-N-methyl LB-01 analogues by a microdilution assay in Mueller-Hinton-I broth (MH-I). The bacterial strains used were *P. aeruginosa* (PA) ATCC27853 and PAO1, and Gram-positive *Staphylococcus aureus* ATCC29213. All analogues were essentially inactive towards *S. aureus*, which is not surprising assuming the same mechanism of action as the parent structure LB-01/L27-11. MIC values are generally two-fold higher for *P. aeruginosa* PAO1 compared to the ATCC27853 strain. Overall, there was a large variation of MIC values. N-methylation at positions Trp2, Leu3, Ala11 and Lys12 lead to a complete loss in activity and a major loss at positions Orn9 and Dab10. Analogues Dab4NMe and Orn5NMe and ^{D}Lys6NMe retained approximately the same activity as LB-01/L27-11 or showed even slightly higher activity. Considering the role of the NH group in intramolecular hydrogen bonding of analogue Orn5NMe, retention of activity was unexpected. Moderate activities were measured for positions Thr1, Arg7 and Trp8. N-methylation at the highly hindered position Thr1 was expected to disrupt the β-hairpin completely but this analogue retained moderate activity (cf. Structural Studies by NMR 3.1.7). From a global view on the scaffold, it seems that modifications near the stem are less tolerated than in the tip region (residues 5-8).

	MIC (µg/mL)	
peptide	**PA ATCC27853**	**PA PAO1**
LB-01	0.008	0.015
Thr1NMe	0.19	0.38
Trp2NMe	>64	>64
Leu3NMe	>64	>64
Dab4NMe	0.005	0.009
Orn5NMe	0.009	0.008
DLys6NMe	0.012	0.025
Arg7NMe	0.38	0.75
Trp8NMe	0.023	0.13
Orn9NMe	12	16
Dab10NMe	1	12
Ala11NMe	>64	>64
Lys12NMe	>64	>64

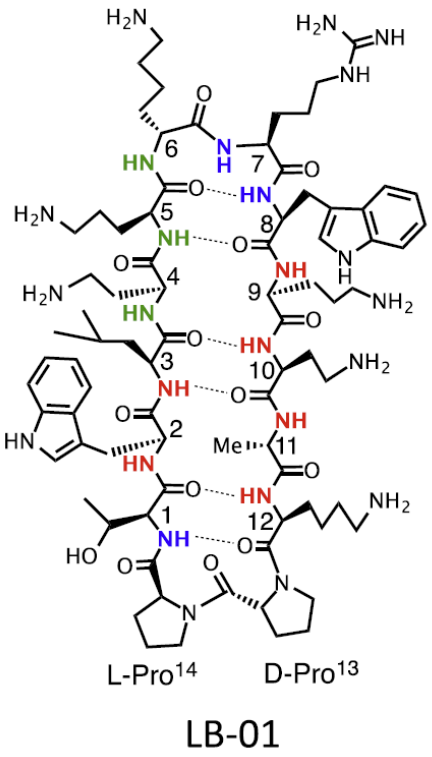

Figure 17 Antimicrobial activity of the N-methyl scan library of LB-01 tested in MH-I with addition of 0.02% BSA. High antimicrobial activity is depicted in green, medium in blue and low activity in red. (Reprinted from Vetterli *et al.*)[39]

It is likely, that N-methylation of amide backbone groups in LB-01 that make important hydrogen-bonding interactions with LptD, will cause major loss of antimicrobial activity. Certain outward-facing NH groups in LB-01 are sensitive to N-methylation such as Trp2, Orn9, and Ala11. N-methylation at those positions leads to a severe loss in activity, highlighting the importance of those H-bonding positions. The also outward-facing NH groups at positions Dab4 and ^{D}Lys6 retain antimicrobial activity upon N-methylation and are therefore unlikely to directly form H-bonds towards LptD. Figure 18 shows a possible binding interaction of LB-01 with two unspecified β-strands from LptD on both sides of the hairpin.[39]

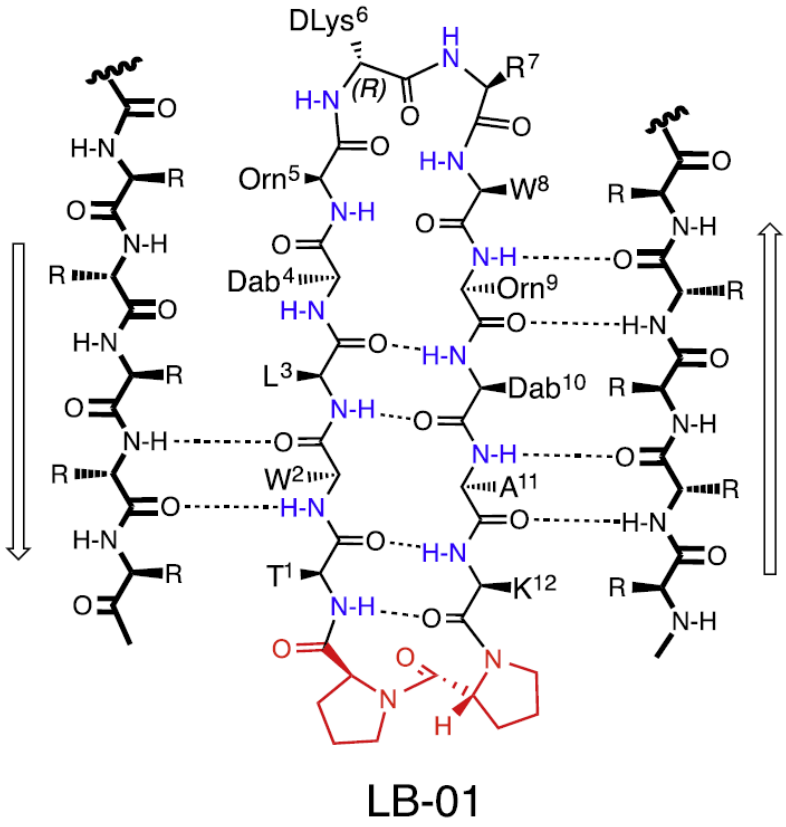

Figure 18 Possible H-bonding interactions of the β-hairpin LB-01 with neighboring β-strands of the target protein LptD. (Reprinted from Vetterli *et al.*)[39]

3.1.7 Structural Studies by NMR

The following NMR studies were carried out in collaboration with Dr. Kerstin Möhle. 1D ^{1}H and 2D [^{1}H, ^{1}H] NMR spectra of each N-methyl analogue were measured in H_2O/D_2O 9:1, pH 2-3. The differences in the shape and dispersion of amide proton resonances with respect to the reference compound LB-01 indicate that the structural behaviour in solution can be strongly influenced by single replacement of an amide proton by a methyl group (Figure 19). The ^{1}H spectra of the N-methylated analogues also displayed the occurrence of major and minor isoforms in solution, which can be related to a *cis-trans* isomerism at the N-methylation site or at the Lys12-^{D}Pro13 peptide bond. The majority of LB-01 N-methyl analogues exist as rotamers with > 90% all-trans peptide bonds along the backbone. However, *cis*-rotamers with higher percentages at the N-methylation site were calculated for Leu3NMe and Trp8NMe, with 25% and 50% of the *cis*-rotamer respectively. In the case of analogue Orn9NMe and Dab10NMe, in addition to the *cis*-rotamer at the N-methylation site (each 25%), *cis*-conformers were detected for the Lys12-^{D}Pro13 peptide bond (12% and 8% respectively). For Trp8NMe, two slowly interconverting isoforms coexist in solution with a ratio of 1:1 arising from *cis-trans* isomerization at the Arg7-Trp8Me peptide bond (Table 6). NMR resonance assignments were completed for all major forms of the analogues (Appendix 6.2) except for Trp8NMe, which shows significant signal overlap of both major forms. The three representative solution structures of analogue Orn5NMe, Ala11NMe, and Thr1NMe are discussed in detail in the following sections. Analogues Orn5NMe and Thr1NMe have peptide NH bonds oriented inwards across the hairpin structure (Figure 17), and so it is of interest to determine whether the regular hairpin structure is retained in these cases. The Thr1NMe substitution, in particular, is at a critical position next to the ^{D}Pro-^{L}Pro template. In addition, the Ala11NMe analogue is of great interest, since the peptide NH at this residue should be oriented outward in a regular hairpin structure, and yet the analogue completely loses antimicrobial activity.

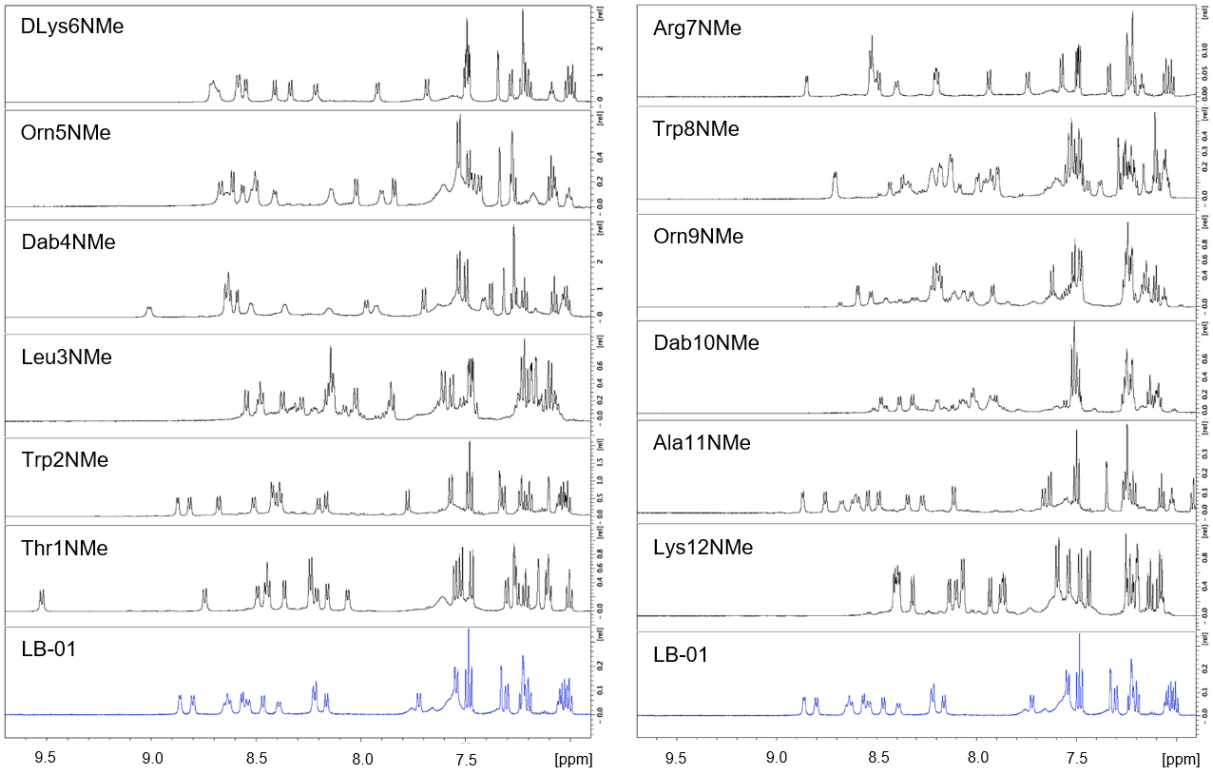

Figure 19 ^{1}H spectra (amide-aromatic region) of N-methyl analogues compared to reference compound LB-01.

Table 6 *cis-trans* peptide bond rotamers in LB-01 N-methyl analogues, calculated from NMR data. (Adapted from Vetterli *et al.*)[39]

Peptide	*cis* rotamer [%]	Peptide bond
LB-01	< 5	-
Thr1NMe	7	^{L}Pro-Thr1NMe
Trp2NMe	7	Thr1-Trp2NMe
Leu3NMe	25	Trp2-Leu3NMe
Dab4NMe	5	Leu3-Dab4NMe
Orn5NMe	< 5	-
^{D}Lys6NMe	< 5	-
Arg7NMe	< 5	-
Trp8NMe	50	Arg7-Trp8NMe
Orn9NMe	25 12	Trp8-Orn9NMe, Lys12-^{D}Pro13
Dab10NMe	25 8	Orn9-Dab10NMe, Lys12-^{D}Pro13
Ala11NMe	8	Dab10-Ala11NMe
Lys12NMe	10	Ala11-Lys12NMe

Solution structure of Orn5NMe. The Orn5NMe analogue was one of the most active compounds in this study. The chemical shifts of amide resonances show a good dispersion in the range of 1 ppm (slightly less than in LB-01)[49] (Figure 19), suggesting that the peptide is predominantly well-structured in solution. As a qualitative indicator for the formation of secondary structures in solution, secondary chemical shifts – namely the deviations of observed Hα chemical shifts from tabulated random coil values ($\Delta\delta = \delta_{observed} - \delta_{random}$)[50] – were determined. These chemical shift deviations (CSDs) are typically negative (upfield shifts) within segments of four or more contiguous residues indicating α-helical conformations and positive (downfield shifts) in β-sheet conformations. The comparison of the CSDs displays similar trends as in LB-01, with positive Δδ Hα's between Thr1-Dab4 and Trp8-Lys12 (except for Ala11), indicating the occurrence of extended conformations in these regions (Figure 23). Characteristic cross-strand nuclear Overhauser effects (NOEs), consistent with a β-hairpin conformation were observed close to the template, in particular, the backbone Hα-Hα NOE between Trp2 and Ala11, and the backbone side-chain HN-Hβ NOEs between Lys12-Thr1 and Dab10-Leu3. In the tip region between Dab4 and Orn9, only few long-range NOEs were observed, indicating that this region is more flexible and/or interconverts between conformations. NOE connectivities occurred between side-chain protons of Trp2 and Trp8, indicating a π-stacking of aromatic side-chains on the same side of the peptide on the one hand, and between Trp2 and Orn9 side-chain protons, as they were observed and expected in a regular β-hairpin fold, on the other hand. The structure calculations performed with the program CYANA[89] gave a bundle of 20 low energy conformations, which revealed a backbone root mean square deviation (rmsd) of 1.3 Å, suggesting a flexible backbone (Table 7). A restricted clustering of the structures by superposition of the backbone atoms close to the template (Dab10-Pro14, Thr1-Leu3) shows a rmsd of 0.8 Å, and clearly indicates the β-hairpin shaped fold of residues close to the template (Figure 20). The $^{3}J_{HNH\alpha}$ coupling constants of most of the amide protons were in the range of 6-8 Hz correlating with fast conformational exchange, except for the N-terminal residues 1, 2, and 4, which exhibit values > 8 Hz – suggestive of predominantly extended conformation in this region.[90] The temperature coefficients of chemical shifts of amides Thr1, Ala11, and Lys12 were < 4 ppb/K which may be due to intermolecular hydrogen bonding (between Thr1 and Lys12), or solvent-shielding effects in the case of Ala11, whereas all other amides show significantly higher Δδ/ΔT shifts, reflecting the exposed nature of these protons (Figure 24).[91] Further, the lower exchange rates of Thr1 and Lys12 agree with the low Δδ/ΔT observations.

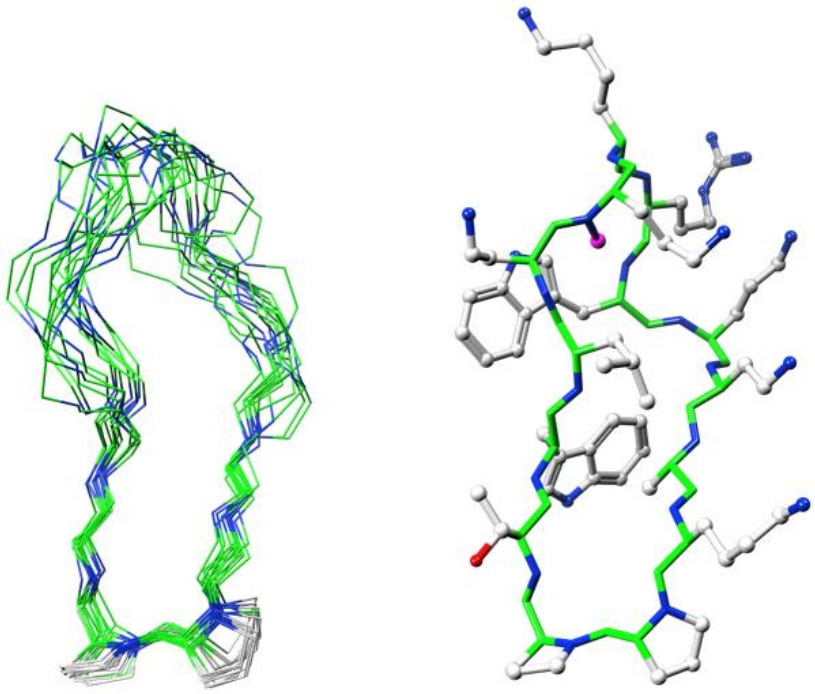

Figure 20 Backbone trace of 20 selected NMR structures of Orn5NMe superimposed to the backbone atoms of Dab10-Pro14, Thr1-Leu3 (left) and a single representative NMR structure with side-chains in ball-and-stick (right). Hydrogen and carbonyl-oxygen are omitted to simplify the view. The N-methyl group was highlighted in magenta.

Solution structure of Ala11NMe. The replacement of the amide proton by a methyl group at position 11, results in a complete loss of antimicrobial activity (cf. Figure 17). The comparison of the 1D ^{1}H spectra of Ala11NMe and LB-01 show high similarity in the dispersion of the NH resonances (over a region of 1.2 ppm). The shifts of the amide proton signals (Figure 19) suggest a similar structure in aqueous solution. The comparison of the Hα CSDs (Figure 23) show the same or slightly stronger tendency of positive values between Trp2-Orn5 and Trp8-Lys12. The resonance assignment of the 2D NOESY/ROESY spectra provides a consistent network of medium and long range NOEs. From the NOE distance restraints, a close bundle of average solution structures was calculated with a backbone rmsd of 0.4 Å (Table 7). The analogue adopts a well-defined β-hairpin structure in aqueous solution (Figure 21). Characteristic backbone cross-strand NOEs were observed, in particular HN-HN between Thr1-Lys12, Hα-Hα NOEs between Trp2-Ala11, and HN-Hα between Leu3-Orn9. Further, numerous cross-strand backbone side-chain and side-chain side-chain NOEs between Trp2-Ala11, Trp2-Orn9, Leu3-Trp8, Leu3-Dab10, and Orn5-Trp8 support the stable β-hairpin fold of Ala11NMe. The conformation of the tip region at ^{D}Lys6 and Arg7 is characterized by two strong sequential backbone NOEs HN-HN between Arg7-Trp8 and Hα-HN between ^{D}Lys6-Trp8, suggesting the formation of a β-turn. The NMR structure exhibits a type II' β-turn with backbone torsion angles (Φ_{i+1}, Ψ_{i+1}) of (81.2 ± 9.5, -89.7 ± 17.4) and (Φ_{i+2}, Ψ_{i+2}) of (-108.8 ± 18.3, -8.2 ±

3.5). The low temperature coefficients of NH chemical shifts ($-\Delta\delta/\Delta T > 5$) at hydrogen bonding positions 1, 5, 8, and 10, as well as slower H/D exchange rates of residue 1, 3, 12, and 8 support the β-hairpin conformation (Figure 24). Finally the $^{3}J_{HNH\alpha}$ coupling constants display values > 8 Hz for the majority of β-strand hosted residues, indicating extended backbone conformation. Interestingly, despite the stable β-hairpin fold in aqueous solution, the peptidomimetic is completely inactive. This leads to the conclusion that the amide group at position 11 is involved in the binding to the target protein. In the β-hairpin register, the group points outward and is basically not involved in the intramolecular hydrogen bonding interactions. However, it can form hydrogen bonds with the protein target (e.g. β-barrel or β-jelly-roll proteins) to stabilize the peptide-LptD complex.

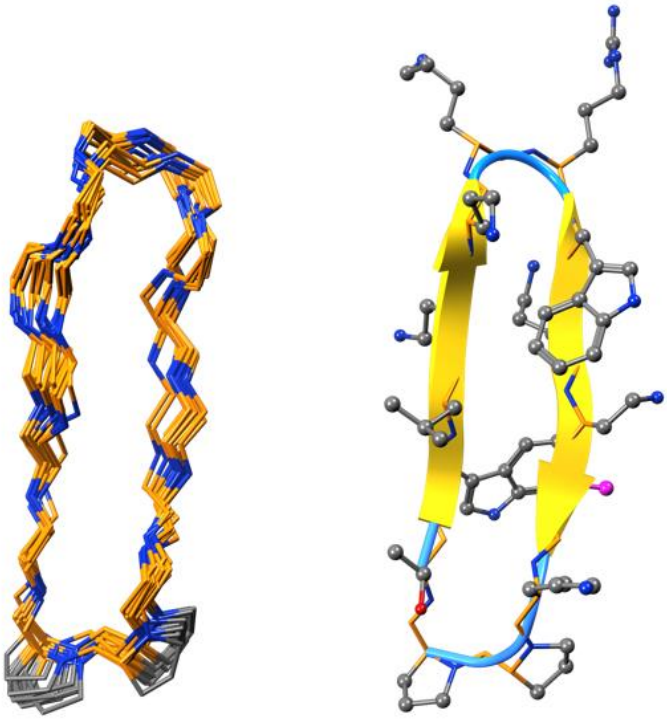

Figure 21 Backbone trace of 20 selected NMR structures of Ala11NMe superimposed to all backbone atoms (left) and a ribbon representation of a single representative NMR structure with side-chains in ball-and-stick (right). Hydrogen and Carbonyl-Oxygen are omitted to simplify the view. The N-methyl group was highlighted in magenta.

Solution structure of Thr1NMe. Residues at position 1 normally occupy a hydrogen-bonding position, which is formed cross-strand between the amide and carbonyl group of Thr1 and Lys12 (cf. Figure 18). Due to the replacement of the amide proton here by a methyl group, the intramolecular hydrogen bond cannot be formed. The 1D ^{1}H spectrum shows well dispersed NH doublets in the amide proton region, with a remarkable downfield shift of an amide proton resonance (9.2 ppm) assigned to Trp2 (Figure 19). The Hα CSDs of Thr1NMe exhibit significant differences in comparison to LB-01 (Figure 23). Most striking is the fact that there is no continuous segment of at least three residues with positive or negative Hα CSDs in the

sequence, indicating the absence of regular secondary structure elements. In contrast to Ala11NMe, most of the observed NOEs in the NOESY spectrum were intraresidual or sequential. Only weak medium and long range NOEs could be observed, indicating that the cyclic peptide adopts non-regular secondary structures or is more flexible in aqueous solution. Furthermore, the observed NOEs indicate proton-proton connectivities, that are not typical for a regular β-hairpin nucleated by the ^{D}Pro-^{L}Pro template. In particular HN-HN NOEs between Leu3-Orn9, Hα-Hα NOEs between Trp2-Dab10, and HN-Hα NOEs between Leu3-Dab10, Orn2-Trp2 were observed. Those backbone NOEs suggest a shifted residue pairing with Trp2 and Dab10 on a non-hydrogen bonding position. Based on the NOE distance restraints, the calculated average NMR structures have a backbone rmsd of 1.5 Å (Figure 22 and Table 7). Despite the spatial orientation of the side-chains that cannot be correlated with a regular β-hairpin structure, two pairs of residues in the middle of the fold – namely Trp2-Dab10 and Leu3-Orn9 – get closer in contact, resulting in the “eight-shaped” overall fold of Thr1NMe. The side-chains of the neighbouring residues Ala11 and Lys12 are pointed to the same side, forming a backbone bulge close to the template. The coupling constants $^{3}J_{HNH\alpha}$ of most of the amide protons lie in the range of 6-8 Hz, suggestive of rapidly interconverting conformers that coexist in solution (Figure 24). The low temperature coefficients of Orn9 and Ala11, with values of 1.8 and 3.2 ppb/K respectively are consistent with the calculated NMR structures. The Orn9 NH appears to be shielded from the solvent by the aliphatic Leu3 side-chain on top and the Trp2 side-chain on the other site. The amide proton of the Ala11 residue is pointed to Thr1 carbonyl allowing hydrogen bond formation.

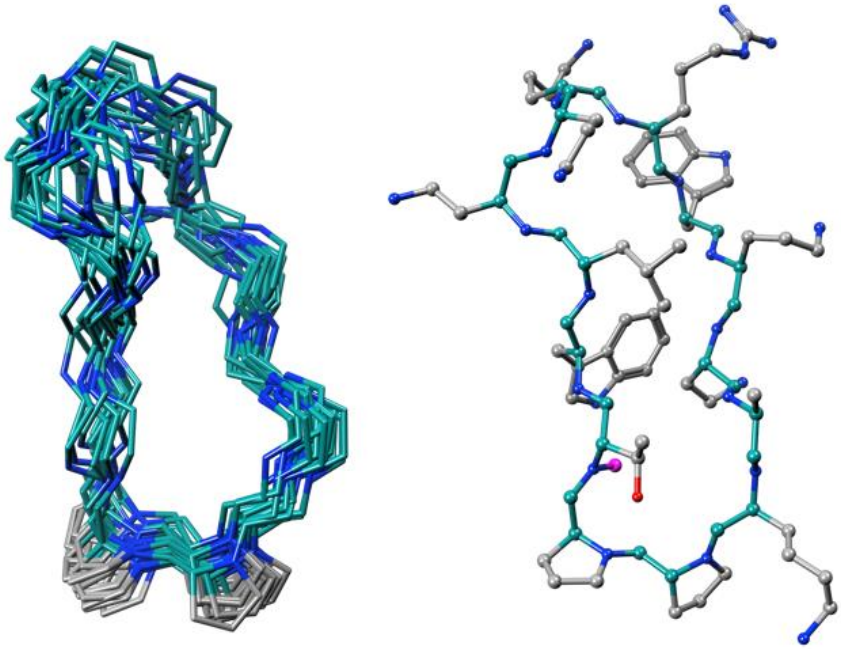

Figure 22 Backbone trace of 20 selected NMR structures of Thr1NMe superimposed to all backbone atoms (left) and a single representative NMR structure with side-chains in ball-and-stick representation (right). Hydrogen and carbonyl-oxygen are omitted to simplify the view. The N-methyl group was highlighted magenta.

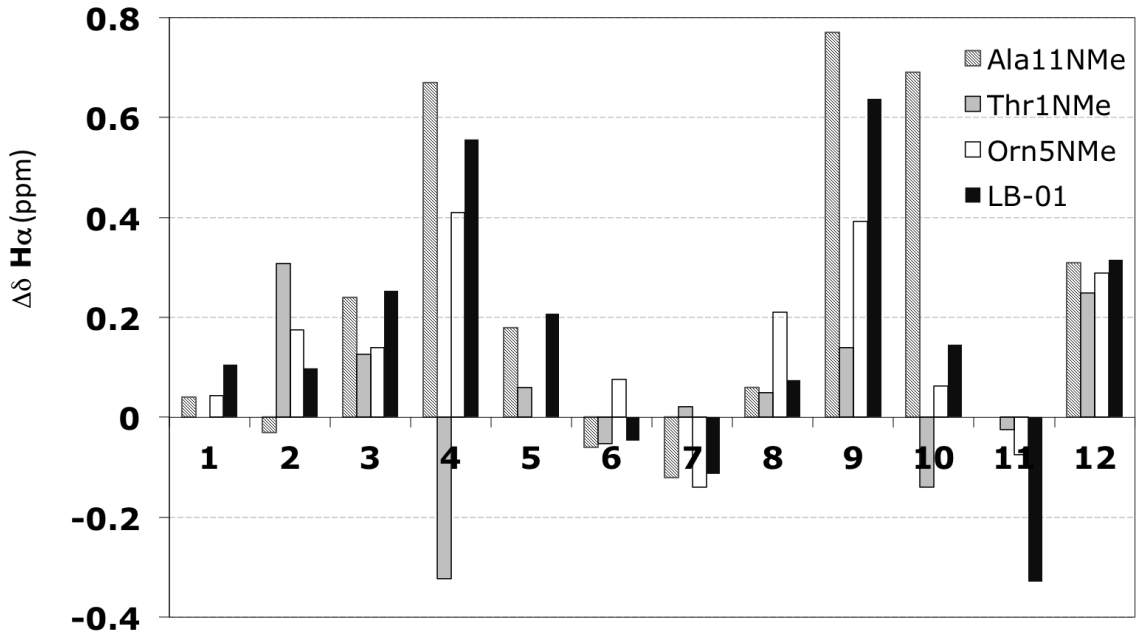

Figure 23 Hα chemical shift deviations (CSDs) from tabulated random coil values[50]. The bars were not displayed for N-methylated residues, because Hα shifts are strongly influenced by N-methylation.

Table 7 Experimental distance restraints and statistics for the final 20 NMR structures calculated for Thr1NMe, Orn5NMe and Ala11NMe.

	Thr1NMe	**Orn5NMe**	**Ala11NMe**
Number of NOE upper-distance limits:	160	250	188
Intraresidue:	73	141	79
Sequential:	61	62	53
Medium- and long-range:	26	47	56
Residual target function value (Å^2):	0.12 ± 0.04	0.26 ± 0.15	0.69 ± 0.11
Mean rmsd values (Å)			
All backbone atoms:	1.47 ± 0.45	1.30 ± 0.34	0.45 ± 0.13
All heavy atoms:	3.06 ± 0.86	2.54 ± 0.60	0.96 ± 0.19
Residual NOE violations			
Number > 0.2 Å:	0	6	2
Maximum (Å):	0.17	0.36	0.38

		residue											
		1	**2**	**3**	**4**	**5**	**6**	**7**	**8**	**9**	**10**	**11**	**12**
Thr1NMe	$^3J_{HNH\alpha}$ [Hz]	-	8.4	8.2	7.5	7.1	6.5	nd	6.7	7.8	7.1	6.7	7.6
	-Δδ/ΔT [ppb/K]	-	7.5	7.9	5.2	5.2	6.4	5.6	9.5	1.8	7.8	3.2	7.7
	$k_{exch.}$	-	○	○	○	○	○	○	○	○	○	○	○
Orn5NMe	$^3J_{HNH\alpha}$ [Hz]	8.0	9.2	nd	9.2	-	7.3	6.4	7.1	7.3	6.8	7.5	7.9
	-Δδ/ΔT [ppb/K]	3.6	10.7	9.2	6.3	-	7.0	7.7	11.0	5.0	7.5	3.7	0.3
	$k_{exch.}$	◐	○	●	○	-	○	○	◐	○	○	○	◐
Ala11NMe	$^3J_{HNH\alpha}$ [Hz]	8.4	9.1	8.2	9.1	7.8	5.0	7.3	7.9	8.3	7.7	-	8.9
	-Δδ/ΔT [ppb/K]	2.0	8.7	6.1	6.8	4.4	8.6	9.1	4.2	4.7	2.9	-	5.3
	$k_{exch.}$	◐	◐	●	○	○	○	○	◐	○	○	-	●

Figure 24 Coupling constants $^3J_{HNH\alpha}$ temperature coefficients Δδ/ΔT of amide NH resonances, and relative peptide NH exchange rates (open circle = fast, half-filled = slower, filled = slowest) for residues 1-12 of Thr1NMe, Orn5NMe and Ala11NMe (nd – determination not possible due to significant resonance overlap).

3.1.8 Circular Dichroism

The far-UV CD spectra of all N-methylated analogues are shown in Figure 25, grouped into three diagrams according to signal intensity and the shape of the graph with respect to LB-01. As judged from the signal intensities at 215 nm, the peptidomimetics Ala11NMe, Arg7NMe, and ^{D}Lys6NMe (group 1) showed similar graphs as LB-01, indicating that the β-hairpin fold remains stable in these analogues. Slightly reduced signal intensities were observed for Orn5NMe, Dab4NMe, Trp2NMe, and Lys12NMe (group 2), which suggests that the β-hairpin content is lower than that of group 1 compounds. Much lower signal intensities were observed for Orn9NMe and Dab10NMe, whereas Thr1NMe, Leu3NMe, and Trp8NMe exhibited a distinctly reduced and shifted negative band (group 3). In the latter compounds, the β-hairpin fold appears to be no longer populated in aqueous solution. The results are in good agreement with the one-dimensional NMR spectra (Appendix 6.2) and the NMR structure determinations of selected analogues described above.

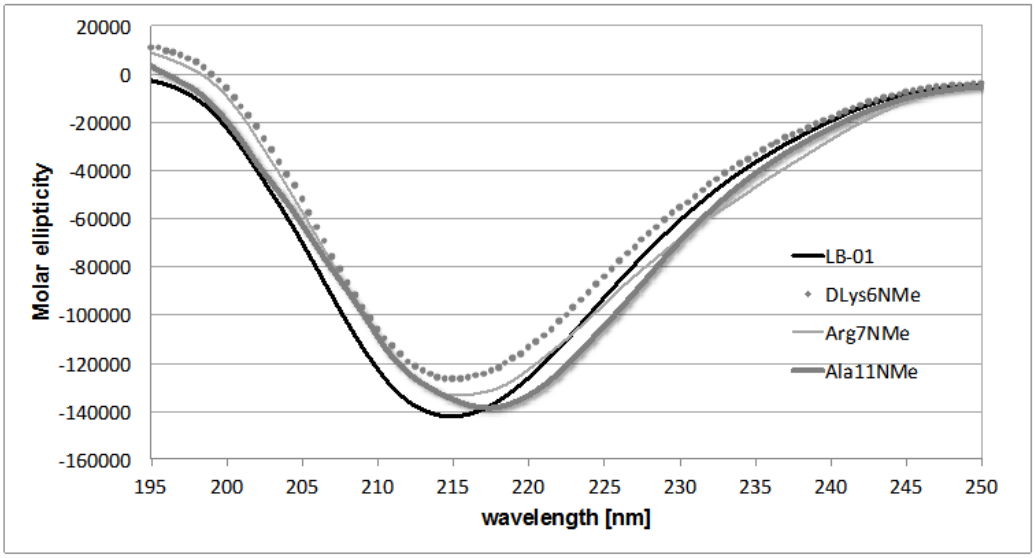

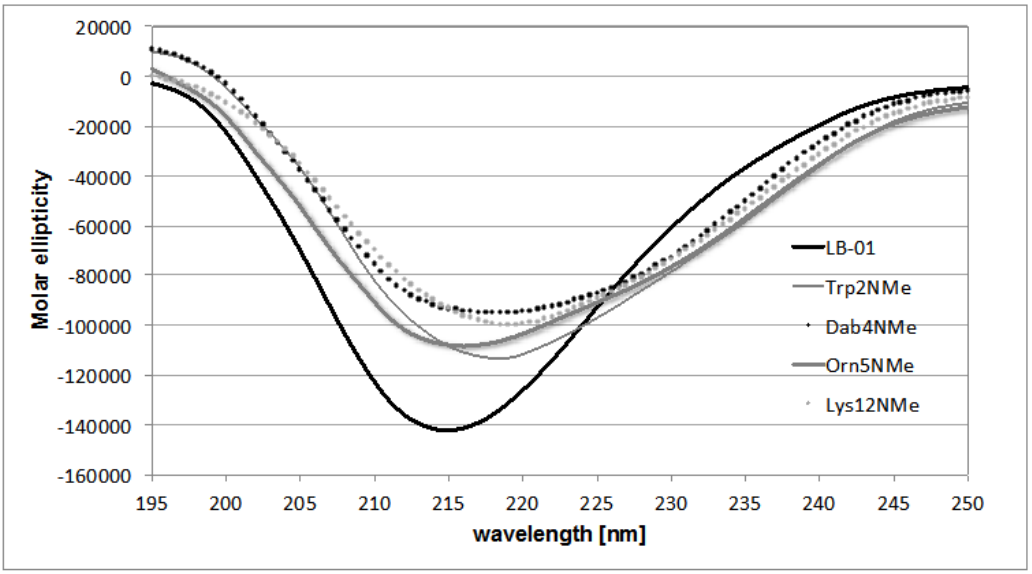

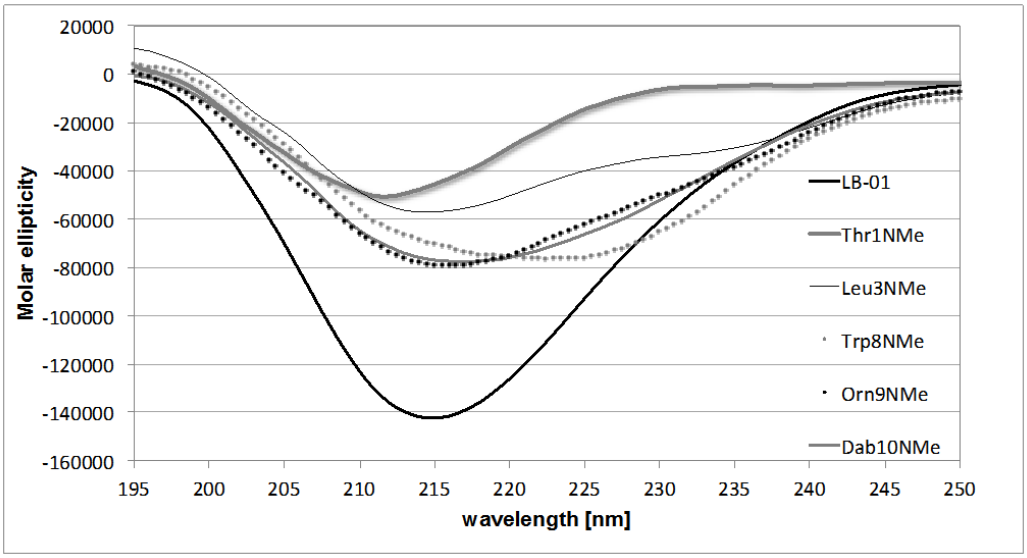

Figure 25 Far-UV CD spectra of N-methylated analogues, comparing β-hairpin propensity to the reference compound LB-01 (thick black line). Molar ellipticity in deg*cm^2/dmol.

3.1.9 Additional Modifications at Positions Dab4 and Orn5

Due to the high activity observed with N-methyl analogues Dab4NMe and Orn5NMe, the positions 4 and 5 were chosen as interesting sites for further modifications. An ethyl group and an aromatic benzyl group were introduced respectively by the *Kessler* method described above, with ethanol (Et) and benzyl alcohol (Bz) as the donor groups. The introduction of an ethyl group retained activity, whereas the introduction of a benzyl group led to a drop in activity, especially in the case of Dab4NBn. Peptoids were introduced to study the influence of chirality at positions 4 and 5. In a peptoid, the amino acid side-chain is directly attached to the nitrogen of the peptide bond, instead of the α-carbon as in regular peptides. The solid phase synthesis of peptoids was first described by Simon *et al.*[16] in 1992 as part of the drug discovery of protease stable peptidomimetics. Peptoid analogues of LB-01 were synthesized according to the refined method of *Zuckermann*[92]. Exemplified here for the synthesis of NDab4 (Scheme 5), the peptoid was installed in two steps; acylation and S_N2 displacement. In the acylation step, bromoacetic acid was activated by diisopropyl-carbodiimide (DIC) and reacted with the free amine of the previous residue. In the following S_N2 reaction, the amine displaced the bromide to form the N-substituted residue. The subsequent amino acid was coupled under standard conditions onto the sterically hindered amine with HATU/HOAt. The NDab4 peptoid showed lower activity compared to Dab4NMe, whereas the NOrn5 peptoid retained its activity, indicating that the chirality of the ornithine side-chain is not essential for activity. A double and a triple N-methylated analogue was synthesized and subjected to MIC testing. For those two analogues, the MIC was determined by a new protocol in MH-II instead of MH-I, which leads to an approximately 8-fold higher MIC value in general. Whereas the activity for the double methylated 4,5-NMe analogue remained high, a significant drop in activity was observed for the triple methylated 4,5,6-NMe analogue. A third N-methylation at position 6 therefore seems to be detrimental to high activity. The purity of all analogues was confirmed by UPLC analysis (Figure 26) and the identity by HR-ESI (Table 8). MIC values of all analogues were determined on *P. aeruginosa* ATCC27853 and PAO1 and are also summarized in Table 8.

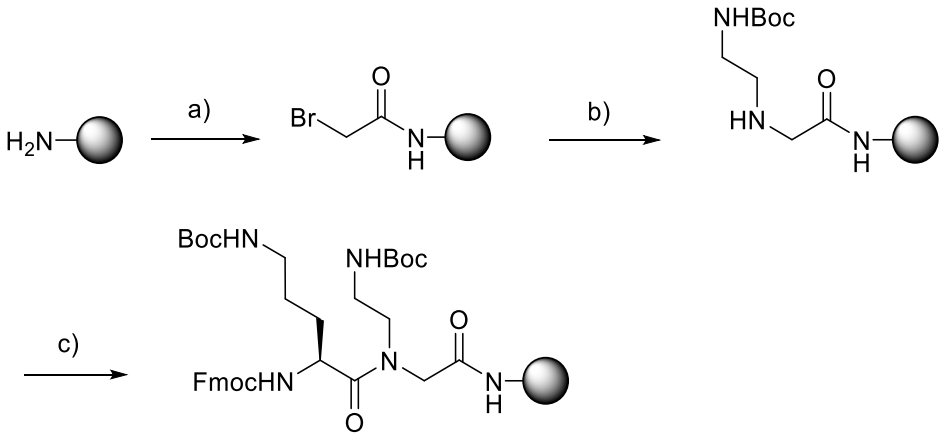

Scheme 5 a) Bromoacetic acid, DIC, DMF, 1 h. b) N-Boc-ethylenediamine, DMF, overnight. c) HATU/HOAt, DIPEA, Fmoc-Orn(Boc)-OH, DMF, 2 h.

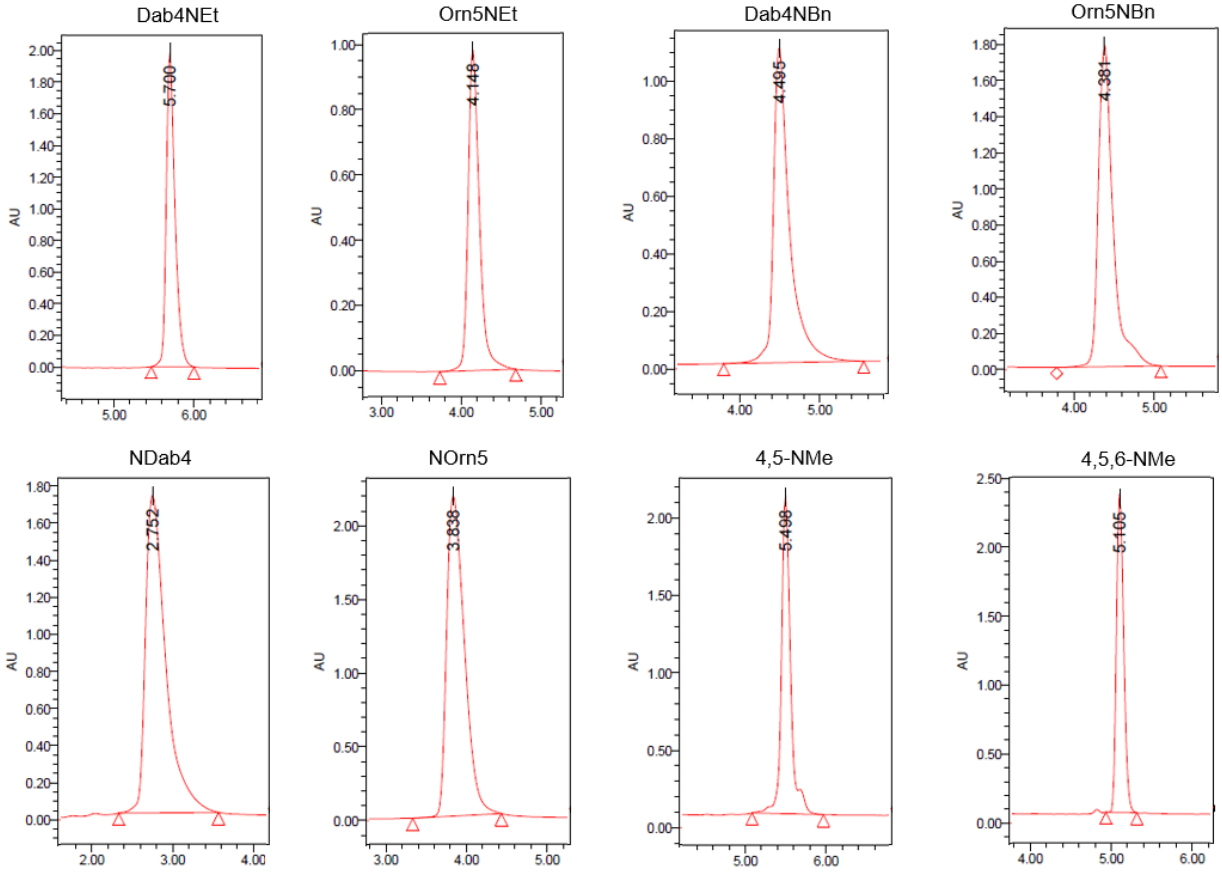

Figure 26 UPLC chromatograms at 226 nm wavelength, run with a linear gradient of 10 to 40% MeCN/H_2O with additional 0.1% TFA on a C18 reverse-phase column.

Table 8 Antimicrobial activity of different LB-01 analogues modified at position 4 and 5 tested on *P. aeruginosa* (PA) ATCC27853 and PAO1 and calculated mass and experimental m/z values measured by high resolution ESI. The two analogues, indicated by a star (*), were tested in MH-II with addition of 0.002% Tween80, all others in MH-I with addition of 0.02% BSA.

Analogue	PA ATCC27853 [µg/ml]	PA PAO1 [µg/ml]	Exact mass (calc.)	m/z (HR-ESI)
Dab4NEt	0.008	0.009	574.3549 $[M+3H]^{3+}$	574.3555 $[M+3H]^{3+}$
Orn5NEt	0.012	0.009	574.3549 $[M+3H]^{3+}$	574.3544 $[M+3H]^{3+}$
Dab4NBn	1.5	0.5	446.5221 $[M+4H]^{4+}$	446.5227 $[M+4H]^{4+}$
Orn5NBn	0.05	0.015	446.5221 $[M+4H]^{4+}$	446.5231 $[M+4H]^{4+}$
NDab4 (peptoid)	0.15	1.5	424.0103 $[M+4H]^{4+}$	424.0106 $[M+4H]^{4+}$
NOrn5 (peptoid)	0.005	0.02	424.0103 $[M+4H]^{4+}$	424.0093 $[M+4H]^{4+}$
4,5-NMe*	0.05	0.06	431.0176 $[M+4H]^{4+}$	431.0180 $[M+4H]^{4+}$
4,5,6-NMe*	1	12	434.5215 $[M+4H]^{4+}$	434.5217 $[M+4H]^{4+}$

3.1.10 Cellular Uptake

Since LB-01 shares many characteristics with known CPPs, namely its size, net positive charge of +7, and a non-lytic mechanism of action, it makes an interesting candidate to study its delivery and uptake into mammalian cells. The eukaryotic model cell line HeLa was used to study the cellular uptake of fluorescence-labelled LB-01. Two labelled LB-01 analogues were synthesized: LB-01-FL with a fluorescein coupled to azidolysine and LB-01-AF647 with an Alexa Fluor® 647 red dye, coupled to a glutamic acid PEG_3-azide linker (Figure 27). Both fluorophores were coupled via Click Chemistry (cf. Experimental Part 4.4). at position 1 of the scaffold, which has been used before in studies of antibacterial analogues for the introduction of different linkers.[46] The purity of the two compounds was confirmed by UPLC (Figure 28) and its identity by HR-ESI (Table 9). Commercially available Tat-FITC (*Anaspec*) served as a positive control in the experiment. The FITC (fluorescein isothiocyanate) fluorophore exhibits the same spectral properties as regular fluorescein, facilitating the comparison and quantification between the two probes. The Tat sequence 47-57 (YGRKKRRQRRR) in Tat-FITC is a well-studied CPP with a high transduction rate.[93]

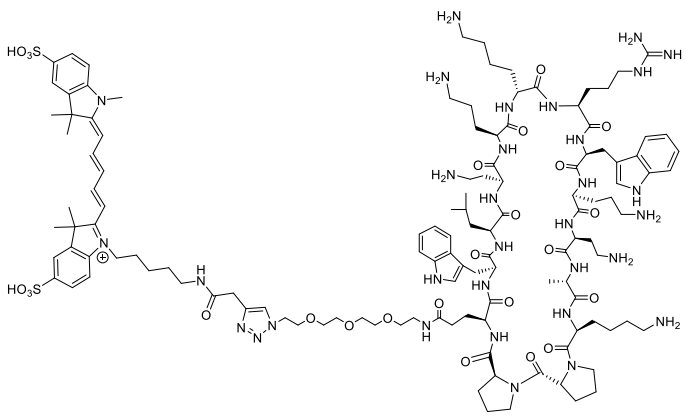

LB-01-AF647

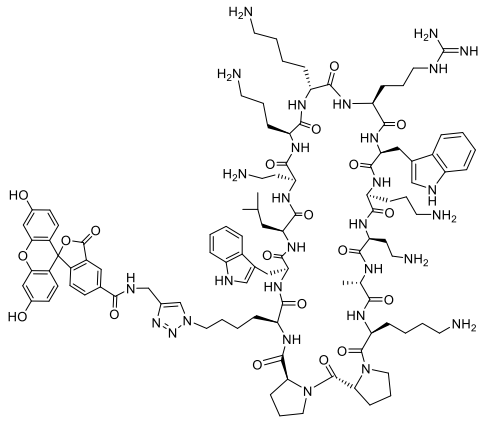

LB-01-FL

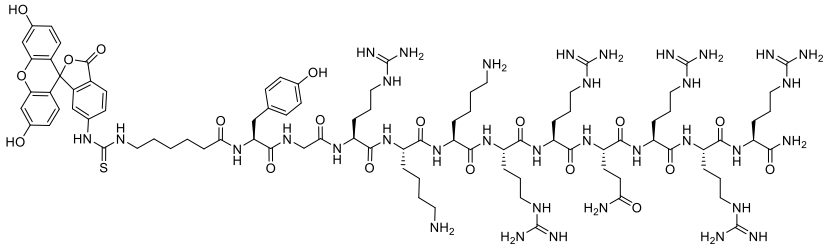

Tat-FITC

Figure 27 Fluorescence-labelled LB-01 analogues LB-01-AF647 and LB-01-FL as well as commercially available Tat-FITC.

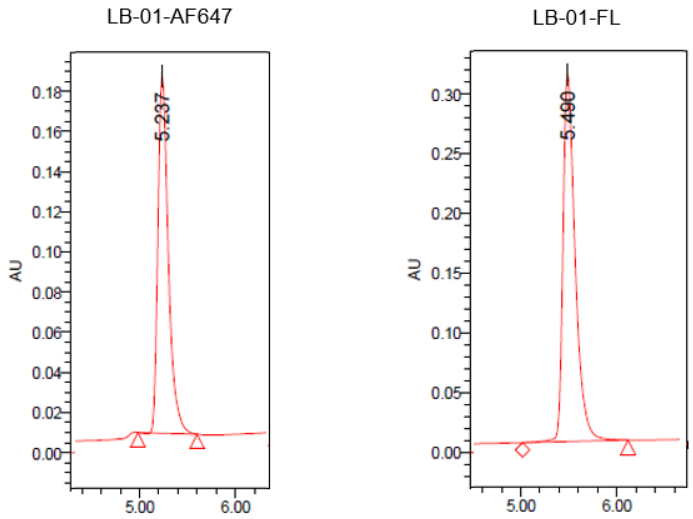

Figure 28 UPLC chromatograms of LB-01-AF647 and LB-01-FL at 226 nm wavelength, run with a linear gradient of 10 to 40% MeCN/H_2O with additional 0.1% TFA on a C18 reverse-phase column.

Table 9 Calculated mass and experimental m/z values of the two compounds measured by high-resolution ESI.

Analogue	Exact mass (calc.)	m/z (HR-ESI)
LB-01-AF647	521.0835 $[M+5H]^{5+}$	521.0825 $[M+5H]^{5+}$
LB-01-FL	540.5423 $[M+4H]^{4+}$	540.5427 $[M+4H]^{4+}$

Confocal fluorescence microscopy. HeLa cells were incubated with 10-20 µg/ml of the individual labelled compound, fixed by paraformaldehyde, mounted with DAPI (4',6-diamidino-2-phenylindole)[94] containing mounting media, and analysed by fluorescence microscopy at the Center of Microscopy and Image Analysis (ZMB) at UZH. The blue dye DAPI used for DNA staining, distinctly highlighted the nucleus of each individual cell as expected. Both Tat-FITC and LB-01-FL at concentrations of 20 µg/ml led to an equal distribution of green fluorescence inside the cells (Figure 29 and Figure 30). Equally, LB-01-AF647 at a concentrations of 10 µg/ml exhibited bright red fluorescence (Figure 31). All three fluorescence-labelled compounds were therefore efficiently taken up and distributed inside the cells under these experimental conditions.

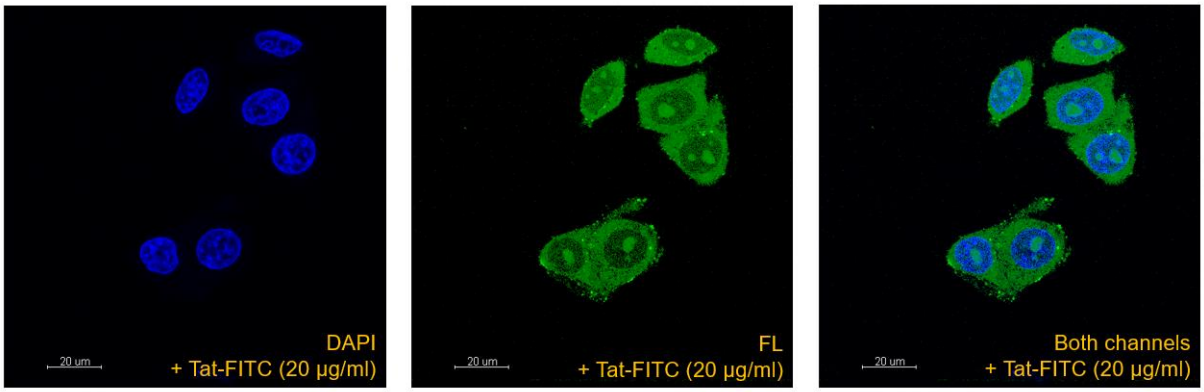

Figure 29 HeLa cells treated with 20 µg/ml Tat-FITC (green) and nucleic acid stain DAPI (blue).

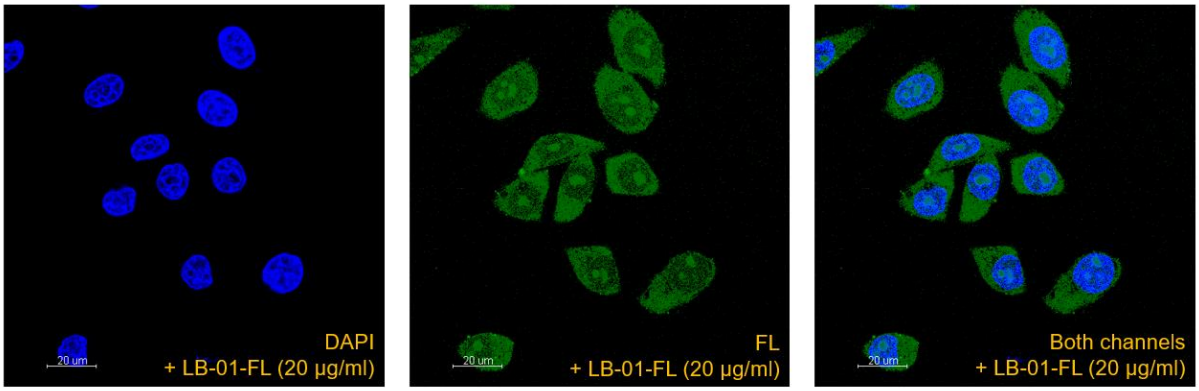

Figure 30 HeLa cells treated with 20 µg/ml LB-01-FL (green) and nucleic acid stain DAPI (blue).

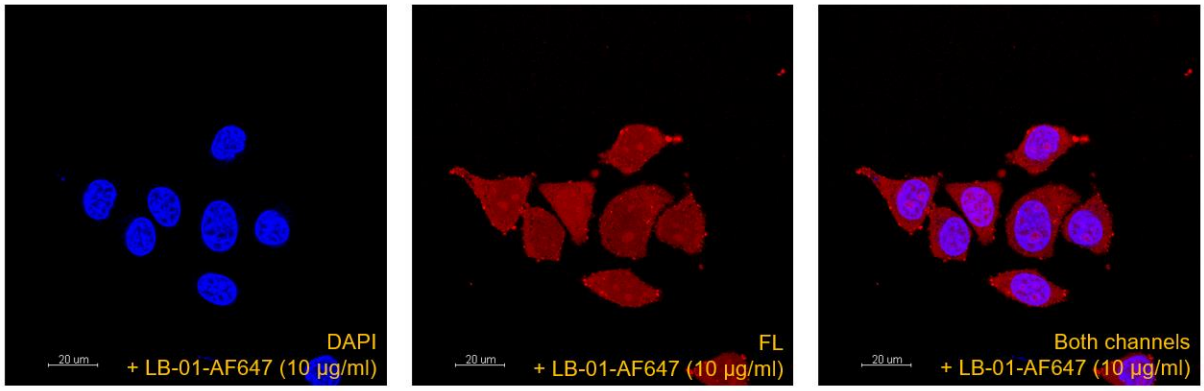

Figure 31 HeLa cells treated with 10 µg/ml LB-01-AF647 (red) and nucleic acid stain DAPI (blue).

Cell lysis assay. A cell lysis assay was performed to quantify the amount of fluorescence-labelled compound LB-01-FL taken up by the cells in direct comparison to Tat-FITC. HeLa cells were grown and incubated with the individual compound in triplicate at a concentration of 6.4 µM for 1 h. Cell lysis was performed, and the lysate was analysed on a fluorescence intensity plate reader to determine the concentration of fluorescence-labelled compounds inside the cells (Figure 32). The concentrations were 118 ± 25 nM for Tat-FITC and 69 ± 8 nM for LB-01-FL. Hence, Tat-FITC has an approximately 40% higher transduction rate than LB-01 into HeLa cells.

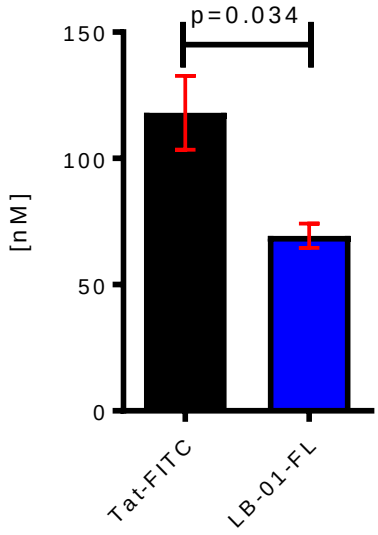

Figure 32 Quantified uptake of Tat-FITC compared to LB-01-FL into HeLa cells.

These results confirm the uptake of LB-01-FL into HeLa cells. Although Tat-FITC exhibits a significantly higher transduction rate than LB-01-FL, the LB-01 scaffold could be potentially used as a non-toxic delivery vehicle into eukaryotic cells.

3.1.11 Conclusion

A reliable synthetic strategy has been applied to synthesize mono and multiple N-methylated LB-01 analogues in high purity of > 95% and yields of 3-15% (Scheme 2). The dipeptide Fmoc-Pro-N-Me-Thr(OtBu)-OH was successfully synthesized in a good overall yield of 59% over three steps (Scheme 4) and incorporated into the sequence of analogue LB-01-ThrNMe. A wide range of MIC values were obtained for the twelve analogues in a complete N-methyl scan (Figure 17). The antimicrobial activity was correlated to the ability to fold a stable β-hairpin by utilising NMR analysis and CD spectroscopy data. However, not only the correct fold of the β-hairpin was shown to be important for high antimicrobial activity, as previously anticipated. Several outward facing NH groups were also crucial. Since they were sensitive to N-methylation, they likely participate in H-bonding interaction with the target protein LptD. A model was proposed, in which LB-01 interacts by antiparallel strand-strand interaction with a β-rich sequence in LptD (Figure 18). Additional modifications were introduced at position 4 and 5 of the scaffold in form of ethyl and benzyl groups, and the regular side-chains were substituted by peptoids. Also, a double and a triple N-methylated analogue was synthesized. However, a clear trend could not be concluded from this, since most of the analogues retained high or moderate activity. During the course of this work, progress has been made by Gloria Andolina in localizing the binding site in LptD, which is now believed to be at the approximately 90 residue insert domain found in *P. aeruginosa spp*. This insert domain is unique for the *Pseudomonas* family, but not found in other Gram-negative bacteria, possibly explaining its selective activity towards this family. A crystal structure of the full *Pseudomonas* LptD sequence and a co-crystal together with L27-11/LB-01 is still highly desirable, but proved to be exceptionally difficult to obtain. Binding studies of this interaction are currently ongoing. The cellular uptake of a fluorescence-labelled LB-01 analogue into mammalian HeLa cells has been confirmed by confocal fluorescence microscopy and a quantitative lysis assay (Figure 30 and Figure 32). Although the transduction rate was lower than the reference compound Tat-FITC, the LB-01 scaffold displays all the characteristics previously described for cell penetrating peptides. However, the influence of N-methylation on the transduction rate remains to be investigated.

3.2 Thanatin

3.2.1 Synthesis and Analysis of Thanatin

Thanatin (GSKKPVPIIYCNRRTGKCQRM, Figure 33) was synthesized following the procedure of Fehlbaum *et al.*[71]. The enantiomeric D-thanatin was synthesized analogously with D-amino acids. The purity of the two compounds was confirmed by UPLC analysis (Figure 34) and the identity by HR-ESI (Table 10). A ^{1}H NMR spectrum was recorded for thanatin (Figure 35).

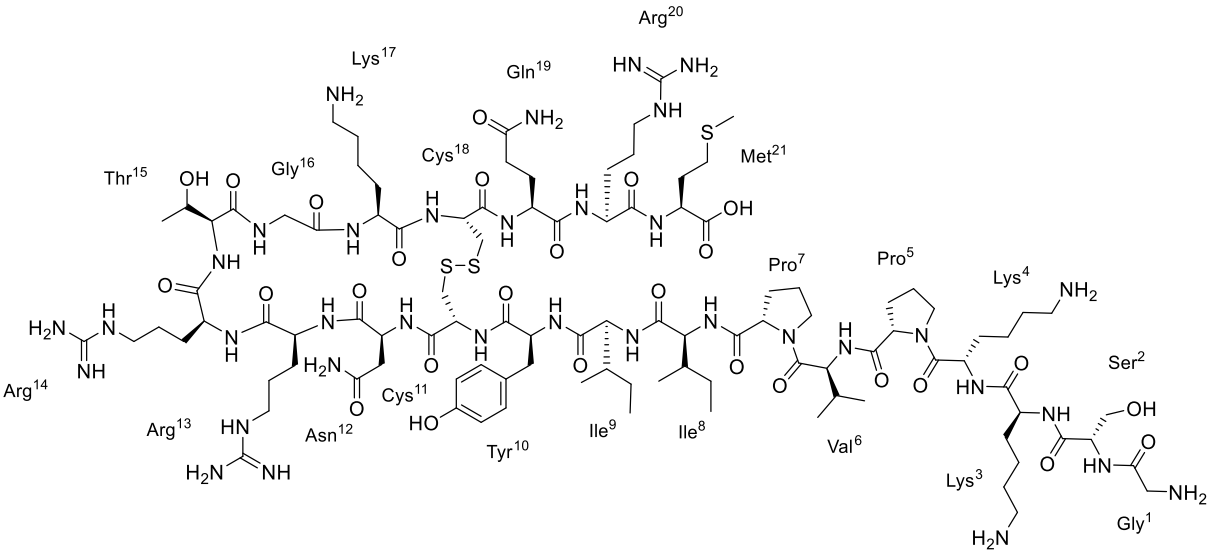

Figure 33 Thanatin drawn in a hairpin structure.

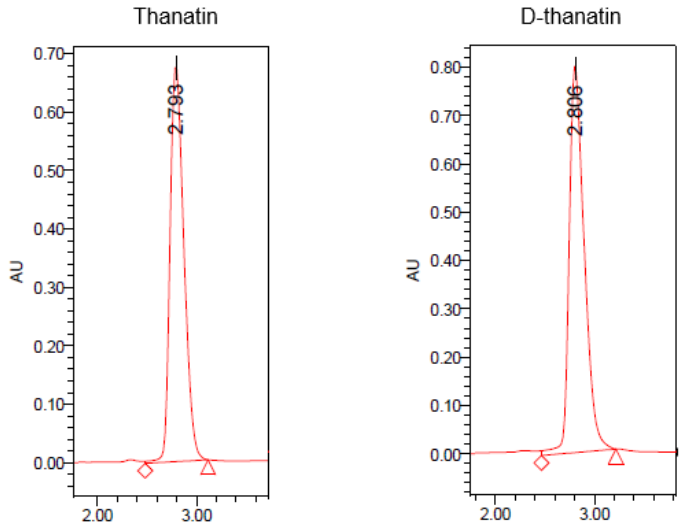

Figure 34 UPLC chromatograms of thanatin and D-thanatin at 226 nm wavelength, run with a linear gradient of 10 to 40% MeCN/H_2O with additional 0.1% TFA on a C18 reverse-phase column.

Table 10 Calculated mass and experimental m/z values of thanatin and D-thanatin measured by high resolution ESI.

Analogue	Exact mass (calc.)	m/z (HR-ESI)
Thanatin	487.4621 $[M+5H]^{5+}$	487.4620 $[M+5H]^{5+}$
D-thanatin	487.4621 $[M+5H]^{5+}$	487.4635 $[M+5H]^{5+}$

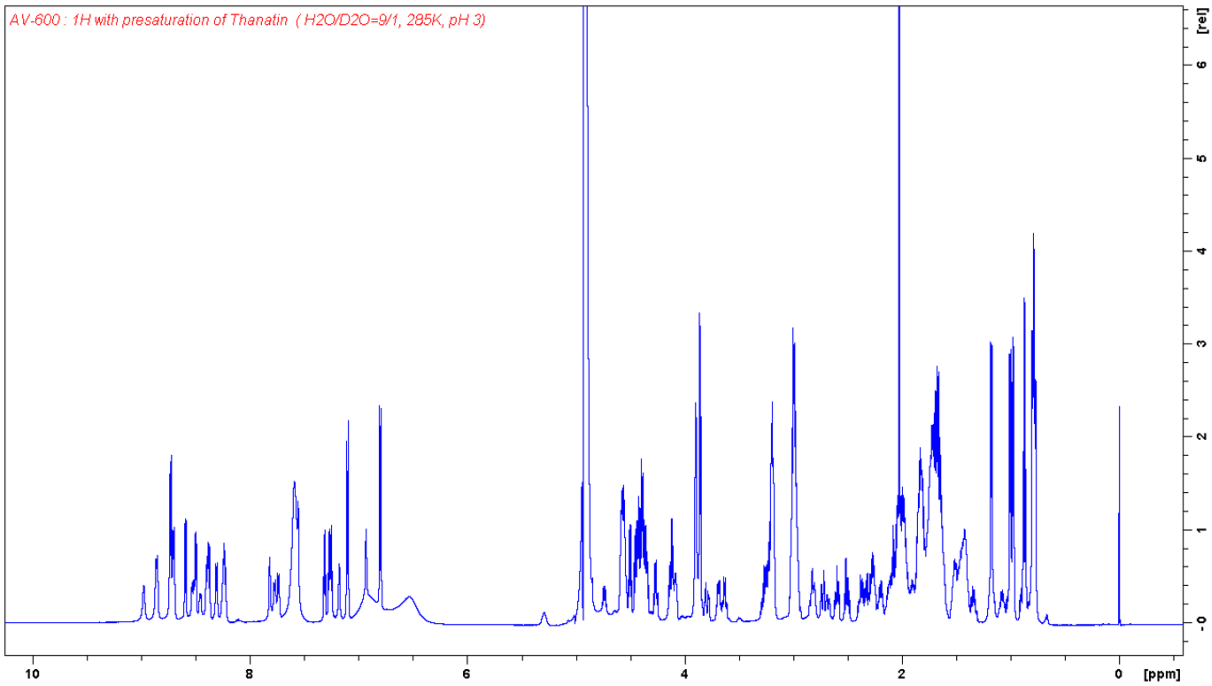

Figure 35 ^{1}H-NMR spectrum of thanatin.

3.2.2 Design of a Stabilized Thanatin β-Hairpin

In an attempt to improve the antimicrobial activity and the metabolic stability towards proteases, the β-hairpin moiety and the flexible N-terminal domain of thanatin were transformed into a more rigid, backbone circular molecule by introduction of the well-established ^{D}Pro-^{L}Pro template. Since the N-terminal truncated isoforms of thanatin retained activity as demonstrated by Fehlbaum *et al.*[71] (cf. Introduction 1.10), the idea was to use Pro5 as an anchor to introduce the ^{D}Pro-^{L}Pro template at this position, and move the two Lys residues at position 3 and 4 to the other side of the hairpin (Figure 36). The compound was synthesized according to the method of Srinivas *et al.*[46]. The purity of the compound was confirmed by UPLC analysis (Figure 37) and the identity was verified by HR-ESI with a calculated mass of 592.8229 $[M+4H]^{4+}$ and a measured m/z value of 592.8224 $[M+4H]^{4+}$.

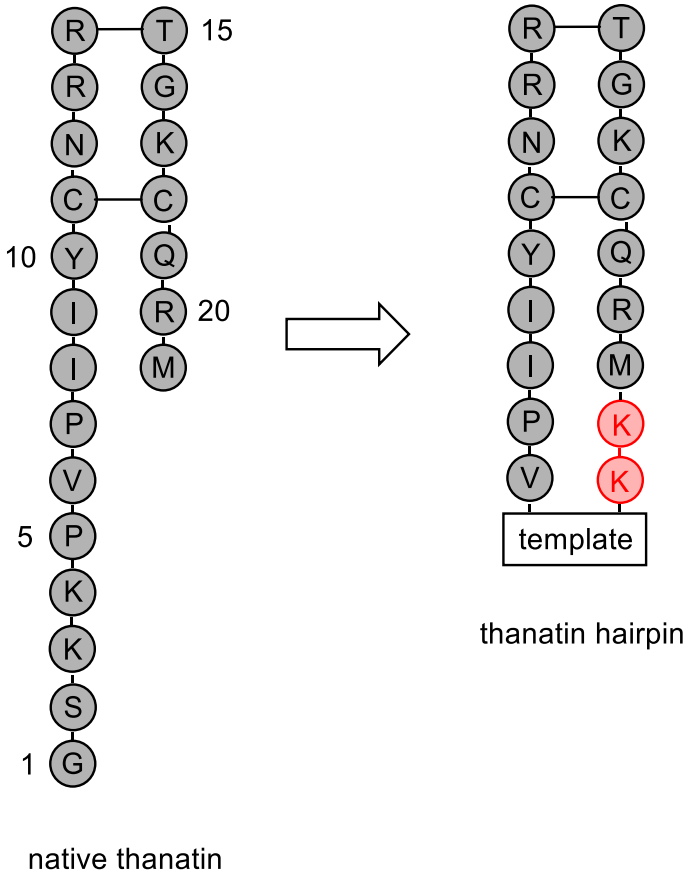

Figure 36 Design of a fully circular thanatin β-hairpin. A ^{D}Pro-^{L}Pro template is introduced and the two Lys residues (red) moved to the other side of the molecule.

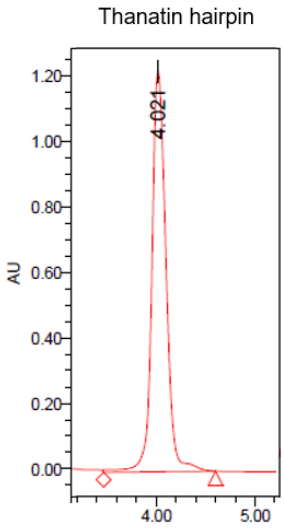

Figure 37 UPLC chromatogram of the circular thanatin hairpin at 226 nm wavelength, run with a linear gradient of 10 to 40% MeCN/H_2O with additional 0.1% TFA on a C18 reverse-phase column.

3.2.3 Antimicrobial Activity

Antimicrobial activity of thanatin on *E. coli ATCC25922* was determined by the MIC microdilution method, yielding an MIC value of 0.5 µg/ml. Enantiomeric D-thanatin was confirmed inactive (> 64 µg/ml). Native thanatin and the newly designed hairpin were tested on a series of Gram-positive and Gram-negative bacteria available in our lab. With the exception of *Bacillus subtilis* DMSZ with a mediocre MIC of 8 µg/ml, none of the treated bacteria in Table 11 showed any response to these two compounds.

Table 11 MIC values of native thanatin compared to the designed circular hairpin. Values were determined by microdilution in MH-II with addition of 0.002% Tween80.

MIC [µg/ml]	Native thanatin	Thanatin hairpin
A. baumanii	>64	>64
S. aureus	>64	>64
***P. aeruginosa* PAO1**	>64	>64
***P. aeruginosa* ATCC27853**	>64	>64
Burkholderia cenocepacia	>64	>64
***Bacillus subtilis* DSMZ**	8	>64

The two compounds were further tested on a series of clinical *E. coli* isolates with broad antimicrobial resistance.[29] Although native thanatin exhibits good activity against all of them except *E. coli* 2144E/2155 (colistin resistant), the hairpin remained completely inactive (Table 12). Unfortunately this particular hairpin design did not lead to improved antimicrobial properties and was therefore abandoned. Studies were continued with native thanatin.

Table 12 MIC values of native thanatin and the designed hairpin compared against clinical *E. coli* isolates (adapted from Urfer *et al.*)[29]. Values were determined by microdilution in MH-II with addition of 0.002% Tween80.

Strain/antibiotic	*E. coli* ATCC 25922	*E. coli* 2138E/ 2151	*E. coli* 2139E/ 2152	*E. coli* 2140E/ 2153	*E. coli* 2143E/ 2154	*E. coli* 2144E/ 2155	*E. coli* 3459E/ 2150
Thanatin	0.5	0.5	0.5	0.5	1	>32	0.5
Thanatin hairpin	>32	>32	>32	>32	>32	>32	>32
Colistin	0.12	0.12	0.03	0.06	0.06	16	0.06
Gentamycin	0.5	1	0.5	8	1	0.06	1
Ceftriaxone	0.06	0.06	0.06	0.06	0.12	1	>64
Ampicillin	16	>64	>64	>64	>64	0.12	>64
Rifampicin	32	64	64	64	>64	0.12	8
Erythromycin	>64	>64	64	64	64	0.12	>64
Azithromycin	8	8	4	8	4	1	4
Ciprofloxacin	0.008	0.12	0.02	0.01	0.02	0.25	0.12

3.2.4 Sytox® Green Assay in MH-I

Sytox® Green is a dye commonly used to measure cell viability and susceptibility to certain antibiotics.[95] The fluorescent dye does not penetrate living cells. However, cells with compromised plasma membranes allow access of the dye to the cytoplasm, which then fluoresces bright green upon interaction with nucleic acids. Polymyxin B is a known membrane permeabilizer and served as a positive control in the following experiments. Although its mechanism of action is still under investigation, it has been shown that cationic polymyxin B interacts with the negatively charged lipid A component of LPS, displacing divalent cations such as Ca^{2+} and Mg^{2+}, leading to a destabilization of the outer membrane.[96] The effect of thanatin on *E. coli* ATCC25922 cells was measured at a high concentration of 100 µg/ml, which is significantly above the MIC. Every spectrum is the mean value of three measurements performed under the same conditions with different cultures over the course of 1 h (Figure 38). The three graphs were normalized to the baseline signal at 440 s. This was done to account for the variations in background signal, stemming from the MH-I media and its residual DNA.

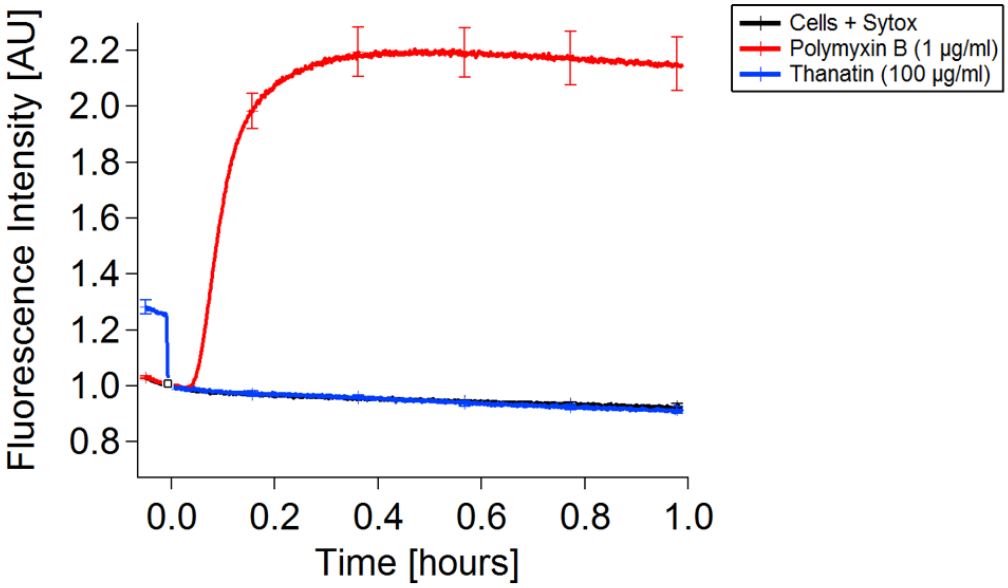

Figure 38 Fluorescence increase of *E. coli* ATCC25922 cells in MH-I treated with polymyxin B and thanatin in presence of Sytox® Green. Control with cells and Sytox® Green but no addition of antibiotics. Signal intensity is normalized to the baseline signal at 440 s.

E. coli cells were mixed with Sytox® Green in MH-I medium and fluorescence intensity was monitored until a stable signal was obtained. Then, addition of polymyxin B at a concentration of 1 µg/ml led to a fast increase of fluorescence by interaction of Sytox® Green with nucleic acid, indicating a strong permeabilization of the inner and outer membrane. As expected, no fluorescence increase was monitored for the negative control, which contained no antibiotic. Even though thanatin was added at a high concentration of 100 µg/ml, it did not lead to any increase in fluorescence, showing that the dye is unable to access the cytoplasm of the cell.

3.2.5 Sytox® Green Assay in HEPES Buffer

In order to repeat the assay in a medium-free environment with a low nucleic acid background, 5 mM HEPES ((4-(2-hydroxyethyl)-1-piperazineethanesulfonic acid)[97] at pH 7.2 was chosen. Under these conditions, cells are not able to grow, while remaining intact over the course of a number of hours. Ciprofloxacin is an inhibitor of DNA replication and served as a negative control. Its mechanism of action comprises binding to topoisomerase II (DNA-gyrase) and topoisomerase IV resulting in strong antimicrobial activity against a wide range of Gram-negative and certain Gram-positive bacteria.[98,99] The effect of thanatin and D-thanatin on *E. coli* ATCC25922 cells was measured at concentrations of 10 µg/ml and 100 µg/ml. Every spectrum is the mean value of three measurements performed under the same conditions with different cultures (Figure 39).

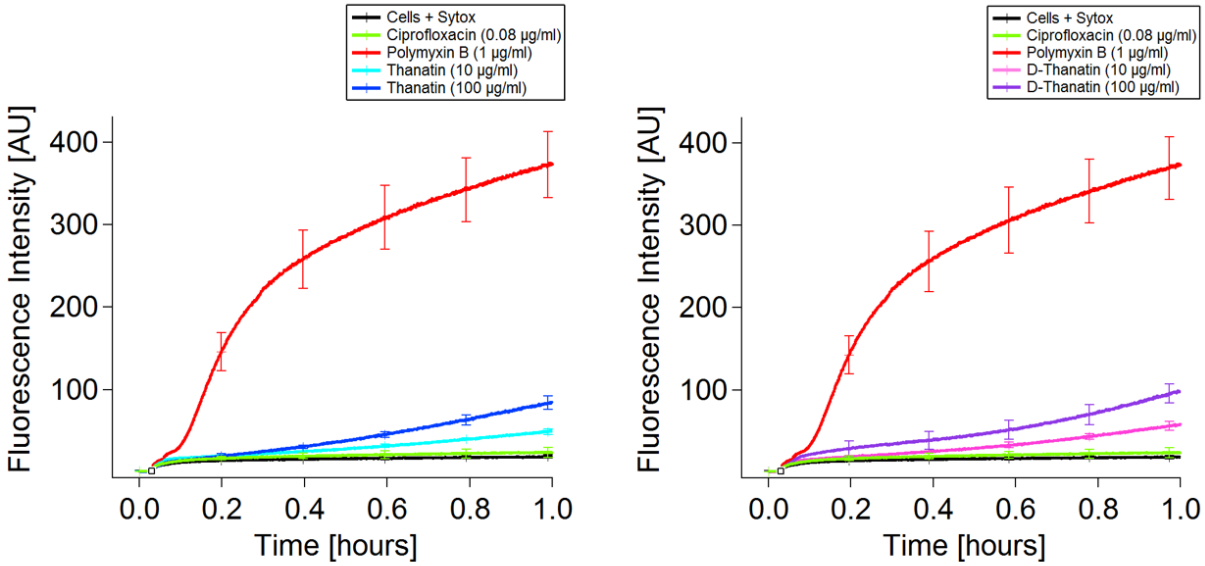

Figure 39 Fluorescence increase of *E. coli* ATCC25922 cells in HEPES (5 mM, pH 7.2) treated with polymyxin B, thanatin and D-thanatin in presence of Sytox® Green.

Addition of polymyxin (1 µg/ml) led to a fast increase in fluorescence similar to the experiment performed in MH-I (cf. Figure 38), though the plateau was reached later. Addition of ciprofloxacin (0.08 µg/ml) or H_2O (control) did not lead to any increase of fluorescence, confirming the assumption that the membrane stayed intact over the 1 h measurement. Thanatin and D-thanatin both led to a similar, small increase in fluorescence with an approximately two-fold higher signal for the 100 µg/ml concentration compared to 10 µg/ml. Since the D-enantiomer of thanatin is completely inactive against *E. coli* ATCC25922, it is apparent that the observed effect was not caused by a stereospecific interaction with a target.

To test whether this observed fluorescence increase is caused by an inherently weakened membrane, the HEPES buffer (5 mM, pH 7.2) was supplemented with $MgCl_2$ (0.5 mM) and $CaCl_2$ (1 mM). This was done in order to strengthen the outer membrane by introducing divalent cations (i.e. Mg^{2+} and Ca^{2+}), which are known to bridge and stabilize the LPS outer membrane monolayer.[96] The effects of polymyxin B (1 µg/ml), thanatin, and D-thanatin (both 100 µg/ml) treatment were determined under the same experimental conditions as described above.

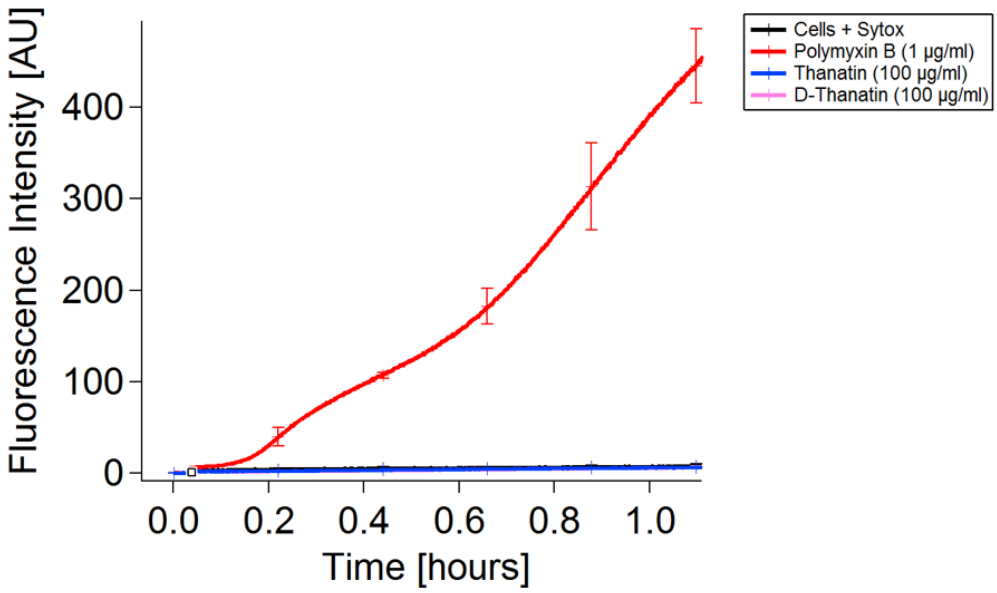

Figure 40 Fluorescence increase of *E. coli* ATCC25922 cells in HEPES (5 mM, pH 7.2) supplemented with $MgCl_2$ (0.5 mM) and $CaCl_2$ (1 mM) treated with polymyxin B, thanatin and D-thanatin in presence of Sytox® Green.

The addition of polymyxin (1 µg/ml) led to an initially slower increase in fluorescence compared to the experiment described above (cf. Figure 39), although a similar intensity of approximately 400 units was reached after 1 h. For thanatin and D-thanatin (both 100 µg/ml), no fluorescence increase was observed.

These results lead to the conclusion, that the mechanism of action of thanatin does not involve full membrane permeabilization under physiological conditions.

3.2.6 β-Galactosidase Assay

An assay that gives additional information on membrane permeabilization is the measurement of β-galactosidase activity towards ONPG (o-nitrophenyl-β-galactoside), a glycoside which can be used in colorimetric assays.[100] The *E. coli* ML-35::pET3a clone used in this experiment exhibits a constitutive (chromosomal) β-galactosidase expression in the cell cytoplasm and is permease deficient.[101] Release of β-galactosidase into the culture media, due to permeabilization of the membrane, can be detected by hydrolysation of the OPNG substrate into yellow coloured ortho-nitrophenol and D-galactose. The effect of protegrin-1 – a known lytic peptide – and thanatin were determined at different concentrations. Ciprofloxacin – an inhibitor of DNA replication – served as a negative control. Data points were averaged from three independent experiments (Figure 41).

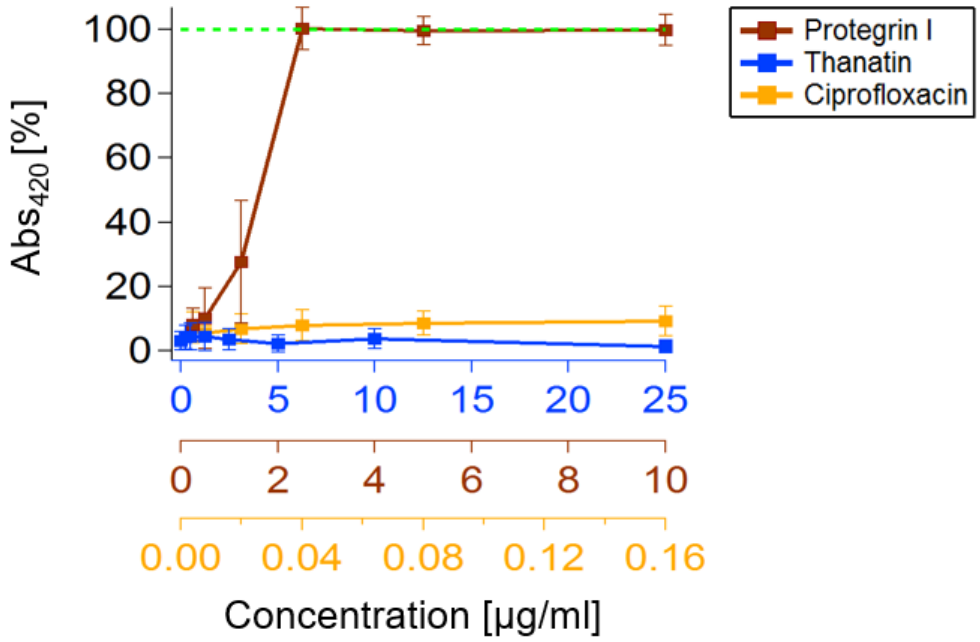

Figure 41 β-Galactosidase assay with ONPG *(o*-nitrophenyl-β-galactoside) as substrate on *E. coli* ML-35::pET3a grown in MH-II media. Light absorption is measured at 420 nm. The green dashed line represent the 100% cell permeabilization (lysed cells).

Protegrin-1 led to a strong release of intracellular β-galactosidase, reaching the 100% plateau achieved by sonication of a control sample, at concentrations higher than 2.5 µg/ml. As expected, ciprofloxacin, with its non-lytic mechanism of action, showed no β-galactosidase activity. Thanatin had no effect on the β-galactosidase release, indicating no permeabilization of the inner and outer membrane.

3.2.7 β-Lactamase Assay

Selective permeabilization of the outer membrane was measured by periplasmatic β-lactamase activity towards CENTA, a chromogenic β-lactamase substrate.[102] The *E. coli* ML-35::pET3a clone described above was also used for this experiment, since the pET3a plasmid carries the necessary *bla* gene coding for β-lactamase. Using this clone, β-lactamase is produced and excreted into the periplasm. Hence, any antibiotic that permeabilizes the outer membrane will lead to a release of the enzyme into the culture medium, where its activity can be detected using CENTA. Data points were averaged from three independent experiments with protegrin-1, thanatin, and ciprofloxacin (Figure 42).

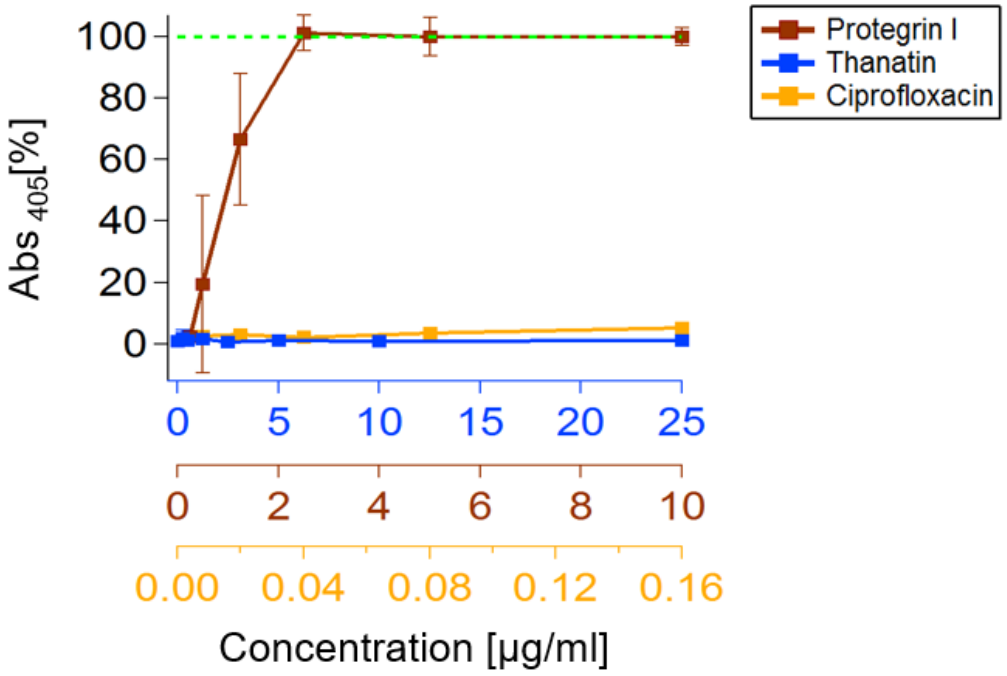

Figure 42 β-Lactamase assay with CENTA as a substrate on *E. coli* ML35::pET3a grown in MH-II media. Light absorption is measured at 405 nm. The green dashed line represents 100% cell permeabilization (lysed cells).

Similar to the β-galactosidase assay (cf. Figure 41), protegrin-1 showed a strong release of periplasmatic β-lactamase at concentrations higher than 2.5 µg/ml, with a stable plateau equal to the 100% maximum. As expected, ciprofloxacin exhibited non-lytic behaviour and therefore no effect on β-lactamase release. Thanatin also has no effect on the β-lactamase release. Taken together, thanatin does not seem to have any perturbation effect on the outer nor the inner membrane.

3.2.8 Macromolecular Synthesis Assay

The following study was carried out in collaboration with Matthias Urfer. Potential inhibition on macromolecular synthesis (i.e. DNA, RNA, proteins, cell wall) was monitored by incorporation of [^{3}H]-labelled precursors in a defined medium (DM) in *E. coli* ATCC25922 using [^{3}H]-thymidine, [^{3}H]-uridine, [^{3}H]-leucine, and [^{3}H]-N-acetylglucosamine. Control experiments were performed with known inhibitors of DNA-synthesis (tobramycin[103]), RNA-polymerase (rifampicin[104]), cell wall biosynthesis (ceftriaxone[105]), and protein biosynthesis (ciprofloxacin[98]). The observed effects are shown in Figure 43.

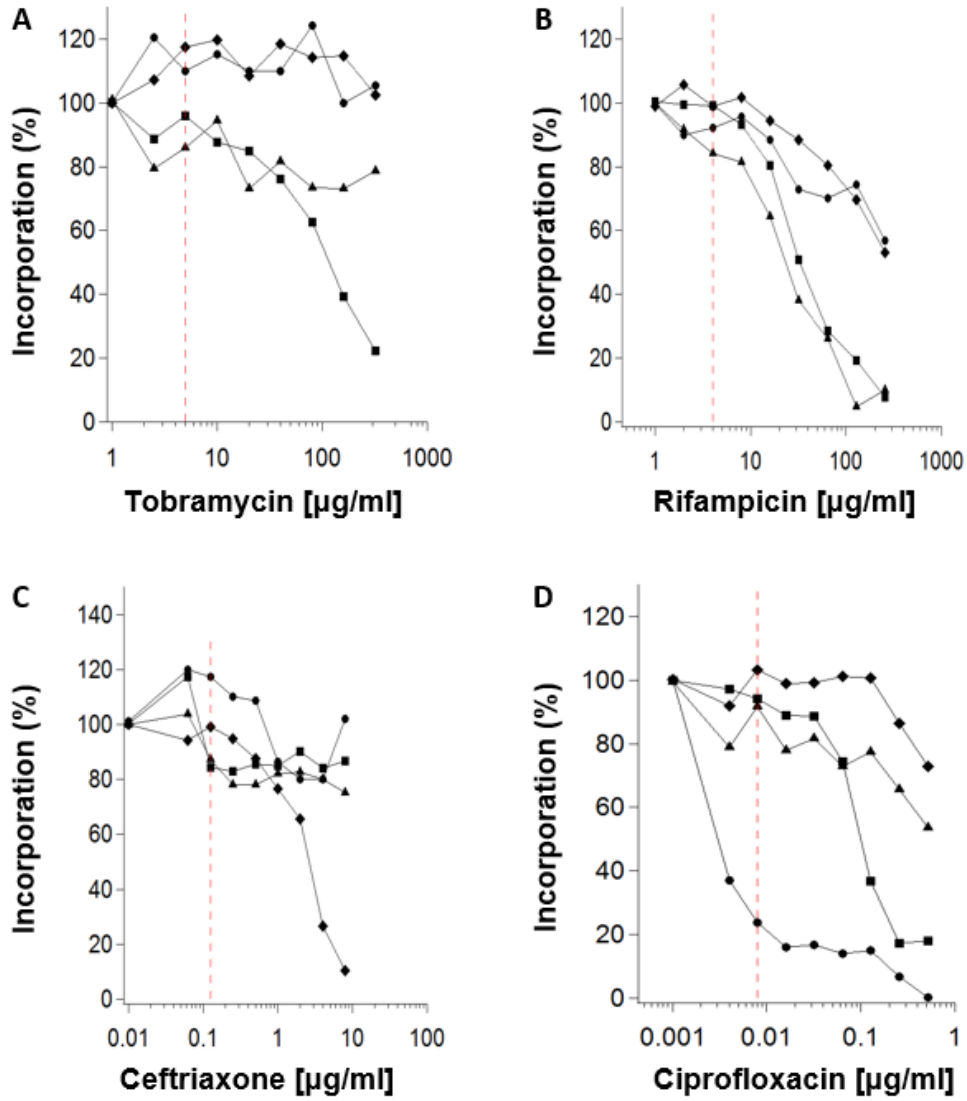

Figure 43 The effect of reference antibiotics tobramycin (A), rifampicin (B), ceftriaxone (C), and ciprofloxacin (D) targeting macromolecular synthesis in *E. coli* ATCC25922. Incorporation of [^{3}H]-precursors of DNA (circles), RNA (triangles), protein (squares), and cell wall (diamonds) were examined. The MIC value for each compound is indicated by a vertical red dashed line.

In the case of thanatin, no effects upon the incorporation of labelled precursors into DNA, RNA, and proteins were observed in three individual experiments (Figure 44). However, the incorporation of [^{3}H]-N-acetylglucosamine was significantly higher than in the control experiments, suggesting a stimulation of the incorporation of this precursor, possibly into components of the polysaccharide coat at the cell surface, or into precursors for LPS biosynthesis.

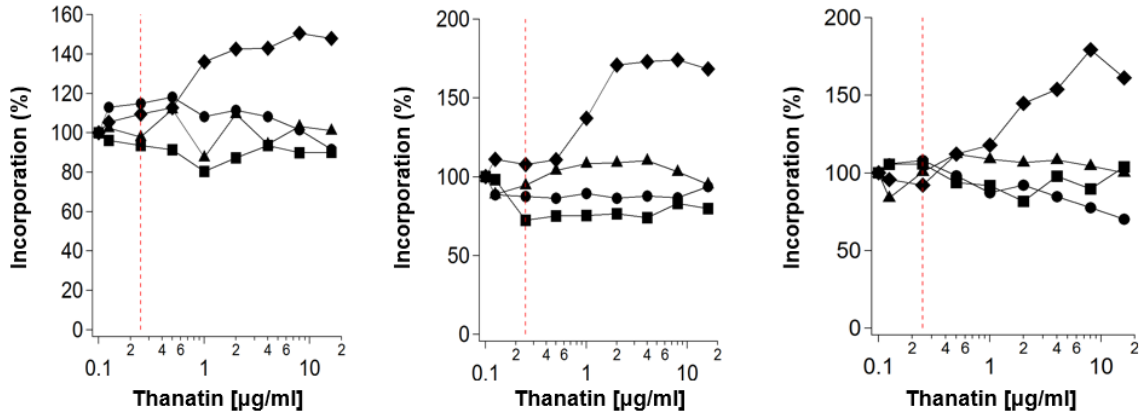

Figure 44 The effect of thanatin on the macromolecular synthesis in *E. coli* ATCC25922 of three individual experiments. Incorporation of [^{3}H]-precursors of DNA (circles), RNA (triangles), protein (squares), and cell wall (diamonds) were examined. An MIC value of 0.25 µg/ml is indicated by a vertical red dashed line.

3.2.9 Live Cell Fluorescence Microscopy

The effect of thanatin on live *E. coli* ATCC25922 cells was studied by confocal fluorescence microscopy. Images were recorded at the Center of Microscopy and Image Analysis (ZMB) UZH by Matthias Urfer. The red dye FM4-64[106] was used to highlight membranes and the blue dye DAPI was used for DNA staining. Sytox® Green was used to identify dead cells. An untreated sample is shown in Figure 45. The cells exhibit a well-rounded shape of single cells or paired cells with a distinct membrane. No detection in the Sytox® Green channel indicated, that all cells were alive during imaging.

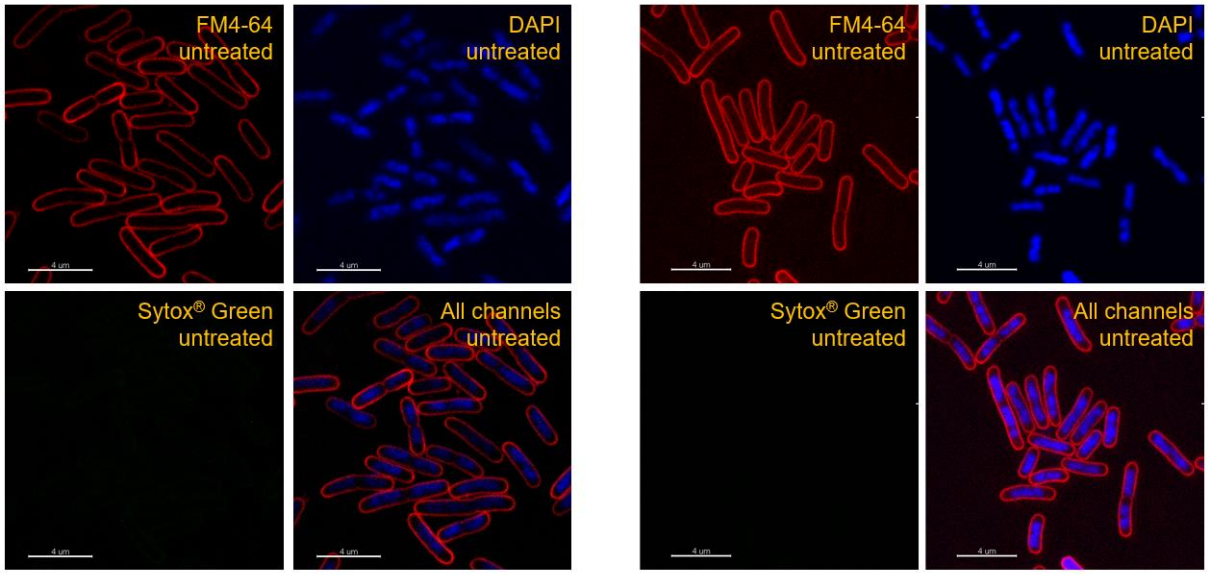

Figure 45 Untreated sample of *E. coli* ATCC25922 with FM4-64 membrane staining (red), DAPI staining of DNA (blue) and Sytox® Green for dead cells staining.

Thanatin was added in a concentration of 5 µg/ml and the cells were incubated for 1 h at 30°C before imaging. Two obvious differences could be observed compared to the untreated sample: An accumulation of unusual membrane-like material highlighted by bright red knobs stained with FM4-64 and an assembly of multiple cells in elongated structures (Figure 46). This assembly can likely be explained by a general stress response and/or difficulties to separate after cell division. However, no permeabilization of the membrane was observed due to lack of a signal in the Sytox® Green channel.

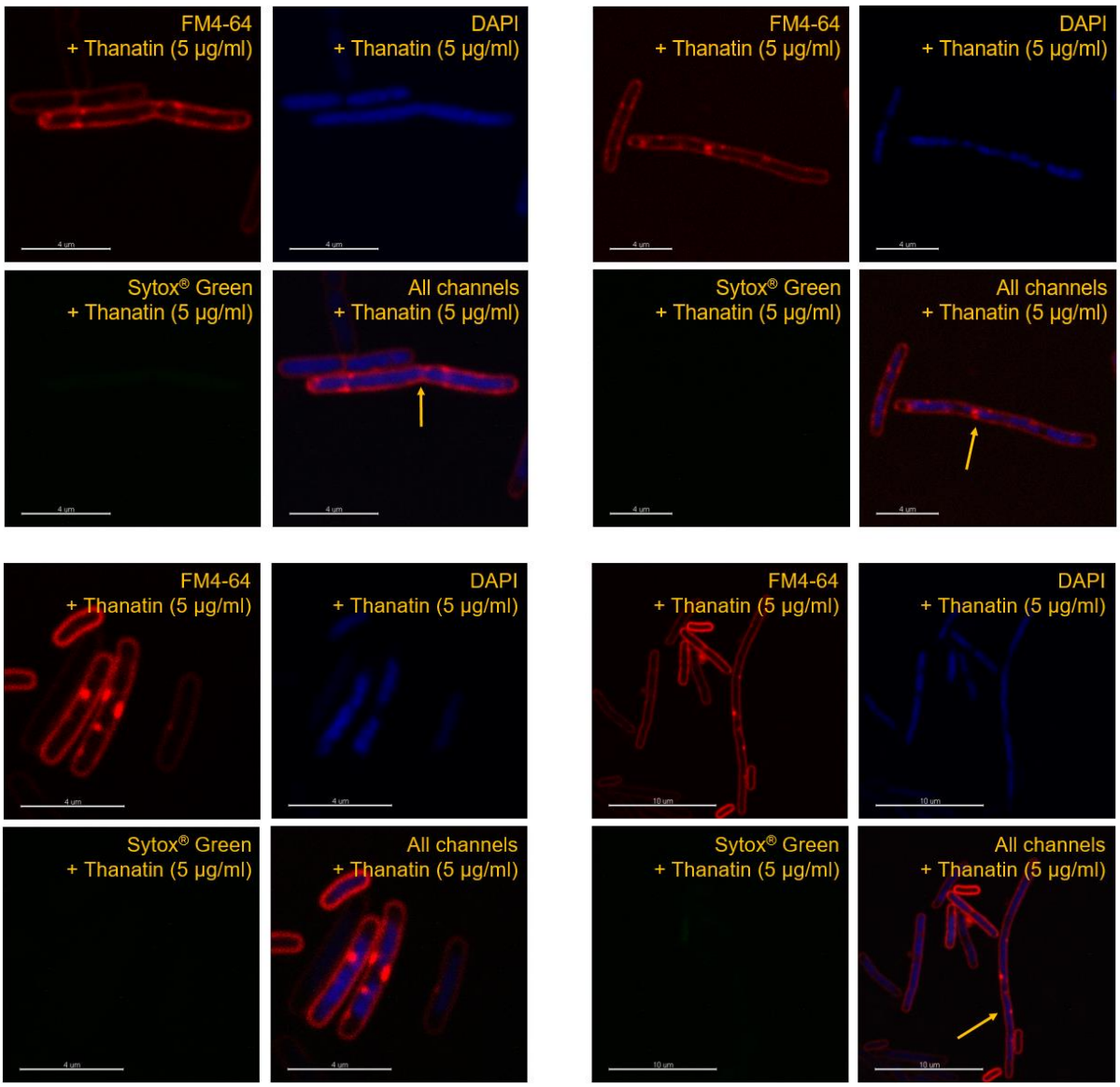

Figure 46 Two sets of images with thanatin (5 µg/ml) treated sample of *E. coli* ATCC25922 with FM4-64 membrane staining (red), DAPI staining of DNA (blue), and Sytox® Green for dead cells staining. Arrows highlight multiple cells in elongated structures and difficulties to separate after cell division.

With higher concentrations of thanatin (10 µg/ml), the elongation effect became even more apparent. A weak signal in the Sytox® Green channel in the bottom left picture was detected (Figure 47), indicating dead cells.

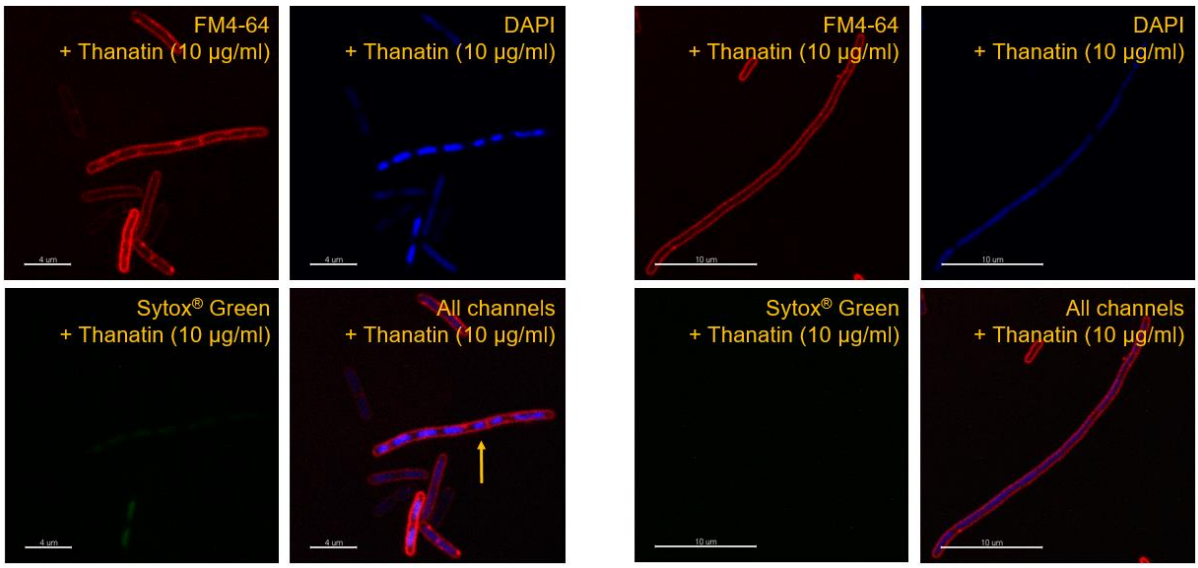

Figure 47 Thanatin (10 µg/ml) treated sample of *E. coli* ATCC25922 with FM4-64 membrane staining (red), DAPI staining of DNA (blue) and Sytox® Green for dead cells staining. Arrow highlights multiple cells in elongated structure and difficulties to separate after cell division.

3.2.10 Fluorescence Microscopy with Probe Thanatin-BDP-FL

A fluorescent probe of thanatin was synthesized by coupling a BODIPY[107] fluorophore at the N-terminus (thanatin-BDP-FL, Scheme 6). This probe was used for confocal fluorescence imaging of paraformaldehyde fixed *E. coli* ATCC25922 cells. The spectral properties of BDP-FL are similar to fluorescein with higher photostability and good water solubility. The linear thanatin sequence was synthesized as described earlier and then a commercially available PEG (polyethylene glycol) spacer carrying an alkyne group (propargyl-PEG_4-acid, *Broadpharm*) was coupled on-resin under standard conditions with HATU/HOAt. After cleavage from the resin, oxidation, and purification of the intermediate by preparative HPLC, BDP-FL-azide (*Lumiprobe*) was coupled by Click Chemistry as described later (Experimental Part 4.4). The purity of thanatin-BDP-FL was confirmed by UPLC (Figure 48) and its identity by HR-ESI with a calculated mass of 763.1505 $[M+4H]^{4+}$ and an experimental m/z value of 763.1500 $[M+4H]^{4+}$. The molecule also showed good antimicrobial activity with an MIC of 0.5 - 2 µg/ml on *E. coli* ATCC25922.

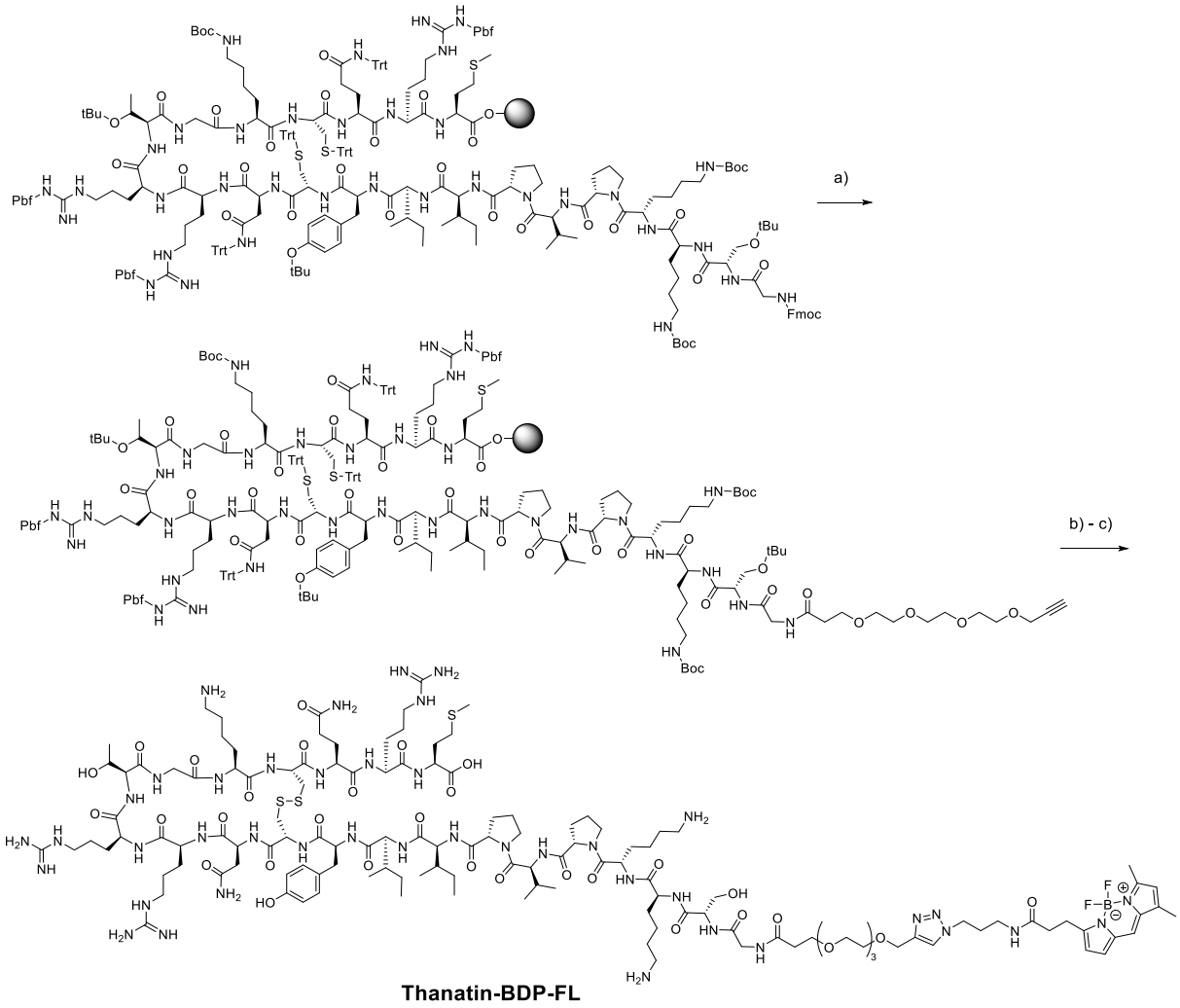

Scheme 6 Synthesis of fluorescent probe thanatin-BDP-FL: a) Piperidine:DMF (1:3), then propargyl-PEG$_4$-acid, HATU, HOAt, DIPEA, DMF. b) TFA:EDT:thioanisole:H_2O:TIS (75:10:10:4:1), then oxidation by air in 0.1 M ammonium acetate pH 8.5. c) BDP-FL-azide, $CuSO_4$, sodium ascorbate, DMSO:H_2O (1:5).

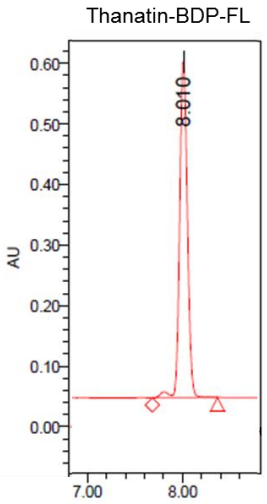

Figure 48 UPLC chromatogram of thanatin-BDP-FL at 226 nm wavelength, run with a linear gradient of 10 to 40% MeCN/H_2O with additional 0.1% TFA on a C18 reverse-phase column.

E. coli ATCC25922 cells were incubated with thanatin-BDP-FL at a concentration of 4 - 8 µg/ml and an incubation time of 2 h. The cells were fixated with paraformaldehyde before imaging. The conjugate was taken up efficiently and with a good distribution inside the cells. Similar to the images described above, elongation of multiple cells was observed along with an accumulation of membrane-like material in green knobs. Additionally, a distinct accumulation of thanatin-BDP-FL at the cell poles and junctions in certain cells was observed (Figure 49).

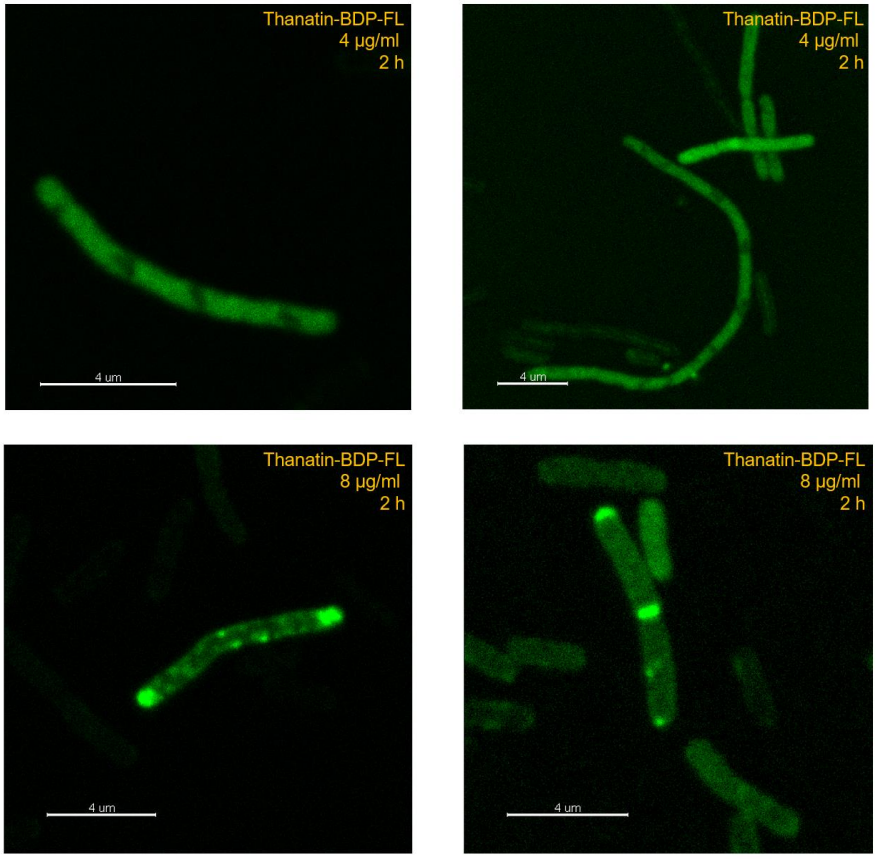

Figure 49 *E. coli* ATCC25922 cells treated with thanatin-BDP-FL (4 and 8 µg/ml) were fixed by paraformaldehyde before imaging.

3.2.11 Photoaffinity Labelling

Photoaffinity labelling (PAL) was applied here to identify possible interaction partners of thanatin. PAL is a technique developed in the 1960's by Westheimer *et al.*[108] to covalently link a photo-reactive label to a larger molecule (e.g. a protein) with UV-light. A recent review by Ewan Smith and Ian Collins describes the broad application range of PAL in studying ligand-protein interactions. In order to facilitate the isolation and detection of a crosslinked binding partner, the incorporation of a reporter group becomes necessary. The most popular affinity tag in use today is biotin, due to its extremely high affinity towards streptavidin. Different photo-reactive groups can be incorporated such as benzophenones, phenylazides, and diazirines to form highly reactive diradicals, nitrenes, and carbenes, respectively. However, diazirines have a number of advantages when applied in a biological system. They are chemically stable and irradiation with a wavelength of 350 nm reduces potential damage to the cellular environment. The reactive singlet-carbene (Figure 50), formed upon irradiation has a short half-live, rapidly forming a covalent crosslink to its target molecule, which leads to fewer side reactions.[109]

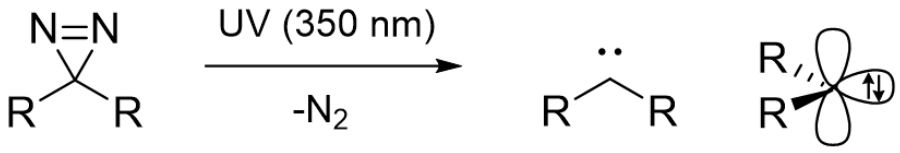

Figure 50 Formation of a highly reactive singlet-carbene upon UV irradiation.

Suchanek *et al*.[110] demonstrated the incorporation of the radioactively labelled diazirine containing amino acids photo-methionine and photo-leucine into proteins by the unmodified mammalian translation machinery, in order to study protein-protein interactions of membrane proteins involved in cellular lipid homeostasis. An efficient synthesis of photo-phenylalanine was described by Nakashima *et al.*[111] and used to specifically label the protein calmodulin (CaM) in a calcium-dependent manner by photo-reactive calmodulin-binding peptide (CaMBP), containing this amino acid together with a biotin linker. Our group previously showed that the incorporation of photo-proline[112] and photo-leucine[113], with a biotin linker, can be used for mechanism of action studies of antibiotics.

PAL probe thanatin-PAL5 was designed with an N-terminal biotin linker and a reactive diazirine group at position Pro5. The synthesis and incorporation of Fmoc-L-photoPro was performed according to the procedure described by van der Meijden and Robinson.[112] The linear thanatin sequence was synthesized as described earlier and the commercially available biotin-PEG_4-acid building block (*Broadpharm*) was coupled on-resin under standard conditions with HATU/HOAt (Scheme 7). After coupling, the peptide was cleaved from the resin, oxidized, and purified by preparative HPLC. The purity of thanatin-PAL5 was confirmed by UPLC (Figure 51)

and its identity by HR-ESI with a calculated mass of 587.3041 $[M+5H]^{5+}$ and an experimental m/z value of 587.3041 $[M+5H]^{5+}$. The diazirine group at position Pro5 is supposed to form a covalent cross-link to any interaction partner upon irradiation, whereas the biotin group is used for detection in a Western blot by chemiluminescence via a horseradish peroxidase NeutrAvidin conjugate (NeutrAvidin-HRP, *Pierce*).

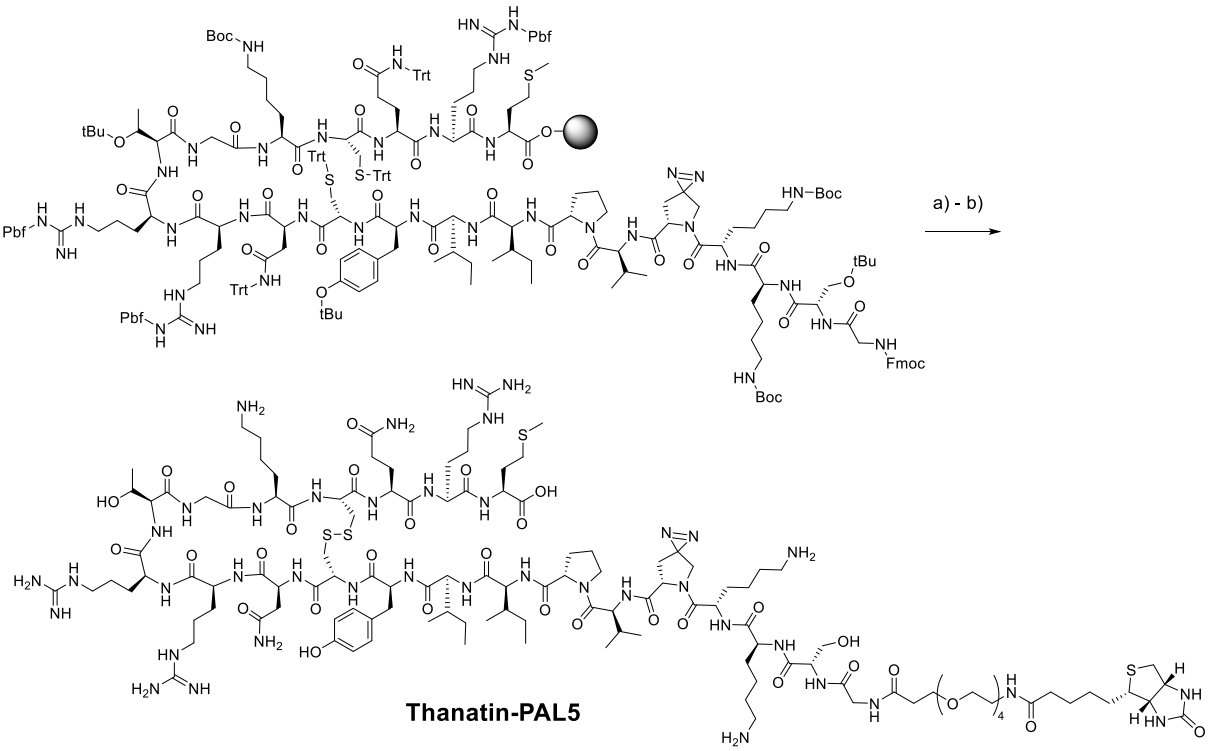

Scheme 7 Synthesis of PAL probe thanatin-PAL5: a) Piperidine:DMF (1:3), then Biotin-PEG_4-acid, HATU, HOAt, DIPEA, DMF. b) TFA:EDT:thioanisole:H_2O:TIS (75:10:10:4:1), then oxidation by air in 0.1 M ammonium acetate pH 8.5.

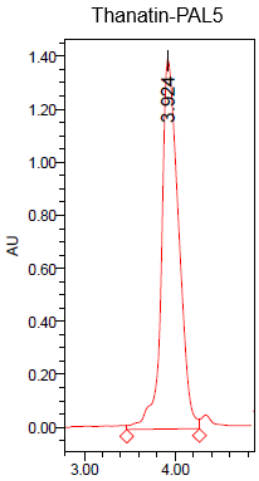

Figure 51 UPLC chromatogram of thanatin-PAL5 at 226 nm wavelength, run with a linear gradient of 10 to 40% MeCN/H_2O with additional 0.1% TFA on a C18 reverse-phase column.

Thanatin-PAL5 showed a 4-8 times higher MIC against *E. coli* ATCC25922 compared to the parent compound (2 - 4 µg/ml versus 0.5 µg/ml). Photolabelling of whole *E. coli* cells was performed at a concentration of 10 µg/ml and 2 µg/ml thanatin-PAL5. Additionally, a competition experiment was performed, in which a 20-fold excess of native thanatin (200 µg/ml) was preincubated with the cells before adding the photoprobe (10 µg/ml). For the control experiment, cells were treated in the same manner as described below, but without addition of the photoprobe. The cells were preincubated for 30 min with the photoprobe and then irradiated at 350 nm wavelength in a Rayonet reactor for 30 min. After cell lysis, the insoluble fractions, containing mainly membrane proteins, were isolated by differential ultracentrifugation and analysed by polyacrylamide gel electrophoresis (SDS-PAGE). Proteins were transferred onto a PVDF (polyvinylidene difluoride) membrane by the Western blotting technique[114] for subsequent biotin detection. The gel was blotted under conditions optimized for larger membrane proteins to ensure optimal transfer.[115] Biotin detection of the sample treated with 10 µg/ml thanatin-PAL5 (lane 2) showed at least four distinct bands in the Western blot around 100 kDa, 45 kDa, 40 kDa, and 20 kDa, plus a faint band below 75 kDa (Figure 52). For the sample treated with 2 µg/ml thanatin-PAL5 (lane 3), the same labelling pattern was observed, when the blot was exposed for a longer period of time. However, the competition with native thanatin led to a disappearance of the 100 kDa band, whereas the other bands remained visible when exposed for a longer time, suggesting a displacement of the photoprobe at the potential binding site within the 100 kDa protein. No signal could be detected for the control sample (lane 1). The Coomassie staining confirmed the loading of approximately equal amounts of protein for all samples.

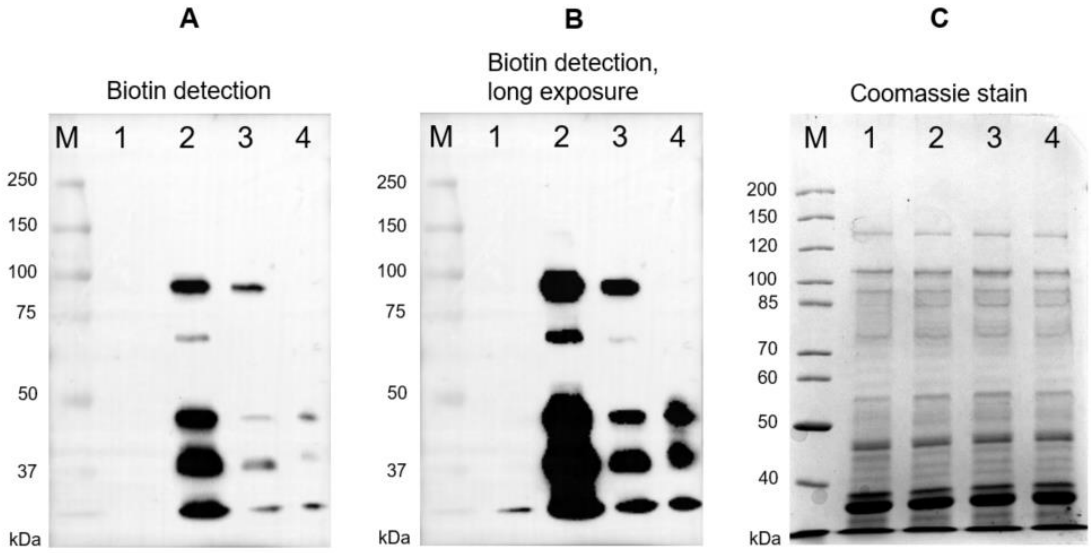

Figure 52 Western blots (A+B) and SDS-PAGE (C) of *E. coli* ATCC25922 membrane fractions from 10% self-casted polyacrylamide gels. Lanes: M) molecular-weight marker, 1) control, 2) thanatin-PAL5 (10 µg/ml), 3) thanatin-PAL5 (2 µg/ml), 4) thanatin-PAL5 (10 µg/ml) + native thanatin (200 µg/ml). Blotting for 2 h (10 V, 0.5 A) with urea transfer buffer. Biotin detection by chemiluminescence with NeutrAvidin-HRP 1:30'000 and WesternBright™ Sirius™ HRP substrate. Exposure times: 92 s (blot A), 536 s (blot B).

Gel electrophoresis of the membrane protein extract treated with 2 µg/ml thanatin-PAL5 was repeated under non-reducing conditions (without DTT) before Western blotting. A distinct mass shift of the band at 100 kDa to approximately 130 kDa was observed (Figure 53). This mass shift was previously described in the literature as a characteristic feature of the outer membrane protein LptD.[40] The effect is caused by a difference in mobility upon reduction of the two disulfide bonds in *E. coli* LptD, in comparison to the unreduced form.

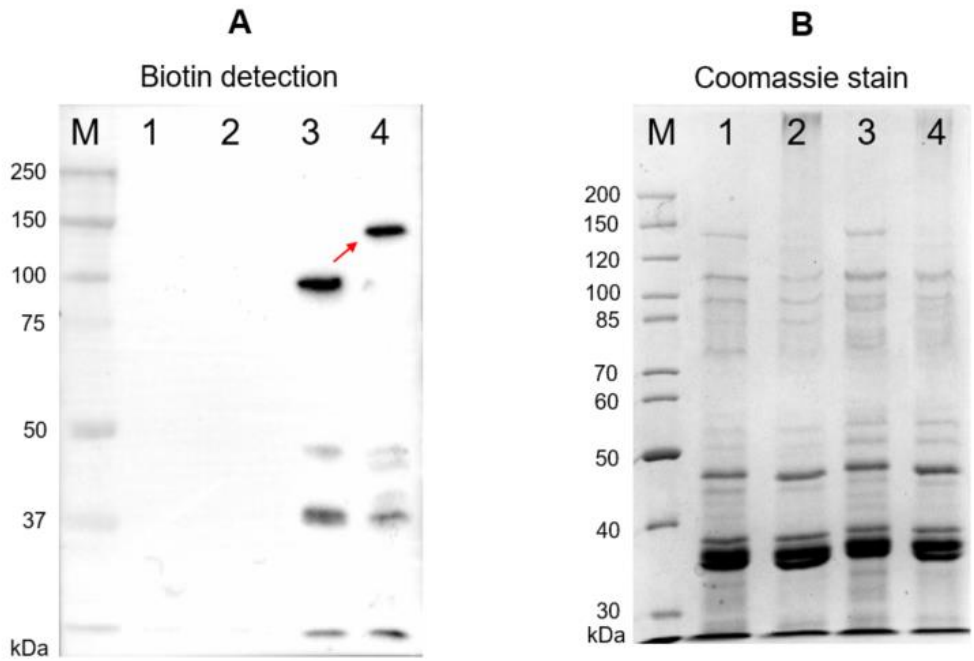

Figure 53 Western blot (A) and SDS-PAGE (B) of *E. coli* ATCC25922 membrane fractions from 10% self-casted polyacrylamide gels. Lanes: M) molecular-weight marker, 1) control, 2) control (non-reducing conditions), 3) thanatin-PAL5 (2 µg/ml), 4) thanatin-PAL5 (2 µg/ml, non-reducing conditions). Blotting for 2 h (10 V, 0.5 A) with urea transfer buffer. Biotin detection by chemiluminescence with NeutrAvidin-HRP 1:30'000 and WesternBright™ Sirius™ HRP substrate. The arrow indicates a mass shift characteristic for LptD. Exposure time: 304 s (blot A).

The photolabelling experiment was repeated with two different *E. coli* strains: *E. coli* K-12 and clinically isolated, multi resistant *E. coli* 926415. The MIC value against *E. coli* K-12 remained unchanged with 0.5 µg/ml. It was, however, 2 - 8 times higher (i.e. 1 - 4 µg/ml) against *E. coli* 926415. A commercially available 4-20% gradient gel (*Bio-Rad*) was used for SDS-PAGE with blotting under the recommended conditions from the supplier for high molecular weight proteins. Those conditions also allowed the investigation of smaller proteins (< 30 kDa). The labelling pattern at a concentration of 2 µg/ml thanatin-PAL5 looked very similar between these two strains (Figure 54) with distinct bands at 100 kDa, 40 kDa, and 20 kDa in both strains, with several additional faint bands for *E. coli* K-12. In comparison to the *E. coli* ATCC25922 strain (cf. Figure 52), only one band was highlighted in the 40-45 kDa region.

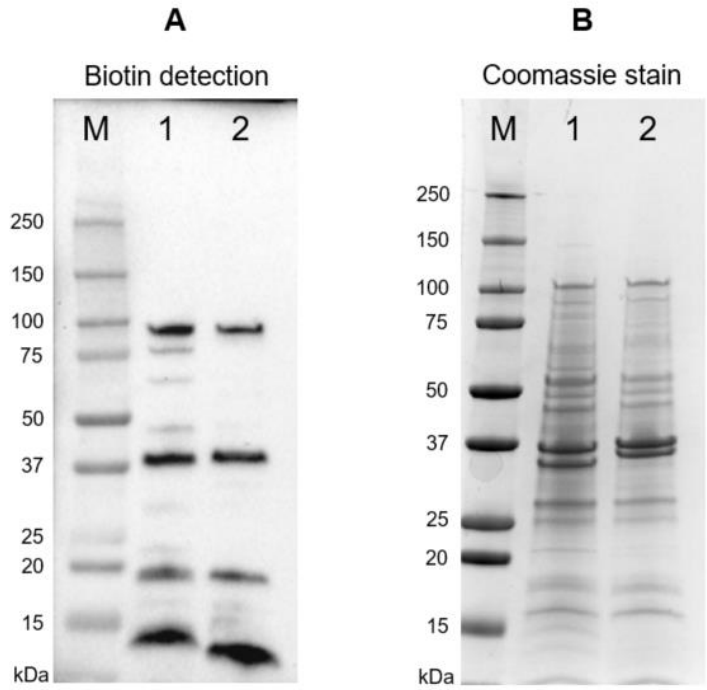

Figure 54 Western blot (A) and SDS-PAGE (B) of *E. coli* K-12 and 926415 membrane fractions from 4-20% gradient polyacrylamide gels. Lanes: M) molecular-weight marker, 1) *E. coli* K-12 with thanatin-PAL5 (2 µg/ml), 2) *E. coli* 926415 with thanatin-PAL5 (2 µg/ml). Blotting for 2x10 min (25 V, 1.3 A). Biotin detection by chemiluminescence with NeutrAvidin-HRP 1:30'000 and WesternBright™ Sirius™ HRP substrate. Exposure time: 193 s (blot A).

Thanatin exhibited no activity against *P. aeruginosa* PAO1 and *P. aeruginosa* ATCC27853 (MIC > 64 µg/ml). However, it has previously been claimed that thanatin shows low activity against *P. aeruginosa* ATCC27853 (MIC = 16 µg/ml) and good activity against a multi-drug resistant, clinical isolate *P. aeruginosa* XJ75297 (MIC = 1 µg/ml).[116] Further, a derivative named S-thanatin, in which residue Thr15 has been substituted by a serine, was used in a co-treatment together with colistin in an *in vivo* study against *P. aeruginosa* ATCC27853 and colistin resistant clinical isolate *P. aeruginosa* AN-09.[117] Photoaffinity labelling of *P. aeruginosa* PAO1 with thanatin-PAL5 (10 µg/ml) revealed a band above 100 kDa (likely LptD), a band at 75 kDa, which was also present in the control and likely stems from the biotin carrying enzymes methyl crotonyl-CoA-carboxylase (MCCase) or geranyl-CoA-carboxylase (GCCase) with respective masses of 78 kDa and 74 kDa[118], a faint band around 60 kDa, and a large band at 50 kDa (Figure 55). It seems therefore, that thanatin interacts with several membrane proteins also in *P. aeruginosa*.

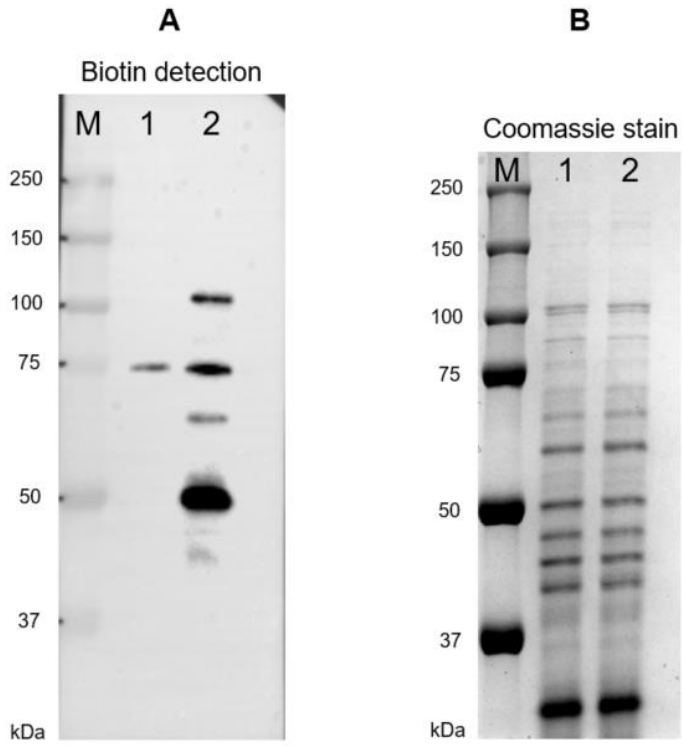

Figure 55 Western blot (A) and SDS-PAGE (B) of membrane fraction of *P. aeruginosa* PAO1 from 10% polyacrylamide gels. Lanes: M) molecular-weight marker, 1) control, 2) thanatin-PAL5 (10 µg/ml). Blotting for 2 h (10 V, 0.5 A) with urea transfer buffer. Biotin detection by chemiluminescence with NeutrAvidin-HRP 1:30'000 and WesternBright™ Sirius™ HRP substrate. Exposure time: 415 s (blot A).

Two dimensional gel electrophoresis was applied in an attempt to identify the labelled proteins. Membrane protein extract from a photolabelling experiment performed with 10 µg/ml thanatin-PAL5 on *E. coli* ATCC25922 was used. The proteins were first separated by isoelectric focusing from pH 4 – 7 by immobilization on pH gradient strips, and then by their molecular weight in the second dimension on a 10% polyacrylamide gel. The crosslinking of thanatin-PAL5 to the individual proteins results in a pI shift corresponding to seven additional positive charges and an increase in molecular weight of +2.9 kDa. The observed labelling pattern (Figure 56) resembles the one from the 1D experiment (cf. Figure 52) with a number of differences: The band around 100 kDa actually stems from two proteins that could not be separated on a 1D gel. The previously observed faint band below 75 kDa was vastly more abundant in this experiment, whereas the 40 kDa band was fainter. Several membrane proteins in *E. coli* ATCC25922 were previously identified by Dr. Fabio Lo Monte by 2D SDS-PAGE and mass spectrometry analysis in collaboration with the Functional Genomics Center Zurich at UZH (FGCZ) (Figure 57). The region around 100 kDa, where the two proteins LptD and BamA were assigned, was further investigated. The other signals in the Western blot could not be correlated to the protein map, since they appeared in a more crowded region with several possible interaction partners.

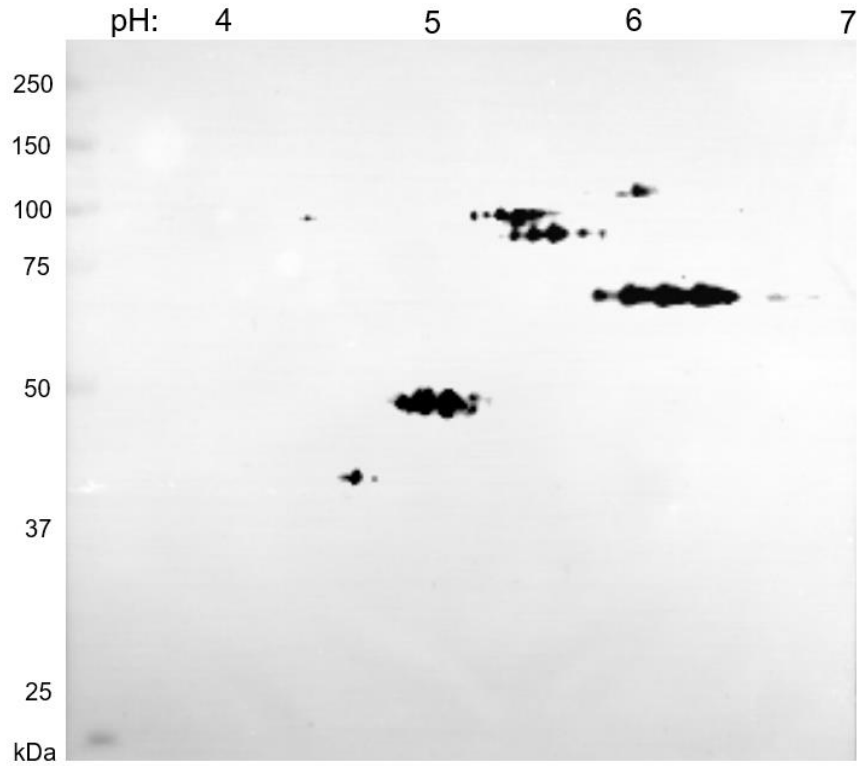

Figure 56 2D Western blot of membrane fractions of *E. coli* ATCC25922, from a 10% polyacrylamide gel. Photolabelling was performed with 10 µg/ml thanatin-PAL5. Blotting for 2 h (10 V, 0.5 A) with urea transfer buffer. Biotin detection by chemiluminescence with NeutrAvidin-HRP 1:30'000 and WesternBright™ Sirius™ HRP substrate. Exposure time: 122 s.

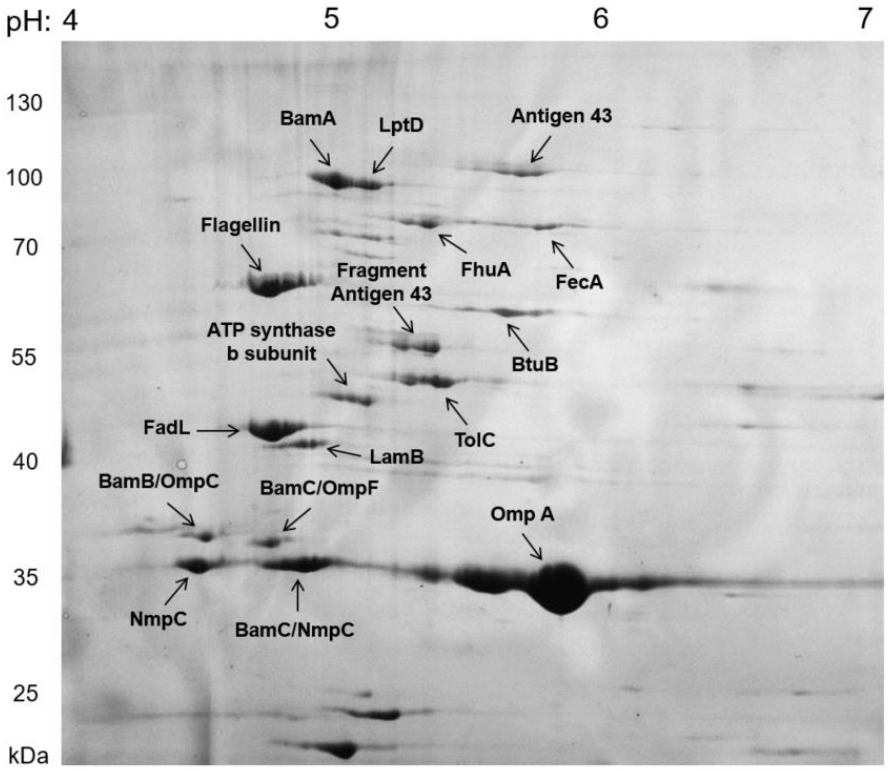

Figure 57 2D SDS-PAGE (10% polyacrylamide) of membrane fractions of *E. coli* ATCC25922 with Coomassie staining. Proteins were assigned by mass spectrometry analysis. Results were obtained by Dr. Fabio Lo Monte.

Gel electrophoresis of the same membrane protein extract of *E. coli* ATCC25922 cells treated with 10 µg/ml thanatin-PAL5 was repeated under non-reducing conditions (i.e. without DTT) to investigate the previously described mass shift of LptD in two dimensions. Indeed, the upper band showed a clear difference in mobility, whereas the lower band remained at the previous position (Figure 58). Compared to the assigned protein map, this signal could be BamA. The calculated pI shift of LptD is 4.98 to 5.22 for the crosslinked product and matched the observation in the Western blot. The calculated pI shift of BamA is 4.87 to 5.08 and appears higher than expected in the Western blot. This provides evidence of a binding of thanatin to LptD and at least four other membrane proteins that remain to be identified.

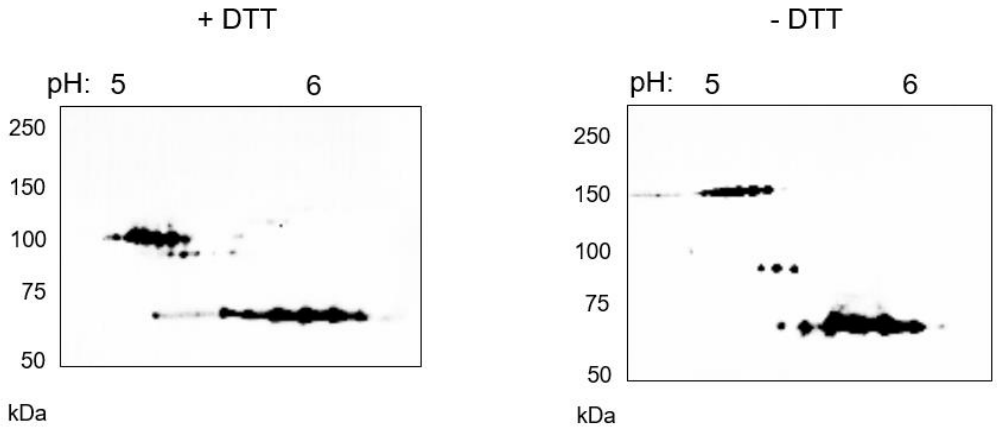

Figure 58 2D Western blot of membrane fractions of *E. coli* ATCC25922, from a 10% polyacrylamide gel. Photolabelling with 10 µg/ml thanatin-PAL5. Reducing conditions (left) and non-reducing conditions (right). Blotting for 2 h (10 V, 0.5 A) with urea transfer buffer. Biotin detection by chemiluminescence with NeutrAvidin-HRP 1:30'000 and WesternBright™ Sirius™ HRP substrate. Exposure times: 75 s (left), 23 s (right).

3.2.12 Protein Identification by Mass Spectrometry

In order to unambiguously identify proteins labelled in the photoaffinity labelling experiments, mass spectrometry based methods were applied in a collaboration with Maik Müller and Prof. Bernd Wollscheid at ETH Zurich. In a first experiment, samples of *E. coli* ATCC25922 cells photolabelled with 10 µg/ml thanatin-PAL5 together with control samples of a photolabelling experiment as described above were analysed in triplicate by MS-methods. The cells were lysed and biotinylated (crosslinked) proteins were collected by streptavidin beads. After on-bead proteolytic digestion with trypsin, data acquisition of protein fragments was performed by HPLC-MS/MS methodology. Peptide quantification and identification were based on the UNIPROT database for *E. coli* K-12[119]. A statistical analysis of cells treated with 10 µg/ml thanatin-PAL5 compared to untreated control samples identified 550 proteins in total, from which 230 proteins could be quantified in both samples, under the prerequisite that at least two peptide fragments derive from the same protein. Three proteins that were enriched in the

labelled sample could be identified with statistical significance above the threshold. LptA and LptD both exhibit high significance, whereas BamB lies just above the threshold (Figure 59). The labelling of LptD was already anticipated from the photoaffinity labelling experiments described above. LptA is directly associated with LptD in the periplasmic space, and both are part of the LPS transport machinery. BamB, however, is part of the outer membrane protein assembly complex (BAM complex), which is involved in assembly and insertion of β-barrel proteins into the outer membrane (cf. Introduction 1.4).

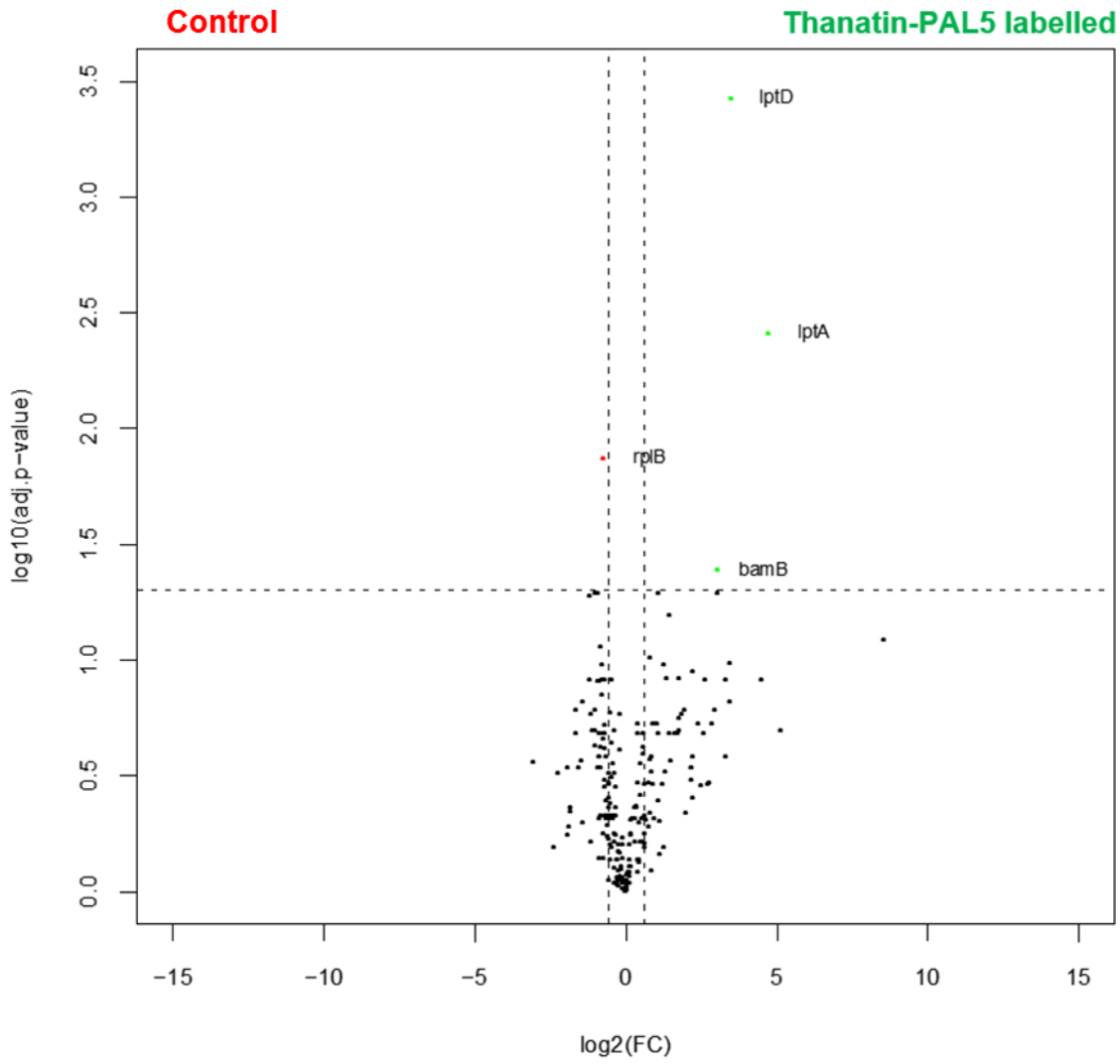

Figure 59 Volcano plot comparing protein abundance of an unlabelled control sample and a sample treated with 10 µg/ml thanatin-PAL5 in a photoaffinity labelling experiment, by quantitation using relative precursor ion signals and significance testing based on the UNIPROT database for E. coli K-12[119]. Significantly enriched (i.e. photo-crosslinked) proteins are LptD, LptA, and BamB (cf. Appendix 6.3 for full protein sequence).

In a second experiment a different approach using a proximity based photo-oxidation method where methylene blue-labelled probe thanatin-PAL5-MB (Scheme 8) was applied. The previously described thanatin-PAL5 precursor (cf. Results and Discussion 3.2.11) was Fmoc deprotected and a propargy-PEG_4 spacer coupled under standard conditions. After resin cleavage, oxidation, and purification by preparative HPLC, commercially available methylene blue azide (Atto-MB2 azide, Atto-Tec) was coupled by Click Chemistry as described later (Experimental Part 4.4). The purity of the compound was confirmed by UPLC analysis (Figure 60) and the identity was verified by HR-ESI with a calculated mass of 652.1353 $[M+6H]^{6+}$ and a measured m/z value of 652.1360 $[M+6H]^{6+}$.

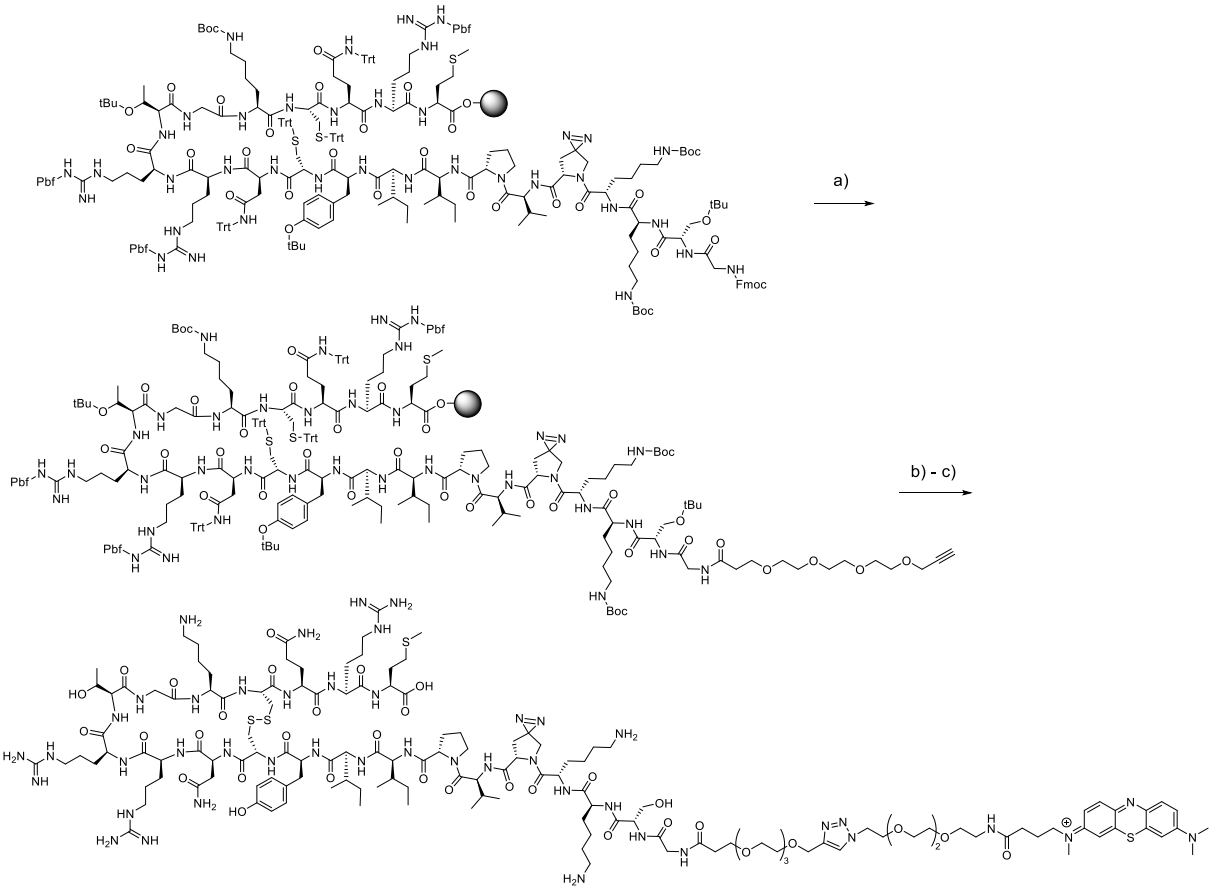

Scheme 8 a) Piperidine:DMF (1:3), then propargyl-PEG_4-acid, HATU, HOAt, DIPEA, DMF. b) TFA:EDT:thioanisole:H_2O:TIS (75:10:10:4:1), then oxidation by air in 0.1 M ammonium acetate pH 8.5. c) Atto-MB2 azide, $CuSO_4$, sodium ascorbate, DMSO:H_2O (1:5).

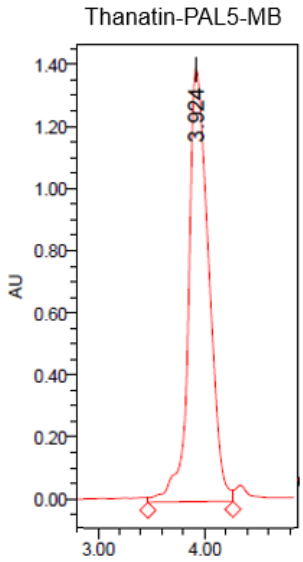

Figure 60 UPLC chromatogram of thanatin-PAL5-MB at 226 nm wavelength, run with a linear gradient of 10 to 40% MeCN/H_2O with additional 0.1% TFA on a C18 reverse-phase column.

Methylene blue is a photosensitizer that upon irradiation creates highly reactive singlet oxygen ($^1O_2$). The reaction of $^1O_2$ with amino acid side chains such as Trp, Cys, His, Tyr and Met has been shown to give rise to further reactive species via radical and ring opening reactions.[120] Trp and Tyr residues can form ketones, which can then be captured by reacting them with a hydrazide-biotin probe via hydrazone formation. If the thanatin-PAL5-MB probe binds to a receptor such as a membrane protein, this method should allow the identification of proteins in the direct vicinity of the binding site. Samples of *E. coli* ATCC25922 cells treated with 3 µM thanatin-PAL5-MB and a control sample (3 µM thanatin-PAL5-MB preincubated with 30 µM native thanatin) were analysed in triplicate. Isolation of the biotinylated proteins and their quantification and analysis by MS-methods was then achieved as described above. An enrichment of protein clusters primarily consisting of periplasmic and membrane proteins was observed, as well as a slight depletion of primarily cytosolic proteins (Figure 61). The two previously identified proteins LptD and LptA were also confirmed with this method as top enriched hits, making it likely that the other enriched proteins are direct neighbors of LptD and LptA. The previously observed BamB signal could also be detected with this method, however, as a non-significantly enriched protein, possibly due to the pre-incubation treatment with native thanatin, blocking most of the unspecific binding sites. Other proteins of the Lpt and Bam family have been detected as enriched hits (LptF, BamA, BamC), and non-significantly enriched (LptB, LptE, LptG). These findings provide strong evidence for a direct interaction of thanatin with components of the LPS transport pathway, and likely an inhibition of LPS transport as the mechanism of action of thanatin in *E. coli*.

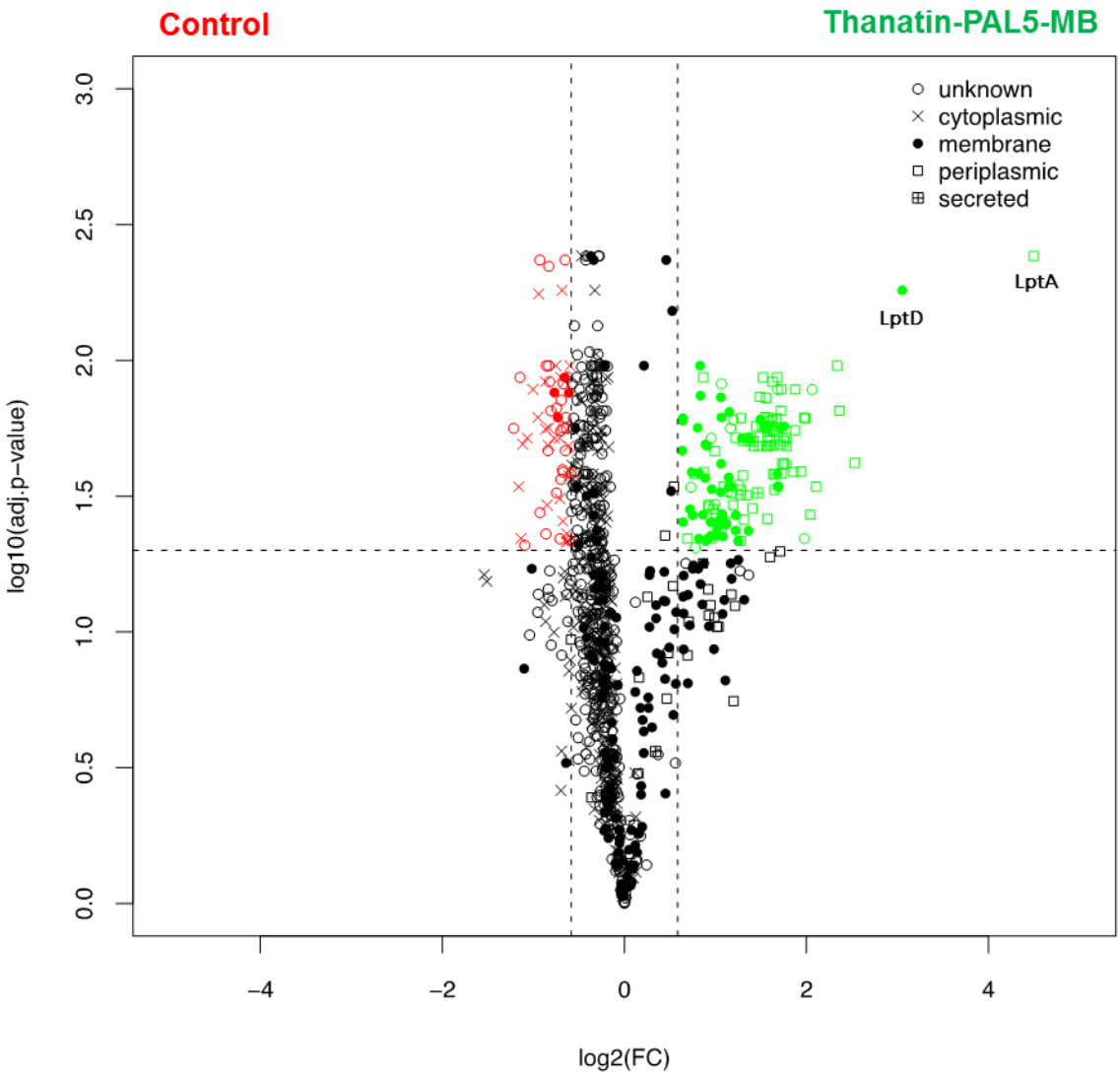

Figure 61 Volcano plot comparing protein abundance of a sample treated with 3 µM thanatin-PAL5-MB and a competition control sample (3 µM thanatin-PAL5-MB preincubated with 30 µM native thanatin) in a light induced proximity based photo-oxidation experiment, by quantitation using relative precursor ion signals and significance testing based on the UNIPROT database for E. coli K-12[119]. Significantly enriched proteins are depicted in green with LptA and LptD as top enriched hits. Depleted proteins are depicted in red.

3.2.13 Production of Recombinant *E.coli* LptA-His$_6$

To study the interaction of thanatin with LptA in an *in-vitro* assay, the protein needed to be produced recombinantly. LptA is part of the lipopolysaccharide transport machinery in Gram-negative bacteria (cf. Introduction 1.5). It is a soluble periplasmic protein consisting of 16 consecutive antiparallel β-strands, folded to resemble a slightly twisted and semi-closed β-jellyroll with two clefts at the ends of each LptA molecule.[121] Its main function is the binding of the Lipid A domain of LPS and the LPS transport along the hydrophobic interior of the β-jellyroll from the homologous domains of LptC to LptD.[122] LptA is assumed to form an oligomeric

channel where LptA molecules are assembled head-to-tail, to form a bridge-like structure through the periplasm. The N-terminal end of LptA has been confirmed by an *in-vivo* photo-crosslinking experiment to make contact with LptC, whereas the C-terminal end interacted with the periplasmic domain of LptD (Figure 62).[123] The oligomerization effect of LptA to form a continuous array of end-to-end structures was also confirmed in solution, as a function of increasing protein concentration.[124] A recent study conducted by Schultz *et al*.[125], focusing on the LPS binding mechanism using site-directed electron paramagnetic resonance (EPR) spin-labelling methods, suggested a 1:1 ratio for the LptA-LPS complex. Binding of thanatin to LptA could therefore either inhibit the build-up of the channel at the interface or LPS transport itself, by occupying the LPS binding site.

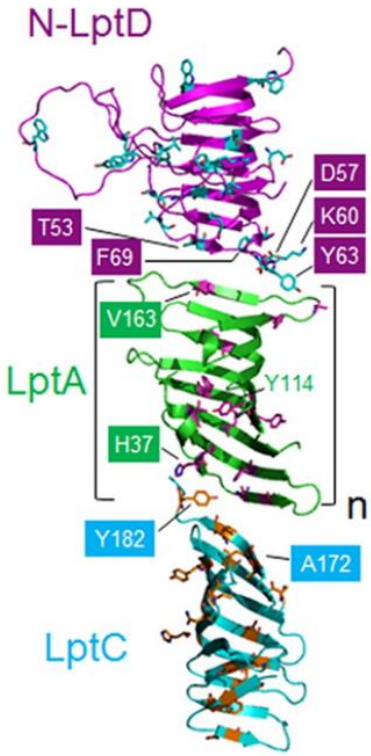

Figure 62 A channel formed of structurally homologous domains of LptC (PDB 3MY2), several monomers of LptA (PDB 2R19), and a model structure of the N-terminal domain of LptD in *E. coli*. Positions where photo-crosslinking of incorporated p-benzoylphenylalanine (pBPA) was observed are highlighted. (Reprinted from Freinkman *et al.*)[123]

Chromosomal DNA was isolated from *E. coli* ATCC25922 and amplified by PCR (polymerase chain reaction) with primers for the *lptA* gene. The PCR product was then purified on a 1% agarose gel and cloned into a pET-22b vector. Transformation of the plasmid into *E. coli* XL1 Blue was achieved by heat shock transformation, for the production of LptA with a C-terminal His_6 tag. An efficient procedure for the production of LptA-His_6 was previously described by Santambrogio *et al.*[126] and was applied as described in the following. The plasmid was transformed into *E. coli* BL21 and protein expression induced by addition of IPTG (isopropyl β-D-1-thiogalactopyranoside). After cell harvesting and disruption by French press,

the soluble protein fractions were purified by Ni-NTA affinity chromatography with a yield of 2.5 mg LptA-His_6 per liter culture media. SDS-PAGE confirmed the purity of the protein (Figure 63). The identity of the fully processed sequence (i.e. without the 27 N-terminal residues of the signal sequence M1–A27) was confirmed by ESI-MS with a calculated molecular weight of 18'360.55 Da and a measured molecular weight of 18'360.5 Da.

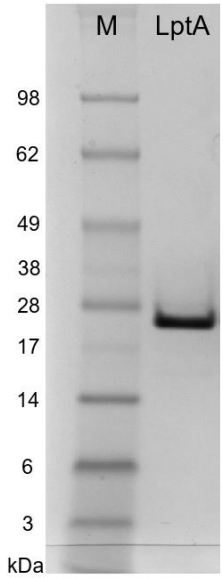

Figure 63 Coomassie stained 4-20% polyacrylamide gradient gel of purified LptA-His_6. M: molecular-weight marker.

With the purified LptA-His_6 in hand, it was decided to study the interaction with thanatin by a fluorescence polarization based binding assay.

3.2.14 Fluorescence Polarization

The binding interaction of labelled thanatin-BDP-FL (cf. Results and Discussion 3.2.10) with LptA-His_6 was studied by fluorescence polarization. Studying the association between biomolecules is crucial in understanding their biological function and activity. Fluorescence polarization provides a non-destructive method to determine the binding affinity of a fluorescent ligand to a macromolecule (i.e. a protein). The theory of fluorescence polarization was first described by Perrin[127] in 1926, as a physical phenomenon in which fluorescent molecules excited with linear polarized light will emit light back in the same (linear) polarization if the molecule remains stationary during excitation. If, however, the molecules move and tumble in solution, the degree of polarization of the emitted light of a fluorophore is inversely related to its molecular rotation. Quantitatively, fluorescence polarization is defined as the difference of the emission light intensity parallel (**I**||) and perpendicular (**I**⊥) to the excitation light plane normalized by the total fluorescence emission intensity (equation E 1), whereas fluorescence anisotropy is defined as equation E 2.[128]

$$\text{Fluorescence polarization} = (\mathbf{I}\| - \mathbf{I}\perp) / (\mathbf{I}\| + \mathbf{I}\perp) \quad \text{E 1}$$

$$\text{Fluorescence anisotropy} = (\mathbf{I}\| - \mathbf{I}\perp) / (\mathbf{I}\| + 2\,\mathbf{I}\perp) \quad \text{E 2}$$

Since a fluorescent ligand bound to a protein exhibits a higher polarization than in free solution, a concentration dependent assay can be applied to determine a dissociation constant (K_d value) for this specific interaction. Further, with the established K_d, the K_d of any competing unlabelled ligand can also be determined accordingly.[129] In a direct assay, a constant concentration of 100 nM thanatin-BDP-FL was titrated with varying concentrations of LptA-His_6 (30.8 µM - 3.7 pM) and fluorescence anisotropy recorded. A distinct lower plateau was apparent at low concentrations of LptA-His_6, whereas at higher LptA-His_6 concentrations, higher anisotropy was detected in a typical sigmoidal behaviour. The upper plateau however, is not entirely flat, probably due to an oligomerization effect of LptA at higher concentrations as described by Merten *et al.*[124] A curve fitting yielded a K_d value of 12 ± 3 nM for this interaction (Figure 64).

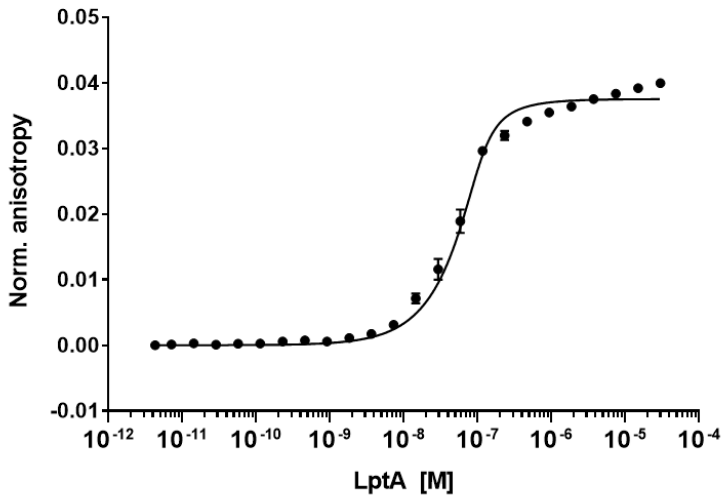

Figure 64 Fluorescence anisotropy of thanatin-BDP-FL interacting with LptA-His_6.

To prove that the binding affinity is caused by a specific interaction with the peptide and not the attached fluorophore, a competition experiment was performed with a constant concentration of thanatin-BDP-FL complexed with LptA-His_6 (both 500 nM), titrated with varying concentrations of native thanatin (2'054 µM - 0.24 nM) as a competitor. Indeed, the free thanatin was able to compete for the binding site occupied by thanatin-BDP-FL at higher concentrations, whereas at lower concentrations of free thanatin, the complex stayed intact, exhibiting higher anisotropy. A curve fitting yielded a competitor K_d value of 10 ± 2 nM, suggesting the same binding affinity for the native thanatin (Figure 65).

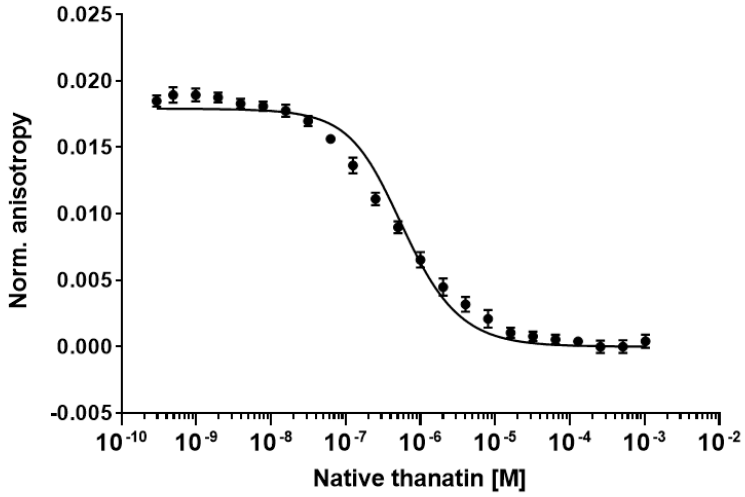

Figure 65 Fluorescence anisotropy of a free thanatin (competitor) against a thanatin-BDP-FL LptA-His_6 complex

The competition experiment was repeated with D-thanatin, the enantiomer consisting of all D-amino acids, within the same concentration range (2054 µM – 0.24 nM) against the thanatin-BDP-FL LptA-His_6 complex (both 500 nM). Although, the enantiomer displays the same molecular weight and charge density, it was not able to compete for the LptA binding site, strongly indicating a stereospecific interaction with LptA-His_6 for the native thanatin (Figure 66).

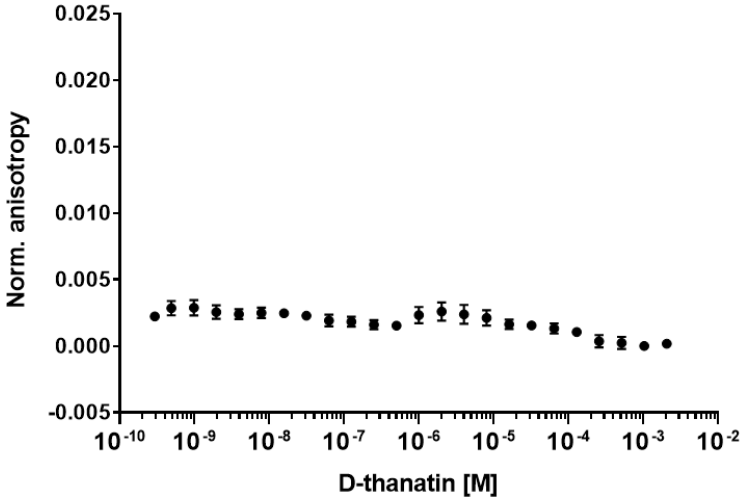

Figure 66 Fluorescence anisotropy of D-thanatin against a thanatin-BDP-FL LptA-His_6 complex.

3.2.15 Isolation and Gene Sequencing of Thanatin-Resistant Mutants

Additional studies were conducted by Dr. Katja Zerbe in order to generate mutants resistant against thanatin (unpublished work). *E. coli* ATCC25922 cells were grown on MH-II agar containing 10 - 50 µg/ml thanatin. It had previously been claimed that the emergence of resistance against thanatin is very low.[130] To our surprise, however, resistant mutants could already be isolated after the first passage with a mutation frequency of approximately 10^{-8}. In two independent experiments, a total of ten thanatin resistant mutants could be isolated, from which five remained stable over at least five subsequent passages on thanatin-free agar, all deriving from conditions where 50 µg/ml thanatin was used for selection. Sequencing of the *lptA* gene revealed two different point mutations, Q62L and D31N, with the Q62L obtained in both independent experiments (Table 13). These two residues (Q62 and D31) are highly conserved in LptA between other Gram-negative bacteria and lie in close proximity to each other on one side of the protein (Figure 67). The thanatin treatment apparently leads to a mutation of these residues to reduce binding affinity, escaping the toxic effect thanatin has on the cells. This might be due to the disruption of crucial H-bonds in the contact region (Q62L) and loss of a salt bridge in the case of D31N.

Table 13 Analysis of thanatin resistant isolates of *E. coli* ATCC25922 and their respective mutations in LptA. ThanRes1 – ThanRes7 and ThanRes8 – ThanRes10 were identified in independent experiments. MIC Values were determined by microdilution in MH-II with addition of 0.002% Tween80.

Mutants	Thanatin conc. on original plate used for selection [µg/ml]	MIC against thanatin [µg/ml]	MIC against thanatin after four passages [µg/ml]	Mutation in LptA sequence
Wild type		1-2	1-2	
ThanRes1	10	2-4	2	-
ThanRes2	50	>64	>64	Q62L
ThanRes3	50	>64	1	-
ThanRes4	50	32	64	D31N
ThanRes5	20	16	4	-
ThanRes6	20	16	4	-
ThanRes7	20	16-32	1	n.d.
ThanRes8	50	>64	>64	Q62L
ThanRes9	50	>64	>64	Q62L
ThanRes10	50	>64	>64	Q62L

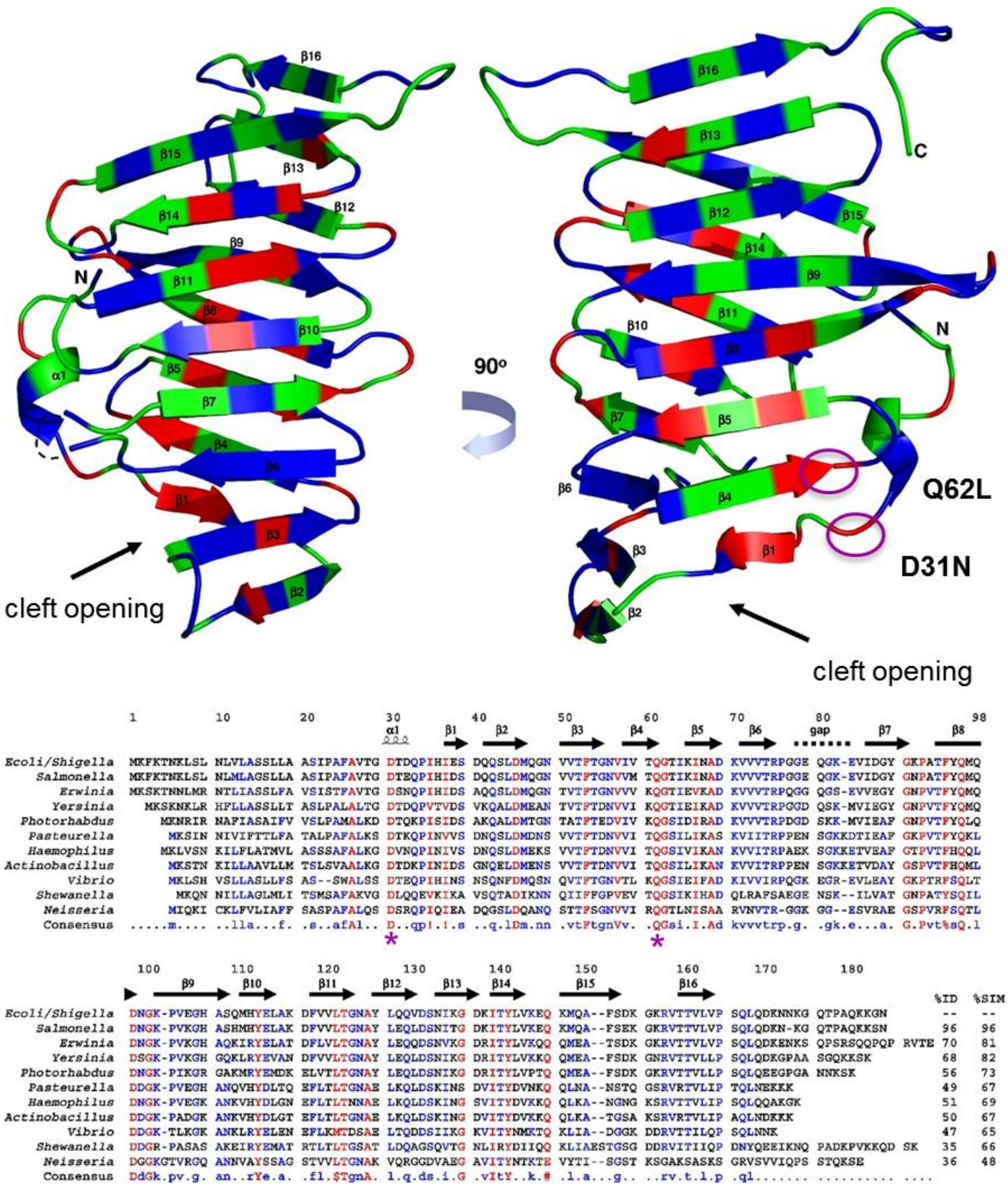

Figure 67 Ribbon diagram of a single *E. coli* LptA molecule (PDB 2R19) and sequence alignment of LptA from various Gram-negative bacterial homologues. The backbone of non-conserved (green), similar (blue), and conserved (red) residues are depicted. Mutation sites are highlighted in magenta. (Adapted from Suits *et al.*)[121]

The three thanatin resistant mutants ThanRes2, ThanRes4, and ThanRes8 were further analysed, and no difference in their growth behaviour (i.e. lag-time, doubling time, and final OD_{600}) in MH-II media compared to the wild type was observed. They did not show an increased sensitivity in the presence of 0.5% SDS and 1 mM EDTA in MH-II media, indicating that the outer membrane remained unaffected. Susceptibility towards a series of standard antibiotics also remained unchanged as shown in the antibiogram in Table 14.

Table 14 Antibiogram of thanatin resistant mutants ThanRes2, ThanRes4, and ThanRes8 compared to the parent strain *E. coli* ATCC25922. Values were determined by microdilution in MH-II with addition of 0.002% P80.

MIC (µg/ml)	***E. coli* ATCC25922**	**ThanRes2 (LptA-Q62L)**	**ThanRes4 (LptA-D31N)**	**ThanRes8 (LptA-Q62L)**
Colistin	0.06	0.03	0.06	0.015
Erythromycin	>64	>64	64	64
Gentamycin	0.5	0.5	0.5	0.5
Vancomycin	>64	>64	>64	n.d.
Rifampicin	8	8	8	16-64
Ampicillin	16	8	16	16
Ciprofloxacin	0.002	0.002	0.002	0.015
Thanatin	**1**	**>64**	**>64**	**>64**

Sequencing of whole genomes was carried out in collaboration with Alessandra Vitale, Dr. Gabriella Pessi, and Prof. Leo Eberl at the Department of Plant and Microbial Biology UZH. Genomic DNA was extracted from thanatin resistant *E. coli* mutants ThanRes2, ThanRes4, and ThanRes8, as well as from the wild type *E. coli* ATCC25922 for comparison. Sequence analysis of the chromosome as well as the two plasmids revealed only a few changes (point mutations, deletions, insertions) which cause modifications on the amino acid level. The genes containing mutations are listed in Table 15. In all mutant genomes a point mutation in *lptA* was confirmed. In ThanRes2 and ThanRes4 additional changes in a small number of proteins were observed, some of them with unknown functions. Interestingly the ThanRes8 mutant showed only a single point mutation compared to the wild type sequence, causing the Q62L mutation in LptA, which further confirms LptA as a main target for thanatin. *LptA* is an essential gene for *E.coli*, which means that this mutation is not completely inhibiting the essential LPS transport. The protein is still functional, but seems to prevent thanatin binding. LptD as a target cannot be ruled out, even though no mutations in *lptD* were observed in this screening. This could be explained by the fact that mutations in LptD are lethal and no mutant colonies might have survived.

Table 15 Observed mutations (+ : mutation found, - : no mutation) in different genes of thanatin-resistant *E.coli* ATCC25922 mutants ThanRes2, ThanRes4, and ThanRes8, compared to the wild type genome, detected by whole genome sequencing. (Results were obtained by Alessandra Vitale and Dr. Gabriella Pessi)

gene	Protein/function	ThanRes2	ThanRes4	ThanRes8
lptA	LPS transport	+	+	+
rpmB	50S ribosomal protein 28L	+	-	-
pckA	Phosphoenolpyruvate-carboxykinase	+	-	-
rplE	50S ribosomal protein L5	+	-	-
thiK	Thiamine kinase	+	+	-
acnB	Aconitate hydratase B	-	+	-
DR76_2839	unknown	+	+	-
DR76_4251	unknown	+	+	-
DR76_2319	unknown	+	-	-
DR76_3425	unknown	-	+	-

The point mutations Q62L and D31N were shown to be dominant resistance markers. If the proteins were expressed from plasmids which were transformed into a wild type *E. coli* strain (ATCC25922 or K-12), they conferred full resistance against thanatin. Higher levels of wild type LptA, when expressed from a plasmid additionally to the chromosomal gene (*E. coli* K-12 + pOCI1548), had no significant effect and thanatin activity was largely retained (MIC approximately two-fold higher) (Table 16).

Table 16 MIC of strains containing plasmid-borne copies of the wild type or mutant LptA genes. MIC Values were determined by microdilution in MH-II with addition of 0.002% Tween80. (pOCI1548: LptA-His_6, pOCI1551: LptA_Q62L-His_6, pOCI1552: LptA_D31N-His_6)

Strain (+ plasmid)	MIC against thanatin [µg/ml]
E. coli ATCC25922	0.5 - 1
E. coli ATCC25922 + pET22b	0.25 - 0.5
E. coli ATCC25922 + pOCI1551	32
E. coli ATCC25922 + pOCI1552	8 - 16

Strain (+ plasmid)	MIC against thanatin [µg/ml]
E. coli K-12	0.5 - 2
E. coli K-12 + pET22b	0.5 - 2
E. coli K-12 +pOCI1551	32 - >64
E. coli K-12 + pOCI1552	16 - 64
E. coli K-12 +pOCI1548	1 - 4

3.2.16 Electron Microscopy

Scanning electron microscopy (SEM) and transmission electron microscopy (TEM) were performed on thanatin treated *E. coli* ATCC25922 by Dr. Katja Zerbe and Dr. Andres Käch from the Center of Microscopy and Image Analysis (ZMB) at UZH (unpublished work). Cells were grown in LB media at a thanatin concentration causing 50% growth inhibition. In comparison to a control sample, assemblies of multiple cells in elongated structures were observed in SEM (Figure 68), possibly due to difficulties to divide and to separate from each other during cell division. Similar results were obtained in fluorescence microscopy experiments described above (cf. Figure 46).

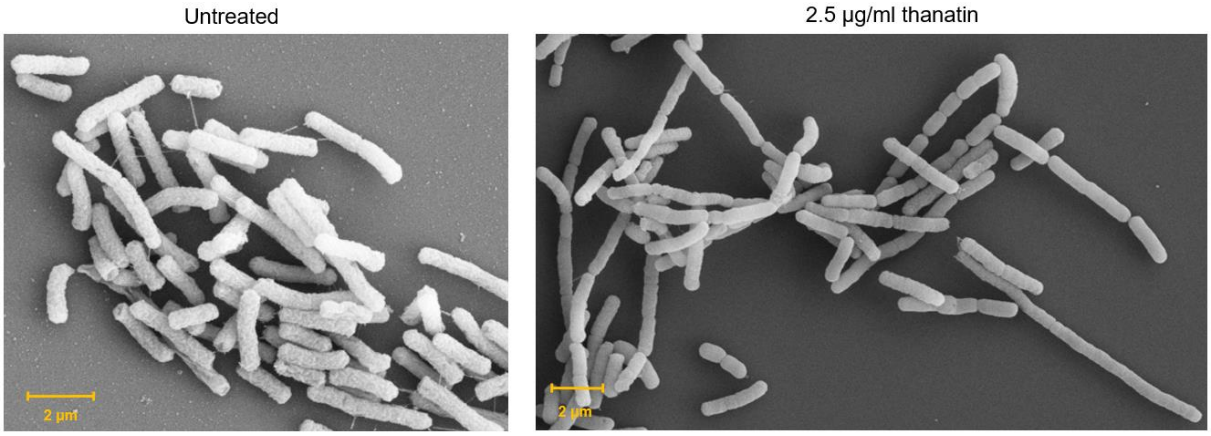

Figure 68 SEM images of *E. coli* ATCC25922 cells grown in LB, untreated (left) and treated with 2.5 µg/ml thanatin (50% growth inhibition) (right).

TEM images of thin sections of *E. coli* ATCC25922 cells grown in MH-II and treated with 2 µg/ml thanatin (74% growth inhibition) showed a lot of modifications compared to untreated cells, predominantly defects in the membrane architecture and unusual accumulations of membrane-like material inside cells and at cell junctions, but also brighter vacuoles at the cell poles, detachment of outer membranes, and black spots/aggregates inside the cytoplasm (Figure 69).

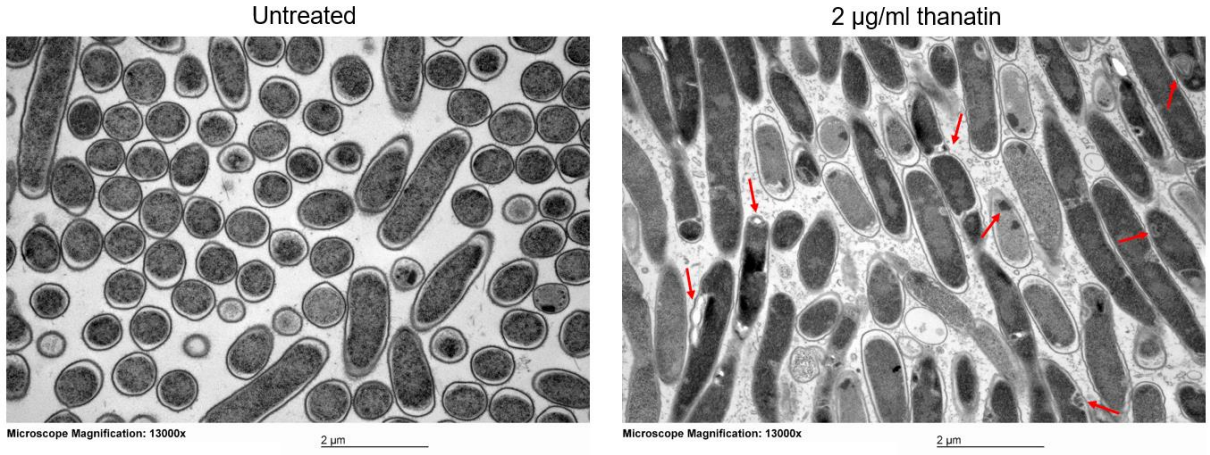

Figure 69 TEM images of *E. coli* ATCC25922 cells grown in MH-II, untreated (left) and treated with 2 µg/ml thanatin (74% growth inhibition) (right). Arrows indicate unusual membrane defects and accumulations.

A representative structure of an interesting multi-layered membrane fold inside the cell is shown in Figure 70. Such modifications are typically observed in cells where LPS transport is inhibited, as previously described for LptA/B, LptC, LptD, and LptE depleted *E. coli* mutants (Figure 71).[131,132] As a consequence, membranous material is accumulated and cell division is arrested. These findings indicate a direct effect of thanatin on the membrane, without causing actual permeabilization, likely by interfering with the biosynthesis or transport of membrane components such as LPS.

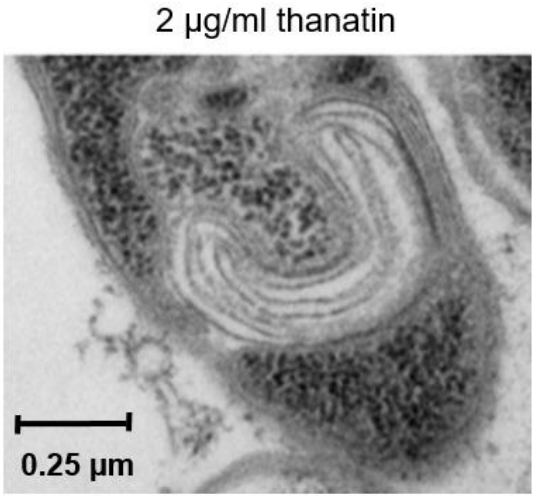

Figure 70 TEM thin section image of an *E. coli* ATCC25922 cell grown in MH-II and treated with 2 µg/ml thanatin (74% growth inhibition) shows a high accumulation of membrane-like material inside the cell.

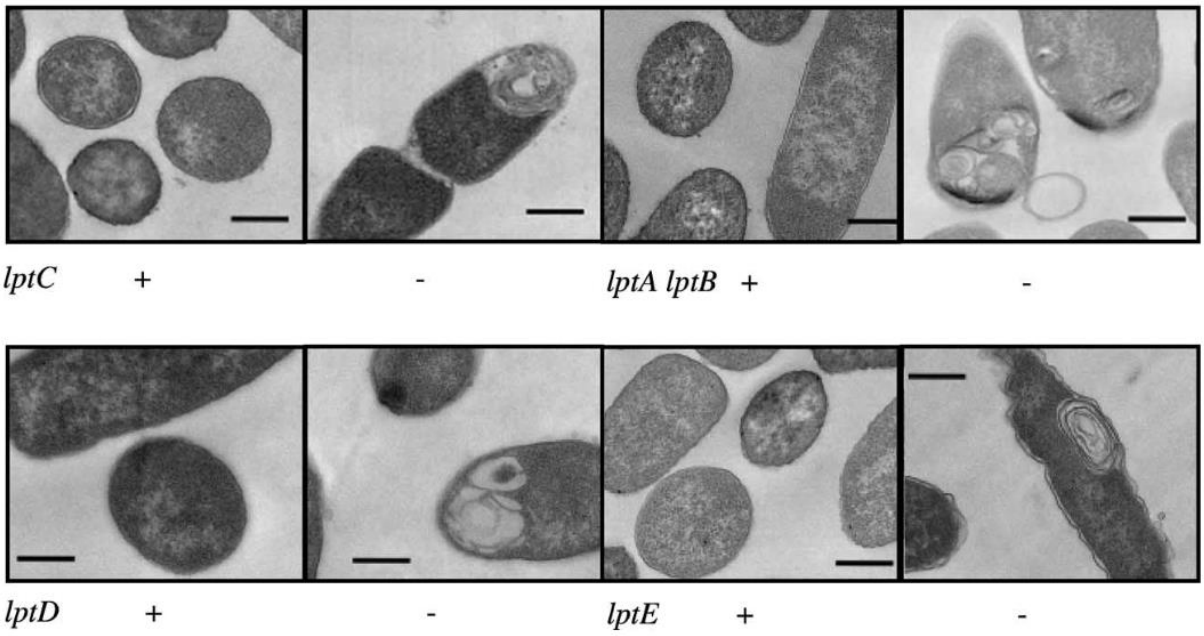

Figure 71 Cell morphology upon depletion of LptA-LptB, LptE, LptD, and LptC. *E. coli* cells were grown in the presence (+) or in the absence (-) of arabinose (arabinose-dependent, conditional mutants). Scale bars indicate 0.5 µm length. (Reprinted from Sperandeo *et al.*)[132]

3.2.17 Conclusion

The antimicrobial activity of thanatin against *E. coli* ATCC25922 and a series of clinical, multi-resistant *E. coli* isolates was confirmed. It was proven that thanatin does not act by a membranolytic mechanism of action by a series of assays. In the Sytox® Green assay performed in MH-I media, no membrane permeability was observed with thanatin concentrations up to 100 µg/ml (Figure 38). Although a signal could be detected when the Sytox® Green assay was performed in HEPES buffer, it was shown that the enantiomeric D-thanatin, which has no antimicrobial activity, exhibited the same effect (Figure 39). This suggests an unspecific permeabilization, likely caused by the positive charge density of the molecule on weakened cells. If the HEPES media was supplemented with Ca^{2+} and Mg^{2+}, again, no effect was observed with thanatin concentrations up to 100 µg/ml (Figure 40). These results were further reinforced by the β-lactamase and β-galactosidase assays, neither of which showed any perturbative effect of the inner or outer membrane (Figure 41 and Figure 42). The effect of thanatin on the macromolecular pathways of DNA, RNA, protein, and cell wall biosynthesis was studied by monitoring the incorporation of radioactive precursors. No inhibition of any pathway was observed, however, an increase of N-acetylglucosamine incorporation was apparent, suggesting a stimulation of its incorporation into components of the polysaccharide coat or into precursors used for LPS biosynthesis (Figure 44). Confocal fluorescence microscopy and scanning and transmission electron microscopy images indicated that the membrane morphology was affected by thanatin. Accumulations of membranous material inside of cells were observed (Figure 70), resembling previously described structures in *E. coli* mutants, where LPS transport was inhibited. The fluorescence-labelled probe thanatin-BDP-FL (Scheme 6) was used to confirm the uptake of the compound into cells (Figure 49). Additionally, elongated assemblies of multiple cells were observed, likely as a general stress response and/or failure to divide (Figure 47). Photoprobe thanatin-PAL5 was synthesized (Scheme 7), carrying an N-terminal biotin tag and a photo-reactive diazirine group at position Pro5 for the use in photoaffinity labelling experiments. SDS-PAGE and Western blotting with subsequent biotin detection of photolabelled membrane proteins identified LptD as a potential interaction partner of thanatin. Mass spectrometry based methods were carried out in a collaboration with the Wollscheid group at ETH Zurich confirming LptD and identifying LptA with high significance as targets of thanatin (Figure 58). Since these proteins are both associated and involved in the LPS transport, it is highly likely that the LPS transport is disturbed by thanatin and is the reason for its antimicrobial activity in Gram-negative bacteria. Thanatin resistant mutants were isolated, and the whole genome sequenced. A key point mutation in LptA (Q62L) was identified, rendering the bacteria completely resistant against thanatin. LptA-His_6 was recombinantly expressed and the purified protein subjected to fluorescence polarization measurements with labelled probe thanatin-

BDP-FL. A K_d value of 12 ± 3 nM was calculated for the specific interaction between thanatin-BDP-FL and LptA-His_6 (Figure 64). In an ongoing collaboration with Peer Mittl from the Department of Biochemistry at UZH a thanatin-LptA co-crystal is being produced for x-ray diffraction analysis. The results of which are expected in the near future to help understand the interaction on a residue-to-residue basis. Taken together, these studies provide an important advance in revealing the mechanism of action of thanatin. So far, no other molecules are known that bind to LptA and so target the LPS transport bridge across the periplasm. The results described in this thesis might therefore be used to develop new classes of antibiotics against this important new target in Gram-negative bacteria. Although *E. coli* LptA displays a high sequence identity among other Gram-negative bacteria (Figure 67), the binding affinity of thanatin to LptA needs to be confirmed for these species. It also remains to be identified how LptD makes contact to thanatin and how the maturation of LPS is affected. It would also be interesting to study the mechanism of action in Gram-positive bacteria and fungi, as they both lack the Lpt system.

4 Experimental Part

4.1 General Procedures and Analytics

All solvents used for reactions were purchased from *Sigma-Aldrich*, *Merck*, or *Acros* (puriss. or p.a.). Solvents for extractions, flash column chromatography and thin layer chromatography (TLC) were purchased as commercial grade and distilled prior to use. High purity H_2O (18 MΩ) was supplied by a Purelab Flex 02 (*Elga Laboratories*) dispenser system. Commercially available reagents and amino acids (*GL Biochem Ltd*) were used without further purification, unless otherwise noted. In general, reactions were magnetically stirred and monitored by TLC performed on *Merck* TLC aluminium sheets (silica gel 60 F254). Spots were visualized with UV light (λ = 254 nm) and through staining with vanillin/H_2SO_4 or anisaldehyde/H_2SO_4. Chromatographic purification of products was performed using silica gel 60 (*Fluka*) for preparative column chromatography (particle size 40-63 µm). ^{1}H, ^{13}C-NMR were recorded in $CDCl_3$, DMSO-d_6, or D_2O on *Bruker* AV-300, AV-400 MHz and AV-500 MHz instruments at RT. Chemical shifts (δ) are reported in ppm and are referenced to TMS and TSP (0 ppm) as an internal standard. Data for NMR spectra are reported as follows: s = singlet, d = doublet, t = triplet, q = quartet, m = multiplet, br = broad signal, *J* = coupling constant in Hz. Routine low resolution mass spectra were recorded on a *Dionex* MSQ Plus spectrometer coupled to an automated *Gilson* liquid handler system 215, a *Dionex* P580 Pump, and a *Dionex* UVD170U detector with an *Agilent* ZORBAX SB-C8/C18 column (3.5 µm, 2.1×150 mm). High resolution mass spectra were recorded by the MS-service of the University of Zurich on a *Bruker* maXis HR-MS instrument.

4.2 Solid Phase Peptide Synthesis

Resin loading. 2-Chlorotrityl chloride resin (*GL Biochem Ltd*) was washed three times with DMF and three times with DCM without prior activation (an additional step of resin activation using acetyl chloride in toluene can be performed if necessary). A loading of 0.75 mmol amino acid per gram of resin was applied. The resin was swelled in DCM for 15 min by bubbling N_2 through the reaction vessel. In a round bottom flask the amino acid was dissolved in DCM (5 ml) and DIPEA (4 eq.) was added. The reaction vessel was drained and the amino acid mixture transferred to the reaction vessel. After a reaction time of 3 h, liquids were drained and the resin washed three times with DCM. Then, the resin was blocked by treatment with a solution of DCM/MeOH/DIPEA (17:2:1; 20 ml) for 2 min. Blocking was repeated five times and the resin finally washed with DCM and dried *in vacuo*.

Determination of the resin loading. Completely dry resin (1-2 mg) was treated with a 25% piperidine/DMF (3 ml) solution for 30 min. The solution was transferred into a quartz UV-cuvette with 10 mm path length. UV absorption was measured at a wavelength of 290 nm against a blank background (25% piperidine/DMF). The resin loading can be calculated by using equation E 3.

$$\text{Loading (mmol/g)} = (A_{290\ nm}\ (\text{sample}) - A_{290\ nm}\ (\text{blank})) / (1.75 * m_{dry\ resin}) \qquad \text{E 3}$$

There is also the possibility of determining the resin loading gravimetrically using equation E 4, where m_{total} = the mass of the loaded resin, m_{resin} = the mass of the unloaded resin and $M_{W,AA}$ = molecular weight of the immobilized amino acid.

$$\text{Loading (mmol/g)} = ((m_{total} - m_{resin}) \times 10^3) / ((M_{w,AA} - 36.46) * m_{total}) \qquad \text{E 4}$$

Fmoc deprotection. The resin was washed three times with DMF and swelled for 15 min. DMF was drained and 25% piperidine/DMF was added to fully cover the resin. The resin was agitated by bubbling N_2 through the reaction vessel for 8 min. This procedure was repeated three times and the resin finally washed three times with DMF and DCM.

Coupling of the next amino acid. The respective amino acid (4 eq.) HBTU (4 eq.), HOBt (4 eq.) and DIPEA (10 eq.) were dissolved in DMF (5 ml) and activated for 2 min. The mixture was then added to the Fmoc deprotected resin and agitated under N_2 for 2 h. The resin was then washed three times with DMF and DCM. The last two steps (deprotection and coupling) were repeated for each subsequent amino acid.

Automated peptide synthesis. Linear peptides were synthesized on a 0.25 mmol scale by an ABI433A automated peptide synthesizer (*Applied Biosystems*) coupled to a *Perkin-Elmer* 785A UV/VIS detector. Cartridges filled with the corresponding amino acids (1 mmol, 4 eq.) were activated with 0.9 mmol of an HBTU/HOBt (0.45 M) stock solution in DMF and transferred to the resin containing reaction vessel, which was vortexed for 20 min in a standard coupling reaction cycle. Fmoc deprotection was achieved by addition of 20% piperidine in NMP for 7 min under vortexing. Complete deprotection was ensured by monitoring the formation of the dibenzofulvene and its piperidine adduct at 301 nm wavelength or by changes in conductivity of the drained solvent. Intermediate and final washing steps with NMP and DCM were performed by vortexing and subsequent draining of the solvents.

Selective cleavage from 2-chlorotrityl chloride resin. The final linear peptide was cleaved from its solid support by repeated treatment with a 0.8% TFA in DCM solution for two min. This procedure was repeated ten times and the TFA immediately quenched by draining the aliquots into a two molar excess of DIPEA. Excess DCM was evaporated *in vacuo* yielding a thick oil that was transferred into a 50 ml falcon tube with as little DMF as possible. Ice cold H_2O was then added causing precipitation of the peptide. The suspension was centrifuged (15 min at 4'000 rpm), the supernatant discarded, and the pellet resuspended with ice cold diethyl ether. This procedure was repeated for two times and the pellet dried overnight *in vacuo*. An improved cleavage method first described by Bollhagen *et al.*[133] was used alternatively: The resin was treated with hexafluoroisopropanol (HFIP), DCM, and trifluoroethanol (65:25:10, 5 ml) three times for 5 min. The combined fractions were dried *in vacuo* and co-evaporated with toluene to obtain a crystalline solid.

Cyclization. HBTU (4 eq.), HOBt (4 eq.) and DIPEA (15 eq.) were dissolved in DMF (10 ml). This mixture was then added dropwise to a solution of the crude linear side-chain protected peptide in DMF at a concentration of approximately 0.01 M. The reaction mixture was stirred for 3 h and excess DMF was then removed under high vacuum.

Global deprotection. A solution of TFA/TIS/H_2O (95:2.5:2.5, 10 ml) was added to the crude cyclized peptide under cooling. The mixture was then allowed to reach room temperature (RT) und stirred for 3 h. Excess TFA was removed *in vacuo* resulting in a thick oil. The oil was then transferred dropwise to a 50 ml falcon tube filled with ice cold diethyl ether to precipitate. The suspension was centrifuged (15 min at 2'400 rpm), the supernatant discarded, and the pellet resuspended in ice cold diethyl ether. This procedure was repeated twice and the pellet finally air-dried yielding a pale solid powder. Cys and Met containing peptides were deprotected under reducing conditions by a solution of TFA:1,2-ethandithiol:thioanisole:H_2O:TIS (75:10:10:4:1, 10 ml), and directly precipitated by dropwise addition into cold diisopropyl ether. Peptides that additionally contain azide groups can suffer from reduction of azides to amines under these conditions, and the use of DTT instead of 1,2-ethandithiol as thioscavenger is advised.[134]

Oxidation. Formation of disulfide bonds was achieved at a concentration of approximately 0.1 mg/ml peptide in 0.1 M ammonium acetate pH 8.5. The solution was stirred at RT overnight in the presence of atmospheric oxygen.[71]

Purification and analysis. Crude cyclic peptides were purified by reverse phase HPLC using a binary gradient from 10 to 60% MeCN in H_2O with additional 0.1% TFA on an ÄKTA purifier

100 system (*Amersham Biosciences*). Columns for analytical chromatography were of the type C18 4.6 × 250 mm with 5 µm particle size and C18 21.2 × 250 mm 7 µm particle size (*Agilent Technologies*) for preparative chromatography. UPLC was performed on an ACQUITY UPLC® system (*Waters*) equipped with a BEH130 C18 column, 2.1 x 100 mm, and 1.7 µm particle size.

4.3 Minimal Inhibitory Concentration

Bacterial strains to be tested were inoculated in water supplemented with 0.9% NaCl from a fresh agar plate. According to the McFarland standard[135], the turbidity of the bacterial suspension was adjusted to 0.5. An aliquot of 100 µl of this suspension was transferred into 10 ml MH-I with 0.02% BSA or MH-II with 0.002% Tween80. The peptide was dissolved in H_2O with 0.01% acetic acid at a concentration of 1 mg/ml, which was determined accurately by UV/VIS spectroscopy at 280 nm. A two-fold dilution series was prepared in a 96 well plate in a range of 64 µg/ml down to 0.0005 µg/ml. 50 µl of the bacterial suspension was then used to inoculate each well for a total volume of 100 µl, corresponding to 5 x 10^5 CFU/ml (colony forming units per ml). The plate was incubated overnight at 37°C and 200 rpm. The minimal inhibitory concentration was assessed visually as the lowest concentration of the antimicrobial agent that inhibits visible growth.[136]

4.4 Coupling of Fluorophores via Click Chemistry

PEG spacer with azide and acid functionality were obtained from *Broadpharm* (propargyl-PEG_4-acid and azido-PEG_4-acid) and coupled on-resin by standard Fmoc chemistry. Amino acid building block Fmoc-Glu(PEG_3-N_3)-OH was synthesized according to Come *et al.*[137]. Different fluorophores obtained from *Lumiprobe* (BDP-FL-azide), *Atto-Tec* (ATTO-MB2), and *Thermo Fisher* (Alexa Fluor® 488 and 647) were coupled according to an adapted protocol from Clavé *et al.*[138] via Click Chemistry. Fluorescein-alkyne for the LB-01-FL synthesis was kindly provided by former group member Jessica Steinmann. As a representative example reaction the coupling of thanatin to BDP-FL-azide (*Lumiprobe*) is described: Intermediate thanatin-PEG_4-azide (8.94 mg, 0.00334 mmol) was dissolved in H_2O (500 µl). Sodium ascorbate (30 µl, 0.1 M, 0.0035 mmol), BDP-FL-azide (0.00134 mmol, 0.25 mg) dissolved in DMSO (100 µl) and $CuSO_4$ (35 µl, 0.1 M, 0.0035 mmol) were sequentially added under stirring. After 15 min the mixture was injected on an LC-MS for reaction control. After another 15 min, the reaction mixture was directly purified by preparative HPLC in a single run with a gradient of 10-50% MeCN/H_2O (0.1% TFA) and a retention time of 19.8 min. The isolated fraction was

lyophilized yielding 4 mg (98%) of red lyophilisate. HRMS (ESI): calculated for $C_{132}H_{220}BF_2N_{41}O_{33}S_3$ $[M+4H]^{4+}$ 763.1505, found 763.1500.

4.5 LB-01

4.5.1 Introduction of N-Methyl Groups

Introduction of N-methyl amino acids. Commercially available N-methylated amino acid building blocks were coupled according to the protocol described above. Fmoc-N-Me-Ala-OH, Fmoc-N-Me-Leu-OH, and Fmoc-N-Me-Trp(Boc)-OH were acquired from *Sigma-Aldrich* or *Bachem*. Subsequent peptide couplings onto an N-methylated terminus proved to be difficult under regular conditions. Higher yields were achieved by double coupling with the use of amino acid (4 eq.), HATU (4 eq.), HOAt (4 eq.), and DIPEA (8 eq.).

On resin methylation (*Kessler* protocol). The resin was washed three times and swelled in DMF for 15 min by bubbling N_2 through the reaction vessel. 2-Nitrobenzenesulfonyl chloride (4 eq.) and sym-collidine (10 eq.) were dissolved in DMF (7 ml) and the resin treated for 15 min with this mixture. This procedure was repeated once. The resin was washed thoroughly with anhydrous THF. In a round bottom flask, triphenylphosphine (5 eq.) was dissolved in anhydrous THF (4 ml) and anhydrous MeOH (10 eq.) was added to the solution and mixed well. The resin was treated with this mixture for 2 min. Diisopropyl azodicarboxylate (DIAD, 5 eq.) was dissolved in THF (4 ml) and added to the reaction mixture in a portion wise manner, taking 1 ml aliquots each time with a reaction time of 10 min. This procedure was repeated once. The resin was washed three times with DMF. Mercaptoethanol (10 eq.) and DBU (5 eq.) were dissolved in DMF (7 ml) and added to the resin with a reaction time of 5 min. This procedure was also repeated once, and the resin was finally washed three times with DCM and dried *in vacuo*.[81]

4.5.2 Synthesis of Dipeptide Fmoc-Pro-N-Me-Thr(OtBu)-OH

(2*S*,3*R*)-methyl 2-(((benzyloxy)carbonyl)(methyl)amino)-3-(*tert*-butoxy)butanoate

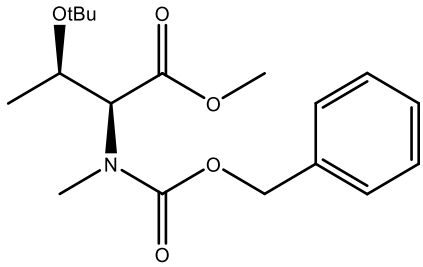

Z-Thr(tBu)-OH dicylohexylamine salt (1.00 g, 2.04 mmol) was converted to the free acid by treatment with aq citric acid 5% and extraction into Et_2O (3 x 20 ml). Ag_2O (1.89 g, 8.16 mmol) was added to a solution of *Z*-Thr(tBu)-OH free acid and MeI (1.91 ml, 30.6 mmol) in DMF (7 ml) and stirred overnight at RT. DCM (15 ml) was then added and the solution was filtered through celite. The filter cake was washed with DCM (3 x 20 mL), and the combined organic phases were washed with 15% aq $Na_2S_2O_3$ (2 x 30 ml), H_2O (3 x 30 mL) and brine (30 ml). After drying ($MgSO_4$), the combined organic phases were concentrated *in vacuo* and the oily residue was purified by flash column chromatography (4:1 cyclohexane/EtOAc) yielding 647 mg of colorless oil (94% yield).

TLC: Rf 0.50 (cyclohexane/EtOAc 4:1, UV, vanillin)
$[\alpha]_D^{24}$: +3.5° (c 0.65, MeOH)

Two rotamers with an approximate ratio of 2:1 are present.
^{1}H-NMR (500 MHz, $CDCl_3$):
Major: δ =7.39 - 7.27 (m, 5H), 5.21 - 5.04 (m, 2H), 4.82 (d, J=4.3 Hz, 1H), 4.41 - 4.35 (m, 1H), 3.70 (s, 3H) 3.14 (s, 3H), 1.19 (d, J = 6.2 Hz, 3H), 1.13 (s, 9H).
Minor: δ =7.39 - 7.27 (m, 5H), 5.21 - 5.04 (m, 2H), 4.59 (d, J= 5.1 Hz, 1H), 4.30 - 4.24 (m, 1H), 3.65 (s, 3H), 3.11 (s, 3H), 1.16 (d, J = 6.2 Hz, 3H), 1.12 (s, 9H).
^{13}C-NMR (100 MHz, $CDCl_3$):
Major: δ = 170.7, 157.6, 136.8, 128.5, 128.0, 127.9, 127.6, 74.0, 68.4, 67.4, 64.1, 51.7, 33.6, 28.7, 20.5.
Minor: δ = 170.5, 156.4, 136.6, 128.5, 128.0, 127.9, 127.6, 74.1, 67.9, 67.4, 64.4, 51.7, 34.1, 28.7, 20.7.

HRMS (ESI): calculated for $C_{22}H_{25}NNaO_4$ $[M+Na]^+$ 390.1676, found 390.1672.[39]

(*R*)-(9H-fluoren-9-yl)methyl 2-(((2*S*,3*R*)-3-(*tert*-butoxy)-1-methoxy-1-oxobutan-2-yl) (methyl)carbamoyl)pyrrolidine-1-carboxylate

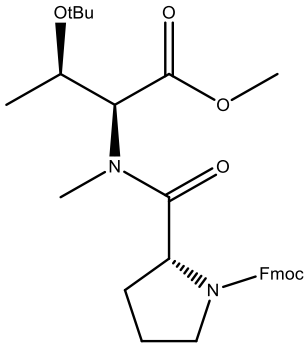

To the foregoing dipeptide (294 mg, 0.87 mmol) in THF (9 mL) was added Pd/C (10%, 93 mg, 0.09 mmol), and stirred for 30 min under H_2. The solution was then filtered through celite, washed with THF, and dried under vacuo. COMU (746 mg, 1.74 mmol) was added to a mixture of Fmoc-Pro-OH (588 mg, 1.74 mmol), the dipeptide, and DIPEA (445 µl, 2.61 mmol) in DMF (9 ml) at 0°C. The reaction mixture was warmed to RT and stirred for 2 h. The mixture was then diluted with EtOAc (25 ml) and washed with aq citric 5% (2 x 15 ml), 1 M $NaHCO_3$ (2 x 15 ml), and saturated NaCl (2 x 15 ml). The organic layer was then dried over $MgSO_4$ and the solvent removed *in vacuo*. The residue was purified by flash column chromatography (2:1 cyclohexane/ EtOAc then 1:1 cyclohexane/EtOAc) yielding 327 mg reddish foam that solidified overnight (72% yield).

Mp 64 - 68°C
TLC: Rf 0.47 (cyclohexane/EtOAc 1:1, $KMnO_4$)
$[\alpha]_D^{24}$: -42.3 ° (c 0.22, MeOH)

Two rotamers with an approximate ratio of 2:1 (Fmoc-amide rotation) are apparent by NMR, each with a low abundance rotamer deriving from the N-methyl-amide (not assigned).

^{1}H-NMR (500 MHz, $CDCl_3$):
Major: δ = 7.78 - 7.73 (m, 2H), 7.67 - 7.55 (m, 2H), 7.42 - 7.35 (m, 2H), 7.34 - 7.27 (m, 2H), 5.35 (s, J = 3.5 Hz, 1H), 4.86 (dd, J = 8.4 Hz, 1H), 4.47 - 4.41 (m, 1H), 4.41 - 4.37 (m, 1H), 4.33 - 4.26 (m, 1H), 4.30 - 4.24 (m, 1H), 3.70 (s, 3H), 3.80 - 3.72 (m, 1H), 3.62 - 3.56 (m, 1H), 3.34 (s, 3H), 2.30 - 2.21 (m, 1H), 2.05 - 1.96 (m, 1H), 2.20 - 2.09 (m, 1H), 2.03 - 1.92 (m, 1H), 1.20 (d, J = 6.3 Hz, 3H), 1.14 (s, 9H).
Minor: δ = 7.78 - 7.73 (m, 2H), 7.67 - 7.55 (m, 2H), 7.42 - 7.35 (m, 2H), 7.34 - 7.27 (m, 2H), 5.29 (s, J = 3.5 Hz, 1H), 4.65 (dd, J = 8.4 Hz, 1H), 4,71 - 4.65 (m, 1H), 4.41 - 4.35 (m, 1H), 4.23 - 4.16 (m, 1H), 4.21 - 4.16 (m, 1H), 3.68 (s, 3H), 3.69 - 3.63 (m, 1H), 3.56 - 3.47 (m, 1H),

3.15 (s, 3H), 2.30 - 2.21 (m, 1H), 2.02 - 1.95 (m, 1H), 2.04 - 1.96 (m, 1H), 2.91 - 1.82 (m, 1H),1.09 (s, 9H), 0.93 (d, J = 6.3 Hz, 3H).

^{13}C-NMR (100 MHz, $CDCl_3$):
Major: δ = 174.1, 170.7, 154.8, 144.3, 144.0, 141.3, 127.6, 127.0, 125.4, 125.2, 119.9, 74.0, 68.8, 67.4, 61.5, 57.0, 51.7, 47.2, 47.6, 34.4, 29.2, 28.7, 24.3, 20.3.

Minor: δ = 173.9, 170.5, 154.3, 144.4, 143.9, 141.3, 127.6, 127.1, 127.0, 125.3, 125.1, 119.9, 119.8, 74.1, 68.5, 66.9, 61.4, 56.8, 51.7, 47.4, 46.9, 34.0, 30.2, 28.7, 23.0, 20.2.

HRMS (ESI): calculated for $C_{22}H_{25}NNaO_4$ $[M+Na]^+$ 390.1676, found 390.1672.[39]

(2*S*,3*R*)-2-((*R*)-1-(((9H-fluoren-9-yl)methoxy)carbonyl)-N-methylpyrrolidine-2-carboxamido)-3-(*tert*-butoxy)butanoic acid

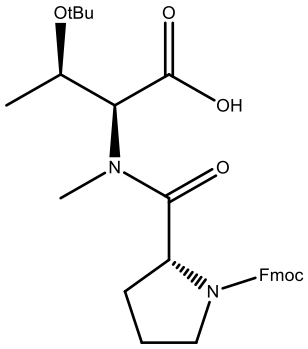

To the foregoing methyl ester (265 mg, 0.51 mmol) in EtOAc (5 mL) was added LiI (679 mg, 5.07 mmol). The mixture was refluxed for 16 h. After cooling, water was added and the solution acidified with aq citric acid 5% to pH 3, and extracted with EtOAc (3 x 20 ml). The combined organic phases were dried over $MgSO_4$ and concentrated *in vacuo*. The product was purified by flash column chromatography (19:1 to 4:1 DCM/MeOH) yielding 203 mg of a white solid (79% yield).

Mp 96 - 99°C
TLC: Rf : 0.51 (9:1 DCM/MeOH, $KMnO_4$)
$[\alpha]_D^{24}$: -34.8° (c 0.23, MeOH)

Two rotamers with an approximate ratio of 1:1 (Fmoc-amide rotation) are apparent by NMR, each with a low abundance rotamer deriving from the N-methyl-amide (not assigned).

^{1}H-NMR (500 MHz, DMSO-d_6):
Rotamer 1: δ = 12.80 - 12.62 (br, 1H), 7.92 - 7.85 (m, 2H), 7.70 - 7.53 (m, 2H), 7.45- 7.39 (m, 2H), 7.37 - 7.26 (m, 2H), 4.79 (d, J=3.7 Hz, 1H), 4.75 - 4.68 (m, 1H), 4.38 - 4.34 (m, 1H), 4.27 - 4.21 (m, 2H), 4.17 - 4.11 (m, 1H), 3.49-3.39 (m, 2H), 3.16 (s, 3H), 2.32 - 2.18 (m, 1H), 1.83 - 1.76 (m, 2H), 1.79 - 1.73 (m, 1H), 1.12 (s, 9H), 1.04 (d, J = 6.3 Hz, 3H),

Rotamer 2: δ = 12.80 - 12.62 (br, 1H), 7.92 - 7.85 (m, 2H), 7.70 - 7.53 (m, 2H), 7.45 - 7.39 (m, 2H), 7.37 - 7.26 (m, 2H), 5.01 (d, J = 3.7Hz, 1H), 4.75 - 4.68 (m, 1H), 4.44 - 4.38 (m, 1H), 4.34 - 4.29 (m, 1H), 4.28 - 4.23 (m, 1H), 4.14 - 4.07 (m, 1H), 3.49 - 3.39 (m, 2H), 3.08 (s, 3H), 2.32 - 2.18 (m, 1H), 1.91 - 1.83 (m, 2H), 1.75 - 1.69 (m, 1H), 1.06 (s, 9H), 0.88 (d, J = 6.3 Hz, 3H),

^{13}C-NMR (100 MHz, DMSO-d_6):
Rotamer 1: δ =172.9, 171.5, 153.6, 143.9, 143.8, 140.7, 127.6, 127.1, 125.2, 120.1, 73.2, 67.9, 66.4, 61.2, 56.6, 47.1, 46.9, 33.7, 29.6, 28.5, 23.7, 20.5.
Rotamer 2: δ = 172.8, 171.3, 153.6, 143.8, 143.4, 140.7, 127.6, 127.1, 125.1, 120.0, 73.2, 67.8, 66.2, 60.9, 56.4, 46.6, 46.4, 33.6, 28.6, 28.5, 23.7, 20.3.

HRMS (ESI): calculated for $C_{29}H_{36}N_2NaO_6$ $[M+Na]^+$ 531.24715, found 531.24656.[39]

4.5.3 Solution NMR of N-methylated Analogues

^{1}H NMR measurements were performed in H_2O/D_2O (9:1) or pure D_2O at pH 2-3, at 10-15 mg/ml. Spectra were acquired on a *Bruker* AV-600 spectrometer at 300K. Water suppression was performed by presaturation. Spectral assignments were made by using 2D DQF-COSY, TOCSY and NOESY spectra. $^{3}J_{HNH\alpha}$ coupling constants were determined from 1D spectra or, in the case of signal overlap from 2D NOESY spectra, by inverse Fourier transformation of in-phase multiplets. Distance restraints were obtained from NOESY spectra with a mixing time of 250 ms. Spectra were typically collected with 1024 x 256 complex data points zero-filled prior to Fourier transformation to 2048 x 1024, and transformed with a cosine-bell weighting function. Data processing was carried out with TOPSPIN (*Bruker*) and XEASY[139]. Temperature coefficients were obtained by measuring the chemical shifts of the amide protons, and calculating their relative change over that temperature range. For the H/D exchange experiments, the lyophilized peptides were dissolved in 99% D_2O, and one-dimensional spectra were acquired every 10 min for 2 h at 300K. The amide region of the spectrum was analysed to determine slow exchanging amide protons. The structure calculations were performed by restrained molecular dynamics in torsion angle space by applying the simulated annealing protocol implemented in the program CYANA[89]. Starting from 100 randomized conformations, a bundle of 20 conformations incurring the lowest

CYANA target energy function were selected. MOE (Molecular Operating Environment, *Chemical Computing Group* Montreal, Canada) was used for structure analysis and visualization of the molecular models.[39]

4.5.4 Circular Dichroism

Circular dichroism spectra were recorded on a J-175 spectropolarimeter (*Jasco*) using a quartz cell of 1 cm path length at RT. The measurement range was 195 to 250 nm with a scan rate of 20 nm/min and standard sensitivity. Two scans were accumulated, corrected for background signal, averaged, and smoothed for each spectra. Concentrations of all compounds were 10 µM in PBS (phosphate buffered saline) pH 7.4. Values are expressed as molar ellipticity (deg*cm^2/dmol).

4.5.5 Cellular Uptake Studies

Cell culture. HeLa cells were kindly provided by the Wang group at the Institute of Experimental Immunology UZH. Cells were cultivated in DMEM with the addition of 10% FBS (fetal bovine serum, *Sigma-Aldrich*) and 1x streptomycin/penicillin (100x stock Gibco®, *Thermo Fisher*). 1x trypsin-EDTA 0.5% (10x stock Gibco®, *Thermo Fisher*) was used for cell dissociation in routine cell culture passaging.

Confocal microscopy. 100'000 HeLa cells, counted with a Neubauer chamber, were seeded on round cover slips in a 12 well plate and grown for 24 h. Media was exchanged with addition of fluorescence-labelled peptides Tat-FITC (20 µg/ml), LB-01-FL (10 µg/ml), or LB-01-AF647 (20 µg/ml). The cells were washed three times with PBS and then incubated in 2% paraformaldehyde in PBS for 10 min. Cells were then aspirated and mounted with mounting media containing DAPI (ProLong® Gold Antifade, *Thermo Fisher*) on microscope slides (Menzel-Gläser, 76x26 mm, *Thermo Fisher*). Fluorescence microscopy was performed on a *Leica* CLSM SP8 inverted microscope, using a 100x oil objective (HC PL APO, *Leica*).

Cell lysis assay. 7 x 100'000 cells were seeded in 12 well plates the day before. Cells were washed three times with PBS (500 µl) and incubated in triplicate with 6.4 µM Tat-FITC, 6.4 µM LB-01-FL, and one control, for 1 h in serum free DMEM (500 µl). Cells were then carefully washed three times with PBS (500 µl). Cell lysis was performed with 100 µl DISC lysis buffer (30 mM Tris-HCl (pH 7.5), 150 mM NaCl, 10% glycerol, 1% Triton X-100, cOmplete™ mini protease inhibitor cocktail (*Roche*)) for 20 min on ice. The lysate was transferred to Eppendorf tubes and centrifuged (5'000 rpm, 5 min). 50 µl of the supernatant was transferred to a white, flat-bottom 96 well plate (*Corning*) and diluted with 50 µl PBS. Fluorescence intensity was then

recorded on a *Tecan* infinite 200 Pro plate reader (Ex. 485 nm / Im. 535 nm). A dilution series of Tat-FITC was used to calculate the concentrations of fluorescence-labelled compound taken up by the cells.

4.6 Thanatin

4.6.1 Sytox® Green Assay in MH-I

20 mL of MH-I were inoculated with 2% (400 µl) of an *E. coli* ATCC25922 overnight culture. The bacteria were grown at 37°C and 200 rpm, to an OD_{600} of 0.3-0.4. The cells were then centrifuged (5 min at 4'000 rpm) and the pellet was resuspended in the right amount of MH-I to obtain an OD_{600} of 0.1. 3 ml of this suspension were transferred into a cuvette containing a magnetic stir bar and 0.002% Polyoxethylene80 (P80 or Tween80). The fluorescence was then recorded using an LS55 Fluorescence Spectrometer (*PerkinElmer*). Excitation and emission wavelengths for Sytox® Green dye were 488 nm and 525 nm respectively. A slit width of 2.5 nm was used to record the spectrum. A blank was first measured for 100 s. After this, Sytox® Green dye from a 500 µM stock solution in DMSO was added to reach a concentration of 0.5 µM, and the signal was observed during 400 s. At this point, the antibiotic was added and the fluorescence intensity was recorded for 1 h.

4.6.2 Sytox® Green Assay in HEPES Buffer

20 mL of MH-I were inoculated with 2% (400 µl) of an *E. coli* ATCC25922 overnight culture. The bacteria were grown at 37°C and 200 rpm, to an OD_{600} of 0.3-0.4. The cells were then centrifuged (5 min at 4'000 rpm) and the pellet was washed a single time and then resuspended in 5 mM HEPES buffer pH 7.2 with or without $MgCl_2$ (0.5 mM) and $CaCl_2$ (1 mM) supplementation to obtain an OD_{600} of 0.1. 3 ml of this suspension were taken into a cuvette containing a magnetic stir bar, 0.002% of Tween80, and the antibiotic. The fluorescence intensity was then recorded as stated above.

4.6.3 β-Galactosidase Assay

MH-II was inoculated with 2% of an overnight culture of *E. coli* ML-35[140] (ATCC43827) in LB (lysogeny broth). The bacteria were grown at 37°C and 200 rpm, to an OD_{600} of 0.4 - 0.6. During this time a 24-well plate was prepared containing the right amount of antibiotic, 0.02% BSA and a solution of H_2O/DMSO (80:20%) to fill up to 50 µl. At an OD_{600} of around 0.6, the cells were centrifuged (5 min at 4'000 rpm), washed in LB media and centrifuged again (5 min at 4'000 rpm). Finally, the cell pellet was resuspended in PBS (containing 1 mM $CaCl_2$ and

0.5 mM $MgCl_2$) to obtain an OD_{600} of 0.5. From this culture, 950 µl were added to each well (except the wells containing PBS only for the controls and the wells containing the supernatant of lysed cells for the 100% β-galactosidase release control). The plate was incubated at 37°C and 200 rpm for 1 h. The content of each well was transferred to Eppendorf tubes and centrifuged (45 s at 11'000 rpm). The supernatant (900 µl) was placed back in a fresh 24-well plate and OPNG (o-nitrophenyl-β-galactoside) was added to a final concentration of 0.25 mM (100 µl of a 0.25 mM a stock solution). After 30 min at RT, the absorbance was measured at 420 nm. H_2O:DMSO (80:20) treated bacteria were used as "zero intensity" controls and sonicated, lysed cell were used as 100% β-galactosidase release controls.[29]

4.6.4 β-Lactamase Assay

For periplasmic β-lactamase expression, *E. coli* ML-35 cells were grown in MH-II containing ampicillin (100 µg/ml) to an OD_{600} of 0.4 - 0.6. During this time, a 24-well plate was prepared containing the right amount antibiotic, 0.02% BSA, and a solution of H_2O:DMSO (80:20%) to fill up to 50 µl. The cells were then collected, washed twice with fresh MH-II, and resuspended in PBS supplemented with $CaCl_2$ (1 mM) and $MgCl_2$ (0.5 mM) to an OD_{600} of 0.3. The cell suspension (950 µl) was distributed to the previously prepared 24-well plate. The plate was incubated at 37°C and 200 rpm for 1 h. The content of each well was transferred to Eppendorf tubes and centrifuged (45 s, 11'000 rpm). The supernatant (900 µl) was placed back in a fresh 24-wells plate, to which CENTA (*Merck-Millipore*) substrate was added to a final concentration of 100 µg/ml. After 30 min at RT, the absorbance was measured at 405 nm. H_2O:DMSO (80:20) treated bacteria were used as "zero intensity" controls and sonicated, lysed cell were used as 100% β-lactamase release.[29]

4.6.5 Macromolecular Synthesis Assay

The radioisotope precursors (10x final concentration, in 2x DM) and an 8-point, two-fold serial dilution of antibiotics (10x final concentration, in H_2O:DMSO (80:20) were prepared (Table 17 and Table 18). The experiments were carried out in 96-well round bottomed polypropylene plates (*Thermo Fisher*). For each [^{3}H]-precursor, a background (without cells), a maximal incorporation (cells without antibiotic), and a duplicate of cells treated with antibiotic dilutions were made. For the background and the maximal incorporation, 10 µl of the 10x radioisotope stock + 10 µl of H_2O:DMSO (80:20) were added. For the antibiotic treated samples, 10 µl of the 10x radioisotope stock and 10 µl of the antibiotic dilution were added. Once prepared, the plates were prewarmed to 37°C.

Table 17 Concentrations and specific activities of precursors used for the macromolecular synthesis assay in E. *coli* ATCC25922.

	Final conc. [µCi/ml]	Final conc. [µM]	Specific activity [Ci/mmol]
[^{3}H]-Leucine	10	0.16	60
[^{3}H]-Uridine	10	0.16	60
[^{3}H]-Thymidine	10	0.14	71
[^{3}H]-NAG	1	0.016	60

Table 18 Concentrations of the 10x antibiotic stock solutions in H_2O:DMSO (80:20).

	Tobramycin [µg/ml]	Rifampicin [µg/ml]	Ciprofloxacin [µg/ml]	Ceftriaxone [µg/ml]	Thanatin [µg/ml]
1	320	2560	5.12	80	160
2	160	1280	2.56	40	80
3	80	640	1.28	20	40
4	40	320	0.64	10	20
5	20	160	0.32	5	10
6	10	80	0.16	2.5	5
7	5	40	0.08	1.25	2.5
8	2.5	20	0.04	0.625	1.25

1x DM (defined growth media) was inoculated with 2% of an overnight culture of E. *coli* ATCC25922 in MH-I (2%) and grown at 37°C and 200 rpm. When the mid-log phase was reached (OD_{600}=0.3), 80 µl of 1x DM was added to the background wells (cell-free blank) and 80 µl of mid-log phase cells were added to the maximum incorporation and the antibiotic treated incorporation wells. Plates were incubated at 37°C and 200 rpm for 20 min, which is approximately half the generation time for E. *coli* ATCC25922 in 1x DM. At this point, the incorporation was terminated by addition of 50 µl of 30% TCA (trichloroacetic acid) to each well. Plates were cooled down for 1 h at 4°C, incubated at 37°C and 200 rpm for 30 min, and cooled again for 15 min at 4°C. During this time, 96-well filter plates (*Merck-Millipore*) were prepared by washing with 200 µl of 5% TCA, according to the manufacturer's instructions. Test aliquots of 120 µl (of a total 150 µl) were transferred to the filter plates, filtered, and washed four times with 5% TCA and one time with 95% EtOH. The filter plates were dried (50°C for 1 h) and the underdrain removed. The filters were punched and transferred to a 96-well isoplate (*Perkin Elmer*). 200 µl of OptiPhase Supermix (*Perkin Elmer*) was added to each well and the top of each plate was sealed with transparent film (*Merck-Millipore*). After one night shaking at 150 rpm, the plates were counted on a Wallac MicroBeta 1'450 scintillation counter

(*PerkinElmer*), with top and bottom PMT counting for a better signal-to-noise ratio (each well 2 min).

Defined growth media (DM). The defined medium used for macromolecular synthesis assays comprised the following: 1xM9 salts; 0.5% glucose (w/v); 1 mM $MgCl_2$; 20 µg/ml $CaCl_2$; 2 µg/ml thiamine; 2 µg/ml nicotinic acid; 100 µM L-alanine, L-asparagine, L-aspartate, L-glutamate, L-glycine, L-proline, and L-serine; and 200 µM L-arginine, L-cysteine, L-histidine, L-isoleucine, L-lysine, L-methionine, L-phenylalanine, L-threonine, L-tryptophan, L-tyrosine, and L-valine; 1 µM L-leucine.

4.6.6 Photoaffinity Labelling

200 ml MH-I medium was inoculated with 2% of an *E. coli* ATCC25922 overnight culture and incubated at 37°C and 200 rpm. After reaching an OD_{600} of 1, 50 ml of this culture were spin down (20 min at 4'000 rpm). The cells were washed once, then taken up in 50 ml PBS and incubated for 30 min at 37°C and 200 rpm in the dark with 2-10 µg/ml thanatin-PAL5 (MIC = 2-4 µg/ml), followed by UV irradiation at 350 nm wavelength in a Rayonet Reactor (16 x 8W *Sylvania* blacklight lamps) for 30 min at 30°C. A control sample was treated in the same manner, without addition of the photoprobe. Cells were harvested by centrifugation (30 min at 4'000 rpm) and washed two times with PBS. Pellets can be stored at -20°C.

Membrane isolation. The cell pellets described above were resuspended in 50 mM Tris-HCl, pH 7.3, with addition of one tablet cOmplete™ mini protease inhibitor cocktail (*Roche*) per 30 ml and lysed by three cycles of sonication using a Branson digital sonifier equipped with a microtip (80 W, 30% intensity, 20 sec on with 20 sec off for 2 min) under cooling on ice. To remove unbroken cells and cell debris, the lysate was centrifuged (30 min at 4'000 rpm, 4°C). The supernatant was then carefully decanted and subjected to ultracentrifugation (200'000 g, 45'000 rpm in a Sorvall T-875 rotor, 1 h, 4°C). The supernatant, containing the soluble cytoplasmic protein fraction, was kept. The pellet was resuspended in 50 mM Tris-HCl, pH 7.3 and again, subjected to ultracentrifugation (1 h at 45'000 rpm, 4°C). The pellets (isolated membrane fraction) can be stored at -20°C.

Determination of protein concentration. Protein concentrations were determination by the Bradford method[141]. H_2O (500 µl) and Bradford reagent (500 µl) (*Sigma-Aldrich*) and 5 µl of the protein suspension were mixed and the absorption was measured at 595 nm. A standard curve was generated using BSA, to determine the sample concentration by linear regression.

1D gel electrophoresis. Aliquots of 1-10 µg of protein from membrane or cytoplasmic fractions were loaded on SDS-polyacrylamide gels in SDS loading buffer containing 100 mM DTT as a final concentration. After 5 min heating at 100°C in a heating block, each sample was loaded onto the gel twice, resulting in 2 half gels, one for Coomassie brilliant blue staining and the other half for Western blotting and biotin detection.

Investigation of proteins with low molecular weight. Precasted 4-20% TGX gradient gels (*Bio-Rad*) were run at 200 V in electrophoresis buffer (25 mM Tris, pH 8.8, 192 mM glycine, 0.1% SDS). Blotting was achieved using the Trans-Blot® Turbo blotter (*Bio-Rad*) with commercially available membrane stacks (PVDF, 0.2 µm pore size, *Bio-Rad*) for 2 x 8 min at 1.3 A, 25 V.

Investigation of proteins with high molecular weight. Self-casted gels with 10% acrylamide (4% acrylamide in stacking gel) according to Laemmli[142] were run in electrophoresis buffer (25 mM Tris-HCl, pH 8.3, 192 mM glycine, 0.1% SDS) with initially 90 V for the stacking and then 130 V for the separating gel. For blotting, a properly sized piece of PVDF membrane (0.45 µm pore size, Immobilon®-P, *Merck*) was activated with MeOH (30 s), then rinsed two times for 2 min with H_2O and pre-equilibrated 5 min with transfer buffer (buffer 1: 12 mM Tris, 96 mM glycine, 0.1 % SDS and buffer 2: 10 mM Na_2HPO_4, 1 % SDS, 6 M Urea. Mix 1:1 and filter (0.22 µm pore size, *Whatman*)). Six filter papers (3 mm, *Whatman*) were cut out in the same size as the gel and the membrane. Filters, membrane and gel were placed on the graphite plate in the following order: i) three filter papers soaked in transfer buffer, ii) pre-equilibrated membrane, iii) gel, iv) three filter papers soaked in transfer buffer. Electrophoretic transfer of proteins from gel onto the membrane was achieved by a *Pierce* G2 Fast Blotter (*Thermo Fisher*) for 2 h at 0.5 A and 10 V. After transfer, the membrane was blocked with blocking buffer (3% BSA, 0.2% Tween20 in PBS) for 1 h at RT or overnight at 4°C. After blocking, the membrane can be stored at -20°C. For detection, the blocked membrane was incubated with Streptavidin-HRP or NeutrAvidin-HRP conjugate (*Pierce*, 1:30'000 from stock, 1% BSA, 0.2% Tween20 in PBS) for 1 h. The membrane was washed 4 x 5 min with PBS. Then, the membrane was covered with WesternBright™ Sirius™ (*Advansta*) HRP substrate (1 - 3x dilution with H_2O) on the tray and covered with plastic foil. Chemiluminescence was detected on a ChemiDoc™ MP Imaging System (*Bio-Rad*) over the course of 1-20 min. The washed (PBS) membrane can be stored at -20°C.

4.6.7 2D Gel Electrophoresis

The protein concentration was determined by the Bradford method after the first ultracentrifugation and resuspension in 50 mM Tris-HCl, pH 7.3 buffer. After the second ultracentrifugation step the samples were resuspended to a concentration of 1.33 mg/ml in rehydration buffer (1% w/v tetradecanoylamido-propyl-dimethylammonio-propane-sulfonate (ASB-14, *Sigma-Aldrich*), 2 mM tributyl phosphine, 7 M urea, 2 M thiourea and 0.5% w/v carrier ampholytes 3-10 (Biolytes pH 3-10, *Bio-Rad,* and a small spatula of bromophenol blue). For Coomassie staining 600 µg protein/gel (450 µl), for biotin detection 200 µg protein/gel (150 µl diluted to 450 µl) were required. Samples were centrifuged (3 min, 13'000 rpm) and loaded by in-gel rehydration onto immobilized pH gradient strips (IPG-strips, pH 4-7, 18 cm, *Bio-Rad*) overnight at RT. Isoelectric focussing was performed using an *Ettan* IPGphor isoelectric focussing system (*Amersham*) for 3 h at 150 V, 3 h at 300 V, and finally 8'000 V for a total of 50 kVh. Subsequently, the IPG-strips were equilibrated in 6 M urea, 20% glycerol, 2% w/v SDS, 5 mM tributyl phosphine and 375 mM Tris (3 ml/strip) for 30 min at RT. The strips were then placed on top of a 10% SDS-PAGE gel (acrylamide/bisacrylamide Roti Gel 40, 375 mM Tris-HCl pH 8.8, 5% glycerol, 0.1% SDS, 1.1 µM TEMED, 0.05% ammonium persulfate) and sealed using 1.5 ml of a 0.5% agarose solution in running buffer, containing a small amount of bromophenol-blue. Precision Plus Protein standard plugs (*Bio-Rad*) or filter papers soaked with pre-stained protein ladder (*Fermentas* Page Ruler™) were added and gels were electrophoresed using an *Ettan* DALT II system (*Amersham*) with 2 W/gel for 45 min and 17 W/gel for 3 h, with electrophoresis buffer (25 mM Tris-HCl, pH 8.3, 192 mM glycine, 0.1% SDS). For Coomassie staining, gels were incubated in fixing solution (20% methanol, 1% phosphoric acid (80%)) for 30 min and stained overnight in 20% RotiBlueTM (*Roth*) concentrate, 20% methanol, and 60% water. Gels were destained for 5 min in 25% methanol/water and stored in MilliQ-water. For Biotin detection the proteins from an unstained gel were blotted onto an PVDF membrane (0.45 µm pore size, Immobilon®-P, *Merck*) in a *Pierce* G2 Fast Blotter (*Thermo Fisher*) for 2 h at 0.5 A and 10 V. After transfer, the membrane was blocked with blocking buffer (3% BSA, 0.2% Tween20 in PBS) for 1 h at RT or overnight at 4°C. After blocking, the membrane can be stored at -20°C.

4.6.8 Fluorescence Microscopy

20 ml of MH-II were inoculated with 400 µl of an overnight culture of *E. coli* ATCC25922 in LB. The bacteria were grown at 37°C and 200 rpm to exponential growth phase (OD_{600} of 0.5 - 0.7). When the exponential phase was reached, 200 µl of the culture was taken and transferred to an Eppendorf tube. Antibiotics in the desired concentration were added. A negative control was done by adding the same amount of H_2O:DMSO (80:20). The samples were incubated for

1 h at 30°C and 200 rpm. In case of thanatin-BDP-FL (BDP-FL-azide, *Lumiprobe*) labelling, the cells were incubated for 1-2 h, washed twice with PBS, and then fixated with 200 µl of 4% paraformaldehyde in PBS for 30 min at RT. After fixation, the cells were again washed in PBS and resuspended in H_2O (20 µl). In the meantime, microscope patches were prepared by boiling 1% agarose solution in water until the agarose was completely dissolved. 800 µl were then poured onto a clean microscope slide (Menzel-Gläser, 76x26 mm, *Thermo Fisher*), covered with a second slide, and cooled down for 5 min. The agarose patches were kept wet. Different dyes were added to the samples and the bacteria were incubated on ice for 1 h. The samples were centrifuged (30 s at 3'300 g) and resuspended in 200 µl medium to wash the cells. The cells were then centrifuged again (30 s at 3'300 g) and concentrated in one tenth of the volume. 3 µl of the sample were added onto the microscope patch and imaged with a fluorescence microscope (CLSM SP8 inverted, *Leica*), using a 100x oil objective (HC PL APO, *Leica*). Fluorescent compounds were used in concentrations according to Table 19.

Table 19 Concentrations of different fluorescent compounds used in the experiments.

Compound	Stock (in DMSO)	Concentration Experiment	Labelling time [min]
FM4-64	100 µg/ml	1 µg/ml	45 - 60
Sytox	50 µM	0.5 µM	10 - 15
DAPI	200 µg/ml	0.2 µg/ml	10
Thanatin-BDP-FL	500 µg/ml (20% H_2O)	4 - 8 µg/ml	60 - 120

4.6.9 Protein Identification by Mass Spectrometry

Cell harvesting. For the photoaffinity labelling experiment, 2 x 200 ml MH-I were inoculated with 2% (4 ml) of an *E. coli* ATCC25922 overnight culture. The cells were harvested at an OD_{600} of 1 by centrifugation (20 min, 4'000 rpm). The cells were washed, and taken up in 200 ml PBS and incubated for 30 min at 37°C with 10 µg/ml thanatin-PAL5 and 0.002% Tween80, followed by UV irradiation (350 nm) for 30 min at 30°C. A control sample was treated in the same manner. The cells from three different cultures of labelled and control samples were washed five times with PBS (50 ml), put on ice, and subjected to mass spectrometric analysis at ETH Zurich. For the proximity based photo-oxidation experiment, 200 ml MH-I were inoculated with 2% (4 ml) of an *E. coli* ATCC25922 overnight culture. The cells were harvested at an OD_{600} of 1.2 by centrifugation (20 min, 4'000 rpm) and washed once with PBS (50 ml) and delivered to ETH Zurich on ice.

Sample preparation photoaffinity labelling. Cell pellets of thanatin-PAL5 labelled (n=3) and unlabelled control samples (n=3) were resuspended in 50 mM ammonium bicarbonate containing protease inhibitor cocktail (cOmplete™ mini protease inhibitor cocktail, *Roche*) and 1% RapiGest (*Waters*). Cells were lysed at 4°C by six intervals of 30 s ultrasound sonication in a vial tweeter (*Hielscher Ultrasonics GmbH*) at a power of 170 W and 80% cycle time. Protein concentration was measured by Nanodrop 2000 Spectrophotometer (*Thermo Fisher*) and 10 mg protein incubated with 200 µl agarose based streptavidin resin (*Thermo Fisher*) for 100 min at 4°C to bind biotinylated proteins. Beads were settled by centrifugation (5 min at 2'000 g). The supernatant was collected and stored at -20°C. Beads were then resuspended in 50 mM ammonium bicarbonate and transferred to Mobicol columns equipped with a 30 µm pore size filter (*MoBiTec GmbH*). On a Vac-Man Laboratory Vacuum Manifold (*Promega*), the beads were extensively washed with 20 times 500 µl aliquots of 5 M NaCl, StimLys buffer (50 mM Tris pH 7.8, 137 mM NaCl, 150 mM Glycerol, 0.5 mM EDTA, 0,1 % Triton X-100), 100 mM $NaHCO_3$ and a final 50 mM ammonium bicarbonate wash to remove non-biotinylated proteins. Beads were transferred to fresh Mobicol columns and proteins reduced with 5 mM Tris(2-carboxyethyl)phosphine (TCEP) in 50 mM ammonium bicarbonate for 40 min at 37°C. Then, proteins were alkylated on-beads by adding iodoacetamide to a final concentration of 10 mM for 30 min at 37°C. Purified biotinylated proteins were proteolytically digested by sequencing grade modified trypsin (*Promega*) for 20 h at 37°C. Peptide containing solution was collected by quick spinning of Mobicols in Eppendorf tubes. Beads were further washed with 50 mM ammonium bicarbonate and the flow-through pooled with peptide solution. Samples were acidified to pH < 3 by addition of formic acid and subjected to C18 purification using 3–30 µg UltraMicroSpin Columns (*The Nest Group*) according to the manufacturer's instructions.

Sample preparation proximity based photo-oxidation. Cell pellets were resuspended in PBS containing 3 µM thanatin-PAL5-MB (n=3) or 3 µM thanatin-PAL5-MB with 30 µM native thanatin (n=3, competition control). Cells were incubated for 30 min at 37°C and then resuspended in ice cold PBS containing 5 mM biocytin-hydrazide (*Pitsch Nucleic Acids*) at pH 6.5. Subsequently, cells were illuminated for 5 min with monochromatic light at a wavelength of 656 nm and an intensity of 58 mW/cm^2 at 4°C, using precision LED spotlights (*Micro Control Instruments Ltd.*). After the photo-oxidation, cells were incubated in the dark for 25 min at 4°C to ensure thorough biotinylation of oxidized proteins. Samples were resuspended in 50 mM ammonium bicarbonate, containing protease inhibitor cocktail (cOmplete™ mini protease inhibitor cocktail, *Roche*) and 0.1% RapiGest (*Waters*). Cells were lysed at 4°C by six intervals of 30 s ultrasound sonication in a vial tweeter (*Hielscher Ultrasonics GmbH*) at a power of 170 W and 80% cycle time. Protein concentration was

measured by a Nanodrop 2'000 spectrophotometer (*Thermo Fisher*) and 8 mg protein per sample was subjected to automated purification and processing of biotinylated proteins. For this, in-house packed tips containing 80 µl streptavidin plus ultraLink resin (*Thermo Fisher*) were coupled to a Versette liquid handling robotic system (*Thermo Fisher*) and incubated with the cell lysate for 1 h at room temperature while pipetting up-and-down. In an automated fashion, bead-bound proteins were subsequently washed with 5 M NaCl, StimLys Buffer (described above), 100 mM $NaHCO_3$ and 50 mM ammonium bicarbonate, reduced with 5 mM TCEP, 3 M urea, 50 mM ammonium bicarbonate for 30 min at 37°C, alkylated with 10 mM iodoacetamide in 3 M urea and 50 mM ammonium bicarbonate for 30 min at 37°C and proteolytically digested with sequencing grade modified trypsin (*Promega*) in 1.5 M urea and 50 mM ammonium bicarbonate for 17 h at 37°C. Eluted peptides were acidified to pH < 3 by addition of formic acid and subjected to C18 purification using 3–30 µg UltraMicroSpin Columns (*The Nest Group*) according to the manufacturer's instructions.

Mass spectrometry acquisition. Peptide samples were separated by reversed-phase chromatography on a HPLC column (75 µm inner diameter, *New Objective*) that was packed in-house with a 15 cm stationary phase (ReproSil-Pur C18-AQ, 1.9 µm) and connected to a nano-flow HPLC combined with an autosampler (EASY-nLC II, *Thermo Fisher*). The HPLC was coupled to a Q-Exactive Plus mass spectrometer (Thermo Fisher) equipped with a nano electrospray ion source (*Thermo Fisher*). Peptides were loaded onto the column with 100% buffer A (99.9% H_2O, 0.1% formic acid) and eluted at a constant flow rate of 300 nl/min with a 30 min linear gradient from 6–20% buffer B (99.9% ACN, 0.1% FA) and 15 min 20-32% followed by a 3 min transition from 32% to 50% buffer B. After the gradient, the column was washed 5 min with 98%, 4 min with 50%, and again 5 min with 98% buffer B. In between runs, the column was further cleaned for 18 min with two steep consecutive gradients of acetonitrile (10% - 98%). Electrospray voltage was set to 2 kV, sheath and auxiliary gas flow to zero, and capillary temperature to 250°C. In data-dependent acquisition (DDA) mode, the mass spectrometer automatically switched between MS and MS/MS detection. Following a high-resolution survey MS spectrum (from 300 to 1'500 m/z) acquired in the Orbitrap with resolution R = 70'000 at m/z 200 (automatic gain control target value $3*10^6$), the 15 most abundant peptide ions with a minimum intensity of $2.5*10^4$ were selected for subsequent HCD fragmentation with an isolation window of 1.4 Da and fragments were detected by MS/MS acquisition at resolution R = 35'000 (automatic gain control target value: $1*10^6$). Target ions already selected for fragmentation were dynamically excluded for 30 s.

Data analysis. Acquired raw files were subjected to peptide and protein identification using Trans Proteomic Pipeline v.4.7 (SPC/ISB Seattle). First, fragment ion spectra acquired in DDA mode were matched against a database of SwissProt (UniProt consortium) reviewed *E. coli* protein sequences and common contaminants.[119] Peptides were required to be fully tryptic with a maximum of 2 missed cleavage sites, carbamidomethylation as fixed modification, and methionine oxidation as a dynamic modification. The precursor and fragment mass tolerance were set to 20 ppm and 0.02 Da, respectively. Identified proteins were quantified by integration of chromatographic traces on MS1 level using Progenesis QI v.2.0 (*Nonlinear Dynamics UK*). Contaminant hits were removed and proteins filtered to obtain a false discovery rate of < 1%. Raw protein abundances based on non-conflicting peptides were exported and differential abundance testing was performed using R-package MSstats v3.5.3[143]. Bacterial proteins with an abundance fold change of +/- 1.5 and adjusted p-value < 0.05 were considered as significantly regulated by photoaffinity labelling or proximity based photo-oxidation.

4.6.10 Production of Recombinant *E. coli* LptA-His$_6$

Gene cloning. Primers for NdeI and XhoI restriction site were ordered from *Sigma-Life Science* (Ndefor: ATCTACATATGAAATTCAAAAACAAAC and Xhorev: TACGTCTCGAGATTACCCTTCTTCTGTGC). Chromosomal DNA from *E. coli* ATCC25922 was isolated (Bacterial Genomic DNA Kit, *GenElute*™) and loaded for PCR (polymerase chain reaction) amplification according to Table 20. The temperature program was run on a GeneAmp® PCR System 2700 (*Applied Biosystems*) with 25 amplification cycles (45 min/95°C, 45 min/45°C, 1 min/72°C). The PCR product was purified on a 1% agarose gel with addition of ethidium bromide (approximately 0.5 µg/ml). Bands were highlighted around 500 bp and cut out under UV light for digestion with restriction enzymes. The pET-22b vector was isolated (QIAprep Spin Miniprep Kit, *Qiagen*) from an overnight culture of a pET-22b containing strain, digested by restriction enzymes NdeI and XhoI, and purified on a 1% agarose gel. One third of the vector band and the whole band of *lptA* were cut out, pooled, and purified using the QIAquick gel extraction Kit (*Qiagen*). Ligation was performed overnight at 16°C.

Table 20 Components used for PCR amplification.

	$MgSO_4$ 3 mM		$MgSO_4$ 4 mM	
	control		**control**	
template genomic 'DNA	0	1	0	1
ddH_2O	41	40	39	38
10xPfu/20 mM $MgSO_4$	5	5	5	5
$MgSO_4$ 25 mM	2	2	4	4
LptA NdeI for 50 µM	0.5	0.5	0.5	0.5
LptA XhoI rev 50 µM	0.5	0.5	0.5	0.5
dNTPs 25 µM	0.5	0.5	0.5	0.5
Pfu Taq Pol (3 U/µl)	0.5	0.5	0.5	0.5
Total volume [µl]	**50**	**50**	**50**	**50**

Transformation. *E. coli* XL1 Blue were taken from a -80°C stock and put on ice for 30 min with the addition of an aliquot of the vector. Then, the cells were put in a water bath at 45°C for 45 min (heat shock transformation) and again put on ice for 2 min. After that, 600 µl of S.O.C. medium (*Thermo Fisher*) was added and the cells incubated for 1 h at 37°C and 200 rpm. Cells were plated out on solid agar supplemented with ampicillin and incubated overnight. Four single colonies were isolated and grown in LB overnight. 1.5 ml of each overnight culture were subjected to DNA extraction (QIAprep Spin Miniprep Kit, *Qiagen*). Then, the plasmid DNA was incubated with restriction enzymes NdeI and XhoI for 1.5 h. Colonies were sent to sequencing analysis (*Microsynth*) and the correct sequence was confirmed.

Protein expression. LptA-His_6 was overexpressed and purified according to the method of Santambrogio *et al.*[126] 4 x 500 ml cultures of transformed *E. coli* BL21 were grown in TB/phosphate buffer (terrific broth Table 21) with 5x glycerol and ampicillin (100 µg/ml) to an OD of 0.80 at 37°C and 200 rpm. The flasks were cooled down to 16°C for 30 min, then IPTG induced (0.1 mM) and grown overnight. Cells were harvested by centrifugation (20 min, 5'000 rpm) and resuspended in buffer A (50 mM sodium phosphate, pH 8.0, 300 mM NaCl, 10 mM imidazole, 10% glycerol) containing lysozyme (1 mg/ml), DNase (100 µg/ml), $MgCl_2$ (10 mM), phenylmethylsulfonyl fluoride (PMSF, 1 mM). Cells were disrupted in three cycles of French press (*SLM Aminco)* at 14'000 psi. Unbroken cells were removed by centrifugation (30 min at 20'000 rpm). The supernatant was loaded on a 1 ml Ni NTA column (*Qiagen*) and eluted stepwise by 5% increments of buffer B (buffer A with 500 mM imidazole) on an ÄKTA start FPLC system (*GE Healthcare*). The 40% and 45% fraction contained the desired protein in high purity. The fractions were combined and dialyzed against 50 mM sodium phosphate (150 mM NaCl, pH 8.0) in 2 l for 3 h and then overnight into 2 l fresh buffer. A sample of LptA-

His_6 was desalted using a C4 ZipTip® (*Merck-Millipore*) and analysed with ESI-MS (FGCZ) confirming the calculated molecular weight of 18'360.55 Da (found 18'360.5 Da).

Table 21 Terrific broth with 5x glycerol: 900 ml A and 100 ml B were mixed after autoclaving.

Part A (900 ml)	Per liter
Tryptone (casein digest)	12 g
Yeast extract	24 g
Glycerol	20 ml

Part B (100 ml)	
KH_2PO_4 (170 mM)	23.14 g
K_2HPO_4 (720 mM)	125.41 g

4.6.11 Fluorescence Polarization

Fluorescence polarization measurements were recorded on a safire^2 plate reader (*Tecan*) in black, flat-bottom, non-binding 96 well plates (*Greiner*). Instrument settings were optimized for BDP-FL (Ex. 470 nm, Im. 508 nm) with a bandwidth of 10 nm and a G-factor of 1.21.

Direct assay. In the direct assay a constant concentration of the fluorescence-labelled reporter (thanatin-BDP-FL) was titrated with the analyte protein LptA-His_6. A 24 fold titration series of LptA-His_6 was prepared starting from a 61.6 µM stock solution in buffer (sodium phosphate 50 mM, NaCl 150 mM, pH 8.0). 100 µl was pipetted in triplicate in a 96 well plate in the first wells, 50 µl was taken and then diluted in a 1:1 fashion with buffer. The concentration of the thanatin-BDP-FL conjugate was kept constant by adding 50 µl of a 200 nM stock solution in buffer supplemented with 0.1% Tween20 to each dilution resulting in an end concentration of 100 nM thanatin-BDP-FL and 0.05% Tween20. After an incubation time of 30 min, fluorescence polarization was recorded. Data were averaged from triplicate and normalized from the concentration point with the lowest anisotropy value. Data were fitted by a one-to-one binding model using GraphPad Prism by implementing equation E 5, where a = -1, b = K_d + x + A_{tot} and c = -x * A_{tot}. m is the amplitude of maximal anisotropy increase, K_d is the dissociation constant and A_{tot} is the total ligand concentration.[144]

$$y = m*((- b + sqrt(b^2 - 4*a*c)) / 2*a) / A_{tot} \quad \text{E 5}$$

Competition assay. In the competition experiments, a constant concentration of thanatin-BDP-FL and LptA-His_6 was titrated with free thanatin and enantiomeric D-thanatin (competitors). A 24 fold titration series of the of free thanatin or enantiomeric D-thanatin was prepared starting from a 2054 µM stock (10 mg/ml) solution in buffer (sodium phosphate 50 mM, NaCl 150 mM, pH 8.0). 100 µl were pipetted in triplicate in a 96 well plate in the first wells, 50 µl were taken and then diluted in a 1:1 fashion with buffer. The concentration of thanatin-BDP-FL and LptA-His_6 was kept constant by adding 50 µl of a 1 µM stock solution in buffer supplemented with 0.1% Tween20 to each dilution, resulting in an end concentration of 0.5 µM thanatin-BDP-FL and LptA-His_6 with 0.05% Tween20. After an incubation time of 30 min, fluorescence polarization was recorded. Data were averaged from triplicate and normalized from the concentration point with the lowest anisotropy value. Data were fitted by a competition binding model using GraphPad Prism by implementing equation E 6, where a=K_a+K_b+A_o+x-P_o, b=K_b*(A_o-P_o)+K_a*(x-P_o)+K_a*K_b, c=-K_a*K_b*P_o, and d=arccos((-2*a^3+9*a*b-27*c)/(2*sqrt((a^2-3*b)^3))).[145] K_b is the competitive K_d value for a certain competitor and K_a the K_d value for thanatin-BDP-FL obtained in the direct assay.

$$y = m*((A_o*(2*sqrt(a^2-3*b)*cos(d/3)-a))/((3*K_a+(2*sqrt(a^2-3*b)*cos(d/3)-a)))/P_o) \quad \text{E 6}$$

5 References

[1] M. Pasupuleti, A. Schmidtchen, M. Malmsten, *Crit. Rev. Biotechnol.* **2012**, *32*, 143.

[2] M. Zasloff, *Nature* **2002**, *415*, 389.

[3] C. B. Park, H. S. Kim, S. C. Kim, *Biochem. Biophys. Res. Commun.* **1998**, *244*, 253.

[4] A. Yonezawa, J. Kuwahara, N. Fujii, Y. Sugiura, *Biochemistry* **1992**, *31*, 2998.

[5] H. Brotz, G. Bierbaum, K. Leopold, P. E. Reynolds, H. G. Sahl, *Antimicrob. Agents Chemother.* **1998**, *42*, 154.

[6] A. Patrzykat, C. L. Friedrich, L. Zhang, V. Mendoza, R. E. W. Hancock, *Antimicrob. Agents Chemother.* **2002**, *46*, 605.

[7] C. Subbalakshmi, N. Sitaram, *FEMS Microbiol. Lett.* **1998**, *160*, 91.

[8] G. Kragol, S. Lovas, G. Varadi, B. A. Condie, R. Hoffmann, L. Otvos, *Biochemistry* **2001**, *40*, 3016.

[9] K. A. Brogden, *Nature Rev. Microbiol.* **2005**, *3*, 238.

[10] L. T. Nguyen, E. F. Haney, H. J. Vogel, *Trends Biotechnol.* **2011**, *29*, 464.

[11] K. L. Brown, R. E. W. Hancock, *Curr. Opin. Immunol.* **2006**, *18*, 24.

[12] R. E. W. Hancock, H.-G. Sahl, *Nat. Biotechnol.* **2006**, *24*, 1551.

[13] R. E. W. Hancock, *Lancet* **1997**, *349*, 418.

[14] D. J. Craik, D. P. Fairlie, S. Liras, D. Price, *Chem. Biol. Drug Des.* **2013**, *81*, 136.

[15] A. Choudhary, R. T. Raines, *ChemBioChem* **2011**, *12*, 1801.

[16] R. J. Simon, R. S. Kania, R. N. Zuckermann, V. D. Huebner, D. A. Jewell, S. Banville, S. Ng, L. Wang, S. Rosenberg, C. K. Marlowe, *Proc. Natl. Acad. Sci. U.S.A.* **1992**, *89*, 9367.

[17] M. D. Fletcher, M. M. Campbell, *Chem. Rev.* **1998**, *98*, 763.

[18] A. Giannis, F. Rübsam, *Adv. Drug Res.* **1997**, 1.

[19] World Health Organization, *Antimicrobial resistance: global report on surveillance*, WHO, **2014**.

[20] R. Laxminarayan, A. Duse, C. Wattal, A. K. M. Zaidi, H. F. L. Wertheim, N. Sumpradit, E. Vlieghe, G. L. Hara, I. M. Gould, H. Goossens et al., *The Lancet* **2013**, *13*, 1057.

[21] Y.-Y. Liu, Y. Wang, T. R. Walsh, L.-X. Yi, R. Zhang, J. Spencer, Y. Doi, G. Tian, B. Dong, X. Huang et al., *Lancet Infect. Dis.* **2016**, *16*, 161.

[22] J. M. A. Blair, M. A. Webber, A. J. Baylay, D. O. Ogbolu, L. J. V. Piddock, *Nature Rev. Microbiol.* **2015**, *13*, 42.

[23] H. W. Boucher, G. H. Talbot, J. S. Bradley, J. E. Edwards, D. Gilbert, L. B. Rice, M. Scheld, B. Spellberg, J. Bartlett, *Clin. Infect. Dis.* **2009**, *48*, 1.

[24] R. R. Uchil, G. S. Kohli, V. M. Katekhaye, O. C. Swami, *J. Clin. Diagn. Res.* **2014**, *8*, 1-4.

[25] J. A. Robinson, *Acc. Chem. Res.* **2008**, *41*, 1278.

[26] C. Toniolo, E. Benedetti, *Crit. Rev. Biochem. Mol. Biol.* **1980**, *9*, 1.

[27] L. R. Whitby, Y. Ando, V. Setola, P. K. Vogt, B. L. Roth, D. L. Boger, *J. Am. Chem. Soc.* **2011**, *133*, 10184.

[28] J. A. Robinson, *J. Pept. Sci.* **2013**, *19*, 127.

[29] M. Urfer, J. Bogdanovic, F. Lo Monte, K. Moehle, K. Zerbe, U. Omasits, C. H. Ahrens, G. Pessi, L. Eberl, J. A. Robinson, *J. Biol. Chem.* **2016**, *291*, 1921.

[30] Polyphor AG, "CXCR4 antagonist POL6326", can be found under http://www.polyphor.com/products/pol6326, **2017**.

[31] M. L. Korsinczky, H. J. Schirra, D. J. Craik, *Curr. Protein Pept. Sci.* **2004**, *5*, 351.

[32] a) Polyphor AG, "Neutrophil elastase inhibitor POL6014", can be found under http://www.polyphor.com/products/pol6014, **2017**; b) D. Obrecht, E. Chevalier, K. Moehle, J. A. Robinson, *Drug Discov. Today Technol.* **2012**, *9*, 63-69.

[33] Alberts, B., Johnson, A., Lewis, J., Raff, M., Roberts, K., and Walter, P, *Molecular Biology of the Cell (5th Ed.)*, John Wiley & Sons Inc, **2008**.

[34] T. Gregersen, *Appl. Microbiol. Biotechnol.* **1978**, *5*, 123.

[35] J. Bakelar, S. K. Buchanan, N. Noinaj, *Science* **2016**, *351*, 180.

[36] Y. Gu, H. Li, H. Dong, Y. Zeng, Z. Zhang, N. G. Paterson, P. J. Stansfeld, Z. Wang, Y. Zhang, W. Wang et al., *Nature* **2016**, *531*, 64.

[37] C. R. H. Raetz, C. Whitfield, *Annu. Rev. Biochem.* **2002**, *71*, 635.

[38] N. Ruiz, D. Kahne, T. J. Silhavy, *Nature Rev. Microbiol.* **2009**, *7*, 677.

[39] S. U. Vetterli, K. Moehle, J. A. Robinson, *Bioorg. Med. Chem.* **2016**, *24*, 6332.

[40] S. Qiao, Q. Luo, Y. Zhao, X. C. Zhang, Y. Huang, *Nature* **2014**, *511*, 108.

[41] I. Botos, N. Majdalani, S. J. Mayclin, J. G. McCarthy, K. Lundquist, D. Wojtowicz, T. J. Barnard, J. C. Gumbart, S. K. Buchanan, *Structure* **2016**, *24*, 965.

[42] H. Dong, Q. Xiang, Y. Gu, Z. Wang, N. G. Paterson, P. J. Stansfeld, C. He, Y. Zhang, W. Wang, C. Dong, *Nature* **2014**, *511*, 52.

[43] D. A. Steinberg, M. A. Hurst, C. A. Fujii, A. H. C. Kung, J. F. Ho, F.-C. Cheng, D. J. Loury, J. C. Fiddes, *Antimicrob. Agents Chemother.* **1997**, *41*, 1738.

[44] S. C. Shankaramma, Z. Athanassiou, O. Zerbe, K. Moehle, C. Mouton, F. Bernardini, J. W. Vrijbloed, D. Obrecht, J. A. Robinson, *ChemBioChem* **2002**, *3*, 1126.

[45] J. M. Andrews, *J. Antimicrob. Chemother.* **2001**, *48*, 5.

[46] N. Srinivas, P. Jetter, B. J. Ueberbacher, M. Werneburg, K. Zerbe, J. Steinmann, B. van der Meijden, F. Bernardini, A. Lederer, R. L. A. Dias et al., *Science* **2010**, *327*, 1010.

[47] M. Werneburg, K. Zerbe, M. Juhas, L. Bigler, U. Stalder, A. Kaech, U. Ziegler, D. Obrecht, L. Eberl, J. A. Robinson, *ChemBioChem* **2012**, *13*, 1767.

[48] Polyphor AG, "Antibiotic POL7080", can be found under http://www.polyphor.com/products/pol7080, **2017**.

[49] J. Schmidt, K. Patora-Komisarska, K. Moehle, D. Obrecht, J. A. Robinson, *Bioorg. Med. Chem.* **2013**, *21*, 5806.

[50] D. S. Wishart, C. G. Bigam, A. Holm, R. S. Hodges, B. D. Sykes, *J. Biomol. NMR* **1995**, *5*, 67.

[51] K. Wüthrich, *NMR of Proteins and Nucleic Acids*, Wiley, **1986**.

[52] T. Jenuwein, C. D. Allis, *Science* **2001**, *293*, 1074.

[53] J. S. Davies, *J. Pept. Sci.* **2003**, *9*, 471.

[54] R. Dornetshuber, P. Heffeter, M.-R. Kamyar, T. Peterbauer, W. Berger, R. Lemmens-Gruber, *Chem. Res. Toxicol.* **2007**, *20*, 465.

[55] K. Hiraga, S. Yamamoto, H. Fukuda, N. Hamanaka, K. Oda, *Biochem. Biophys. Res. Commun.* **2005**, *328*, 1119.

[56] F. Loganzo, C. M. Discafani, T. Annable, C. Beyer, S. Musto, M. Hari, X. Tan, C. Hardy, R. Hernandez, M. Baxter et al., *Cancer Res.* **2003**, *63*, 1838.

[57] a) K. Watanabe, H. Oguri, H. Oikawa, *Molec. Divers.* **2009**, *13*, 189; b) F. Leng, J. B. Chaires, M. J. Waring, *Nucleic Acids Res.* **2003**, *31*, 6191.

[58] J. Liu, J. D. Farmer, W. S. Lane, J. Friedman, I. Weissman, S. L. Schreiber, *Cell* **1991**, *66*, 807.

[59] D. J. Cohen, R. Loertscher, M. F. Rubin, N. L. Tilney, C. B. Carpenter, T. B. Strom, *Ann. Intern. Med.* **1984**, *101*, 667.

[60] J. Chatterjee, F. Rechenmacher, H. Kessler, *Angew. Chem. Int. Ed.* **2013**, *52*, 254.

[61] A. I. Fernández-Llamazares, J. Spengler, F. Albericio, *Biopolymers* **2015**, *104*, 435.

[62] C. K. Wang, S. E. Northfield, B. Colless, S. Chaousis, I. Hamernig, R.-J. Lohman, D. S. Nielsen, C. I. Schroeder, S. Liras, D. A. Price et al., *Proc. Natl. Acad. Sci. U.S.A.* **2014**, *111*, 17504.

[63] S. V. Fiacco, R. W. Roberts, *ChemBioChem* **2008**, *9*, 2200.

[64] Y. Li, N. Bionda, A. Yongye, P. Geer, M. Stawikowski, P. Cudic, K. Martinez, R. A. Houghten, *ChemMedChem* **2013**, *8*, 1865.

[65] a) E. Biron, J. Chatterjee, O. Ovadia, D. Langenegger, J. Brueggen, D. Hoyer, H. A. Schmid, R. Jelinek, C. Gilon, A. Hoffman et al., *Angew. Chem. Int. Ed.* **2008**, *47*, 2595; b) L. Doedens, F. Opperer, M. Cai, J. G. Beck, M. Dedek, E. Palmer, V. J. Hruby, H. Kessler, *J. Am. Chem. Soc.* **2010**, *132*, 8115.

[66] a) M. Green, P. M. Loewenstein, *Cell* **1988**, *55*, 1179; b) A. D. Frankel, C. O. Pabo, *Cell* **1988**, *55*, 1189.

[67] a) S. R. Schwarze, A. Ho, A. Vocero-Akbani, S. F. Dowdy, *Science* **1999**, *285*, 1569; b) H. Nagahara, A. M. Vocero-Akbani, E. L. Snyder, A. Ho, D. G. Latham, N. A. Lissy, M. Becker-Hapak, S. A. Ezhevsky, S. F. Dowdy, *Nat. Med.* **1998**, *4*, 1449.

[68] D. J. Mitchell, L. Steinman, D. T. Kim, C. G. Fathman, J. B. Rothbard, *J. Pept. Res.* **2000**, *56*, 318.

[69] F. Madani, S. Lindberg, Ü. Langel, Lo, S. Futaki, A. Gräslund, *J Biophys* **2011**, *2011*, 1.

[70] M. Rizzuti, M. Nizzardo, C. Zanetta, A. Ramirez, S. Corti, *Drug Discov. Today* **2015**, *20*, 76.

[71] P. Fehlbaum, P. Bulet, S. Chernysh, J. P. Briand, J. P. Roussel, L. Letellier, C. Hetru, J. A. Hoffmann, *Proc. Natl. Acad. Sci. U.S.A.* **1996**, *93*, 1221.

[72] P. Bulet, C. Hetru, J. L. Dimarcq, D. Hoffmann, *Dev. Comp. Immunol.* **1999**, *23*, 329.

[73] N. Mandard, P. Sodano, H. Labbe, J.-M. Bonmatin, P. Bulet, C. Hetru, M. Ptak, F. Vovelle, *Eur. J. Biochem.* **1998**, *256*, 404.

[74] T. Imamura, N. Yamamoto, A. Tamura, S. Murabayashi, S. Hashimoto, H. Shimada, S. Taguchi, *Biochem. Biophys. Res. Commun.* **2008**, *369*, 609.

[75] E. Robert, T. Lefèvre, M. Fillion, B. Martial, J. Dionne, M. Auger, *Biochemistry* **2015**, *54*, 3932.

[76] G. Wu, J. Ding, H. Li, L. Li, R. Zhao, Z. Shen, X. Fan, T. Xi, *Curr. Microbiol.* **2008**, *57*, 552.

[77] G. Wu, X. Fan, L. Li, H. Wang, J. Ding, W. Hongbin, R. Zhao, L. Gou, Z. Shen, T. Xi, *Int. J. Antimicrob. Agents* **2010**, *35*, 250.

[78] G. Wu, X. Li, X. Deng, X. Fan, S. Wang, Z. Shen, T. Xi, *Peptides* **2011**, *32*, 353.

[79] T. Imamura, M. Yasuda, H. Kusano, H. Nakashita, Y. Ohno, T. Kamakura, S. Taguchi, H. Shimada, *Transgenic Res.* **2010**, *19*, 415.

[80] a) A. Koch, W. Khalifa, G. Langen, A. Vilcinskas, K.-H. Kogel, J. Imani, *J. Phytopathol.* **2012**, *160*, 606; b) T. Wu, D. Tang, W. Chen, H. Huang, R. Wang, Y. Chen, *Gene* **2013**, *527*, 235.

[81] J. Chatterjee, B. Laufer, H. Kessler, *Nat. Protoc.* **2012**, *7*, 432.

[82] W. Chan, P. White, *Fmoc Solid Phase Peptide Synthesis*. *A Practical Approach*, OUP Oxford, **2000**.

[83] T. Kan, T. Fukuyama, *Chem. Commun.* **2004**, 353.

[84] S. C. Miller, T. S. Scanlan, *J. Am. Chem. Soc.* **1997**, *119*, 2301.

[85] L. A. Carpino, H. Imazumi, A. El-Faham, F. J. Ferrer, C. Zhang, Y. Lee, B. M. Foxman, P. Henklein, C. Hanay, C. Mügge et al., *Angew. Chem. Int. Ed.* **2002**, *41*, 441.

[86] A. El-Faham, F. Albericio, *J. Pept. Sci.* **2010**, *16*, 6.

[87] J. Fölling, S. Polyakova, V. Belov, A. van Blaaderen, M. L. Bossi, S. W. Hell, *Small* **2008**, *4*, 134.

[88] J. W. Fisher, K. L. Trinkle, *Tetrahedron Lett.* **1994**, *35*, 2505.

[89] P. Güntert, *Automated NMR Structure Calculation with CYANA*, Humana Press, **2004**.

[90] K. Wuthrich, *NMR of proteins and nucleic acids*, John Wiley & Sons, New York, **1986**.

[91] a) N. J. Baxter, M. P. Williamson, *J. Biomol. NMR* **1997**, *9*, 359; b) T. Cierpicki, J. Otlewski, *J. Biomol. NMR* **2001**, *21*, 249.

[92] R. N. Zuckermann, J. M. Kerr, Kent, Stephen B. H., W. H. Moos, *J. Am. Chem. Soc.* **1992**, *114*, 10646.

[93] A. Ho, S. R. Schwarze, S. J. Mermelstein, G. Waksman, S. F. Dowdy, *Cancer Res.* **2001**, *61*, 474.

[94] J. Kapuscinski, *Biotech. Histochem.* **1995**, *70*, 220.

[95] B. L. Roth, M. Poot, S. T. Yue, P. J. Millard, *Appl. Environ. Microbiol.* **1997**, *63*, 2421.

[96] T. Velkov, P. E. Thompson, R. L. Nation, J. Li, *J. Med. Chem.* **2010**, *53*, 1898.

[97] C. Shipman, *Proc. Soc. Exp. Biol. Med.* **1969**, *130*, 305.

[98] C. C. Sanders, *Rev. Infect. Dis.* **1988**, *10*, 516.

[99] D. C. Hooper, *Drugs* **1999**, *58*, 6.

[100] S. T. Smale, *Cold Spring Harb Protoc* **2010**, *2010*, 5423.

[101] R. I. Lehrer, A. Barton, K. A. Daher, S. S. Harwig, T. Ganz, M. E. Selsted, *J. Clin. Invest.* **1989**, *84*, 553.

[102] C. Bebrone, C. Moali, F. Mahy, S. Rival, J. D. Docquier, G. M. Rossolini, J. Fastrez, R. F. Pratt, J. M. Frere, M. Galleni, *Antimicrob. Agents Chemother.* **2001**, *45*, 1868.

[103] L. P. Kotra, J. Haddad, S. Mobashery, *Antimicrob. Agents Chemother.* **2000**, *44*, 3249.

[104] W. Wehrli, *Rev. Infect. Dis.* **1983**, *5*, 407-411.

[105] N. H. Georgopapadakou, A. Bertasso, K. K. Chan, J. S. Chapman, R. Cleeland, L. M. Cummings, B. A. Dix, D. D. Keith, *Antimicrob. Agents Chemother.* **1989**, *33*, 1067.

[106] S. Fischer-Parton, R. M. Parton, P. C. Hickey, J. Dijksterhuis, H. A. Atkinson, N. D. Read, *J. Microsc.* **2000**, *198*, 246.

[107] A. Loudet, K. Burgess, *Chem. Rev.* **2007**, *107*, 4891.

[108] A. Singh, E. R. Thornton, F. H. Westheimer, *J. Biol. Chem.* **1962**, *237*, 3006.

[109] E. Smith, I. Collins, *Future Med. Chem.* **2015**, *7*, 159.

[110] M. Suchanek, A. Radzikowska, C. Thiele, *Nat. Methods* **2005**, *2*, 261.

[111] H. Nakashima, M. Hashimoto, Y. Sadakane, T. Tomohiro, Y. Hatanaka, *J. Am. Chem. Soc.* **2006**, *128*, 15092.

[112] B. van der Meijden, J. A. Robinson, *Arkivoc* **2011**, 130.

[113] B. van der Meijden, J. A. Robinson, *J. Pept. Sci.* **2015**, *21*, 231.

[114] B. T. Kurien, H. R. Scofield, *Western Blotting*. *Methods and Protocols*, Humana Press, **2005**.

[115] P. D. Abeyrathne, J. S. Lam, *Can. J. Microbiol.* **2007**, *53*, 526.

[116] B. Ma, C. Niu, Y. Zhou, X. Xue, J. Meng, X. Luo, Z. Hou, *Antimicrob. Agents Chemother.* **2016**, *60*, 4283.

[117] O. Cirioni, G. Wu, L. Li, F. Orlando, C. Silvestri, R. Ghiselli, Z. Shen, E. Gabrielli, L. Brescini, G. Lezoche et al., *Peptides* **2011**, *32*, 697.

[118] J. A. Aguilar, C. Diaz-Perez, A. L. Diaz-Perez, J. S. Rodriguez-Zavala, B. J. Nikolau, J. Campos-Garcia, *J. Bacteriol.* **2008**, *190*, 4888.

[119] "Reviewed proteins in Escherichia coli (strain K-12)", can be found under http://www.uniprot.org/taxonomy/83333, **2017**.

[120] a) M. J. Davies, *Photochem. Photobiol. Sci.* **2004**, *3*, 17; b) D. I. Pattison, A. S. Rahmanto, M. J. Davies, *Photochem. Photobiol. Sci.* **2012**, *11*, 38.

[121] M. D. Suits, P. Sperandeo, G. Dehò, A. Polissi, Z. Jia, *J. Mol. Biol.* **2008**, *380*, 476.

[122] a) A. X. Tran, M. S. Trent, C. Whitfield, *J. Biol. Chem.* **2008**, *283*, 20342; b) S. Okuda, E. Freinkman, D. Kahne, *Science* **2012**, *338*, 1214.

[123] E. Freinkman, S. Okuda, N. Ruiz, D. Kahne, *Biochemistry* **2012**, *51*, 4800.

[124] J. A. Merten, K. M. Schultz, C. S. Klug, *Protein Sci.* **2012**, *21*, 211.

[125] K. M. Schultz, T. J. Lundquist, C. S. Klug, *Protein Sci.* **2017**, ahead of print: DOI: 10.1002/pro.3177.

[126] C. Santambrogio, P. Sperandeo, R. Villa, F. Sobott, A. Polissi, R. Grandori, *J. Am. Soc. Mass Spectrom.* **2013**, *24*, 1593.

[127] F. Perrin, *J. Phys. Radium* **1926**, *7*, 390.

[128] W. A. Lea, A. Simeonov, *Exp. Op. Drug Disc.* **2011**, *6*, 17.

[129] A. M. Rossi, C. W. Taylor, *Nat. Protoc.* **2011**, *6*, 365.

[130] Z. Hou, J. Lu, C. Fang, Y. Zhou, H. Bai, X. Zhang, X. Xue, Y. Chen, X. Luo, *J. Infect. Dis.* **2011**, *203*, 273.

[131] M. Benedet, F. A. Falchi, S. Puccio, C. Di Benedetto, C. Peano, A. Polissi, G. Dehò, *PLOS ONE* **2016**, *11*, 1-21.

[132] P. Sperandeo, F. K. Lau, A. Carpentieri, C. de Castro, A. Molinaro, G. Dehò, T. J. Silhavy, A. Polissi, *J. Bacteriol.* **2008**, *190*, 4460.

[133] R. Bollhagen, M. Schmiedberger, K. Barlos, E. Grell, *J. Chem. Soc., Chem. Commun.* **1994**, 2559.

[134] P. E. Schneggenburger, B. Worbs, U. Diederichsen, *J. Pept. Sci.* **2010**, *16*, 10.

[135] J. McFarland, *JAMA* **1907**, 1176.

[136] I. Wiegand, K. Hilpert, R. E. W. Hancock, *Nat. Protoc.* **2008**, *3*, 163.

[137] J. H. Come, F. Becker, N. A. Kiey, C. Reichel, US 2004/0043388A1, **2004**.

[138] G. Clave, H. Volland, M. Flaender, D. Gasparutto, A. Romieu, P.-Y. Renard, *Org. Biomol. Chem.* **2010**, *8*, 4329.

[139] C. Bartels, T.-h. Xia, M. Billeter, P. Güntert, K. Wüthrich, *J. Biomol. NMR* **1995**, *6*, 1.

[140] T. J. Falla, D. N. Karunaratne, R. E. Hancock, *J. Biol. Chem.* **1996**, *271*, 19298.

[141] M. M. Bradford, *Anal. Biochem.* **1976**, *72*, 248.

[142] U. K. Laemmli, M. Favre, *J. Mol. Biol.* **1973**, *80*, 575.

[143] M. Choi, C.-Y. Chang, T. Clough, D. Broudy, T. Killeen, B. MacLean, O. Vitek, *Bioinformatics* **2014**, *30*, 2524.

[144] S. Hansen, D. Tremmel, C. Madhurantakam, C. Reichen, P. R. E. Mittl, A. Pluckthun, *J. Am. Chem. Soc.* **2016**, *138*, 3526.

[145] Z.-X. Wang, *FEBS Lett.* **1995**, *360*, 111.

6 Appendix

6.1 Abbreviations

AMPs	Antimicrobial peptides
Boc	*tert*-Butyloxycarbonyl
BSA	Bovine serum albumin
Cbz or Z	Benzyloxycarbonyl
CFU	Colony-forming unit
COMU	(1-Cyano-2-ethoxy-2-oxoethylidenaminooxy)dimethylamino-morpholino-carbenium hexafluorophosphate
CPP	Cell-penetrating peptide
CSDs	Chemical shift deviations
DAPI	4',6-diamidino-2-phenylindole
Dab	2,4-Diaminobutyric acid
DBU	1,8-Diazabicyclo[5.4.0]undec-7-ene
DCM	Dichloromethane
DIAD	Diisopropyl azodicarboxylate
DIPEA	N,N-Diisopropylethylamine
DM	Defined growth media
DMF	Dimethylformamide
DMSO	Dimethyl sulfoxide
DTT	Dithiothreitol
EDT	1,2-Ethanedithiol
EDTA	Ethylenediaminetetraacetic acid
eq.	Equivalents
Fmoc	N-9H-Fluoren-2-ylmethoxycarbonyl
HATU	1-[Bis(dimethylamino)methylene]-1H-1,2,3-triazolo[4,5-b]pyridinium 3-oxid hexafluorophosphate
HBTU	N,N,N',N'-Tetramethyl-O-(1H-benzotriazol-1-yl)uronium hexafluorophosphate
HEPES	4-(2-hydroxyethyl)-1-piperazineethanesulfonic acid
HOAt	3-Hydroxytriazolo[4,5-*b*]pyridine
HOBt	N-Hydroxybenzotriazole
HPLC	High performance liquid chromatography
HR-ESI	High-resolution electron spray ionization
HRP	Horse radish peroxidise

IPTG	Isopropyl β-D-1-thiogalactopyranoside
LB	Lysogeny broth
LPS	Lipopolysaccharides
MH-I/II	Müller-Hinton broth I/II
MIC	Minimal inhibitory concentration
NOE	Nuclear Overhauser effect
OMPs	Outer membrane proteins
PAL	Photoaffinity labelling
Pbf	2,2,4,6,7-Pentamethyldihydrobenzofuran-5-sulfonyl
PBS	Phosphate-buffered saline
PCR	Polymerase chain reaction
PDB	Protein Data Bank
PEG	Polyethylene glycol
PEM	Protein epitope mimetic
pI	Isoelectric point
PVDF	Polyvinylidene difluoride
rmsd	Root mean square deviation
rpm	Revolutions per minute
RT	Room temperature
SAR	Structure activity relationship
SDS-PAGE	Sodium dodecyl sulfate polyacrylamide gel electrophoresis
SPPS	Solid phase peptide synthesis
TCA	Trichloroacetic acid
TCEP	Tris(2-carboxyethyl)phosphine
TFA	Trifluoroacetic acid
THF	Tetrahydrofuran
TIS	Triisopropylsilane
TMS	Tetramethylsilane
Tris	Tris(hydroxymethyl)aminomethane
TSP	Trimethylsilyl propanoic acid
Trt	Trityl
UPLC	Ultra performance liquid chromatography

6.2 NMR Spectra of LB-01 N-Methyl Analogues

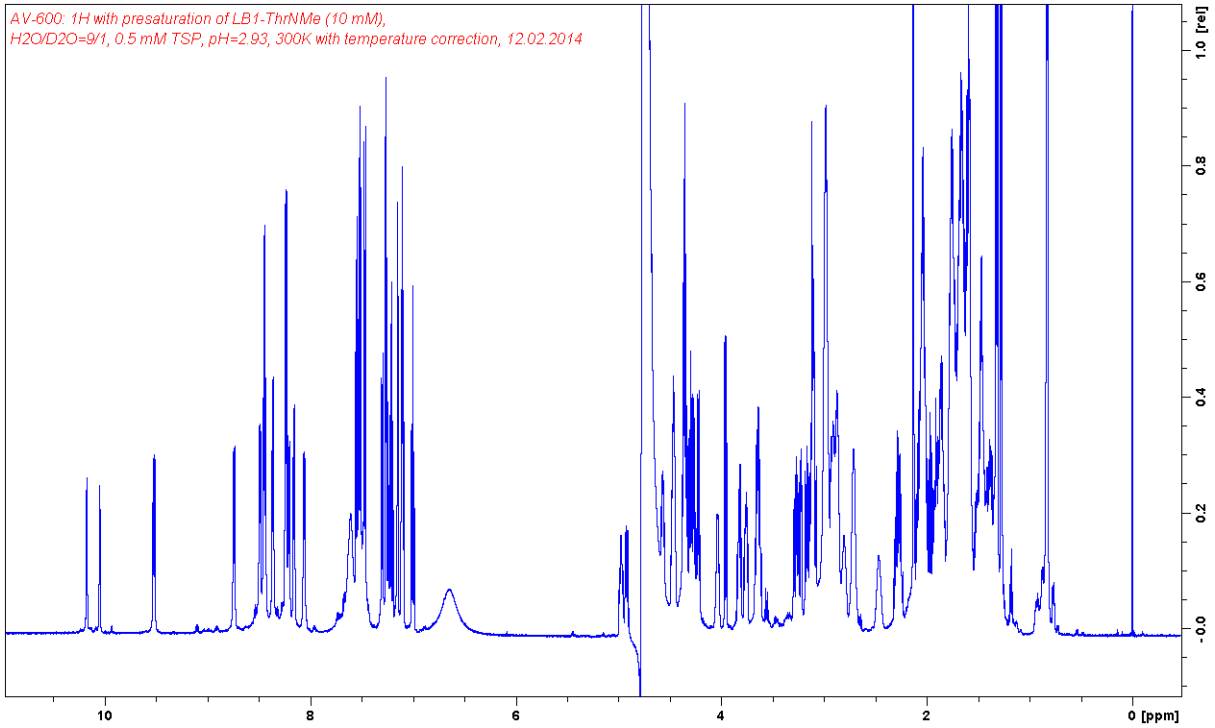

Figure 72 ^{1}H-NMR spectrum of Thr1NMe.

Table 22 ^{1}H-NMR shift assignments of analogue Thr1NMe.

	H	HA	HB	HG	HD	HE	HZ	HH
Thr1	2.12	3.96	4.93	1.28	-	-	-	-
Trp2	9.52	4.97	3.10,3.23	-	7.26	7.55,10.17	7.10,7.53	7.26
Leu3	8.74	4.47	1.51,1.63	1.5	0.82	-	-	-
Dab4	8.44	4.04	1.86,2.04	2.46,2.80	-	-	-	-
Orn5	8.06	4.36	1.74,1.87	1.66	-	-	-	-
^{D}Lys6	8.36	4.27	1.72,1.75	1.33,1.42	-	-	-	-
Arg7	8.24	4.36	1.65,1.74	1.47	-	-	-	-
Trp8	8.44	4.71	3.16,3.26	-	7.15	7.29,10.05	7.00,7.46	7.21
Orn9	8.21	4.46	1.59,1.75	1.58	-	-	-	-
Dab10	8.49	4.22	1.84,2.02	2.71	-	-	-	-
Ala11	8.16	4.3	1.31	-	-	-	-	-
Lys12	8.23	4.57	1.68,1.76	1.39,1.46	1.67	-	-	-
^{D}Pro13	-	4.68	1.92,2.26	2.04	3.63,3.75	-	-	-
Pro14	-	4.34	1.94,2.28	2.06,2.08	3.65,3.82	-	-	-

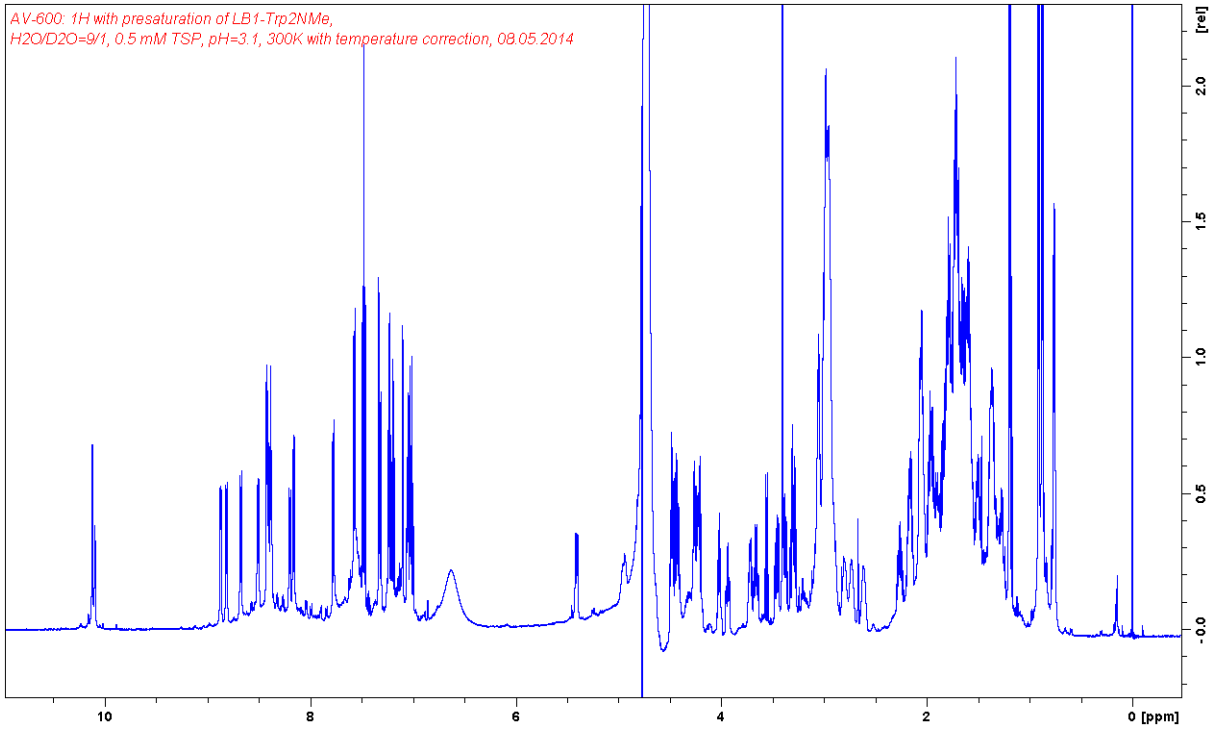

Figure 73 ^{1}H-NMR spectrum of Trp2NMe.

Table 23 ^{1}H-NMR shift assignments of analogue Trp2NMe.

	H	HA	HB	HG	HD	HE	HZ	HH
Thr1	7.78	4.82	4.2	1.2	-	-	-	-
Trp2	3.4	5.41	3.00,3.30	-	7.1	7.32,10.10	7.01,7.48	7.24
Leu3	8.51	4.48	1.59,1.73	1.57	0.9	-	-	-
Dab4	8.68	4.97	2.06,2.16	2.91,2.98	-	-	-	-
Orn5	8.42	4.48	1.79,1.89	1.58,1.63	2.95	-	-	-
^{D}Lys6	8.87	4.26	1.72,1.78	1.37,1.49	1.7	2.99	-	-
Arg7	8.82	4.23	1.59,1.73	1.30,1.38	3.05	7.06	-	-
Trp8	8.16	4.71	3.29,3.46	-	7.34	7.57,10.12	7.03,7.47	7.2
Orn9	8.2	4.94	1.72,1.82	1.6	2.62,2.73	-	-	-
Dab10	8.38	4.42	1.80,1.98	2.80,2.98	-	-	-	-
Ala11	8.42	4.02	0.76	-	-	-	-	-
Lys12	8.39	4.67	1.51,1.74	1.26,1.36	1.65	2.95	-	-
^{D}Pro13	-	4.72	1.84,2.27	1.96,2.04	3.38,3.72	-	-	-
Pro14	-	4.44	2.06,2.16	1.93,2.05	3.66,3.94	-	-	-

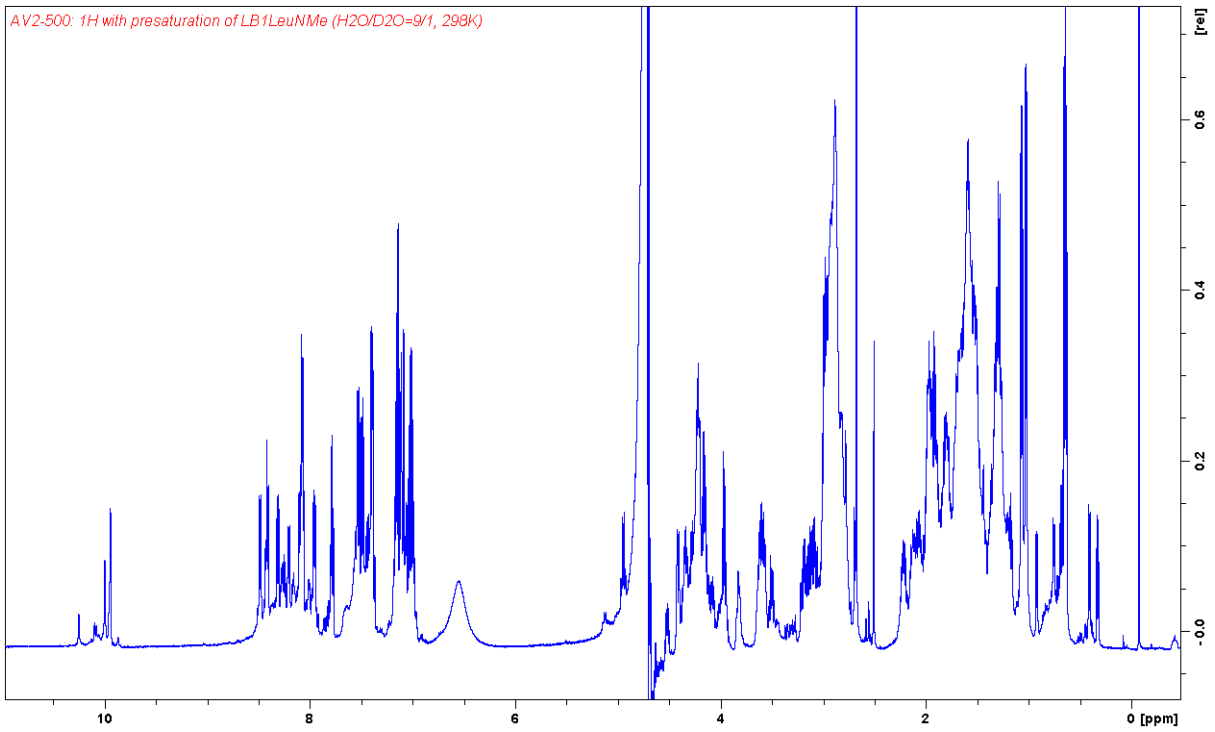

Figure 74 ^{1}H-NMR spectrum of Leu3NMe.

Table 24 ^{1}H-NMR shift assignments of analogue Leu3NMe.

	H	HA	HB	HG	HD	HE	HZ	HH
Thr1	7.86	4.24	4.04	1.1	-	-	-	-
Trp2	8.49	5.03	3.07,3.22	-	7.17	7.57,10.08	7.09,7.48	7.23
Leu3	2.76	4.48	1.45,1.51	1.12	0.72	-	-	-
Dab4	7.87	4.29	1.92,2.13	2.87,2.95	-	-	-	-
Orn5	8.18	4.42	1.79,1.88	1.7	3	-	-	-
^{D}Lys6	8.56	4.35	1.70,1.76	1.37,1.40	1.7	2.99	-	-
Arg7	8.39	4.28	1.60,1.66	1.38	3.06	7.07	-	-
Trp8	8.15	4.59	3.16,3.27	-	7.19	7.61,10.02	7.10,7.47	7.22
Orn9	8.28	4.32	1.63,1.86	1.58	2.95	-	-	-
Dab10	8.04	4.3	1.99,2.15	3.04	-	-	-	-
Ala11	8.15	4.04	1.15	-	-	-	-	-
Lys12	8.14	4.71	1.54,1.74	1.28,1.34	1.59	2.91	-	-
^{D}Pro13	-	4.71	1.90,2.29	1.99,2.06	3.58,3.71	-	-	-
Pro14	-	4.49	2.06,2.20	1.96,2.04	3.67,3.90	-	-	-

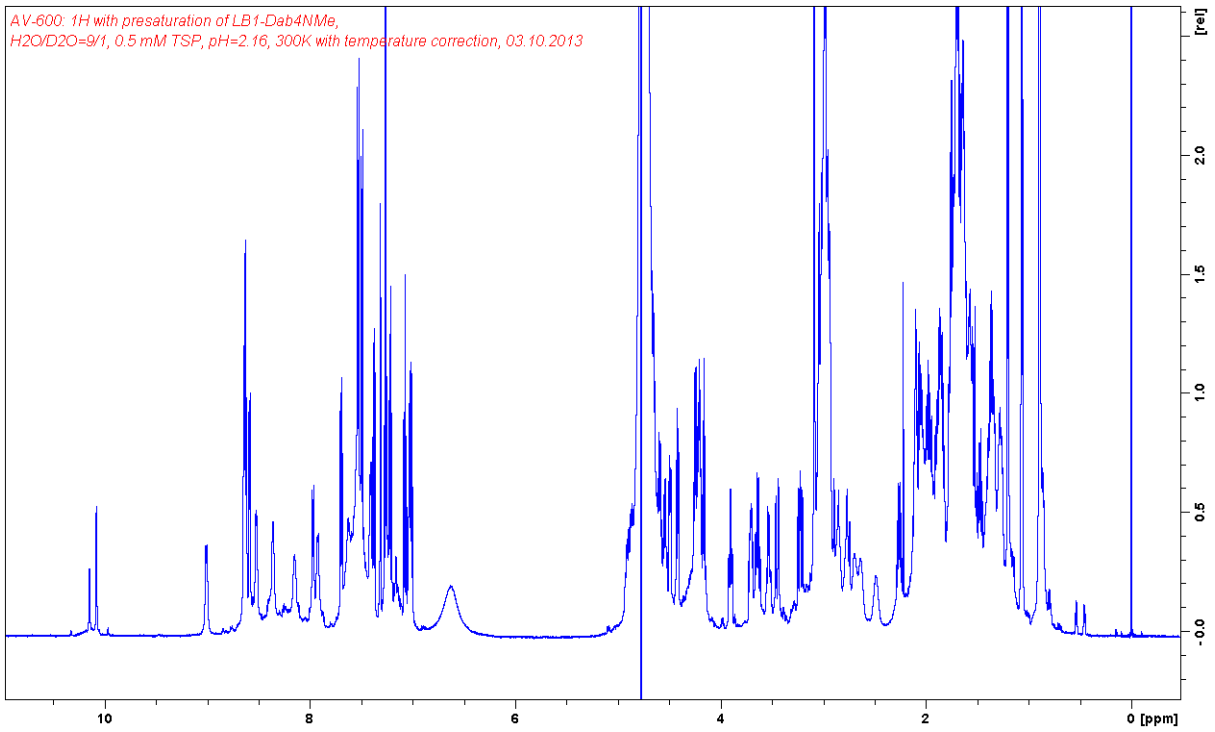

Figure 75 ^{1}H-NMR spectrum of Dab4NMe.

Table 25 ^{1}H-NMR shift assignments of analogue Dab4Me.

	H	HA	HB	HG	HD	HE	HZ	HH
Thr1	7.7	4.42	4.17	1.21	-	-	-	-
Trp2	8.64	4.88	2.97,3.03	-	7.27	7.38,10.15	7.08,7.54	7.26
Leu3	9.01	4.92	1.59,1.71	1.56	0.9	-	-	-
Dab4	3.09	4.55	1.96	2.07,2.48	-	-	-	-
Orn5	7.97	4.55	1.71,1.88	1.66	3	-	-	-
^{D}Lys6	8.59	4.25	1.77	1.37,1.48	1.71	2.98	-	-
Arg7	8.62	4.21	1.57,1.61	1.29,1.35	3.04	7.04	-	-
Trp8	8.36	4.81	3.23,3.45	-	7.32	7.41,10.08	7.03,7.50	7.22
Orn9	8.15	4.87	1.72,1.84	1.65	2.64,2.77	-	-	-
Dab10	8.64	4.25	1.75,2.01	2.70,2.86	-	-	-	-
Ala11	8.52	4.21	1.07	-	-	-	-	-
Lys12	7.93	4.6	1.59,1.73	1.28,1.40	1.65	2.94	-	-
^{D}Pro13	-	4.66	1.90,2.28	1.99,2.07	3.53,3.71	-	-	-
Pro14	-	4.49	1.89,2.10	1.89,2.05	3.64,3.90	-	-	-

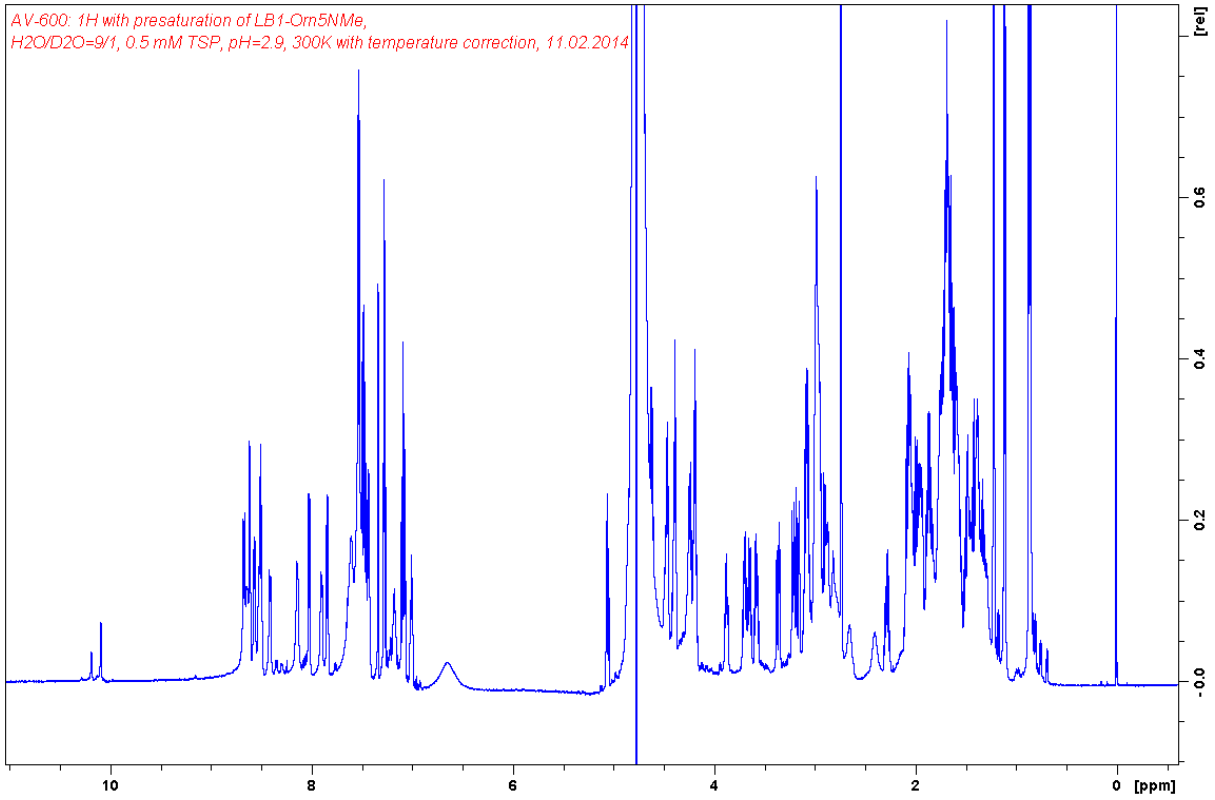

Figure 76 ^{1}H-NMR spectrum of Orn5NMe.

Table 26 ^{1}H-NMR shift assignments of analogue Orn5NMe.

	H	HA	HB	HG	HD	HE	HZ	HH
Thr1	7.84	4.38	4.18	1.21	-	-	-	-
Trp2	8.51	4.82	3.07,3.16	-	7.28	7.49,10.19	7.09,7.52	7.27
Leu3	8.64	4.47	1.49,1.61	1.47	0.86	-	-	-
Dab4	8.67	4.7	1.75,1.97	2.39,2.65	-	-	-	-
Orn5	2.73	5.06	1.69,1.93	1.57	2.99	-	-	-
^{D}Lys6	8.02	4.4	1.69,1.73	1.33,1.44	1.68	2.98	-	-
Arg7	8.61	4.19	1.58,1.65	1.37	3.07	7.07	-	-
Trp8	8.13	4.85	3.20,3.35	-	7.33	7.43,10.09	7.00,7.45	7.17
Orn9	8.41	4.69	1.75,1.84	1.69	2.81,2.87	-	-	-
Dab10	8.56	4.25	1.81,2.04	2.78,2.89	-	-	-	-
Ala11	8.49	4.23	1.1	-	-	-	-	-
Lys12	7.9	4.61	1.59,1.73	1.29,1.40	1.64	2.95	-	-
^{D}Pro13	-	4.67	1.88,2.28	1.98,2.06	3.58,3.69	-	-	-
Pro14	-	4.46	1.94,2.07	1.87,2.03	3.65,3.87	-	-	-

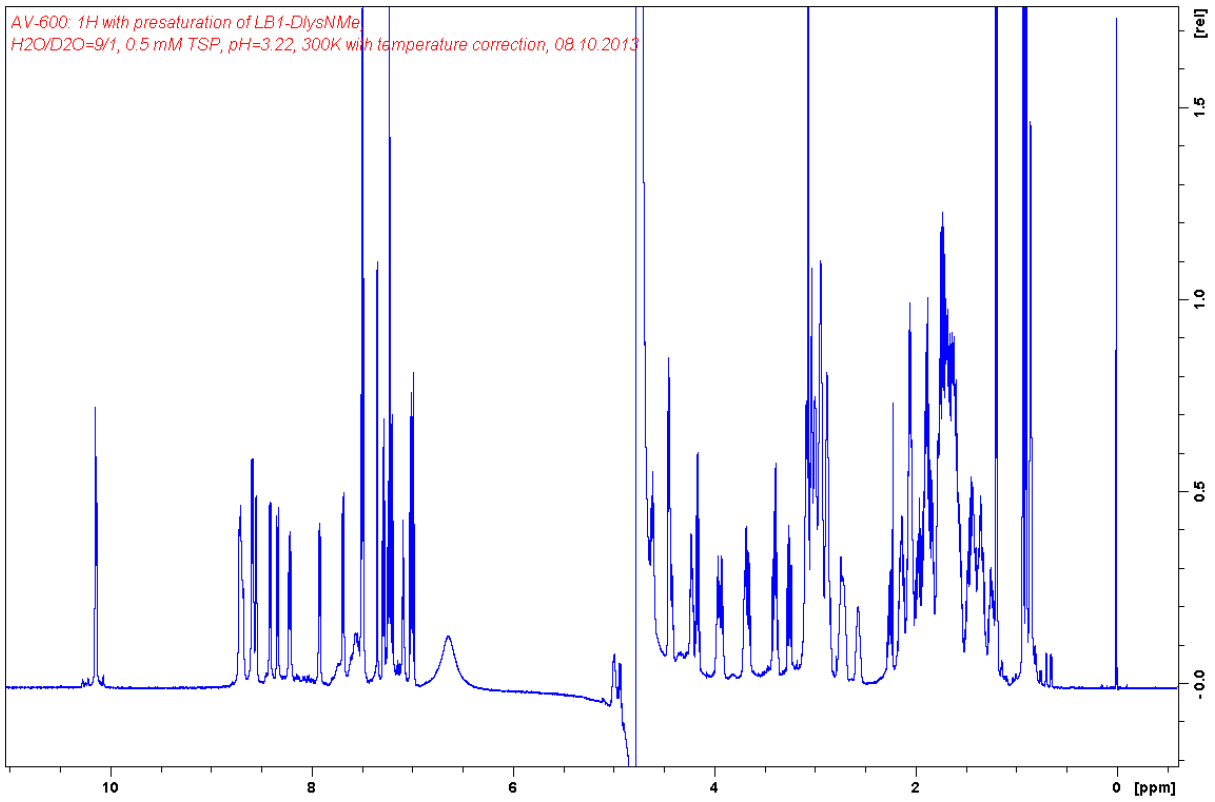

Figure 77 ^{1}H-NMR spectrum of ^{D}Lys6NMe.

Table 27 ^{1}H-NMR shift assignments of analogue ^{D}Lys6NMe.

	H	HA	HB	HG	HD	HE	HZ	HH
Thr1	7.68	4.44	4.16	1.2	-	-	-	-
Trp2	8.59	4.94	3.04	-	7.23	7.28,10.13	6.98,7.48	7.26
Leu3	8.7	4.6	1.68	1.55	0.90,0.93	-	-	-
Dab4	8.71	4.97	2.07,2.13	2.88,2.94	7.71	-	-	-
Orn5	8.59	4.93	1.77,1.90	1.68	2.88,3.02	7.56	-	-
^{D}Lys6	3.07	4.73	1.88	1.34,1.44	1.73	3.00	-	-
Arg7	8.68	4.23	1.60,1.75	1.42	3.08	7.09	-	-
Trp8	7.92	4.7	3.25,3.41	-	7.34	7.50,10.14	7.01,7.48	7.2
Orn9	8.33	4.98	1.70,1.83	1.59	2.57,2.71	7.36	-	-
Dab10	8.41	4.43	1.77,1.98	2.74,2.94	7.74	-	-	-
Ala11	8.55	3.96	0.85	-	-	-	-	-
Lys12	8.21	4.6	1.47,1.69	1.24,1.35	1.65	2.95	7.54	-
^{D}Pro13	-	4.69	1.88,2.27	1.97,2.07	3.38,3.69	-	-	-
Pro14	-	4.46	2.05,2.13	1.90,2.06	3.66,3.93	-	-	-

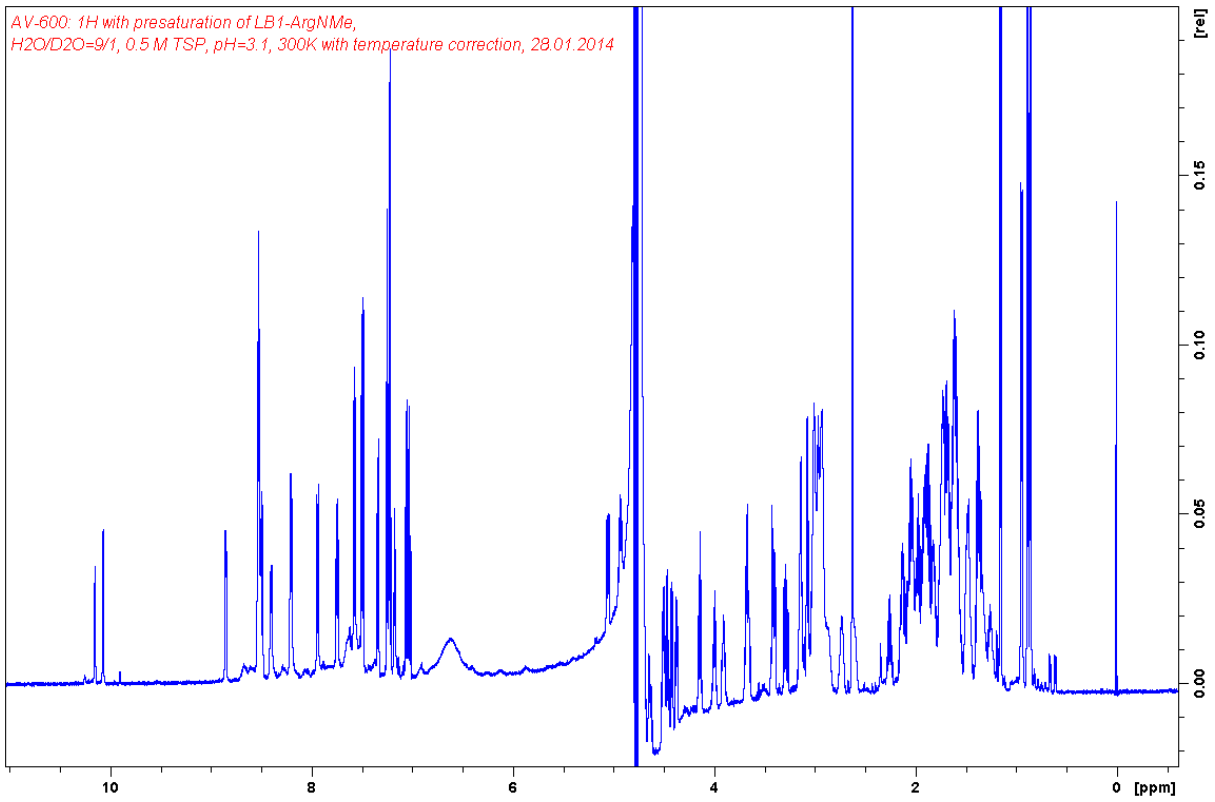

Figure 78 ^{1}H-NMR spectrum of Arg7NMe.

Table 28 ^{1}H-NMR shift assignments of analogue Arg7NMe.

	H	HA	HB	HG	HD	HE	HZ	HH
Thr1	7.75	4.37	4.15	1.16	-	-	-	-
Trp2	8.4	4.74	3.08,3.08	-	7.22	7.34,10.15	7.03,7.50	7.23
Leu3	8.52	4.5	1.61	1.48	0.86	-	-	-
Dab4	8.51	4.82	2.02,2.12	2.87,2.94	7.65	-	-	-
Orn5	8.21	4.47	1.82,1.87	1.62,1.70	2.93,3.01	7.63	-	-
^{D}Lys6	8.85	4.65	1.73	1.33,1.47	1.66	2.96	7.56	-
Arg7	2.63	5.06	1.57,1.90	1.38	3.14	7.17	-	-
Trp8	7.94	4.94	3.29,3.41	-	7.25	7.57,10.07	7.05,7.48	7.22
Orn9	8.49	4.92	1.73,1.82	1.60,1.61	2.61,2.73	7.37	-	-
Dab10	8.53	4.5	1.92,2.07	2.91,3.00	7.75	-	-	-
Ala11	8.53	4	0.95	-	-	-	-	-
Lys12	8.2	4.63	1.50,1.70	1.25,1.36	1.65	2.95	7.53	-
^{D}Pro13	-	4.7	1.88,2.26	1.97,2.05	3.42,3.68	-	-	-
Pro14	-	4.41	1.98,2.14	1.91,2.04	3.66,3.91	-	-	-

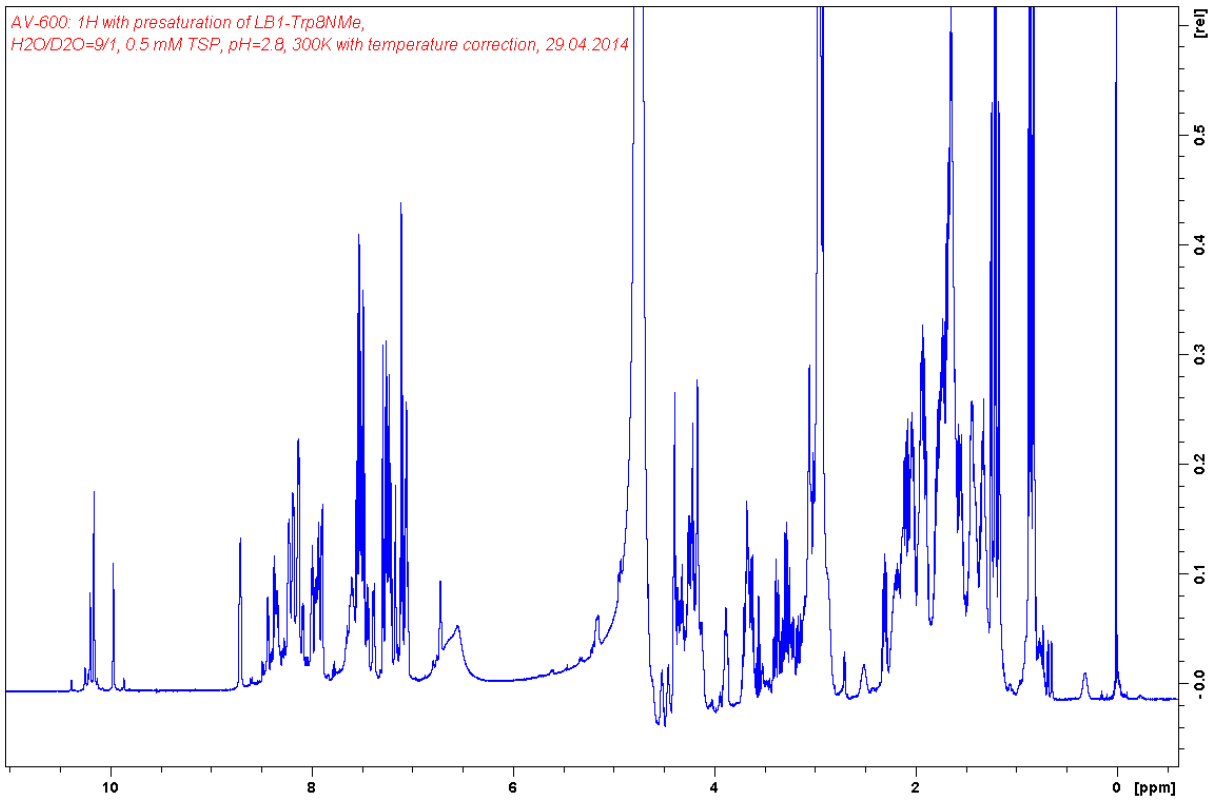

Figure 79 ^{1}H-NMR spectrum of Trp8NMe.

Note: For analogue Trp8NMe complete assignments could not be determined, due to signal overlap and rotational isomers (cf. Structural Studies by NMR 3.1.7).

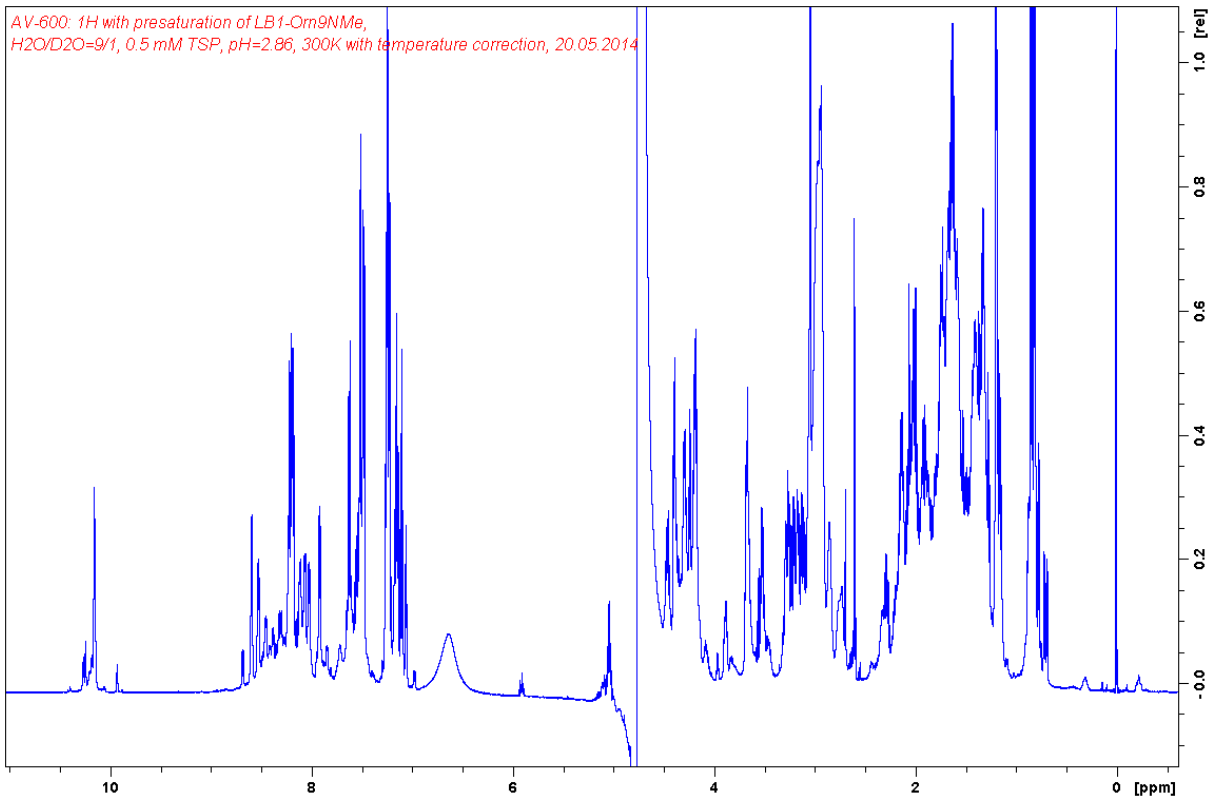

Figure 80 ^{1}H-NMR spectrum of Orn9NMe.

Table 29 ^{1}H-NMR shift assignments of analogue Orn9NMe.

	H	HA	HB	HG	HD	HE	HZ	HH
Thr1	7.92	4.24	4.18	1.2	-	-	-	-
Trp2	8.06	4.69	3.11,3.21	-	7.22	7.48,10.15	7.22,7.47	7.23
Leu3	8.22	4.27	1.56,1.56	1.44	0.82	-	-	-
Dab4	8.12	4.47	2.03,2.13	2.95,2.95	7.65	-	-	-
Orn5	8.19	4.45	1.75,1.85	1.61,1.68	2.85	7.54	-	-
^{D}Lys6	8.59	4.29	1.61,1.61	1.33,1.39	1.66	2.94	7.52	-
Arg7	8.53	4.19	1.57,1.65	1.33,1.33	3.05	7.06	-	-
Trp8	8.18	5.04	3.15,3.27	-	7.24	7.62,10.15	7.14,7.51	7.26
Orn9	3.04	4.94	1.73,1.82	1.33,1.41	2.74	7.43	-	-
Dab10	8.03	4.38	1.99,2.15	2.99,2.99	7.71	-	-	-
Ala11	8.2	4.19	1.19	-	-	-	-	-
Lys12	8.21	4.67	1.57,1.75	1.31,1.40	1.66	2.96,2.96	-	-
^{D}Pro13	-	4.7	1.92,2.29	1.99,2.07	3.51,3.67	-	-	-
Pro14	-	4.39	1.88,2.13	1.91,2.02	3.68,3.89	-	-	-

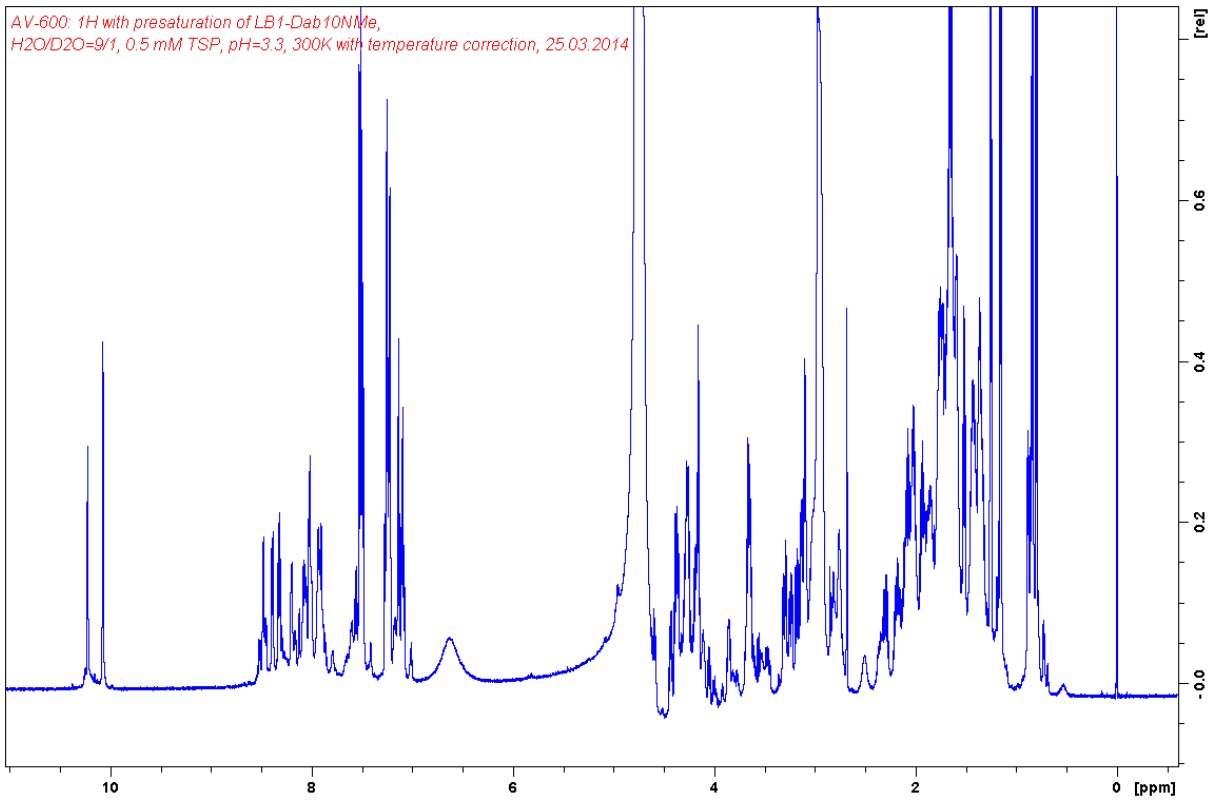

Figure 81 ^{1}H-NMR spectrum of Dab10NMe.

Table 30 ^{1}H-NMR shift assignments of analogue Dab10NMe.

	H	HA	HB	HG	HD	HE	HZ	HH
Thr1	8.02	4.16	4.14	1.15	-	-	-	-
Trp2	8	4.59	3.13,3.24	-	7.25	7.52,10.22	7.14,7.52	7.26
Leu3	7.94	4.19	1.51	1.36	0.81,0.82	-	-	-
Dab4	8.08	4.11	1.89,2.01	2.50,2.82	7.57	-	-	-
Orn5	8.06	4.43	1.74,1.86	1.64,1.71	2.93	7.58	-	-
^{D}Lys6	8.47	4.27	1.66	1.36,1.42	1.66	2.97	7.53,7.53	-
Arg7	8.39	4.28	1.64,1.74	1.43	3.09	7.07	-	-
Trp8	8.2	4.71	3.17,3.29	-	7.22	7.51,10.06	7.09,7.50	7.23
Orn9	8.32	4.72	1.59,1.77	1.56	2.94	7.57	-	-
Dab10	2.97	4.38	1.87,2.18	2.76	7.59	-	-	-
Ala11	7.9	4.25	1.25	-	-	-	-	-
Lys12	7.93	4.66	1.65,1.77	1.35,1.41	1.66	2.96	-	-
^{D}Pro13	-	4.7	1.93,2.29	2.02,2.07	3.63	-	-	-
Pro14	-	4.36	1.84,2.09	1.94,2.02	3.65,3.85	-	-	-

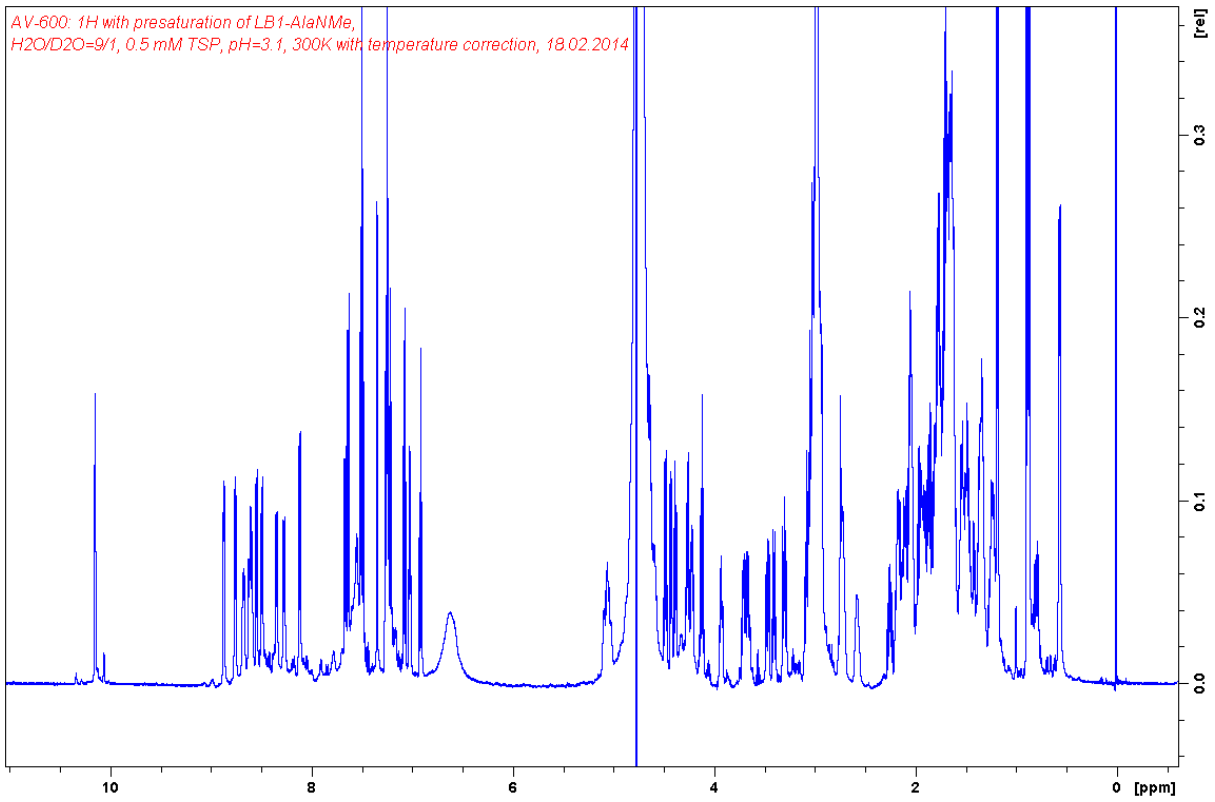

Figure 82 ^{1}H-NMR spectrum of Ala11NMe.

Table 31 ^{1}H-NMR shift assignments of analogue Ala11NMe.

	H	HA	HB	HG	HD	HE	HZ	HH
Thr1	7.66	4.39	4.13	1.19	-	-	-	-
Trp2	8.59	4.63	3.06,3.07	-	7.24	7.25,10.14	6.91,7.50	7.24
Leu3	8.67	4.58	1.54,1.67	1.47	0.88	-	-	-
Dab4	8.61	5.03	2.11,2.19	2.99,3.00	-	-	-	-
Orn5	8.48	4.48	1.80,1.91	1.66,1.73	2.99	-	-	-
^{D}Lys6	8.86	4.26	1.70,1.76	1.37,1.50	1.70	2.97	-	-
Arg7	8.75	4.22	1.53,1.67	1.23,1.34	3.03	7.02	-	-
Trp8	8.11	4.72	3.30,3.46	-	7.34	7.63,10.14	7.07,7.49	7.21
Orn9	8.34	5.09	1.75,1.86	1.64,1.64	2.58,2.71	-	-	-
Dab10	8.54	5.05	1.80,2.12	2.73,2.98	-	-	-	-
Ala11	2.97	4.71	0.57	-	-	-	-	-
Lys12	8.26	4.63	1.48,1.71	1.23,1.34	1.66	2.94,2.94	-	-
^{D}Pro13	-	4.68	1.85,2.26	1.97,2.06	3.40,3.70	-	-	-
Pro14	-	4.42	2.04,2.16	1.93,2.03	3.66,3.92	-	-	-

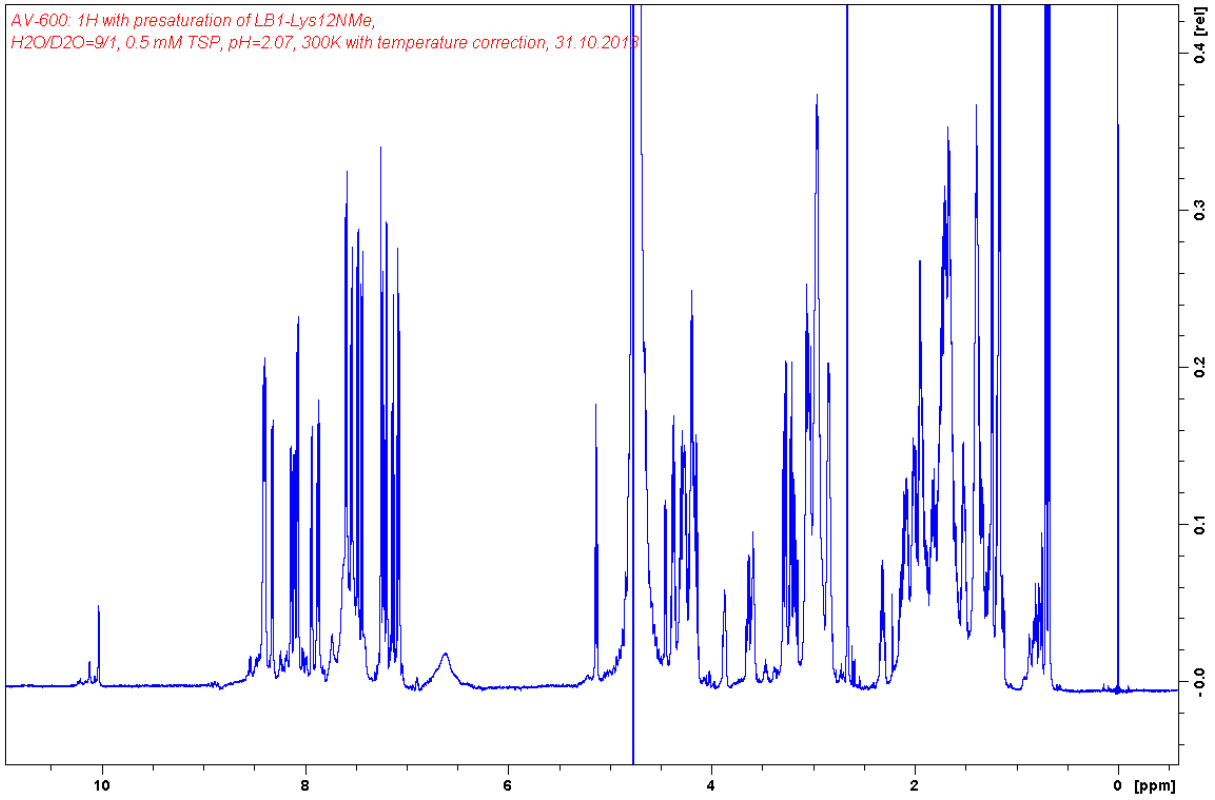

Figure 83 ^{1}H-NMR spectrum of Lys12NMe.

Table 32 ^{1}H-NMR shift assignments of analogue Lys12NMe.

	H	HA	HB	HG	HD	HE	HZ	HH
Thr1	7.86	4.2	4.15	1.17	-	-	-	-
Trp2	8.07	4.64	3.21,3.28	-	7.25	7.59,10.12	7.13,7.48	7.23
Leu3	7.88	4.19	1.38	1.26	0.69	-	-	-
Dab4	8.11	4.17	1.96,2.09	2.85,2.91	7.63	-	-	-
Orn5	8.07	4.37	1.73,1.84	1.66	2.95	7.59	-	-
^{D}Lys6	8.39	4.3	1.76	1.34,1.39	1.66	2.96	7.53,7.53	-
Arg7	8.32	4.26	1.61,1.67	1.39	3.07	7.07	-	-
Trp8	8.14	4.66	3.18,3.29	-	7.2	7.54,10.03	7.07,7.43	7.2
Orn9	8.4	4.28	1.73,1.90	1.67	2.98	7.59	-	-
Dab10	7.93	4.38	2.01,2.13	3.04	7.74	-	-	-
Ala11	8.41	4.2	1.24	-	-	-	-	-
Lys12	2.66	5.13	1.40,1.71	1.18	1.53	2.85	7.42	-
^{D}Pro13	-	-	1.81,2.31	1.92,2.00	3.22,3.59	-	-	-
Pro14	-	4.45	1.98,2.07	1.95,2.03	3.64,3.87	-	-	-

6.3 Protein Identification by Mass Spectrometry

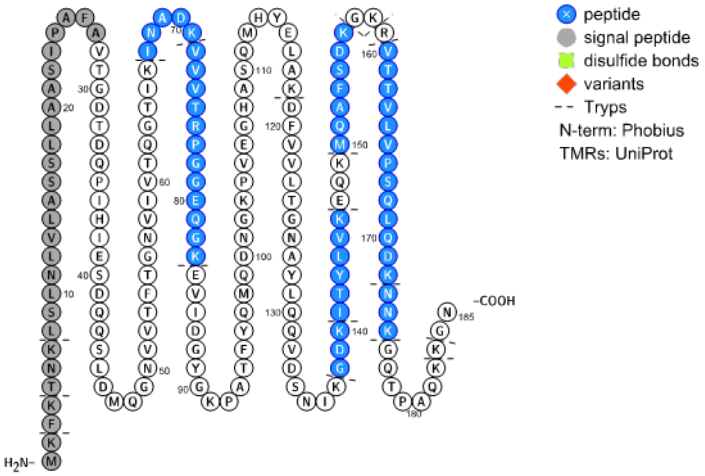

Figure 84 Full LptA sequence and peptide fragments (blue), identified by protein mass spectrometry. The signal sequence is shown in grey.

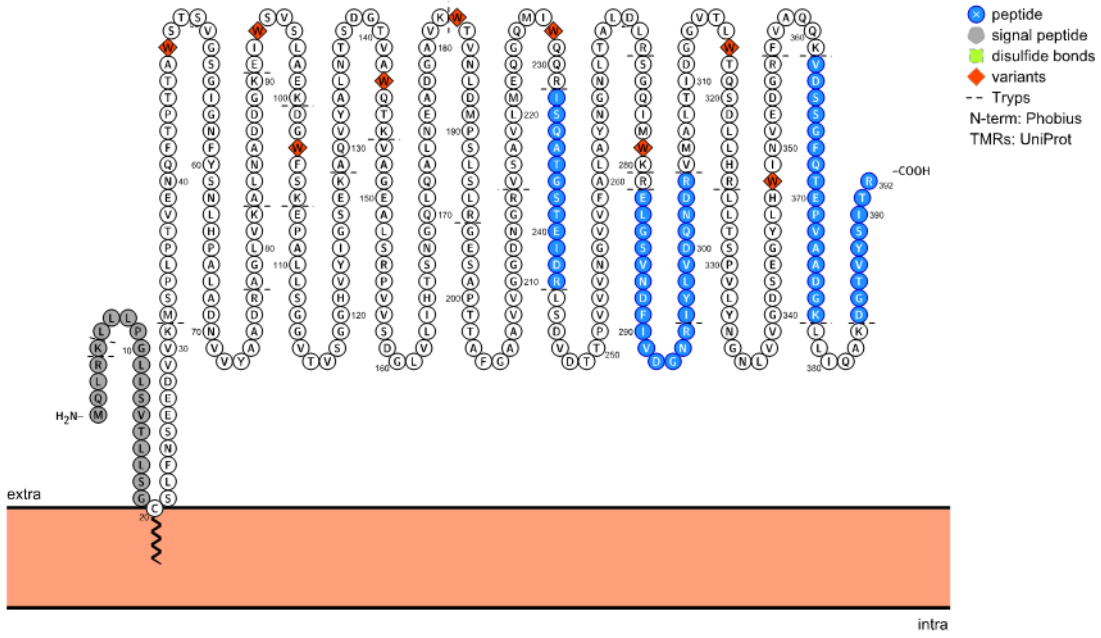

Figure 85 Full BamB sequence and peptide fragments (blue), identified by protein mass spectrometry. The signal sequence is shown in grey.

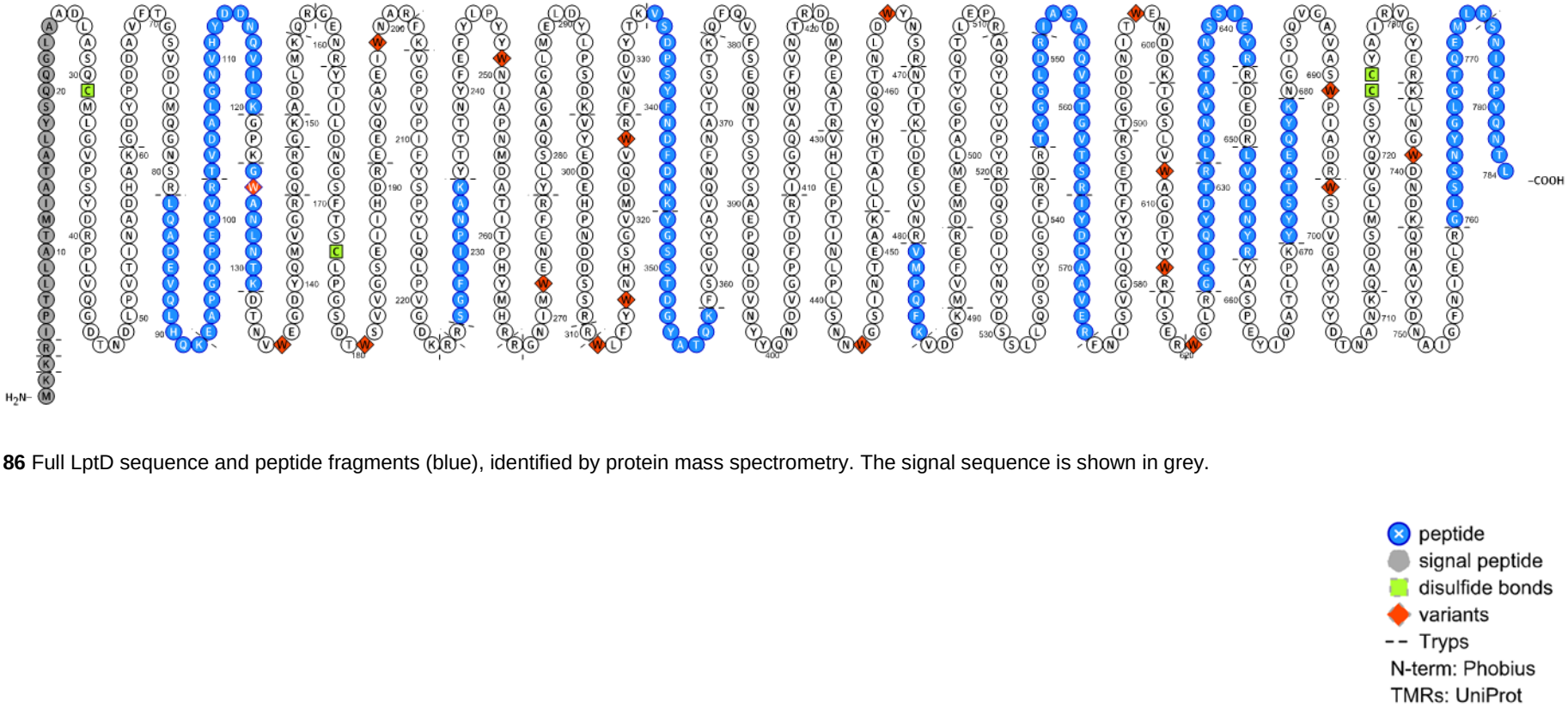

Figure 86 Full LptD sequence and peptide fragments (blue), identified by protein mass spectrometry. The signal sequence is shown in grey.

Acknowledgements

I would like to thank my supervisor, Prof. John A. Robinson, for giving me the opportunity to carry out my Ph.D. thesis in his group and for his excellent guidance throughout the years. I am also very grateful to the committee members Prof. Oliver Zerbe and Prof. Nathan Luedtke, as well as co-referee Prof. Donald Hilvert for critically reviewing my work.

I want to thank all the current and former members of the Robinson group for the friendly atmosphere in the lab, and the following persons in particular for their efforts in supporting this work:

- Dr. Katja Zerbe, for her assistance and for introducing me to the basics of microbiology and biochemistry.
- Dr. Kerstin Möhle, for her NMR analysis and structure calculations in the LB-01 project.
- Matthias Urfer, for being a great colleague in the lab and for his contributions in the thanatin project.
- Annelies Meier, for carrying out all the MIC measurements in the LB-01 project and Myriam Gwerder, for MIC measurements, cloning, and protein purification in the thanatin project.
- Maik Müller, from the Wollscheid group at ETH Zurich, for the successful collaboration and for his key findings in the thanatin project.
- Alessandra Vitale and Dr. Gabriella Pessi, from the Eberl group at UZH, for carrying out whole genome sequencing in the thanatin project.
- Yvonne Stark, from the Plückthun group, for introducing me to fluorescence polarization.
- Dr. Andres Käch, from the Center for Microscopy and Image Analysis UZH, for carrying out electron microscopy experiments.
- Dr. Kay Hänggi, from the Wang group, for being a good friend and his support in the LB-01 uptake studies.

I would also like to thank the NMR and MS service, and the FGCZ for providing analytical services, as well and the graduate school CMSZH for general support.

Finally, I would like to thank my family and my girlfriend Tara, who have always supported and encouraged me throughout my studies.

Curriculum vitae

Personal details

Name:	Stefan Urs Vetterli
Date of birth:	26th of August, 1985
Place of origin:	Stäfa (ZH)
Nationality:	Swiss

Education

2013 – 2017: **Ph.D. in Chemical and Molecular Sciences** at University of Zurich. Ph.D. thesis under the supervision of Prof. Dr. John A. Robinson: Synthesis and Antimicrobial Activity of β-Hairpin Peptidomimetics Against *Pseudomonas aeruginosa* and Understanding the Mechanism of Action of the Insect Antimicrobial Peptide Thanatin.

2010 – 2012: **MSc in Biology (Major: Biological Chemistry)** at ETH Zurich. Master thesis under the supervision of Prof. Dr. K-H. Altmann: Synthesis of Hypermodified Epothilone A Analogues.

2006 – 2010: **BSc in Pharmaceutical Sciences** at ETH Zurich.

2001 – 2005: **Eidgenössische Matura (Major: Economics and Law)** at Mittelschule Dr. Buchmann, Zurich.

Publications

Synthesis and antimicrobial activity against Pseudomonas aeruginosa of macrocyclic β-hairpin peptidomimetic antibiotics containing N-methylated amino acids. S. U. Vetterli, K. Moehle, J. A. Robinson, *Bioorg. Med. Chem.* **2016**, *24*, 6332.